ISSN 0021-9673

VOL. 690 NO. 1 20 JANUARY 1995

JOURNAL OF CHROMATOGRAPHY A

INCLUDING ELECTROPHORESIS AND OTHER SEPARATION METHODS

ELSEVIER

JOURNAL OF CHROMATOGRAPHY A

INCLUDING ELECTROPHORESIS AND OTHER SEPARATION METHODS

Scope. The *Journal of Chromatography A* publishes papers on all aspects of **chromatography, electrophoresis** and related methods. Contributions consist mainly of research papers dealing with chromatographic theory, instrumental developments and their applications. In the *Symposium volumes*, which are under separate editorship, proceedings of symposia on chromatography, electrophoresis and related methods are published. *Journal of Chromatography B: Biomedical Applications* —This journal, which is under separate editorship, deals with the following aspects: developments in and applications of chromatographic and electrophoretic techniques related to clinical diagnosis or alterations during medical treatment; screening and profiling of body fluids or tissues related to the analysis of active substances and to metabolic disorders; drug level monitoring and pharmacokinetic studies; clinical toxicology; forensic medicine; veterinary medicine; occupational medicine; results from basic medical research with direct consequences in clinical practice.

Submission of Papers. The preferred medium of submission is on disk with accompanying manuscript (see *Electronic manuscripts* in the Instructions to Authors, which can be obtained from the publisher, Elsevier Science B.V., P.O. Box 330, 1000 AH Amsterdam, Netherlands). Manuscripts (in English; *four* copies are required) should be submitted to: Editorial Office of *Journal of Chromatography A*, P.O. Box 681, 1000 AR Amsterdam, Netherlands, Telefax (+31-20) 485 2304, or to: The Editor of *Journal of Chromatography B: Biomedical Applications*, P.O. Box 681, 1000 AR Amsterdam, Netherlands. Review articles are invited or proposed in writing to the Editors who welcome suggestions for subjects. An outline of the proposed review should first be forwarded to the Editors for preliminary discussion prior to preparation. Submission of an article is understood to imply that the article is original and unpublished and is not being considered for publication elsewhere. For copyright regulations, see below.

Publication information. *Journal of Chromatography A* (ISSN 0021-9673): for 1995 Vols. 683–714 are scheduled for publication. *Journal of Chromatography B: Biomedical Applications* (ISSN 0378-4347): for 1995 Vols. 663–674 are scheduled for publication. Subscription prices for *Journal of Chromatography A*, *Journal of Chromatography B: Biomedical Applications* or a combined subscription are available upon request from the publisher. Subscriptions are accepted on a prepaid basis only and are entered on a calendar year basis. Issues are sent by surface mail except to the following countries where air delivery via SAL is ensured: Argentina, Australia, Brazil, Canada, China, Hong Kong, India, Israel, Japan, Malaysia, Mexico, New Zealand, Pakistan, Singapore, South Africa, South Korea, Taiwan, Thailand, USA. For all other countries airmail rates are available upon request. Claims for missing issues must be made within six months of our publication (mailing) date. Please address all your requests regarding orders and subscription queries to: Elsevier Science B.V., Journal Department, P.O. Box 211, 1000 AE Amsterdam, Netherlands. Tel.: (+31-20) 485 3642; Fax: (+31-20) 485 3598. Customers in the USA and Canada wishing information on this and other Elsevier journals, please contact Journal Information Center, Elsevier Science Inc., 655 Avenue of the Americas, New York, NY 10010, USA, Tel. (+1-212) 633 3750, Telefax (+1-212) 633 3764.

Abstracts/Contents Lists published in Analytical Abstracts, Biochemical Abstracts, Biological Abstracts, Chemical Abstracts, Chemical Titles, Chromatography Abstracts, Current Awareness in Biological Sciences (CABS), Current Contents/Life Sciences, Current Contents/Physical, Chemical & Earth Sciences, Deep-Sea Research/Part B: Oceanographic Literature Review, Excerpta Medica, Index Medicus, Mass Spectrometry Bulletin, PASCAL-CNRS, Referativnyi Zhurnal, Research Alert and Science Citation Index.

US Mailing Notice. *Journal of Chromatography A* (ISSN 0021-9673) is published weekly (total 52 issues) by Elsevier Science B.V., (Sara Burgerhartstraat 25, P.O. Box 211, 1000 AE Amsterdam, Netherlands). Annual subscription price in the USA US$ 5389.00 (US$ price valid in North, Central and South America only) including air speed delivery. Second class postage paid at Jamaica, NY 11431. **USA POSTMASTERS**: Send address changes to *Journal of Chromatography A*, Publications Expediting, Inc., 200 Meacham Avenue, Elmont, NY 11003. Airfreight and mailing in the USA by Publications Expediting.

See inside back cover for Publication Schedule, Information for Authors and information on Advertisements.

0021-9673/95/$09.50

Printed in the Netherlands

CONTENTS

(Abstracts/Contents Lists published in Analytical Abstracts, Biochemical Abstracts, Biological Abstracts, Chemical Abstracts, Chemical Titles, Chromatography Abstracts, Current Awareness in Biological Sciences (CABS), Current Contents/Life Sciences, Current Contents/Physical, Chemical & Earth Sciences, Deep-Sea Research/Part B: Oceanographic Literature Review, Excerpta Medica, Index Medicus, Mass Spectrometry Bulletin, PASCAL-CNRS, Referativnyi Zhurnal, Research Alert and Science Citation Index)

REGULAR PAPERS

Column Liquid Chromatography

Gas Chromatography

(Continued overleaf)

Contents (continued)

JOURNAL OF CHROMATOGRAPHY A

VOL. 690 (1995)

JOURNAL OF CHROMATOGRAPHY A

INCLUDING ELECTROPHORESIS AND OTHER SEPARATION METHODS

ELSEVIER

Amsterdam – Lausanne – New York – Oxford – Shannon – Tokyo

J. Chromatogr. A, Vol. 690 (1995)

0021-9673/95/$09.50

ELSEVIER

Journal of Chromatography A, 690 (1995) 1–8

JOURNAL OF CHROMATOGRAPHY A

Axial dispersion in liquid magnetically stabilized fluidized beds

Motonobu Goto*, Takahiro Imamura, Tsutomu Hirose

Department of Applied Chemistry, Kumamoto University, Kumamoto 860, Japan

First received 9 August 1994; revised manuscript received 17 October 1994; accepted 17 October 1994

Abstract

Magnetic stabilization permits the expansion of a packed bed without mixing of solid particles. This allows operation with a low pressure drop, free from clogging, and high column efficiency. The performance of magnetically stabilized fluidized beds (MSFB), developed for affinity separation, was studied in terms of axial dispersion, the controlling factor in column efficiency. Porous beads of chitosan-containing magnetite particles were used as the stationary phase. Bed expansion increased with increase in flow-rate and with decrease in magnetic field strength. The axial dispersion coefficient was evaluated by moment analysis of the impulse response curves. The axial dispersion for the MSFB was comparable to that of a packed bed and smaller than that of a fluidized bed. The chromatographic behaviour of the MSFB was consistent with the above results.

1. Introduction

The use of a magnetically stabilized fluidized bed (MSFB) is an alternative to conventional column operation, such as with a packed bed (PB) or fluidized bed (FB), for the large-scale purification of biological products. The fluidization is stabilized by a magnetic field so that the bed can be maintained in a quiescently fluidized state without turbulent solids mixing. The MSFB has advantages of both packed and fluidized beds, such as efficient fluid–solid contact, low pressure drop, resistance to clogging and continuous counter-current operation.

The performance of the MSFB has been studied for both gas [1] and liquid [2] systems. The MSFB behaves like a packed bed but has lower operational pressure drops while still having sharp breakthrough and narrow elution bands of solute with high column capacity [1]. The application of a magnetic field to a liquid fluidized bed produces several different operating regimes depending on the liquid velocity and the strength of the magnetic field. There exists an operating regime termed "stabilized" where the bed is fluidized without mixing motion of the particles. The adsorption efficiency for the bed may be defined by the dynamic capacity adsorbed until the breakthrough point, which depends on the shape of the breakthrough curve. In that regime, the adsorption efficiency would be higher than for a conventional fluidized bed, because of the smaller axial dispersion without mixing of particles in the bed.

The adsorption efficiency decreased due to the band spreading resulting from axial dispersion and rate processes, such as intraparticle diffusion, external fluid–solid mass transfer and in-

* Corresponding author.

0021-9673/95/$09.50
SSDI 0021-9673(94)00993-7

trinsic adsorption rate. The intraparticle diffusion and intrinsic adsorption rate are inherent in the adsorbate–adsorbent system. As external mass transfer is not usually dominant, the evaluation of the axial dispersion is most important for the analysis of adsorption systems.

The objective of this paper is to evaluate axial dispersion in the MSFB in comparison with the PB and the FB. The axial dispersion reported in the literature was measured for nickel powder on a relatively small scale (solid 95 or 20–45 μm, column 6.35 and 9.53 mm I.D.) [3] and for steel spheres on a relatively large scale (spheres 30–140 mesh, column 76.2 mm I.D.) [2] as a solid. We have measured the axial dispersion coefficient with porous adsorbent particles that had been prepared for affinity separation of trypsin or lysozyme [4].

2. Experimental

2.1. Preparation of magnetic adsorbent

A magnetic affinity adsorbent was prepared from chitosan. As chitosan is a very hydrophilic polysaccharide and has amino groups, it is suitable as an affinity adsorbent.

Magnetite fine particles were synthesized from iron(II) sulfate by moderate oxidation with potassium nitrate in the presence of ammonia under a nitrogen atmosphere at boiling temperature. The average diameter of the magnetite particles obtained was 580 nm.

Magnetite-containing porous chitosan beads were prepared as follows. Chitosan (from crab shells; Sigma) was dissolved in 4% acetic acid to obtain a 3% (w/v) chitosan solution. After filtration and degassing, the chitosan solution was mixed with the magnetite particles prepared as above. The mixture was forced into a nitrogen stream through a needle nozzle by means of the aerosol jet technique [5]. The sol particles extruded from the nozzle were immediately gelled in sodium hydroxide solution located about 0.10 m downstream from the jet nozzle. After the magnetic chitosan beads had been sufficiently washed with water, the beads were cross-linked with glutaraldehyde. The size of the beads could be controlled by the chitosan concentration, extrusion speed, nozzle size and nitrogen flow-rate. The average diameter of the particles used was 0.550 mm with a standard deviation of 0.0787 mm. The content of the magnetite was 5% (w/v). The apparent density of the adsorbent was 1210 kg/m^3 and the void fraction was 0.911. The minimum fluidizing velocity was $0.90 \cdot 10^{-3}$ m/s.

The prepared adsorbent was used for the affinity adsorption of lysozyme by a group-specific affinity interaction with the glucosamines of the chitosan matrix, and of trypsin after introducing soy bean trypsin inhibitor as a ligand [4].

2.2. Impulse response measurement

The experimental apparatus is shown schematically in Fig. 1. The column was a C10/20 (200 mm × 10 mm I.D.) (Pharmacia–LKB Biotechnology) with an adapter that allowed adjustment of the bed height. The position of the adapter was controlled at the top of the fluidized bed so as to eliminate the dead space above the bed. For packed-bed operation, the adapter was controlled at the top of the unfluidized bed so as to prevent expansion of the bed. The column was cooled at 277 K with a water-jacket. A magnetic field was applied collinear with that of the mobile phase by surrounding the column with two wire-wound solenoid electromagnets. D.c. power was supplied by a regulated d.c.

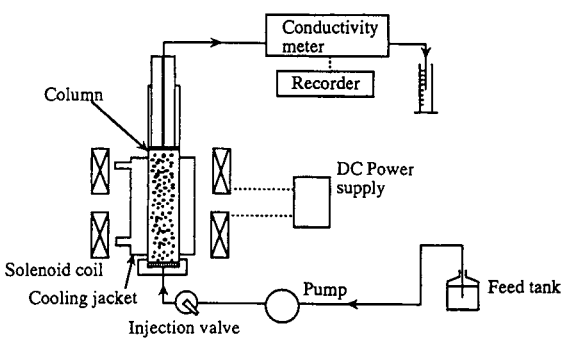

Fig. 1. Experimental apparatus for magnetically stabilized fluidized bed operation.

power supply (Model GP035-10; Takasago, Tokyo, Japan) and the magnetic field strength was controlled by the current applied. The solenoid coil (30 mm × 68 mm I.D.) consisted of approximately 550 turns of 1-mm copper wire. The fluidizing liquid flow was provided by an HPLC pump (Model PU-880; JASCO, Tokyo, Japan).

All the experiments were carried out in the "flow-first" mode [2] where the bed was fluidized by first flowing the liquid and then applying a magnetic field. The "flow-first" mode was better than the "field-first" mode with regard to reproducibility. A 25-μl pulse of aqueous 40 m*M* NaCl solution was injected into the column with a seven-port injection valve (Pharmacia–LKB Biotechnology). The response of the pulse was measured with an electric conductivity meter (Model 213A; Wescan Instruments, Santa Clara, CA, USA). The response curve recorded was analysed by the moment method. The magnetic field applied was 25 kA/m unless stated otherwise. NaCl was chosen as a tracer because the adsorption of Na^+ and Cl^- ions is weak or negligible even if they diffuse into the particles.

2.3. Affinity chromatography

Purification of lysozyme was demonstrated by the magnetically stabilized fluidized bed filled with the magnetic chitosan beads. Lysozyme dissolved in 0.1 *M* Tris–HCl buffer solution (pH 7.4) was used as a feed solution. The feed solution was supplied to the column until the adsorbent was saturated with lysozyme. Then, the lysozyme adsorbed was eluted with a 0.1 *M* acetic acid. The magnetic field applied was 25 kA/m.

3. Results and discussion

3.1. Behaviour of magnetically stabilized fluidized bed

Without a magnetic field, the particles in the bed became fluidized at the minimum fluidizing velocity, and moved within the bed as it expanded. With a magnetic field, the bed started to expand at the minimum fluidizing velocity but without relative motion of the particles (stably fluidized). When the flow-rate was increased further, the bed height increased and the particles started to move (unstably fluidized).

The behaviour of the magnetic fluidized bed was classified from visual observation of different regimes depending on the strength of the magnetic field and the flow-rate as shown in Fig. 2. The bed changed from an unfluidized bed (dense packed) to a stably fluidized bed (quiescent) and then finally an unstably fluidized bed (turbulent solids mixing) regime as the flow-rate increased at a given magnetic field. The particles in the stable regime were fixed in place in the expanded bed where the void volume is larger than that in the packed bed, that is, the particle motion is arrested. On the other hand, particles move in a circulatory manner in the bed with turbulent liquid flow in the unstably fluidized regime. The particle behaviour in the unstably fluidized state was "gulf streaming" [3] or "circulatory motion of the overall bed" rather than "roll cell" motion [2]. The behaviour shifted from gulf streaming to circulatory motion and finally to random motion as the flow-rate increased.

Ideal performance of the fluidized-bed operation may be attained by minimizing bed expansion and extending the stably fluidized state to

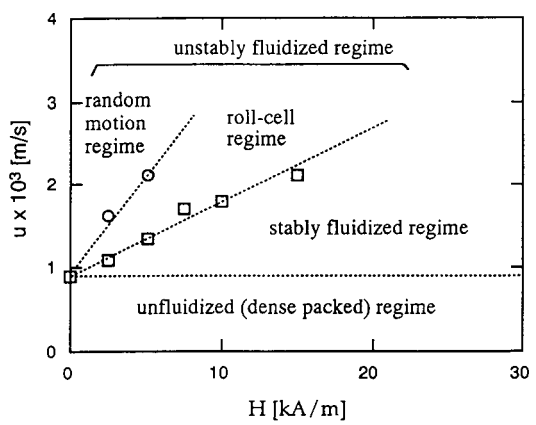

Fig. 2. Effect of magnetic field strength on the fluidization characteristics of bed (packed-bed length = 0.0647 m). ○ = Transition between random motion and roll-cell regime; □ = transition between roll-cell and stably fluidized regime.

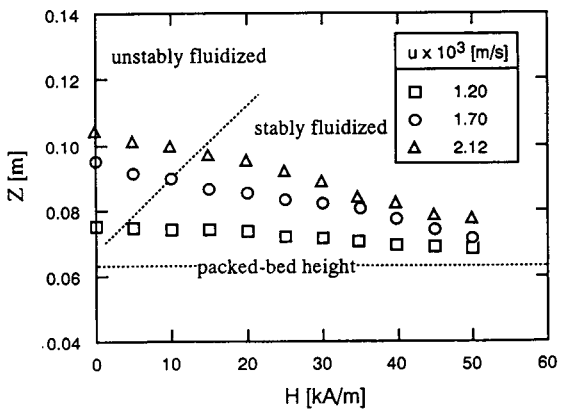

Fig. 3. Effect of magnetic field strength and flow-rate on the fluidized bed length.

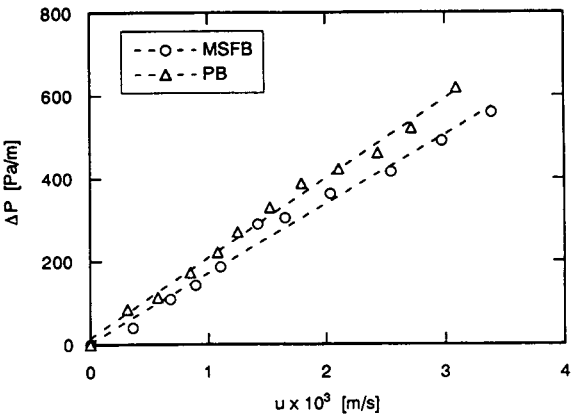

Fig. 4. Comparison of pressure drops between the MSFB and PB.

higher flow-rates while maintaining a low pressure drop. Fig. 3 shows the expansion of the bed as a function of the magnetic field strength and the flow-rate. Larger bed heights were observed for higher flow-rates. The bed expansion decreased as the magnetic field increased. The largest decrease in the bed height was observed in the unstable regime. Once the bed had stabilized, its height did not decrease further with increasing magnetic field. The magnetic field extended the quiescent state to higher flow-rates, decreased bed expansion and minimized axial mixing by inhibiting axial motion of the particles. This behaviour may result in higher efficiency of adsorption in the bed.

3.2. Pressure drops

Pressure drops in the PB and MSFB are shown in Fig. 4. The pressure drop in the MSFB was smaller than that in the PB because of the larger bed voidage. As the column size was relatively small and the particle size was large, the pressure drop was not large in this experiment. As the pressure drop is a function of bed voidage, particle size and flow-rate [6], a larger bed voidage leads to a smaller pressure drop. If the particle size were much smaller, the pressure drop in the PB would be much larger.

In addition to the lower pressure drop, the MSFB can avoid consolidation of the bed. One of the problems with chromatography using a soft gel as the stationary phase is consolidation of the bed at higher flow-rates, resulting in a significant increase in pressure drop [7]. As particles in the MSFB are fixed in the bed with a large bed voidage by a magnetic field even at high flow-rates, consolidation of the bed does not occur. Therefore, a soft gel can be used without consolidation at high flow-rates.

3.3. Impulse response analysis

The theoretical model developed for a packed bed is not strictly applicable to a fluidized bed system, because the adsorbent particles move in the bed so that there is axial mixing of solids in addition to fluid mixing. However, a packed-bed model was used in order to compare the behaviours among the PB, FB and MSFB.

The impulse response in a packed column is governed by a system of coupled partial differential equations which include axial dispersion, external fluid–particle mass transfer and intraparticle diffusion [8]. On the assumption of linear adsorption equilibrium, the moments can be derived [9]. The first absolute and the second central moments of the response curve for the system are

$$\mu_1' = \frac{z}{v}\left[1 + \frac{1-\varepsilon_B}{\varepsilon_B} \cdot K\right] + \frac{t_0}{2} \quad (1)$$

$$\mu_2 = \frac{2z}{v}\left[\frac{1-\varepsilon_B}{\varepsilon_B}\cdot\frac{K^2R^2}{3}\left(\frac{1}{5D_e}+\frac{1}{k_fR}\right) + \frac{D_{ax}}{v^2}\left(1+\frac{1-\varepsilon_B}{\varepsilon_B}\cdot K\right)^2\right] + \frac{t_0^2}{12} \quad (2)$$

The first absolute moment, μ_1', characterizes the position of the centre of gravity of the response peak, whereas the second central moment, μ_2, characterizes the width of the peak.

The first and second moments of the experimental response curve are calculated by

$$\mu_1' = \int_0^\infty Ct\,dt \Big/ \int_0^\infty C\,dt \quad (3)$$

$$\mu_2 = \int_0^\infty C(t-\mu_1')^2\,dt \Big/ \int_0^\infty C\,dt \quad (4)$$

The governing equations were solved analytically [10] in the time domain and the analytical solution was given in terms of an infinite integral.

The response curves are compared in Fig. 5 among the PB, FB and the MSFB at a flow-rate of $3.6\cdot10^{-4}$ m/s. The peaks for the MSFB and FB eluted later than that for the PB because of larger bed void space. The shapes of the curves were similar between the PB and the MSFB. The peak for the FB was broader than the other two peaks. Hence, the axial dispersion for the MSFB and PB were almost the same and that for the FB was larger.

The height equivalent to a theoretical plate (HETP), H, reduced HETP, h, and plate number, N, are given by

$$H = z\mu_2/\mu_1'^2 \quad (5)$$

$$N = \mu_1'^2/\mu_2 \quad (6)$$

$$h = H/2R \quad (7)$$

The HETP and the reduced HETP are shown in Fig. 6. The FB had the largest HETP owing to the large axial dispersion. The HETPs for the MSFB and PB were comparable. As the bed was expanded for the MSFB, the HETP was even smaller than that for the PB. The reduced HETP seems to be larger than typical value ($h = 2$–3), because the operation was not optimum.

3.4. Parameter evaluation for packed bed

To evaluate the axial dispersion coefficient, D_{ax}, unknown parameters, K, D_e and k_f, in the second moment must be previously determined. Values of the bed length, z, and the bed porisity, ε_B, are constant for the PB, whereas they are a function of flow-rate for the FB and the MSFB. Thus, the linear regression analysis where the moments are plotted against inverse of the flow-rate to give a straight line is not applicable for the FB and MSFB. Therefore, the parameters K and D_e were first obtained from the experiment

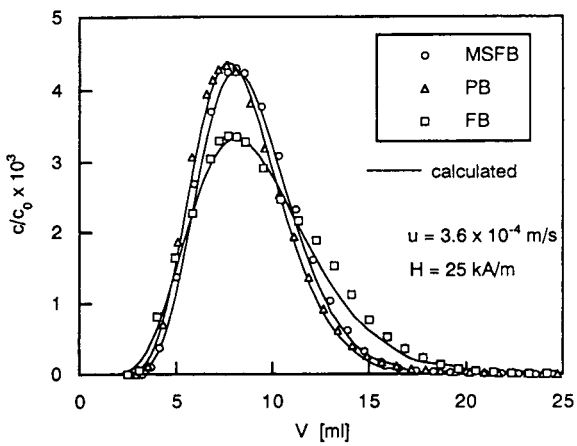

Fig. 5. Comparison of impulse response curve among the MSFB, PB and FB.

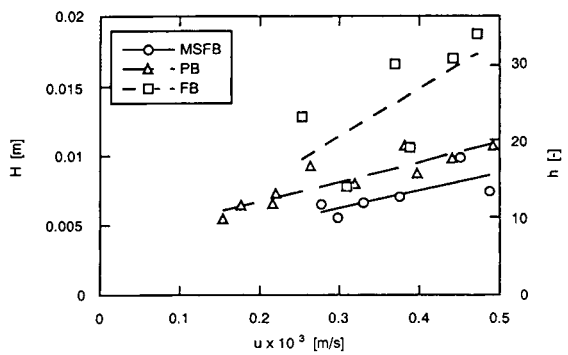

Fig. 6. Comparison of HETP and reduced HETP among the MSFB, PB and FB.

for the PB, because these parameters should be inherent in the adsorbent regardless of the bed state.

The adsorption equilibrium constant, K, was first calculated from the first moment, μ_1'. The slope of the regression line in the plot of $(\mu_1'-t_0/2)$ versus z/v was $1+(1-\varepsilon_B)K/\varepsilon_B$, which gave $K=1.15$. This value includes the effect of pore volume and intrinsic adsorption at the inner surface.

When the influence of external mass transfer on the second moment is small, the second moment can be analysed by the linear regression method from the plot of $(\mu_2-t_0^2/12)v/(2z)$ versus $1/v$. As the contribution of k_f is not expected to be negligible and then the mass transfer term in second moment is a function of the flow-rate, the parameters, D_e and D_{ax} were estimated by non-linear regression. The external mass transfer coefficient, k_f, was estimated by a correlation proposed by Wakao and Kaguei [11] where diffusivity of NaCl was estimated by the Nernst–Haskell equation [12].

The axial dispersion coefficient is usually proportional to the flow-rate for liquid systems except for extremely small flow-rates where molecular diffusion has an influence. Hence, the value of D_{ax}/v was assumed to be constant. D_e and D_{ax}/v were evaluated to be $8.59\cdot10^{-10}$ m^2/s and $1.51\cdot10^{-3}$ m, respectively for the PB.

3.5. Axial dispersion coefficient for a fluidized bed and a magnetically stabilized fluidized bed

For the evaluation of the axial dispersion coefficient of the FB and MSFB, the values of K and D_e determined from the PB were used. The axial dispersion coefficient was calculated from the second moment, Eq. 2, by direct substitution of z, ε_B, K, D_e and k_f for each run at various flow-rates. The bed voidage was calculated from the bed height for the packed state and the fluidized state; the bed voidage for the PB was 0.429.

The axial dispersion coefficients obtained are shown as a function of flow-rate in Fig. 7. As the axial dispersion coefficient for the PB was estimated by linear regression of the entire data, the result for the PB is represented as a straight line. It is evident that the axial dispersion for the MSFB is nearly the same as for the PB, whereas the axial dispersion coefficient for the FB is larger than that for the PB and MSFB. The FB has a large axial dispersion coefficient, because of the mixing of fluid induced by the movement of solid particles. As the solid particles are fixed by the magnetic field for the MSFB, the mixing of fluid for the MSFB is similar to that for the PB. The only difference between the PB and MSFB is the bed voidage. A larger bed voidage results in a lower pressure drop and avoidance of clogging problems of the bed caused by suspended solids in the feed solution.

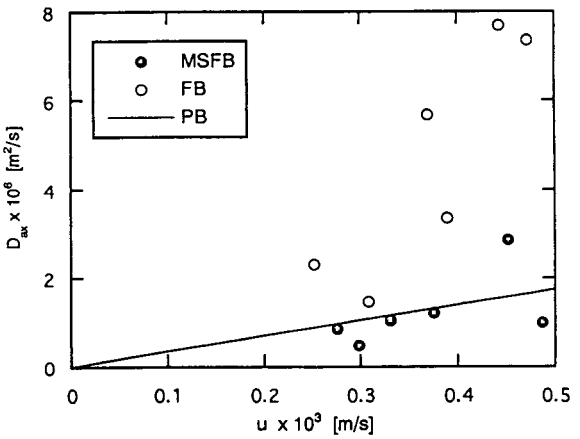

Fig. 7. Comparison of axial dispersion coefficient among the MSFB, FB and PB.

The axial dispersion coefficient is shown in dimensionless form as Pe^{-1} versus Re in Fig. 8. Literature data [2,3,13] are given for comparison. The region of Reynolds number in this work is located in the same region as reported by Goetz and Graves [3]. One of the main differences between this work and the literature [1,12] is that porous chitosan particles were used here whereas non-porous metal particles were used by others [2,3]. The Peclet number obtained in this work almost coincides with the published values. The axial dispersion for the MSFB is nearly the same as for the PB, as reported previously [2,3].

The response curves were simulated with the parameters obtained by moment analysis. An

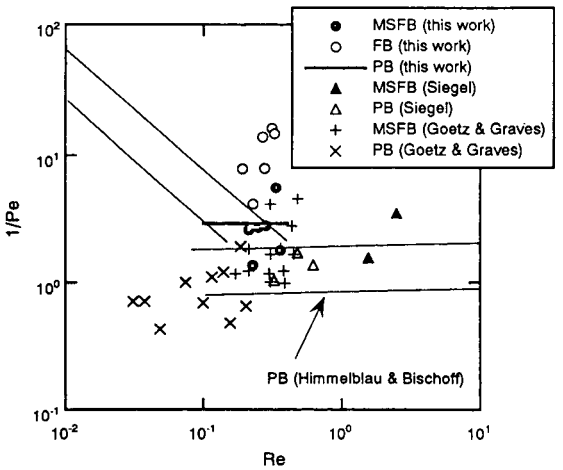

Fig. 8. Comparison of $1/Pe$ with literature data (Siegell [2]; Goetz and Graves [3]; Himmelblau and Bischoff [13]).

analytical solution [10] was used for the simulation. The solid lines in Fig. 5 indicate the calculated curves. The agreement between the experimental and calculated curves indicates that the parameters obtained by moment analysis were reliable.

3.6. *Affinity chromatography*

An affinity separation, which consisted of a series of adsorption, washing and elution steps, was carried out, for lysozyme with the magnetic chitosan beads. The histories of the effluent lysozyme concentration during the operation are compared among the MSFB, FB and PB in Fig. 9. As the adsorbent beads were fixed in the bed by magnetic force, the performance of the MSFB was almost the same as for the PB and better than for the FB. The breakthrough curve in the adsorption step was slightly gentler for the MSFB than that for the PB because of the larger bed voidage. The amounts of adsorbed lyozyme were $0.306 \cdot 10^{-3}$, $0.278 \cdot 10^{-3}$ and $0.181 \cdot 10^{-3}$ g/cm^3 bed for the PB, MSFB and FB, respectively, under the same conditions. Hence, the efficiency of the adsorption for the MSFB is located between those for the PB and FB. The result agrees with the axial dispersion behaviour. As the particle size used in this study is relatively

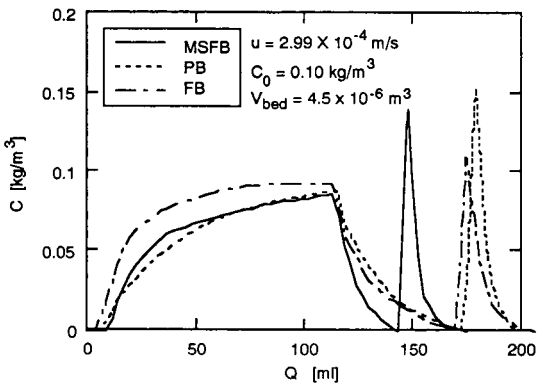

Fig. 9. Comparison between the MSFB, PB and FB with respect to the performance of affinity separation of lysozyme by magnetic chitosan beads.

large, the mass transfer resistance in a particle may dominate. For smaller particles, the difference between the MSFB and FB must be large, because axial dispersion may have a considerable influence on peak broadening.

4. Conclusion

The performance of the MSFB was evaluated in terms of the axial dispersion in the bed. The impulse response measured was analysed by the moment method. The axial dispersion coefficient obtained for the MSFB was comparable to that for the PB and smaller than that for the FB. Therefore, the performance of the MSFB was similar to that of the PB.

As the MSFB is aimed at large-scale preparative operation, the system used in this work may not be suitable for practical operation where larger columns and smaller particles may be used. The advantages of the MSFB may become evident for practical systems. Further work is needed for systems close to a practical scale.

Symbols

C Concentration (M)
D_{ax} Axial dispersion coefficient (m^2/s)
D_e Intraparticle effective diffusivity (m^2/s)

H Magnetic field strength (kA/m)
K Adsorption equilibrium constant
k_f Fluid-to-particle mass transfer coefficient (m/s)
Pe $=2R\,v/D_{ax}$; Peclet number
R Particle radius (m)
Re $=2R\,v\rho/\mu$; Reynolds number
t Time (s)
t_0 Injection time (s)
u Superficial fluid velocity (m/s)
V Effluent volume (m^3)
v Interstitial fluid velocity (m/s)
z Bed height (m)
ε_B Bed void fraction
μ Fluid viscosity (kg/m s)
μ_1' First absolute moment (s)
μ_2 Second central moment (s^2)
ρ Fluid density (kg/m^3)

Acknowledgements

Financial support from the Miyajima Toshiharu Foundation is gratefully acknowledged. The authors are grateful to Mr. S. Morisaki for experimental assistance.

References

[1] R.E. Rosensweig, *Science*, 204 (1979) 57.
[2] J.H. Siegell, *Powder Technol.*, 52 (1987) 139.
[3] V. Goetz and D.J. Graves, *Powder Technol.*, 64 (1991) 81.
[4] M. Goto, T. Imamura and T. Hirose, in M. Suzuki (Editor), *Fundamentals of Adsorption –Proceedings of the IVth International Conference on Fundamentals of Adsorption*, Kodansha, Tokyo, 1993, p. 227.
[5] C.H. Lochmüller and L.S. Wigman, *Sep. Sci. Technol.*, 22 (1987) 2111.
[6] R.M. Nicoud and M. Perrut, *Chromatographic and Membrane Processes in Biotechnology*, Kluwer, Dordrecht, 1991, p. 53.
[7] E. Sada, S. Katoh and M. Shiozawa, *Biotechnol. Bioeng.*, 24 (1982) 2279.
[8] M. Goto, N. Hayashi and S. Goto, *Sep. Sci. Technol.*, 18 (1983) 475.
[9] M. Kubin, *Collect. Czech. Chem. Commun.*, 30 (1965) 1104, 2900.
[10] A. Rasmuson and I. Neretnieks, *AIChE J.*, 26 (1980) 686.
[11] N. Wakao and S. Kaguei, *Heat and Mass Transfer in Packed Beds*, Gordon and Breach, New York, 1982.
[12] R.C. Reid, J.M. Prausnitz and B.E. Poling, *The Properties of Gases and Liquids*, McGraw-Hill, New York, 4th ed., 1987.
[13] D.M. Himmelblau and K.B. Bischoff, *Process Analysis and Simulation*, Wiley, New York, 1967.

ELSEVIER

Journal of Chromatography A, 690 (1995) 9–19

JOURNAL OF CHROMATOGRAPHY A

High velocity reversed-phase chromatography of proteins and peptides: use of conventional C18, 300 Å, 15 μm particles

William Kopaciewicz[a,*], Elizabeth Kellard[a], Geoffrey B. Cox[b]

[a]*Amicon Inc., Beverly, MA 01985, USA*

[b]*Prochrom R&D, 54250 Champigneulles, France*

First received 22 July 1994; revised manuscript received 17 October 1994

Abstract

Experiments were conducted to study the effects of mobile phase velocity on the reversed-phase chromatography of peptides and proteins using a mono-modal pore size (300 Å) C18 spherical silica packing. This material was packed into several 5 × 0.46 cm columns for gradient elution studies using ribonuclease A, insulin, lysozyme and myoglobin. Baseline separation of these proteins was achieved within 90 seconds. Using a two-minute linear gradient from 15 to 65% acetonitrile (in 0.1% trifluoroacetic acid), resolution improved with velocity. Enhanced performance was attributed to the concurrent increase in gradient volume with higher mobile phase velocity.

The frontal adsorption capacity of lysozyme was 25 and 23 mg/ml at 220 and 3600 cm/h on the 300 Å packing material. These values are equivalent (within an experimental error of ± 2 mg/ml) clearly demonstrating that lysozyme (M_r 14 300) fully permeates the 300 Å pores during operation at high mobile phase velocity. Comparison of protein diffusion velocity with the distances involved in pore penetration substantiates the feasibility of this observation. Loading studies were conducted at both 360 and 3600 cm/h using the protein test mixture. The resulting chromatograms were very similar indicating that, under certain circumstances, separations can be run on conventional particles at velocities 5 to 10 times greater than currently practised. The preparative implications are discussed.

1. Introduction

From its inception, high-performance liquid chromatography has been principally concerned with separation speed. Indeed, one of the earlier designations for the technique was high speed liquid chromatography (HSLC). The driving force behind the quest for speed in analytical liquid chromatography has ostensibly been the need to perform more and more analyses per unit time, especially (but not exclusively) in the pharmaceutical industry. Although speed is also of importance in preparative chromatography, it does not seem to be as significant. Whereas for analysis the objective is to resolve and quantitate all components of a mixture, as quickly as possible (on the analytical scale, the most costly component is time), the goal in preparative chromatography is to isolate the maximum amount of pure material (yield) as economically as possible within a given time constraint. There is a classic interrelationship between load, yield and speed in preparative LC as indicated in Fig. 1.

* Corresponding author.

0021-9673/95/$09.50
SSDI 0021-9673(94)01013-7

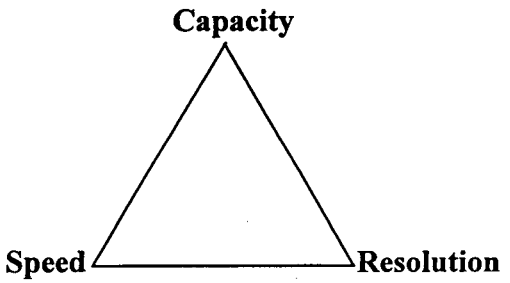

Fig. 1. The Preparative Triangle.

The utility of speed in preparative chromatography cannot be represented by separation time alone, but by the amount of purified material isolated per unit time (production rate) or alternatively, by the cost of producing the desired quantity of product in the required time. If accelerating the process decreases the production costs, then it can be justified. If, however, the acceleration is achieved at the expense of yield, the net value diminishes. This is especially important in the separation of biomolecules which have a potential value in great excess of the other associated purification costs.

In recent years, there have been several publications which discuss the advantages of speed for the preparative chromatography of proteins and peptides [1–5]. Although much of this work involved the use of macro-reticulated packings with bi-modal pore distributions for the ion exchange purification of proteins, results have also been presented for the preparative reversed-phase chromatography of peptides and small proteins [6,7]. These papers implied that the test mixtures chosen could be separated at velocities 5 to 10 times greater than those used conventionally on packings with mono-modal intraparticle pore size distributions.

The application of reversed-phase chromatography for the analysis and isolation of small proteins and peptides has been well established [8–10]. In fact, the technique is so powerful that it is often the only method capable of separating polypeptide chains which differ only in oxidation state or have undergone deamination. In general, silica-based packings with pore diameters of around 150 to 300 Å have been widely used for these separations, with great success. The wide pores are thought to be necessary for the facile access of larger biomolecules, although some data exists [11] which suggest that preparative separations could be carried out on even smaller pore diameter packings to take advantage of the higher surface area. Although there are numerous publications on the conventional use of these silica packings (i.e. at flow velocities of around 300–1000 cm/h), none have investigated the limits of speed.

The work presented here addresses the issue of speed as it applies to the preparative reversed-phase chromatography of small proteins and peptides using a spherical, 300 Å, C18 silica. The 300 Å pore diameter is commonly employed in polypeptide chromatography and silica gels of this type have surface areas which are acceptable for preparative applications [11]. Material of 15 μm particle diameter was chosen, since it offered a good compromise between efficiency and interstitial permeability. A sample mixture consisting of insulin (M_r 6000), ribonuclease A (M_r 13 700), lysozyme (M_r 14 300) and myoglobin (M_r 17 200) was used. These biomolecules have diffusion coefficients in the order of 1×10^{-6} cm^2/s [12] and facile access to the intraparticle surface area [11]. As such, chromatography at higher velocities (>500 cm/h) appeared plausible.

2. Experimental

2.1. Equipment

A Waters Millennium 2010 HPLC system (Waters Associates, Hartford, CT, USA) consisting of two 510 pumps and a photodiode array detector was used. System operation and data acquisition were performed by Millennium software.

2.2. (Bio)chemicals and solvents

Phe-Gly-Phe-Gly, ribonuclease A (bovine), insulin (bovine), lysozyme (egg white) and myoglobin (equine) were obtained from Sigma Chemical Co. (St. Louis, MO, USA). The ace-

tonitrile (ACN) and trifluoroacetic acid (TFA) were HPLC grade and purchased from a local distributor. Bulk Poros 20 R-2 was purchased from Perceptive Biosystems (Cambridge, MA, USA).

2.3. Physical testing

Mercury porosimetry and Malvern particle size analyses (by laser light scattering) were conducted by the analytical services department of the W.R. Grace Washington Research Center (Columbia, MD, USA).

2.4. Chromatography

The C18-300Å-15 μm spherical silica was prepared from Amicon 300 Å, 15 μm spherical silica gel by standard silanization techniques. The C18-250Å-20 μm granular packing was prepared from an Amicon 250 Å, 20 μm irregular silica gel. Approximately 600 mg of each C18 silica were required to fill a 5 × 0.46 cm HPLC column. Columns were packed by a downward slurry protocol using methanol as push solvent. A stock solution of 1 mg/ml each of insulin, ribonuclease A, lysozyme and myoglobin was prepared in 15% acetonitrile, in 0.1% aqueous TFA. Mass loads were varied by changing the injection volume. Mobile phases for the gradients were: Solvent A, 10% acetonitrile in 0.1% aqueous TFA; Solvent B, 70% acetonitrile also in 0.1% aqueous TFA. The instrument was then used to adjust the gradient time and mobile phase acetonitrile composition, accordingly.

3. Results and discussion

3.1. Physical characterization

Several physical analyses were conducted to characterize the C18-300Å-15 μm spherical silica gel. Microscopic examination at 400 × showed that more than 95% of the particles were spherical, based upon manual counting of a 500-particle field. Furthermore, Malvern particle size analysis (by laser light scattering) showed the average particle diameter to be 15 μm with a d_{90}/d_{10} ratio of 2.5. These results, along with other analyses, are listed in Table 1.

Single point BET (nitrogen adsorption) analysis has been used widely for the determination of surface area. This information, in addition to pore volume data, can be used to calculate pore diameter [13]. An alternative method of determining pore diameter is by mercury porosimetry (or Hg intrusion analysis), where mercury is forced around and into the particles under increasingly higher pressure [14]. The resulting (semi-log) pore volume versus pore diameter plot can then be related to the material's interstitial volume (macropores), intraparticle pore volume (micropores) and pore size distribution. It is the preferred technique for the analysis of wider pore particles which are out of the nitrogen sorption measurement range [14].

Fig. 2a illustrates the porosimetry results for the (unbonded) 15 μm spherical silica used in this study. As expected, the average intraparticle diameter was 300 Å with a reasonably tight distribution. The average interstitial space was about 5 μm. These results are typical for a "conventional" (i.e. mono-modal pore distribution) silica-based HPLC packing material. In contrast, Fig. 2b shows the pore distribution for Poros 20 R-2 which is a polymeric, reversed-phase, "perfusive" type particle. Although, in our hands, the bi-modal pore distribution is not evident (as reported in previous literature [1–5]), the mean pore diameter (1800 Å) was substantially larger than that of the silica gel (300 Å).

Table 1
Physical properties of C18-300Å-15 μm spherical silica

Shape	>95% spherical
Nominal particle diameter	15 μm
d_{90}/d_{10}	2.5
Pore volume	0.8 ml/g
Surface area	85 m^2/g
Nominal pore diameter	300 Å
Carbon content	7% (w/w)
Packing density	0.48 g/ml

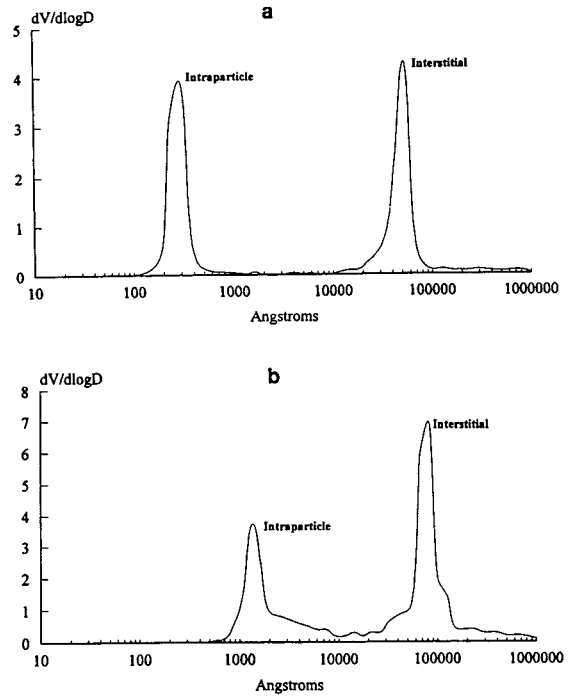

Fig. 2. Mercury porosimetry analyses conducted on the 300 Å-15 μm bare silica (a) and Poros 20 R-2 (b). The data has been plotted in a semi-log format as the change in pore volume/log of the pore diameter (dV/dlog D) vs. pore diameter.

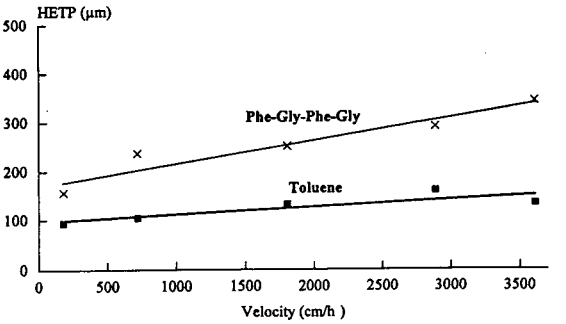

Fig. 3. HETP vs. velocity curves under retained conditions generated for both toluene and Phe-Gly-Phe-Gly on a 5 × 0.46 cm column containing C18-300Å-15 μm. Analytical injections (10 μl of a 1 mg/ml sample) were made at the indicated velocities. HETP's were calculated per the half-height equation. Mobile phases of ACN–H_2O (50:50, v/v) and (18:82, v/v) (both with 0.1% TFA) were used for toluene and Phe-Gly-Phe-Gly, respectively. The capacity factor for both solutes was ca. 2 and detection was by absorbance at 254 or 220 nm.

3.2. Chromatographic characterization

Several 5 × 0.46 cm columns with C18-300Å-15 μm were packed for the study. A representative graph plotting HETP vs. flow velocity for both toluene and the tetrapeptide Phe-Gly-Phe-Gly is shown in Fig. 3. The mobile phases used were 50% aqueous acetonitrile for toluene and 18% acetonitrile in aqueous 0.1% TFA for the peptide. HETP values where measured under retained conditions with a capacity factor of around 2. Although HETP values derived from non-retained solutes have been used to characterize packings for high speed operation [1], the physical meaning of these data has been unclear.

The number of plates in the 5 cm column ranged from 500 to 310 for toluene and from 210 to 150 for the tetrapeptide over the range of linear velocities from 500 to 3600 cm/h. The experimental plots were fitted to the Knox equation using a "B" term of 2 and reasonable values for the diffusion coefficients. The Knox "A" coefficient value was 2.5 indicating that the column was not ideally packed. However, the performance was sufficient for the purposes of this study.

3.3. Influence of velocity on gradient elution

High velocity reversed-phase gradient elution chromatography of proteins was conducted on C18-300Å-15 μm particles achieving separation times under 90 s (see Fig. 4). This separation was performed using a flow rate of 10 ml/min (superficial velocity 3600 cm/h) with a 2-min gradient. Given the current thinking that proteins diffuse too slowly for rapid separations on conventional (or mono-modal) 15 μm particles, the data were somewhat unexpected. One possible hypothesis may reside in the fact that the reversed-phase separation of these four proteins was relatively easy, since the column has only a few hundred theoretical plates. Difficult separations would (by definition) require more plates and therefore would not be amenable to operation at higher

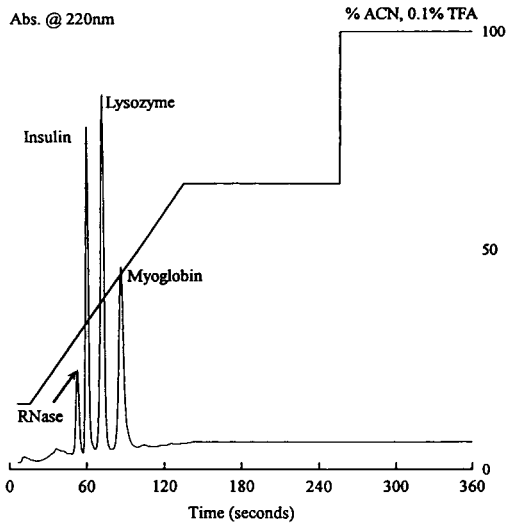

Fig. 4. High velocity reversed-phase chromatography of proteins. The separation was conducted on a 5 × 0.46 cm column of Amicon C18-300Å-15 μm spherical silica. The injection was 20 μl of a 1 mg/ml sample (each) of ribonuclease A, insulin, lysozyme and myoglobin. Proteins were eluted during a 2-min linear gradient at 3600 cm/h (10 ml/min) from 15% ACN to 65% ACN (with 0.1% TFA). Solutes were detected by absorbance at 220 nm.

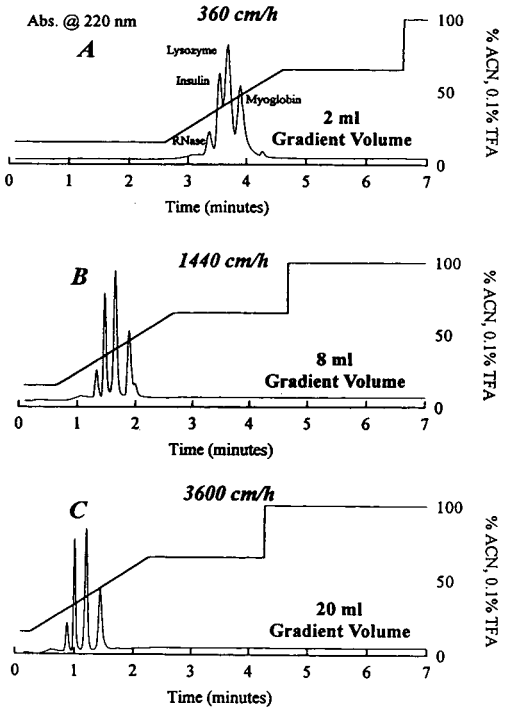

Fig. 5. Influence of velocity on resolution using a C18-300 Å-15 μm spherical silica gel. Chromatograms A–C illustrate the gradient elution profiles of ribonuclease A, insulin, lysozyme and myoglobin, as a function of linear velocity using a 5 × 0.46 cm column containing C18-300Å-15 μm spherical silica. The volumetric flow rates corresponding to 360, 1440 and 3600 cm/h were 1, 4 and 10 ml/min, respectively. A 20-μl injection was made of a solution containing 1 mg/ml of each protein. A 2-min linear gradient from 15% ACN to 65% ACN (with 0.1% TFA) was maintained and the gradient volumes are indicated in each figure. Solutes were detected by absorbance at 220 nm.

mobile phase velocity. Obviously, difficult separations tend to be the norm.

The elution of adjacent protein bands from the C18 surface differed by about 3 to 5% acetonitrile. Desorption appears to be relatively rapid. During the course of gradient elution, the proteins will rapidly desorb when the critical concentration of acetonitrile is achieved. As such, improved resolution can be attained by increasing the mobile phase velocity which concurrently increases the gradient volume (at constant gradient time). In effect, more volume is interjected between the peaks, thus improving the apparent resolution. It should be noted, therefore, that comparisons of gradient experiments in which the gradient volume is *not* held constant are at best misleading. The influence of velocity on the separation of the test proteins during a 2-min gradient is illustrated in Fig. 5. Clearly, resolution was directly related to mobile phase velocity (and gradient volume) rather than to column efficiency. Nearly identical results were seen with a C18-250Å-20 μm granular silica gel packing (160 m^2/g surface area), strongly suggesting that this is a general phenomenon (Fig. 6).

3.4. Frontal uptake of lysozyme

The gradient elution data demonstrated that high velocity analytical reversed-phase protein separations are possible. However, a question that must be addressed is whether the proteins had penetrated the particles, or if the adsorption was pellicular. One accepted experimental ap-

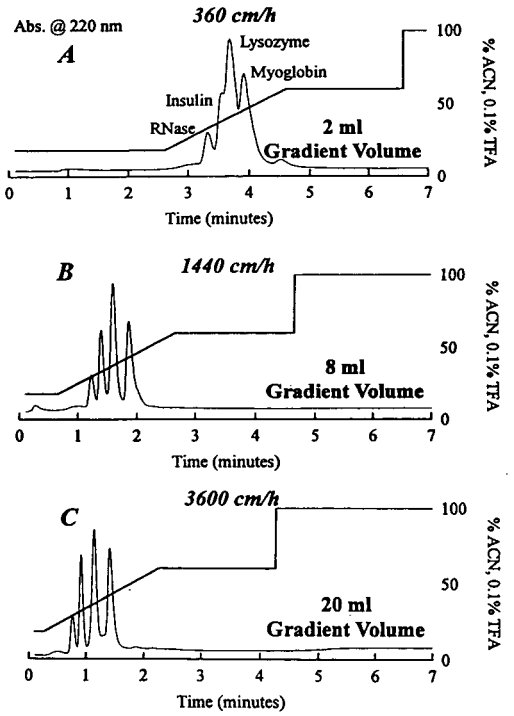

Fig. 6. Influence of velocity on resolution using a C18-250Å-20 μm granular silica gel. Experimental conditions as in Fig. 5.

proach to investigate this issue is frontal adsorption chromatography [15]. During such experiments, solute (lysozyme, 2.5 mg/ml) is pumped through a packed column at various flow rates until it saturates the stationary phase and appears in the column effluent. The column adsorption capacity can then be determined by:

1. Measurement of the mobile phase volume which passed through the column at breakthrough (ca. 10% of feed).
2. Multiplication of this volume by the feed concentration.
3. Division by the column volume.

At slower mobile phase velocities, the solutes have sufficient time to adsorb on the accessible surface area. In experiments at higher velocity, the frontal adsorption capacity would be expected to decrease, if diffusion was limited and the surface area could not be accessed. However, this was not the case for the frontal adsorption of lysozyme on the C18-300Å-15 μm silica (see Fig. 7). The frontal capacities were 25 and 23 mg/ml at 220 and 3600 cm/h, respectively. These data are equivalent given an experimental error of ± 2 mg/ml. In addition, the breakthrough curves at higher velocities remained relatively sharp (further) demonstrating that lysozyme indeed penetrated the pores.

3.5. Diffusion path length, residence time and mean square displacement

Intuitively, one would not expect the frontal adsorption of lysozyme to be so insensitive to flow velocity. Indeed, much of the recent literature on higher speed protein and peptide sepa-

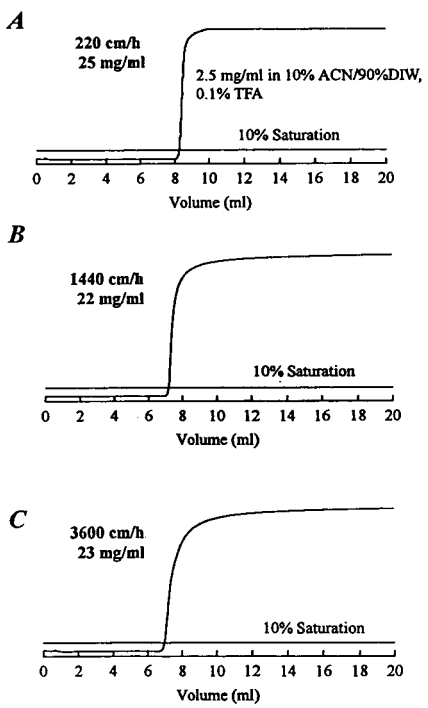

Fig. 7. Lysozyme frontal uptake. Lysozyme frontal uptake curves at 220, 1440 and 3600 cm/h are illustrated in Figs. A–C. Experiments were conducted by pumping a 2.5 mg/ml solution of lysozyme (in 10% ACN with 0.1% TFA) through a 5×0.46 cm column packed with C18-300Å-15 μm. Using 10% of feed absorbance (UV 290 nm) in the effluent as the end-point, adsorption capacities of 25, 22 and 23 mg/ml column volume were determined.

rations has suggested that this was not possible [1–5]. However, Kopaciewicz et al. [15] showed the uptake of α-lactalbumin (M_r 17 500) on 10 and 20 μm anion exchange packings with a 500 Å pore diameter to be velocity insensitive, so this result is perhaps not so surprising.

Although not a rigorous description of the processes involved in the solute mass transfer within a column, comparison of the diffusion path length, solute residence time and mean square displacement is instructive. At the very least, this approach provokes thought toward an explanation of the scientific data. The distance from the center of interstitial space to the center of the 15 μm particle (ignoring pore tortuosity) is in the order of 10.5 μm. Furthermore, an unretained solute spends a certain length of time in the column, given by the product of the column porosity (0.6) and the ratio of the column volume (0.83 ml) to the flow rate (0.165 ml/s). In this case, the solute requires around 3 s (residence time) to traverse a 5 × 0.46 cm column packed with C18-300Å-15 μm spherical silica at a linear velocity of 3600 cm/h. In 1905, Einstein derived an equation which related time (t) to both distance and diffusion coefficient:

$$t = \frac{\langle x^2 \rangle}{2D}$$

where x is the diffusion distance and D is the diffusion coefficient [12]. Solving the equation for time, using 10.5 μm as the path length and the diffusion coefficient for lysozyme of 11.5×10^{-7} cm^2/s, results in a value of 0.49 s. Such an analysis obviously assumes that the intra-particle diffusion coefficient of lysozyme (within the 300 Å pore) is similar to that seen in bulk solution. The assumption is reasonable taking into consideration the relative similarity of the lysozyme frontal uptake curves at 360 to 3600 cm/h (see Fig. 7). Given the residence time in the column of 3 s, this implies that a solute molecule could reach the center of the particle in the same time as it would take to traverse about 1/6th of the column length. At a lower velocity of 1440 cm/h, the protein could reach the center of the particle by the time it traveled 1/15th of the bed length, which in this case is equal to only 3 millimeters down a 50-mm bed. This hypothesis is admittedly an oversimplification. Nevertheless, it does provide an interesting perspective as to why high speed separations are possible on conventional particles. Namely, the diffusion of small proteins (i.e. less than ca. M_r 20 000) and peptides is apparently rapid and relatively unhindered across the dimensions of ca. 300 Å, 15 μm chromatography particles.

3.6. Bandwidth

The distances traveled within the column suggest that the eluted protein bandwidths would be very large. Under the normal solvent elution conditions for reversed-phase protein separations, the typical "small molecule" would have a diffusion coefficient is in the range of 5–10 times larger than that of lysozyme. As such, this implies that the protein elution bands would be broader than that of a small organic compound, but only up to an order of magnitude in comparison. However, the isocratic retention of large molecules tends to change dramatically as a function of solvent composition. During gradient chromatography, biomolecules tend to remain tightly adsorbed to the surface until the critical strong solvent condition is achieved, at which point they are desorbed over a very narrow change in solvent strength. In fact, steep gradients may actually have a band sharpening affect especially at high velocity where desorbed solutes are rapidly swept through the (short) column. Consequently, for such selectivity dominated separations (which require few theoretical plates), elution bandwidth is likely to be more related to gradient shape than the distribution of solute within the column, under non-overload conditions. Obviously, the situation is inverse for those separations which require efficiency.

3.7. Influence of velocity on loadability

As stated in the introduction, the goal of preparative chromatography is to isolate a quantity of pure product. As such, separation speed must not come at the expense of loading.

A packing which can be operated at four times the speed, but has one-fifth the capacity is no bargain. To determine the influence of mobile phase velocity (*at constant gradient volume*) on loadability, increasing mass loads of the protein mixture were eluted using a 20 or 2-min gradient at 360 or 3600 cm/h, respectively (Figs. 8 and 9).

There appeared to be only a minimal difference in the resolution of the major components with velocity, especially at higher mass loads. This is because the thermodynamic band broadening due to overload becomes large compared with the kinetic effects, which are best seen at lower loads. Further inspection of these chromatograms reveals that at high speed the resolution of minor components in the protein

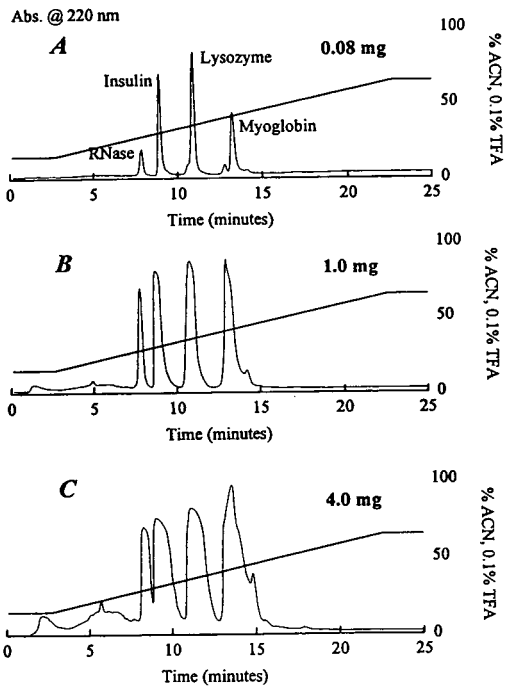

Fig. 8. Resolution vs. load at conventional linear velocity. Chromatograms A–C illustrate the gradient elution profiles of ribonuclease A, insulin, lysozyme and myoglobin at various mass loads. Separations were conducted on a 5 × 0.46 cm column of C18-300Å-15 μm at 360 cm/h (1 ml/min) during a 20-min linear gradient from 15 to 65% ACN containing 0.1% TFA. Total protein loads of 0.08, 1 and 4 mg were chromatographed, as indicated. Solutes were detected by absorbance at 220 nm.

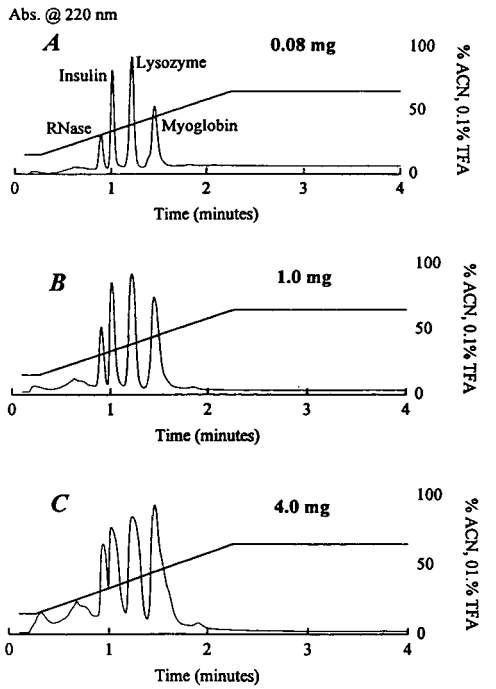

Fig. 9. Resolution vs. load at high linear velocity. Experimental conditions as in Fig. 8, except a velocity of 3600 cm/h (10 ml/min) during 2 minutes.

standards was lost. These data indicate that the ability to increase mobile phase velocity, and thus separation speed is clearly dependent upon separation difficulty. Certainly, for those separations where the adjacent solute bands differ in elution by ca. 3 to 5% acetonitrile, the mobile phase velocity can be increased 5 to 10 fold over "conventional" practice, if the gradient volume is maintained. Increasing the speed for solutes which are less well separated becomes problematic, since such separations are controlled not by the selectivity, but by column efficiency. Under these circumstances, it is necessary to operate at lower flow velocities in order to maximize column efficiency and product yield [10].

3.8. Column pressure analysis

Although smaller particles could be run at high velocity, we chose to investigate materials

of 15 μm. Particles of this size are well established in preparative chromatography as giving an acceptable balance between efficiency and pressure drop. In larger diameter preparative axial compression columns, beds packed with 15 μm spherical silica gels commonly give a reduced plate height of ca. 2.5 which equates to 27 000 plates per meter. In addition, a 15 μm packing will develop a pressure drop just under half that of a 10 μm bead and therefore can be operated at twice the flow rate for a given operating pressure. Since high velocity operation involves increased column pressure drops, it is of value to re-visit the engineering tradeoffs. A more detailed analysis can be found in Ref. [16]. The pressure drop across a packed bed is described by an equation [17] derived from Darcy's law:

$$P = \frac{\phi \eta L u}{d_p^2}$$

where P is the pressure drop, d_p the particle diameter, L the length, u the flow velocity, η the solvent viscosity and ϕ is the resistance parameter (500–600 for spherical particles and 1000 for irregular media). Column pressure is thus linearly related to length and flow rate, and inversely to the square of the particle diameter. Table 2 attempts to provide some perspective regarding the anticipated pressures as a function of length and velocity for spherical monodispersed 15 μm particles. The calculated values should be considered as guidelines.

Short beds have a lower pressure drop at a given flow rate, but also less operational loadability. The longer the bed, the larger the volume and therefore mass load, albeit (for a given velocity and particle diameter) at the expense of pressure and a gain in efficiency. When operated at constant flow velocity, the columns of Table 2 are equivalent in terms of throughput, since both the run time and column load are proportional to length. However, this assumes that they all have the same diameter and the shortest column has a sufficient number of plates to perform the separation. If we consider that the operating pressure is the limiting factor, then it is clear from Table 2 that the 5 cm column can be operated at a flow rate four times that of the 20 cm column. In this case, again provided that the separation can be achieved on the short column, the production rate of the 5 cm column (per unit column volume) is also 4 times that possible using the 20 cm column. Given that real world difficult separations tend to be the norm, this situation is rarely encountered. When working within the practical limits of maximum operating (ca. 1000 psi at large scale), high flow rates can only be achieved with short bed (or larger particles) which concomitantly results in a plate number reduction. Once the efficiency required for the separation is established and the Knox parameters are known, it is relatively easy to calculate for any given maximum operating pressure what is the highest possible flow rate together with the suitable column and particle dimensions. Obviously, this also assumes that the selectivity of the packing material does not appreciable change as a function of particle size. In practice, therefore, the extra production rate possible with short

Table 2
Calculated column pressures for 15 μm spherical particles

Column length (cm)	Column pressure (p.s.i.) at indicated velocity[a]			
	1000 cm/h	2000 cm/h	3000 cm/h	4000 cm/h
5	56	112	168	224
10	112	224	336	448
15	168	336	504	672
20	224	448	672	896

[a] Assuming $\phi = 500$ and $\eta = 1$ (mPa · s).

columns operated at high velocity is often offset by the loss of column efficiency relative to longer columns. For the present purpose, it can be argued that a relatively easy separation can be achieved with high productivity using a column of perhaps 1500 plates which would be 15 to 20 cm in length and packed with 15 μm particles. This column could be run at flow velocities of 1000 to 2000 cm/h (corresponding 330 to 660 ml/min on a 50 mm I.D. column) and would require up to 600 p.s.i. (1 p.s.i. = 6894.76 Pa) depending on the system (extra-column) pressure.

3.9. Other considerations

It is not the intent of this paper to suggest that every reversed-phase protein and peptide separation currently conducted on conventional media should be accelerated. However, the results do indicate that speed should be one of the variables considered in the optimization of preparative separation processes. In reality, there are other operational issues which also require consideration when optimizing separation speed. For example, during a 2-min gradient separation carried out at 3600 cm/h, the band widths may be as small as 18 s. At best, this may complicate accurate fraction collection. An additional factor is that of temperature effects within the columns [18]. As flow rates are increased, the operating pressure also increases and the effects of solvent frictional heating become appreciable. At very high velocities, radial temperature gradients can be established which may distort peak shape. This would have a negative impact upon the purity–recovery relationship. In practice, the separations are probably better operated at more modest velocities. Subsequently, our example above may be more realistically run at 1440 cm/h with a 5-min gradient. Under these conditions, the typical peak width would be approximately 45 s, frictional heat is of little concern and the productivity is still enhanced by a factor of four over "conventional" operation at ca. 360 cm/h.

4. Conclusions

The results clearly demonstrate that high velocity protein and peptide chromatography can be conducted on a conventional C18-300Å-15 μm packing. The separation of ribonuclease A, insulin, lysozyme and myoglobin was achieved in 90 s at a mobile velocity of 3600 cm/h during a two-min linear gradient. However, the ability to conduct such a high speed separation resulted more from the high inherent chromatographic selectivity observed for this separation, rather than any unique physical property of the matrix. Since the elution of adjacent protein bands differed by about 3 to 5% acetonitrile, the separation was selectivity controlled and few theoretical plates are required. This allows mobile phase velocity to have a positive influence on resolution as more eluent can be interposed between eluting peaks.

The frontal uptake capacity of lysozyme on a 5×0.46 cm column was constant within experimental error at linear velocities ranging from 220 to 3600 cm/h. These data demonstrate that the adsorption of small proteins into packings with pores in the order of 300 Å was velocity insensitive. Comparison of the diffusion coefficients with particle geometry suggested that the diffusion of a small protein such as lysozyme is reasonably rapid and unhindered across the dimensions of a ca. 300 Å, 15 μm HPLC particle.

Loading studies using the four proteins gave similar results at both 360 and 3600 cm/h. For the separation of major components, this represents a 10-fold increase in column throughput. However, the resolution of minor components, which represented a more difficult separation (requiring more theoretical plates), was compromised.

In situations where selectivity dominates and the separation can be justifiably accelerated, 15 μm particles offer a favorable balance between efficiency and pressure of operation. A 20 cm bed of 15 μm spherical particles has a (calculated) pressure drop of ca. 450 p.s.i., when run at 2000 cm/h with a mixture of acetonitrile and

water. This value is well within the limits of preparative HPLC systems.

With the current emphasis in high speed separations being placed upon new particle configurations, it is important to be familiar with the performance available from what might be considered conventional particles (mono-modal pore distribution). Certainly, it is clear that under certain conditions the "conventional" reversed-phase chromatography of small proteins and peptides can be substantially accelerated, thus increasing throughput without incurring losses in resolution and loadability. Therefore, speed should be exploited when appropriate. Nevertheless, our conclusions are somewhat circular in that they return to one of the most quintessential paradigms of chromatography, i.e., whereas easy separations can be run fast, difficult ones must walk . . .

Acknowledgments

We wish to thank James Neville (Amicon R&D) and Edward Pfannkoch (W.R. Grace, Washington Research Center) for their technical assistance. We also acknowledge the help of Nick Triano (W.R. Grace Patent Office) for his legal opinion on this manuscript.

References

[1] N.B. Afeyan, N.F. Gordon, I. Mazsaroff, L. Varady, S.P. Fulton, Y.B. Yang and F.E. Regnier, *J. Chromatogr.*, 519 (1990) 1.
[2] N.B. Afeyan, S.P. Fulton, N.F. Gordon, I. Mazsaroff, L. Varady and F.E. Regnier, *Bio/Technology*, 8 (1990) 203.
[3] S.P. Fulton, N.B. Afeyan, N.F. Gordon and F.E. Regnier, *J. Chromatogr.*, 547 (1991) 452.
[4] N.B. Afeyan, S.P. Fulton and F.E. Regnier, *LC-GC*, 9 (1991) 824.
[5] S.P. Fulton, A.J. Shahidi, N.F. Gordon and N.B. Afeyan, *Bio/Technology*, 10 (1992) 635.
[6] S.P. Fulton, M. Meys, J. Protentis, N.B. Afeyan, J. Carlton and J. Haycock, *BioTechniques*, 12 (1992) 742.
[7] D.E. Lehman, J.G. Joyce, D.K. Freymeyer, J.F. Bailey, W.K. Herber and W.J. Miller, *Bio/Technology*, 11 (1993) 207.
[8] M.T.W. Hearn, *Methods Enzymol.*, 104 (1984) 190.
[9] R.W.A. Oliver (Editor), *HPLC of Macromolecules: A Practical Approach*, IRL Press, NY, 1989, p. 127.
[10] E.P. Kroeff, R.A. Owens, E.L. Cambel, R.D. Johnson and H.I. Marks, *J. Chromatogr.*, 461 (1989) 45.
[11] G.B. Cox, L.R. Snyder and J.W. Dolan, *J. Chromatogr.*, 484 (1989) 409.
[12] I. Tinoco, K. Sauer and J. Wang, *Physical Chemistry: Principles ands Applications in Biological Sciences*, Prentice-Hall, NJ, 1978, p. 210.
[13] A. Berthod, *J. Chromatogr.*, 549 (1991) 1.
[14] H.E. Bergna (Editor), *The Colloid Chemistry of Silica*, Maple Press, PA, 1994, p. 341.
[15] W. Kopaciewicz, S.P. Fulton and S.Y. Lee, *J. Chromatogr.*, 409 (1987) 111.
[16] L.R. Synder and G.B. Cox, *J. Chromatogr.*, 483 (1989) 85.
[17] V.R. Meyer, *J. Chromatogr.*, 334 (1985) 197.
[18] B. Porsch, *J. Chromatogr.*, 658 (1994) 179.

ELSEVIER

Journal of Chromatography A, 690 (1995) 21–28

JOURNAL OF CHROMATOGRAPHY A

Uniform-size hydrophobic polymer-based separation media selectively modified with a hydrophilic external polymeric layer

Ken Hosoya[a,*], Yutaka Kishii[a], Kazuhiro Kimata[a], Takeo Araki[a], Nobuo Tanaka[a], Frantisek Svec[b], Jean M.J. Fréchet[b]

[a]*Department of Polymer Science, Kyoto Institute of Technology, Matsugasaki, Sakyo-ku, Kyoto 606, Japan*
[b]*Department of Chemistry, Cornell University, Baker Laboratory, Ithaca, NY 14853-1301, USA*

First received 18 March 1994; revised manuscript received 13 September 1994

Abstract

A simple procedure for the preparation of macroporous hydrophobic styrene–divinylbenzene polymeric separation media with a hydrophilic outer surface has been developed. A hydrophilic monomer and water-soluble polymerization initiator are added to the reaction mixture during the final polymerization step of the preparation of size-monodisperse particles. Because the hydrophobic styrene–divinylbenzene framework of the beads is already formed, and the hydrophilic monomer does not penetrate the pores of the beads that are filled with a hydrophobic porogen, the hydrophilic layer is formed only at the surface of the beads. The hydrophilic monomers used included glycerol monomethacrylate and glycerol dimethacrylate and toluene was used as the porogen for the poly(styrene–co-divinylbenzene) beads. Comparative experiments involving beads with or without a hydrophilic medium showed that the separation selectivity of the media towards hydrophobic solutes remains unchanged. However, the modified medium with a hydrophilic layer could be used to analyse mixtures that also contained large peptide molecules as these do not adsorb at its surface as is the case with the unmodified hydrophobic beads.

1. Introduction

The control of surface chemistry is an important challenge in the design of porous materials. In the field of liquid chromatography, where polymers and C_{18} silica are used most frequently for size-exclusion and reversed-phase chromatography, respectively, difficulties are frequently encountered with analytical samples that contain proteins or other biopolymers. This is because these biopolymers are frequently absorbed irreversibly at the surface of the medium, causing the rapid clogging of its pores and a general deterioration of the separation properties of the column. The C_{18} hydrophobic materials are not wettable with water, which precludes their use in open-column liquid chromatography. Therefore, a modification method has been developed that renders the outer surface of hydrophobic silica beads water-wettable [1]. The C_{18} chains are removed from the external surface by acid hydrolysis and glycol groups are attached to the plain silica. This material can be used for both open-column liquid chromatography using an aqueous mobile phase and for the direct-injection chromatography of complex samples [2]. A drawback of this approach is that the surface modification method is not completely site-selec-

* Corresponding author.

0021-9673/95/$09.50
SSDI 0021-9673(94)00899-X

tive and the hydrophobicity of the internal surface is also impaired.

Polymer-based separation media such as poly(styrene–co-divinylbenzene) are stable over the entire pH range and exhibit an enhanced selectivity towards some classes of compounds, such as halogenated hydrocarbons and aromatic compounds, which is advantageous for monitoring these pollutants in the environment [3]. Unfortunately, the poly(styrene–co-divinylbenzene) media shrink in mobile phases that are rich in water and the column efficiency is therefore deteriorated. The shrinkage can be reduced through the introduction of a more hydrophilic monomer into the beads but the hydrophilic groups also decrease the required hydrophobicity. Moreover, the addition of the new monomer changes the composition of the polymerization system and affects the porous properties of the resulting beads [4].

This paper presents a new concept that allows the preparation of hydrophobic macroporous media that have a very hydrophilic external surface. The usefulness of the process is demonstrated in the preparation of novel polymeric stationary phases specifically designed for direct injection assays.

2. Experimental

2.1. Materials

Styrene, divinylbenzene (55% of divinyl monomer), methyl methacrylate and ethylene dimethacrylate were purchased from Nacalai Tesque (Kyoto, Japan). Glycerol monomethacrylate (**I**) and glycerol dimethacrylate (**II**) (Fig. 1) were gifts from Fuso Chemical (Osaka, Japan). All other reagents were purchased from Nacalai Tesque and used as received.

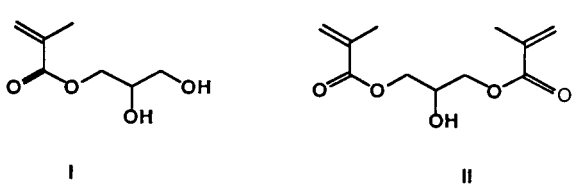

I II

Fig. 1. Structures of glycerol monomethacrylate (**I**) and glycerol dimethacrylate (**II**).

2.2. Preparation of monodisperse beads

Uniform-size polystyrene-shape templates were prepared and purified by the previously reported method [5]. The diameter of the particles was ca. 1 μm.

The preparation of uniformly sized hydrophobic beads with a hydrophilic surface was carried out using a multi-step swelling and polymerization method. A 1.4-ml volume of a water dispersion of the uniformly sized polystyrene seed particles ($9.5 \cdot 10^{-2}$ g/ml) was admixed with a microemulsion prepared by sonication of 0.95 ml of dibutyl phthalate used as the activating solvent for the swelling procedure, 0.085 g of benzoyl peroxide, 0.04 g of sodium dodecyl sulfate and 10 ml of distilled water. This first swelling step was carried out at room temperature while stirring at 125 rpm. Completion of the first swelling step was determined by optical microscopy. A dispersion of 5 ml of the hydrophobic monomer (e.g., styrene or methyl methacrylate), 5 ml of cross-linking agent (e.g., divinylbenzene or ethylene dimethacrylate) and 10 ml of toluene used as porogenic solvent was prepared in 90 ml of water containing 1.92 g of poly(vinyl alcohol) ($d_p = 500$, saponification value = 86.5–89 mol-%) used as the dispersion stabilizer. This dispersion was added to the dispersion of swollen seed particles and the second swelling step was carried out at room temperature for 2–24 h while stirring at 125 rpm. After this second swelling was complete, polymerization was started at 80°C under an argon atmosphere with slow stirring. After 4 h of polymerization, the hydrophilic monomers, with or without potassium peroxodisulfate, were added to the polymerizing beads. After a further 20 h of stirring at the same temperature, the dispersion of polymerized particles was poured into 250 ml of a hot water–methanol mixture and the supernatant was discarded after sedimentation of the particles. The polymer particles were redispersed into methanol and the supernatant was again discarded after sedimentation. This

procedure was repeated three times in methanol and twice in tetrahydrofuran (THF). The resulting 5–6-μm polymer particles were collected using a membrane filter, washed with THF and then with acetone and finally dried at room temperature.

The same polymerization procedure, omitting the addition of the hydrophilic monomers, was used for the preparation of porous poly(styrene–co-divinylbenzene) beads that served as a blank for comparison with the modified beads in the chromatographic experiments. The yield calculated from the amount of monomers used was ca. 85–100%.

2.3. Determination of monomer and polymer distribution between phases

Glycerol monomethacrylate, glycerol dimethacrylate or poly(glycerol monomethacrylate) was added to water–toluene (10:1, v/v) and stirred for 12 h at room temperature. The mixture was allowed to separate into aqueous and organic phases, an aliquot from each phase was taken, water or toluene was evaporated and the amount of the remaining component was determined.

2.4. Chromatography

The porous beads were slurry packed into stainless-steel columns (150 mm × 4.6 mm I.D.) using aqueous acetonitrile or aqueous methanol as the dispersion liquid.

High-performance liquid chromatography was performed with a Jasco Model 880-PU intelligent pump or a Shimadzu, LC-4A ternary gradient pump equipped with a Rheodyne Model 7125 valve loop injector. Peak monitoring was carried out with a Jasco, Uvidec-100-III or a Shimadzu SPD-2A UV detector set at 254 or 280 nm and a Waters RI 401 differential refractometer. Peaks were recorded with a Shimadzu C-R4A Chromatopak. Recoveries of proteins were determined from their peak areas, taking the peak areas in the absence of a column as 100%.

3. Results and discussion

3.1. The concept of site-selective modification

Monodisperse macroporous particles are prepared by the swelling of "activated" shape templates with emulsified mixtures of monomers and porogenic diluents followed by polymerization. The properties of these beads are largely controlled by the properties of the monomers that are used. The traditional technique used for the preparation of monodispersed beads does not allow the modification of specific areas of the beads during their polymerization, which proceeds unabated until all the monomers are consumed. Therefore, the resulting beads are chemically homogeneous. However, we have discovered [6,7] that if another monomer is added to the polymerizing mixture once the structural framework of the beads has already been established, this monomer will not be incorporated into the bulk of the beads but will only form a layer of polymer in those areas where of the beads where it can diffuse. Typically, this would only be the external surface and the surface of the pores within the porous matrix. In addition, both size-exclusion and solubility effects can be used to localize further the site of functionalization. For example, if the aqueous phase contains a water-soluble free-radical initiator, any water-soluble monomer added to the warm aqueous suspension would start polymerizing immediately. Because the resulting polymer molecules cannot penetrate into the pores that are filled with a hydrophobic porogen, they would simply attach themselves to the outer surface of the beads. This very simple procedure allows the preparation of a macroporous medium in which each individual bead exhibits a sharp gradient of very different surface and interior chemistries.

3.2. Hydrophilization of porous poly(styrene–co-divinylbenzene) beads

A study of the preparation of porous polymer beads from styrene and divinylbenzene under conditions similar to those used in this work has

shown that nearly quantitative conversion of the monomers is achieved after 4–5 h of polymerization at 80°C [4]. Therefore, when the hydrophilic monomers are added 4 h after the start of the polymerization, the framework of the hydrophobic poly(styrene–co-divinylbenzene) beads is already well established, and phase separation between the cross-linked polymer and the porogenic solvent filling its pores has been achieved [3]. Because the hydrophilic monomer is added directly to the polymerization medium, it is expected to partition between the water phase and the porogenic solvent according to its partition coefficient.

To determine the distribution of glycerol monomethacrylate, glycerol dimethacrylate and poly(glycerol monomethacrylate) between toluene and water, separate experiments were carried out using a mixture of water and toluene in the ratio typically used for a standard polymerization mixture. The results obtained are summarized in Table 1. These experiments demonstrate that glycerol monomethacrylate, and also its polymer, partition preferentially into the aqueous phase, in contrast to glycerol dimethacrylate, which is found exclusively in the toluene phase. In practical terms, this means that both glycerol monomethacrylate and its polymer would remain in the aqueous polymerization medium but would not penetrate the pores of the poly(styrene–co-divinylbenzene) beads that are filled with toluene porogen. Therefore, if each monomer is added separately, glycerol dimethacrylate can be used to modify the internal surface of the pores, while glycerol monomethacrylate would only polymerize outside the beads to modify their external surface.

If the added monomer is able to partition into the toluene phase, its polymerization should lead to a decrease in the pore volume for the modified particles when compared with the pore volume of the unmodified particles. Table 2 shows the pore volumes of the particles prepared under a variety of modification conditions. As expected from its partitioning between the aqueous and toluene phases, the addition of 2 ml of glycerol dimethacrylate caused a 23% decrease in pore volume when compared with the unmodified base particles. This correlates well with the fact that the volume of added glycerol dimethacrylate represents 20% (w/w) of the toluene that was initially added to the polymerization mixture and therefore then eventually became localized in the pores.

On the other hand, the addition of glycerol monomethacrylate does not affect the pore volume despite the fact that it is incorporated completely on to the beads, as verified by elemental analysis. As seen from a comparison of scanning electron micrographs of the beads shown in Fig. 2a and b, the added glycerol monomethacrylate does not affect the size uniformity of the base particles, but it does change their external appearance (Fig. 2b), suggesting again that the attachment of poly(glycerol monomethacrylate) occurs mainly on the external surface of the poly(styrene–co-divinylbenzene) particles. These findings correlate well with the results of the partition experiments reported in Table 1.

Table 1
Partitioning of additives between toluene and water

Additive	Concentration (%, w/w) in	
	Toluene	Water
Glycerol monomethacrylate	2	98
Glycerol dimethacrylate	100	0
Poly(glycerol monomethacrylate)	8	92

The ratio of toluene to water (1:10) was selected to match that of the actual polymerization mixture.

Table 2
Pore volumes of particles modified with hydrophilic monomers

Added monomer	Volume[a] (ml)	Initiator[b] (%, w/w)	Pore volume[c] (ml/g)
None[d]	–	None	0.94
GMMA[e]	1	None	0.90
GDMA[f]	2	None	0.72
GMMA + GDMA	1 + 1	None	0.78
GMMA + GDMA	1 + 1	1	0.92

[a] Volume of monomer added to the mixture during polymerization.
[b] Potassium peroxodisulfate. The percentage is given relative to the added monomers.
[c] Determined by size-exclusions chromatography.
[d] Poly(styrene–co-divinylbenzene) beads prepared without addition of hydrophilic monomers.
[e] Glycerol monomethacrylate.
[f] Glycerol dimethacrylate.

Also, the addition of both glycerol monomethacrylate and glycerol dimethacrylate in the absence of a water-soluble initiator results in a 16 vol.-% decrease in the pore volume. In contrast, when both glycerol monomethacrylate and glycerol dimethacrylate are added together with a water-soluble initiator such as potassium peroxodisulfate, the resulting beads undergo no change in pore volume. They again maintain their size uniformity but their appearance (Fig. 2c) is similar to those of the glycerol monomethacrylate-modified beads (Fig. 2b). This finding suggests that the radical polymerization initiated by the water-soluble initiator proceeds mainly in the aqueous phase and the cross-linked copolymer is attached only at the surface of the poly(styrene–co-divinylbenzene) beads.

3.3. Chromatographic properties of the prepared particles

While the above findings suggest that glycerol monomethacrylate can modify only the external surface of the poly(styrene–co-divinylbenzene) particles owing to its insolubility in toluene, a column packed with these modified particles is not useful. The back-pressure increases dramatically when a mobile phase rich in water is used. This is most likely due to swelling of the water-soluble poly(glycerol monomethacrylate) attached to the bead surface. The column also provides very poor efficiency.

In contrast, the modification with glycerol dimethacrylate affords particles that provide both high efficiencies and reasonable back-pressures even when water is used as the mobile phase. A previous study [8] indicated that poly(glycerol dimethacrylate) particles are hydrophilic enough to prevent the occurrence of protein absorption. If glycerol dimethacrylate is used for the modification during the preparation of porous poly(styrene–co-divinylbenzene) beads, it dissolves in the toluene that has became localized in the pores, it then polymerizes and thus decreases the pore volume while making the pore surface hydrophilic. This is not advantageous for the preparation of separation media for direct-injection HPLC because these require that the internal surface be highly hydrophobic [9–12]. However, this approach can be used for the preparation of porous beads with completely hydrophilized internal surfaces that can find an application in other modes of HPLC such as aqueous size-exclusion chromatography.

Even if glycerol monomethacrylate is added together with glycerol dimethacrylate but in the absence of a water-soluble free radical initiator, the pore volume of the poly(styrene–co-divinylbenzene) particles is decreased, which implies that modification of the internal surface of

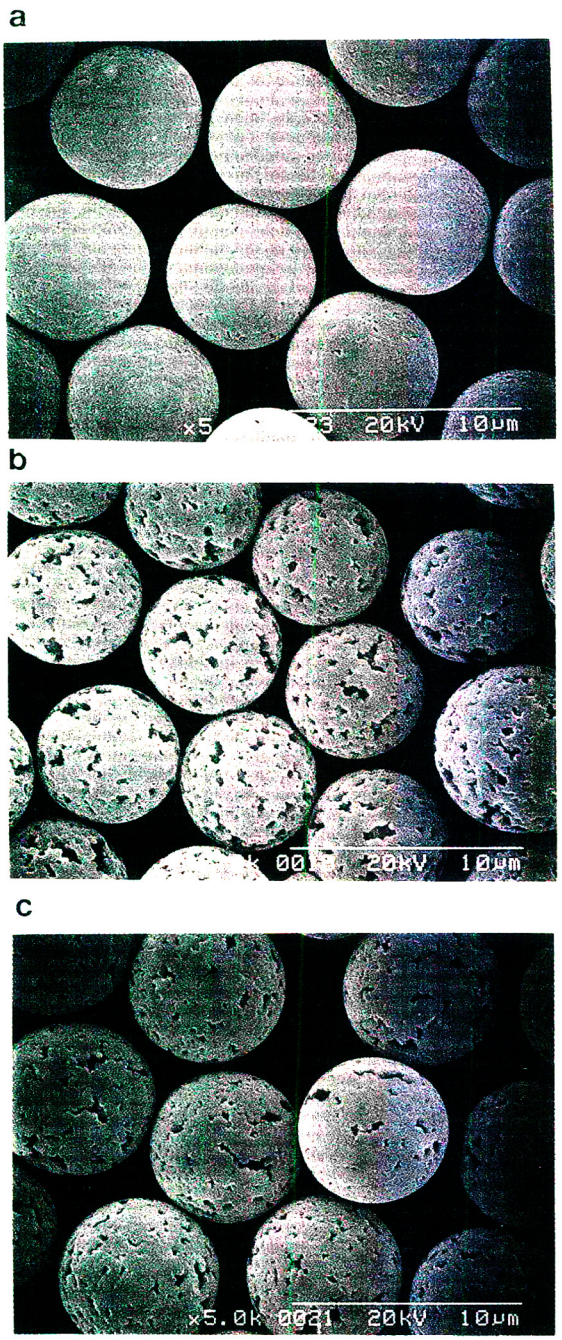

Fig. 2. Scanning electron micrographs of the particles. (a) Unmodified poly(styrene–co-divinylbenzene) beads; (b) beads modified with glycerol monomethacrylate in absence of water soluble initiator; (c) beads modified with a mixture of glycerol monomethacrylate and glycerol dimethacrylate in the presence of potassium peroxodisulfate.

the beads is also carried out and the hydrophobicity of the internal surface is decreased.

Therefore, on the basis of these results, we selected a modification method in which both glycerol monomethacrylate and glycerol dimethacrylate were copolymerized in presence of a water-soluble radical initiator. Fig. 3 shows a comparison of the separation selectivity towards hydrophobic small molecules in water–acetonitrile (80:20) for the particles modified as indicated above and the unmodified poly(styrene–co-divinylbenzene) particles. Despite the quantitative introduction of significant amounts of added monomers, the retention selectivity and hydrophobicity of the modified particles are found to be identical with those of the base particles. This observation further supports our contention that the modification occurs only at the outer surface of the beads, as only such a modification would have no effect on the re-

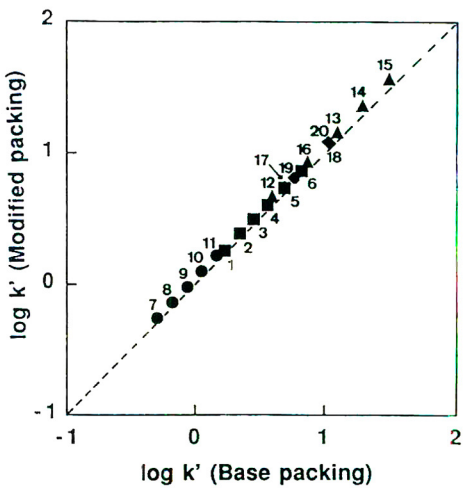

Fig. 3. Separation selectivity of unmodified poly(styrene–co-divinylbenzene) beads and the same beads modified with glycerol monomethacrylate and glycerol dimethacrylate in the presence of potassium peroxodisulfate. Chromatographic conditions: column, 150 mm × 4.6 mm I.D.; mobile phase, acetonitrile–water (20:80); flow-rate, 1 ml/min. Solutes: 1 = benzene; 2 = toluene; 3 = ethylbenzene; 4 = propylbenzene; 5 = butylbenzene; 6 = amylbenzene; 7 = hexanol; 8 = heptanol; 9 = octanol; 10 = nonanol; 11 = dodecanol; 12 = naphthalene; 13 = anthracene; 14 = pyrene; 15 = triphenylene; 16 = fluorene; 17 = diphenylmethane; 18 = triphenylmethane; 19 = triptycene; 20 = *o*-terphenyl.

tention selectivity of the small hydrophobic solutes.

The usefulness of the modification process is clearly demonstrated in separations involving mixtures in a water-rich mobile phase. For example, the separation of a mixture of two drugs and bovine serum albumin (BSA) was attempted with bone the modified particles and the base particles (Fig. 4). With the unmodified particles, albumin is not eluted before the void volume of the column owing to its absorption on the hydrophobic surface of the particles. In addition, and despite their different hydrophobic properties, the two drugs are eluted nearly at the void volume of the column with no separation at all, demonstrating the inability of the stationary phase to work effectively in this mobile phase (Fig. 4a). Actually, the packed bed consisting of the unmodified base particles was found to shrink by about 10% in the column. On the other hand, the modified particles afford complete recovery of BSA before the void volume of the column and the two drugs are well separated according to their respective hydrophobicities (Fig. 4b). The complete recovery of BSA suggests that the external surface of the modified particle is hydrophilic enough to prevent the troublesome absorption of the protein.

This surface-selective modification procedure can also be applied to other hydrophobic base particles. For example, we have used this method for the modification of poly(methyl methacrylate–co-ethylene dimethacrylate) particles with glycerol monomethacrylate and glycerol dimethacrylate in the presence of potassium peroxodisulfate initiator. The modified methacrylate particles were tested in the actual analysis of drugs in human serum as shown in Fig. 5. Once again, the surface-modified particles allow the complete recovery of the proteins near the void volume of the column while the hydrophilic

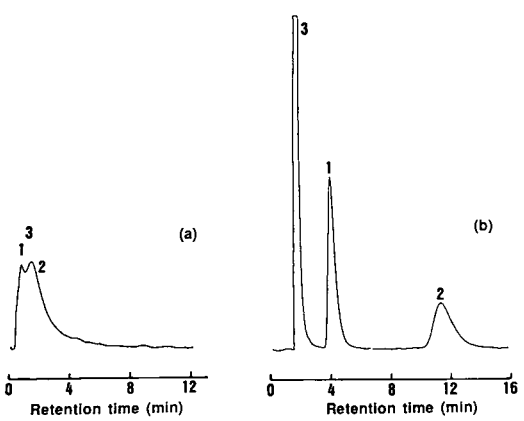

Fig. 4. Separation of drugs in the presence of BSA in a column packed with (a) unmodified poly(styrene–co-divinylbenzene) beads and (b) the same beads modified with a mixture of glycerol monomethacrylate and glycerol dimethacrylate in presence of potassium peroxodisulfate. Chromatographic conditions: column, 150 mm × 4.6 mm I.D.; mobile phase, acetonitrile–0.02 mol/l phosphate buffer containing 0.1 mol/l sodium sulfate (pH 7) (10:90); flow-rate, 1 ml/min. Solutes: 1 = theophylline (1 mg/ml, 0.3 μl); 2 = barbital (1 mg/ml, 5 μl); 3 = BSA (20 mg/ml, 5 μl).

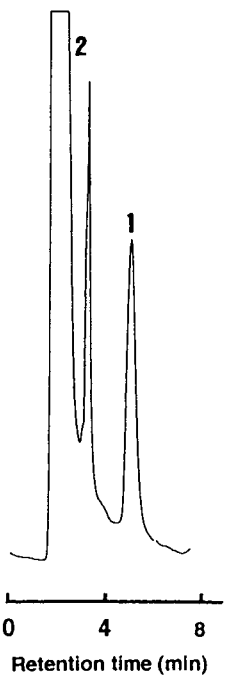

Fig. 5. Direct injection separation of a spiked human serum sample. Chromatographic conditions: column, 150 mm × 4.6 mm I.D.; packing, poly(methyl methacrylate–CO-ethylene dimethacrylate) beads modified with a mixture of glycerol monomethacrylate and glycerol dimethacrylate in the presence of potassium peroxodisulfate; mobile phase, acetonitrile–0.02 mol/l phosphate buffer containing 0.1 mol/l sodium sulfate (pH 7) (30:70); flow-rate, 1 ml/min. Solutes: 1 = theophylline (1 mg/ml, 1 μl); 2 = human serum (20 μl).

drug theophylline is retained by the columns and can therefore be detected. In contrast, this separation proved impossible with unmodified poly(methyl methacrylate–co-ethylene dimethacrylate) particles.

4. Conclusion

Simple concepts involving sequential polymerizations and the partitioning of monomers between immiscible aqueous and organic phases can be used to prepare surface-modified macroporous media. The surface modification with glycerol monomethacrylate of hydrophobic macroporous particles prepared with toluene as a porogen was found to occur selectively on the external surface of the base particles, in accordance with the preferred partitioning of the monomer into the water phase. However, because the separation performance of the modified particles was hampered as a result of the swelling of their surface layer in the water–rich mobile phase, an alternative modification was preferred. In this process, incorporation of both glycerol monomethacrylate and glycerol dimethacrylate was achieved in the presence of a water-soluble initiator to afford dimensionally stable modified particles. As the modification was restricted to the surface layer, the original separation selectivity and hydrophobicity of the base particles toward hydrophobic small solutes was preserved, while the presence of a hydrophilic external surface prevented the absorption of proteins. These characteristics make the surface modification process extremely useful in the design of separation media that can be used for the direct determination of drugs in blood serum.

Another advantage of this surface modification process is that it can be used to provide wettability to a polymeric sorbent without loss of its original retention properties. Because it is well known [3,13] that polymer-based separation media are better suited for the preferential retention of organohalides and also aromatic hydrocarbons than silica-based hydrophobic stationary phases such as C_{18}, new applications of the surface-modified porous polymers are possible. For example, it is expected that our surface-modified media will be very effective for the solid-phase extraction of aqueous environmental pollutants such as halogenated hydrocarbons or toxic dioxins. This is because water wettability of the absorbent is very important in order to obtain reproducible results. Further improvements and tests of our modified macroporous media in these applications are in progress.

Acknowledgement

Financial support of this research by the National Institutes of Health (GM 44885-05) is gratefully acknowledged.

References

[1] K. Kimata, R. Tsuboi, K. Hosoya, N. Tanaka and T. Araki, *J. Chromatogr.*, 515 (1990) 73.
[2] K. Kimata, K. Hosoya, N. Tanaka, T. Araki and J. Haginaka, *J. Chromatogr.*, 558 (1991) 19.
[3] K. Hosoya, E. Sawada, K. Kimata, T. Araki and N. Tanaka, *J. Chromatogr. A*, 662 (1994) 37.
[4] A. Guyot, in D.C. Sherrington and P. Hodge (Editors), *Syntheses and Separations Using Functional Polymers*, Wiley, New York, 1988, p. 1.
[5] V. Smigol, F. Svec, K. Hosoya, Q.C. Wang and J.M.J. Fréchet, *Angew. Makromol. Chem.*, 195 (1992) 151.
[6] K. Hosoya, E. Sawada, K. Kimata, T. Araki, N. Tanaka and J.M.J. Fréchet, *Macromolecules*, 27 (1994) 3973.
[7] J.M.J. Fréchet and K. Hosoya, *US Pat.*, 5, 306 and 561 (1994).
[8] K. Hosoya, Y. Kishii, N. Tanaka, K. Kimata, T. Araki and H. Kiniwa, *Chem. Lett.*, (1993) 745.
[9] H.I. Hagestam and T.C. Pinkerton, *Anal. Chem.*, 57 (1985) 1757.
[10] T.C. Pinkerton, *J. Chromatogr.*, 544 (1991) 13.
[11] J. Haginaka, *Trends Anal. Chem.*, 10 (1991) 17.
[12] D.J. Anderson, *Anal. Chem.*, 65 (1993) 434R.
[13] N. Tanaka, T. Ebata, K. Hashizume, K. Hosoya and M. Araki, *J. Chromatogr.*, 475 (1989) 195.

ELSEVIER

Journal of Chromatography A, 690 (1995) 29–39

JOURNAL OF CHROMATOGRAPHY A

Origin of peak asymmetry and the effect of temperature on solute retention in enantiomer separations on imprinted chiral stationary phases

Börje Sellergren[a,*], Kenneth J. Shea[b]

[a]*Department of Inorganic and Analytical Chemistry, Johannes Gutenberg University Mainz, Joh.-Joachim-Becherweg 24, D-55099 Mainz, Germany*

[b]*Department of Chemistry, University of California, Irvine, CA 92717, USA*

First received 5 April 1994; revised manuscript received 17 August 1994

Abstract

In enantiomer separations of D- and L-phenylalanine anilide (D,L-PA) on L-PA-imprinted chiral stationary phases (CSPs), the use of an aqueous buffer–organic solvent mixture as mobile phase resulted in improved column efficiency compared with what has previously been observed using mobile phases containing acetic acid as modifier. The dependence of the chromatographic parameters on flow-rate and sample load was studied. A strong dependence of the asymmetry factor (A_s) of the L-form on sample load and a weak dependence on flow-rate indicate that the non-linear adsorption isotherm is the main reason for the broad peaks observed in this system. Depending on the method used for the preparation of the materials, different shapes of the plots of retention and selectivity versus sample load were obtained, indicating differences in the site distribution between the polymers. A slow mass transfer was still present but this was in agreement with results from other ion-exchange separations or separations using large porous particles. The band widths of both enantiomers showed a similar dependence on flow-rate and temperature, which is in contrast to earlier reports on imprinted polymers using reversible covalent bonding in the chromatographic separation. As expected from these results, the separation factor (α) and the capacity factor (k') showed no or only a weak dependence on flow-rate. In a study of the effect of temperature on retention and selectivity, linear Van 't Hoff plots were obtained giving ΔH and $\Delta S'$ values (binding of D- or L-PA, absolute values for the D-form and apparent values for the L-form) and $\Delta\Delta H_{app}$ and $\Delta\Delta S_{app}$ values (differential binding of D,L-PA) that showed an exothermic process. Changing the mobile phase pH from 7 to 4 resulted in an increase, mainly in $\Delta S'$ and $\Delta\Delta S_{app}$. Using an acetic acid-containing mobile phase mixture, an endothermic process was observed with positive ΔH, ΔS, $\Delta\Delta H_{app}$ and $\Delta\Delta S_{app}$ values. The results were interpreted in terms of extensive solvation of the solute ammonium groups, the effect being most pronounced in the acetic acid-containing mobile phase.

* Corresponding author.

0021-9673/95/$09.50
SSDI 0021-9673(94)00905-8

1. Introduction

When a solute band passes a chromatographic column it is continuously broadened owing to various dispersion processes [1,2]. These include processes that show little or no flow-rate dependence, such as eddy diffusion or extra-column effects, and flow-rate-dependent processes such as axial diffusion, mass transfer processes including mobile phase, intraparticle and stationary phase diffusion and slow kinetic processes on interaction with the stationary phase. On the other hand, factors such as sample overloading and slow desorption kinetics mainly affect the shape of the peak ([3]; for a review on peak distortion and non-linear chromatography, see Ref. [4]). Altogether these processes counteract the separation of two compounds and lead to lower resolutions. An understanding of their origin is important in order to improve the separations and to gain an insight into the kinetics and mechanism of solute retention. Usually conclusions about the relative importance of these effects can be drawn from chromatographic results at various sample loads, flow-rates and column temperatures. Results from the latter study may further provide valuable information about the energetics of the separation [5–9].

Molecular imprinting is a technique for the preparation of tailor-made chiral stationary phases (CSPs) [10–17]. In our approach, directed non-covalent interactions have been used both in the preparation and in the subsequent evaluation of the phases [12–17]. One enantiomer of the molecule that is the target for the separation is mixed with functionalized monomers in solution (see Fig. 1). The resulting template assemblies are copolymerized with a cross-linking monomer to form a network polymer that can be freed from template by simple extraction. In the chromatographic mode the polymer can then be used for baseline resolution of the original racemic target compound. Mainly owing to the excessive peak broadening observed using these phases, their use for analytical purposes has been limited [12]. Recently we reported on improved chromatographic performance for polymers imprinted with L-phenylalanine anilide (L-PA) using aqueous buffer–organic solvent mobile phase mixtures or after subjecting the polymer to heat treatment [16].

We report here on an attempt to gain a better understanding of the dynamics and energetics controlling the separations on these imprinted phases. First we decided to determine what factors are mainly responsible for the broad and asymmetric peaks in this system. This was followed by a study of the effect of temperature on solute retention and enantioselectivity.

2. Experimental

The imprinted polymers were prepared following a general procedure [16] previously described, by low-temperature photoinitiated free radical polymerization of EDMA (ethylene glycol dimethacrylate) (80 mol%) and MAA (methacrylic acid) (16 mol%) in presence of L-PA (3.8 mol%) as template, using acetonitrile (polymer P1), or methylene chloride (polymer P2) as solvents ($V_{solvent}/V_{total} = 0.57$) (Fig. 1). Prior to work-up of the polymer, P1 was post-treated at 120°C for 24 h.

In the chromatographic evaluation the polymers with a 25–38-μm particle size fraction were slurry packed into 100 mm × 5 mm I.D. stainless-steel columns using as mobile phase MeCN–H_2O–HOAc 92.5:2.5:5, v/v/v). After having passed ca. 50 ml at a flow-rate of 10 ml/min, the columns were equilibrated at 1 ml/min until a stable baseline was reached. Polymer P2 was subjected to thermal treatment by leaving the column overnight in a vacuum oven set at 120°C. Then the column was reconnected to the HPLC system. In the chromatographic studies at variable temperature the columns were immersed in a constant-temperature water-bath together with an additional 50-cm stainless-steel tube connected between the injector and the column. The aqueous buffer–organic mobile phases were acetonitrile (MeCN)–0.05 *M* potassium phosphate (KP) buffer (7:3, v/v). The pH of the buffer was

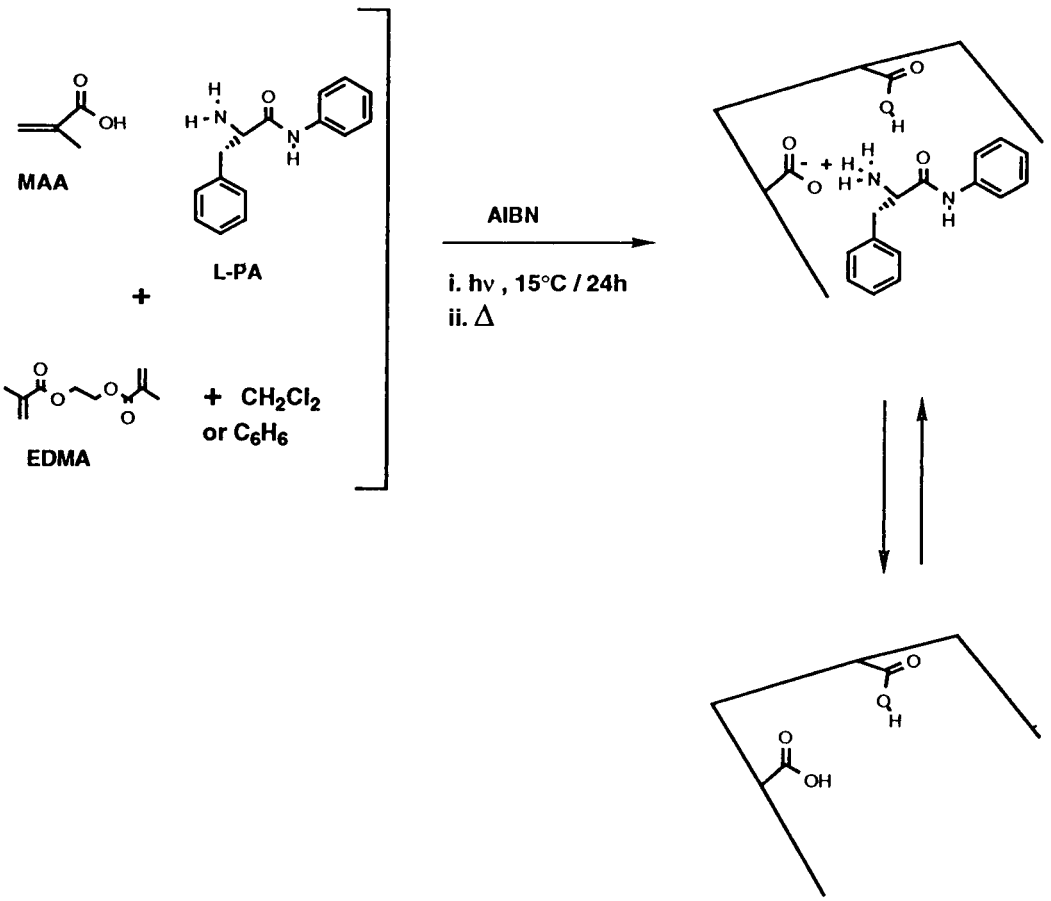

Fig. 1. Preparation of imprinted polymers.

adjusted to 4 or 7 corresponding to a pH of approximately 5 and 8 when measured on the whole system [17].

The capacity factor (k') was calculated as $(t - t_0)/t_0$, where t is the retention time of the solute and t_0 the retention time of a non-retained void marker ($NaNO_3$) (measured to the peak maxima and determined at each temperature). The use of other void markers (acetone, MeCN, HOAc) gave similar results since the solutes were usually retained by more than one void volume. The separation factor (α) measures the relative retention between the enantiomers ($\alpha = k'_L/k'_D$) and the asymmetry factor (A_s) was determined graphically at 10% of the peak maximum as described elsewhere [18]. The reduced plate height (h) was calculated as $h = L/d_pN$, where L = column length, d_p = average particle diameter (32.5 μm) and $N = 5.55(t/t_{1/2})^2$, where $t_{1/2}$ = peak width at half-height, The linear interstitial mobile phase velocity (u) was calculated as $u = F/A\varepsilon$, where F = volumetric flow-rate, A = inner cross-sectional area of column and ε = interstitial porosity (= 0.6), determined as the ratio of the lowest measured void volume (1.2 ml) to the total column volume (2.0 ml). The flow-rate was 1 ml/min, the column temperature 23°C, the volume of solute (D,L-PA, $NaNO_3$ or acetone) injected 10 μl and the UV detection wavelength 260 nm, unless stated otherwise. After the elevated temperature runs a repeat run was performed in order to ensure the stability of the CSP.

3. Results and discussion

3.1. Peak asymmetry and column overload

The peak shape, reflected in the peak asymmetry factor (A_s), is informative about the existence of non-linear binding isotherms and slow adsorption or desorption of solute to the stationary phase. According to Giddings [3], it is possible to distinguish these effects by studying the dependence of A_s on flow-rate and sample load. Thus, if the asymmetry increases with increasing sample load and shows less dependence on flow-rate, the asymmetry is caused mainly by the non-linear binding isotherm. On the other hand, a weak dependence of A_s on sample load and a strong flow-rate dependence are indicative of a slow adsorption/desorption rate. Figs. 2 and 3 show A_s as a function of sample load and flow-rate on two L-PA-selective CSPs prepared by a thermal treatment promoting higher column efficiency [16] (see Experimental). While A_s increases rapidly with increasing sample load, it changes less with flow-rate. Note that the slight decrease in A_s with flow-rate can also be attributed to a non-linear adsorption isotherm [19]. In the same experiment we observed no change in k' and α. The non-linear adsorption isotherm is therefore the main cause of the peak asymmetry. This is reflected in the plots of the capacity factor (k') and separation factor (α) versus sample load (Fig. 4). The shapes of the curves for the two materials are different. Thus k'_L and α on P2 are high with low sample loads but fall off rapidly with increasing sample load to level off above a 10-nmol sample load. On P1, on the other hand, the curves exhibit a small plateau at low sample loads and a less pronounced fall-off at higher sample loads. The corresponding elution profiles on P2 show that the peaks become progressively narrower with increasing sample load (Fig. 5). This is a typical case of an overloaded column with a low plate count where deviation from the "right triangle approximation" [20] is expected to occur [21]. In a study of the binding of 9-ethyladenine to an imprinted polymer [22], the isotherm could be fitted with a Langmuir binary site model composed of a small number of high-energy selective binding sites and a large number of weaker, less selective sites. The corresponding plot of k' versus sample load turns out similar to that obtained for P2 (Fig. 4a), indicating that polymer P2 contains a similar distribution of binding sites. It is noteworthy that a binary site model was also used by Jacobson et al. [23] for

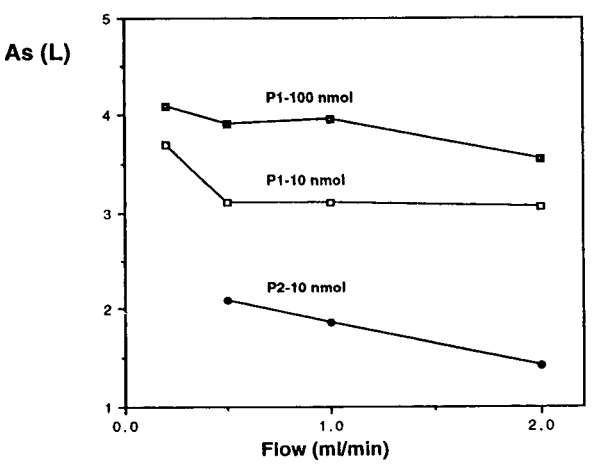

Fig. 2. Asymmetry factor (A_s) versus flow-rate for L-PA at two different sample loads on a column packed with P1 or P2. Mobile phase, MeCN–0.05 *M* KP (pH 7) (7:3, v/v).

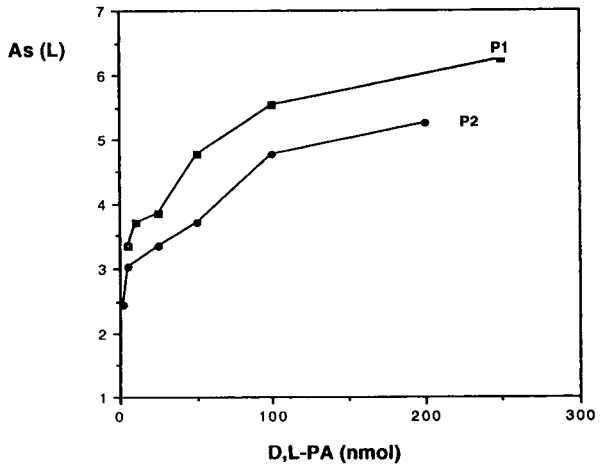

Fig. 3. Asymmetry factor (A_s) of the L-enantiomer versus sample load of D,L-PA on P1 and P2. Flow-rate, 1.0 ml/min; mobile phase, MeCN–0.05 *M* KP (pH 7) (7:3, v/v).

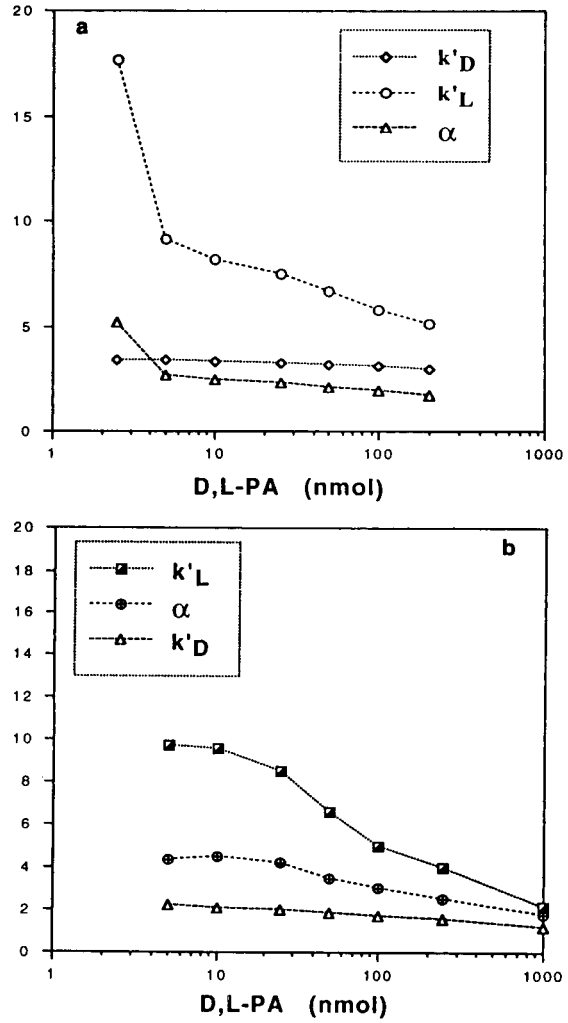

Fig. 4. Capacity factor (k') and separation factor (α) versus sample load of D,L-PA on (a) P2 and (b) P1. Flow-rate, 1.0 ml/min; mobile phase, MeCN–0.05 *M* KP (pH 7) (7:3, v/v).

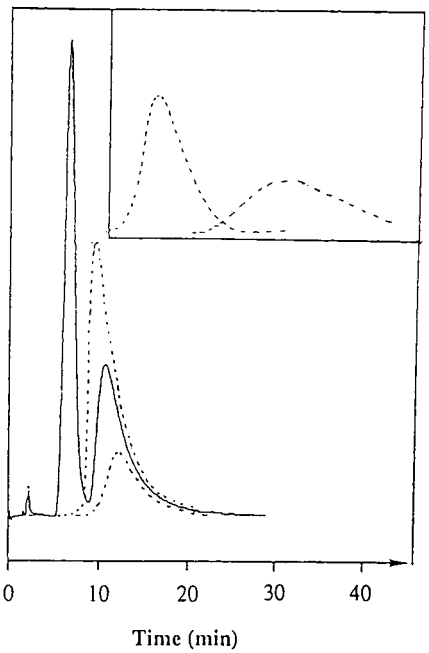

Fig. 5. Elution profiles of increasing loads of D,L-PA applied on P2. Flow-rate, 1.0 ml/min; mobile phase, MeCN–0.05 *M* KP (pH 7) (7:3, v/v). The sample loads from right to left in the chromatogram were 2.5, 5, 50, 100 and 200 nmol. The D-enantiomer is shown only at the 100 nmol sample load.

describing the site distribution in protein-based chiral stationary phases.

What, then, are the possible origins of the different site distributions in the materials? It is noted that P1 and P2 have the same chemical composition but are different only with respect to structure and morphology. This is controlled both by the pore-forming solvent and, by the thermal post-treatment of the materials [16]. Thus, P2 was characterized as gel-like with a low pore volume and surface area but with a relatively high swellability (1.90 ml/ml) that was slightly lower than for the corresponding material not subjected to heat treatment (2.01 ml/ml). P1 was mesoporous with a lower swellabiltiy (1.35 ml/ml), equal to the swellability of the corresponding untreated material. The materials, when not subjected to heat treatment, showed a similar chromatographic dependence on sample load when one was compared with the other [16]. Moreover, higher selectivities and retentions were seen at low sample loads compared with the heat-treated materials. We also found that by subjecting a mesoporous material to heat-treatment in the dry state, that is, the same thermal treatment as used in the preparation of P2, both binding and selectivity were lost. It seems that the structure of the binding sites is more unstable in the porous than in the non-porous materials. Hence a reasonable explana-

tion for the different site distribution in P2 is that unstable and probably highly selective binding sites have been deformed on heat treatment. Apparently these can now stronger bind the D-enantiomer as seen in the higher k'_D values measured on P2 compared with the situation prior to heat treatment. We further note that the saturation capacity of P1 is higher than that of the corresponding material not subjected to heat treatment. This indicates that the heat treatment results in improved site accessibility. Obviously, more detailed studies on the effect of heat treatment need to be carried out, including measurements of the complete binding isotherms [4].

3.2. Peak dispersion

As the retention of the complementary solute (L-PA) on the imprinted polymers follow a non-linear binding isotherm as indicated from the plots of k' versus sample load (Fig. 4), the resulting peaks are asymmetric (see Fig. 5) and the theoretical models describing the various dispersion processes are not applicable [1,2]. On P2, the column efficiency improved at higher temperature (Fig. 6) but with little effect on peak asymmetry. Nevertheless, the bands of the less retained enantiomer (D-PA) and of the void marker, acetone, are fairly gaussian (see Fig. 5) and their retention time changes marginally with sample load. The associated band widths are therefore expected to be mainly a result of the band-broadening mechanisms that are considered in the models. Previously we showed that the solute retention on this type of CSP can be accurately described by a theoretical model for weak cation exchange [17].

In Fig. 7, double logarithmic plots of reduced plate height (h) versus linear mobile phase

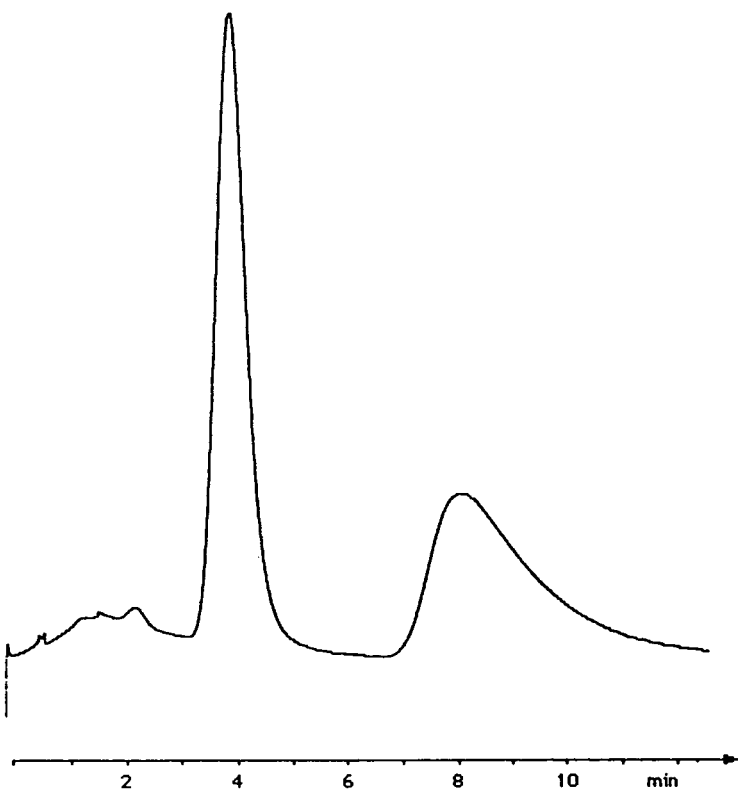

Fig. 6. Elution profile of D,L-PA (10 nmol) applied on P2. Flow-rate, 1.0 ml/min; mobile phase, MeCN–0.5 *M* KP (pH 4) (7:3, v/v); column temperature, 60°C. The reduced plate heights were $h_D = 12$ and $h_L = 35$.

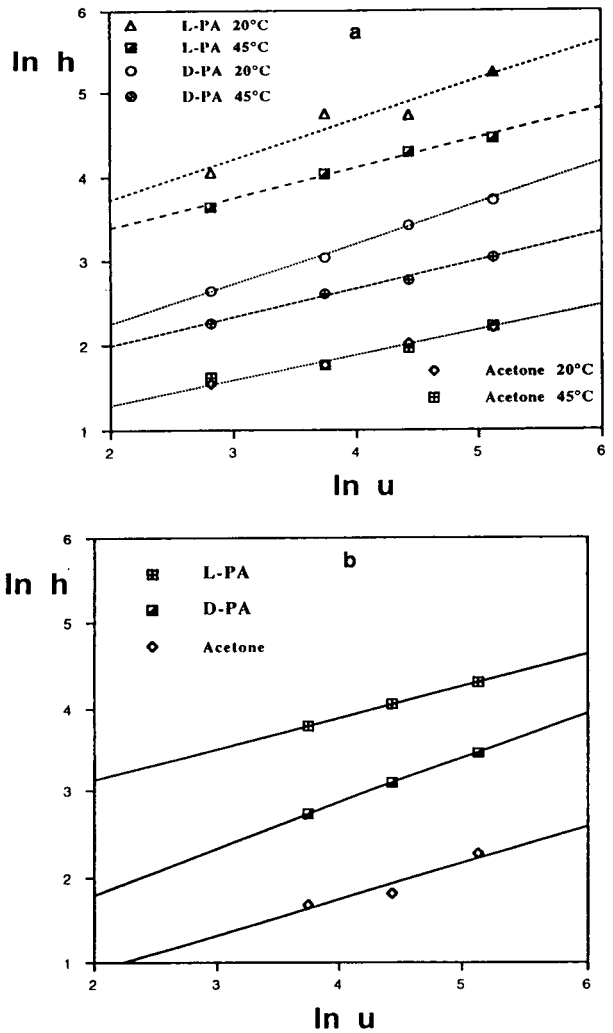

Fig. 7. Double logarithmic plot of reduced plate height (h) versus linear mobile phase velocity (u) in the chromatography of D,L-PA (100 nmol) on (a) a polymer prepared using benzene as porogen at two different column temperatures: at 20°C, $k'_L \approx 6$, $k'_D \approx 2.5$, and at 45°C, $k'_L \approx 2.1$, $k'_D \approx 1.0$; (b) polymer P2 at 20°C. Mobile phase, MeCN–0.05 M KP (pH 7) (7/3, v/v).

velocity (u) are shown for D- and L-PA and the non-retained acetone marker on polymer P2 and a polymer prepared using benzene as porogen. Note that the data for the L-enantiomer have been included for comparative purposes. The plots are all linear and the slope changes with temperature in agreement with other types of ion-exchange separations using porous particles [24–26]. The mass transfer here was believed to be limited by a slow intraparticle diffusion. In this context we note that the plots of acetone do not change with temperature, indicating that the mobile phase diffusion of the neutral void marker is not limiting the mass transfer.

Although the peak of the L-enantiomer is strongly asymmetric, it is interesting that the plots are essentially parallel with those of the D-form. Together with the small change in relative plate heights with temperature (data not shown), this indicates that the enantioselective resistance to mass transfer is small at this sample load (100 nmol). This should be compared with the strongly temperature-dependent relative plate heights observed in the separation of sugar enantiomers on imprinted polymers based on reversible boronate ester formation [11].

3.3. Effect of temperature

Chromatographic retention data from variable-temperature runs may be used to estimate thermodynamic properties according to the well known Van 't Hoff relation [5–9]:

$$\ln k' = -\Delta H/RT + \Delta S/R + \ln \phi \quad (1)$$

where ϕ = phase volume ratio and R = gas constant. Thus linear portions of these plots give enthalpies (ΔH) and entropies (ΔS) of the solute adsorption from the slope and intercept, respectively. The ΔH and ΔS values thereby obtained can rarely be ascribed to a single process but are rather a complex combination of various contributions such as solute–site solvation and desolvation, the unsolvated solute–site interaction, solvation of bound solute, conformational changes, multiple equilibria and mixed retention mechanisms [1]. By plotting $\ln \alpha$ ($\alpha = k'_L/k'_D$ = separation factor) versus $1/T$, all processes that do not contribute to the enantiomeric discrimination cancel out and information about the energetics of the separation can be obtained from

$$\ln \alpha = -\Delta\Delta H/RT + \Delta\Delta S/R \quad (2)$$

The dependence of the chromatographic parameters on temperature were investigated in three different solvent systems. Based on the stable α and k' values obtained on P2 with

respect to flow-rate (at a sample load of 100 nmol at pH 7, the retention data were $k'_L = 4.21 \rightarrow 4.25$ and $\alpha = 1.52 \rightarrow 1.54$ for a flow-rate increase from 0.5 to 2 ml/min; at pH 4 and in the HOAc-containing mobile phase, however, a slight decrease in k'_L and α was observed: pH 4, $k'_L = 3.93 \rightarrow 3.40$ and $\alpha = 3.10 \rightarrow 2.70$; HOAc, $k'_L = 11 \rightarrow 8$ and $\alpha = 6.5 \rightarrow 5.8$; for a flow-rate increase from 0.2 to 2 ml/min), we considered that a discussion of the thermodynamic behaviour of this phase would be justified. For the D-enantiomer the linear isotherm, as indicated by the stable k' values in Fig. 4a, allows thermodynamic quantities to be determined. For the L-form, however, the contribution from thermodynamic band broadening only allow qualitative conclusions. Nevertheless, as the sample load between 10 and 100 nmol had little influence on the corresponding Van 't Hoff plots, the slope and intercept were determined giving values assigned as apparent thermodynamic quantities (ΔH_{Lapp} and ΔS_{Lapp}).

Figs. 8–10 show the plots of ln k' versus $1/RT$ at a mobile phase pH of 7 and 4 and in a mobile phase containing acetic acid as additive [MeCN–H_2O–HOAc (92.5:2.5:5)]. In the latter instance, a larger sample load had to be applied (100 nmol) because of the excessive peak broadening of L-PA. At pH 7 a linear dependence of ln k' on $1/RT$ is seen with decreasing k' with increasing temperature. On lowering the pH to 4, a non-linear plot is obtained with a linear portion at higher temperature. The linear portions of these plots were fitted by least-squares linear regression analysis, giving ΔH and $\Delta S'$ values (for the

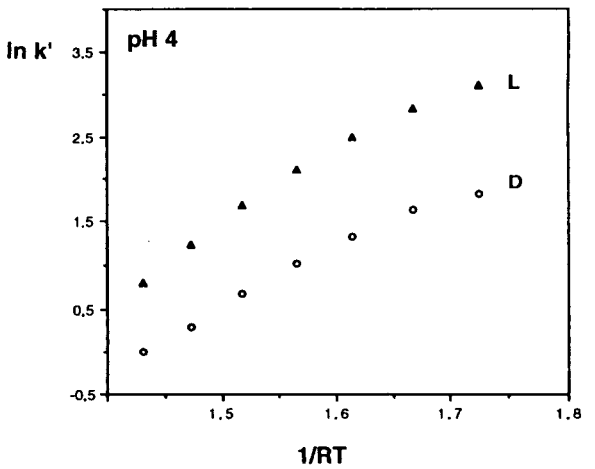

Fig. 9. Van 't Hoff plot as in Fig. 8 but at pH 4. The column temperature was increased from 20 to 80°C in 10°C increments.

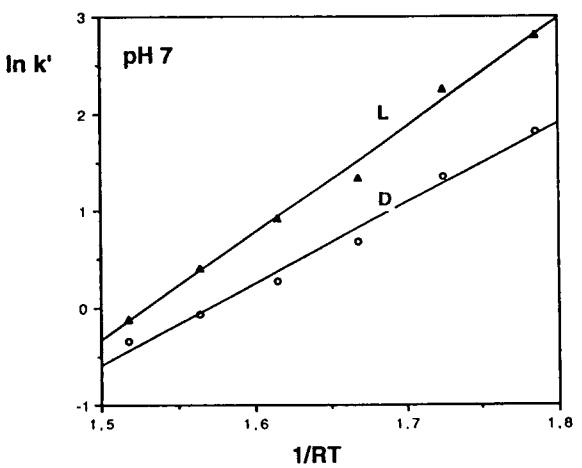

Fig. 8. Van 't Hoff plots of the capacity factors (k') for 10 nmol of D,L-PA chromatographed on P2. Mobile phase, MeCN–0.05 *M* KP (pH 7) (7:3, v/v). The column temperature was increased from 10 to 60°C in 10°C increments.

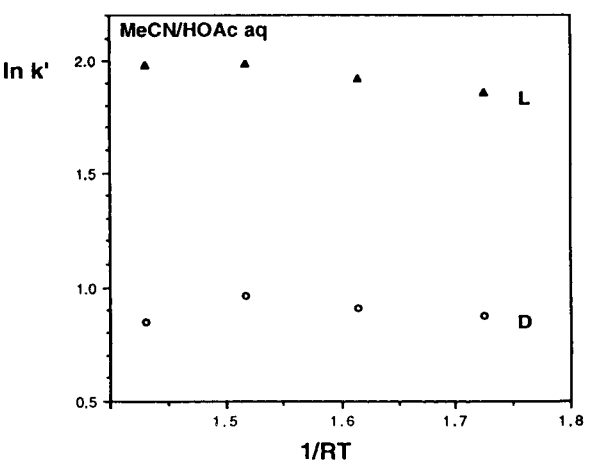

Fig. 10. Van 't Hoff plots of the capacity factors (k') for D- and L-PA (100 nmol) on an L-selective polymer. Mobile phase, MeCN–H_2O–HOAc (92.5:2.5:5). The column temperature was increased from 20 to 80°C in 20°C increments.

Table 1
Chromatographic determination of enthalpies and entropies of binding of D- and L-PA to an L-PA-imprinted polymer (P2) from the data in Figs. 8–11

Mobile phase	D,L- (nmol)	ΔH_D (kcal/mol)	ΔH_{Lapp} (kcal/mol)	$\Delta S'_D$ (cal/mol · K)	$\Delta S'_{Lapp}$ (cal/mol · K)	$\Delta\Delta H_{D,Lapp}$ (kcal/mol)	$\Delta\Delta S_{D,Lapp}$ (cal/mol · K)
MeCN–H_2O–HOAc (92.5:2.5:5)	100	0.43	0.64	3.2	5.9	0.47	3.5
MeCN–0.05 *M* KP (pH 4) (7:3)	10	−7.6	−9.9	−22	−26	−1.7	−3.1
	100	−7.0	−9.0	−20	−25	−1.7	−3.6
MeCN–0.05 *M* KP (pH 7) (7:3)	10	−8.4	−11	−26	−34	−2.7	−7.6
	100	−9.4	−11	−30	−35	−1.7	−4.8

The enthalpies (ΔH) and entropies (ΔS) (absolute values for the D-enantiomer and apparent values for the L-enantiomer) were obtained from linear regression of the linear portion of corresponding Van 't Hoff plots of $\ln k$ versus $1/RT$. The $\Delta\Delta H_{app}$ and $\Delta\Delta S_{app}$ values were obtained from $\ln \alpha$ versus $1/RT$. These plots were apparently linear throughout the temperature interval used in the study. The plots had a correlation factor of at least 0.96. $\Delta S' = \Delta S + R \ln \phi$, where ϕ = column phase volume ratio. 1 cal = 4.184 J.

L-form only apparent values) as shown in Table 1 at two different sample loads. On changing from pH 7 to pH 4, ΔH and $\Delta S'$ increase. As protonation of the solute occurs in this pH interval, a major change in solvation–desolvation effects affecting the separation is to be expected. Interactions requiring desolvation of extensively solvated species are usually associated with a more positive entropy term than the corresponding non-solvated interactions. This effect can be expected for interactions between solvated ammonium and carboxylate groups. Note that aqueous solvation of ammonium ions is strong and can involve four shells of water molecules with a $\Delta H°$ of 30–80 kcal/mol [27]. The solvation of the solute at pH values below its pK_a value (pK_a = 5.4 in this solvent system) [17] is thus likely to have a major influence on the binding process. Apparently solvation is even more pronounced using the organic–acetic acid mobile phase, reflected in the positive values of both ΔH and $\Delta S'$. This is in agreement with our earlier study on the stability of complexes formed between methacrylic acid and L-PA prior to polymerization and between acetic acid and L-PA in the mobile phase [14]. It should be noted that such a rare type of chromatographic temperature dependence was recently observed also in the separation of chiral amines on chiral crown ethers [28]. The endothermic behaviour here was also explained by solute desolvation on formation of electrostatic interactions between the site and the solute.

From the plots in Fig. 11, $\Delta\Delta H_{app}$ and $\Delta\Delta S_{app}$, describing the enantioselective contribution to

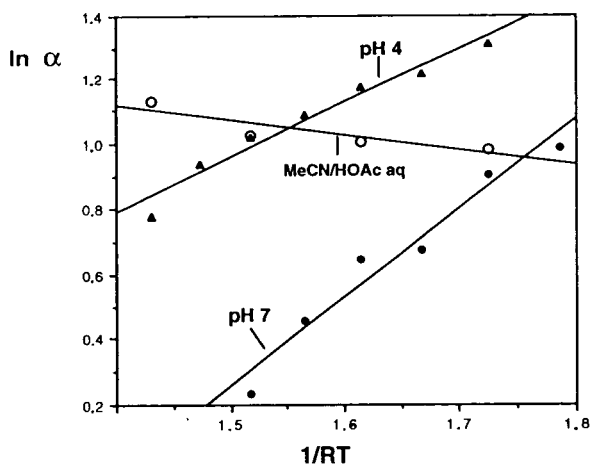

Fig. 11. Van 't Hoff plots of the separation factor (α) for the experiments described in Figs. 8–10. Using the HOAc-containing mobile phase, the amount applied was 100 nmol.

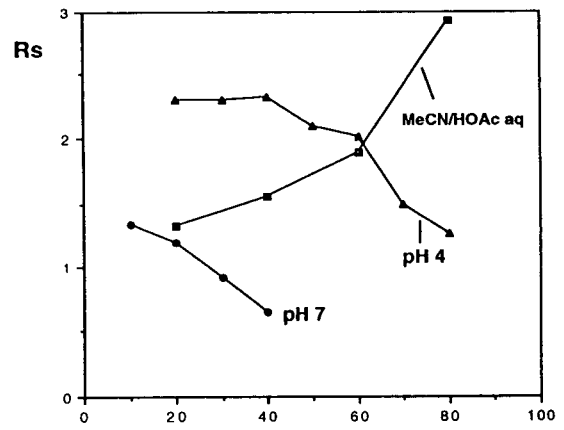

Fig. 12. Resolution factor (R_s) versus column temperature for the experiments in Figs. 8–11.

binding (see Table 1), were calculated. Similar trends are observed here as in the plot of ln k'. Thus $\Delta\Delta S_{app}$ and to some extent $\Delta\Delta H_{app}$ increase with decreasing pH. Again, these changes can be attributed to solvation–desolvation phenomena. At low pH the ammonium ions of the solute are strongly solvated. On binding to the negatively charged sites, the most strongly bound enantiomer will require more desolvation than the antipode, which may bind to the sites while still being partly solvated. In the acetic acid-containing mobile phase this effect is apparently important enough to cause an endothermic behaviour. At pH 7, however, most of the solute is deprotonated and thus less strongly solvated [27]. The polymer is abundant in non-ionized carboxylic acid groups [17]. Hence interactions between non-ionized solute and non-ionized sites, a process likely to involve less solvation–desolvation of the interacting species, may account for the lower $\Delta\Delta S_{app}$ and slightly lower $\Delta\Delta H_{app}$ found at pH 7. The temperature effects are clearly reflected in the dependence of resolution (R_s) on temperature. Whereas at pH 7 an increase in temperature leads to a decrease in resolution, the other extreme is seen using the acetic acid-containing mobile phase, namely an increase in R_s with increase in temperature (Fig. 12).

4. Conclusions

The present results indicate that the peak asymmetry in a buffered mobile phase system is mainly due to the non-linear binding isotherm resulting in a continuous overloading of sites. The site distribution depends on the method used in the preparation of the materials where various heat treatments can be applied in order to change the binding site distributions or accessibility. Kinetic factors such as slow solute adsorption or desorption appears to be of less importance, although mass transfer limitations are still present. At pH 7, the dependence of the plate height for the least retained enantiomer (gaussian peak) on the mobile phase velocity was similar to those commonly observed in ion-exchange separations. Neither the retention nor selectivity changed here with variations in flow-rate. It should be noted that polymers imprinted by reversible boronate ester formation showed a different chromatographic behaviour [10]. The separation factor and retention increased significantly here with decreasing flow-rate whereas the plate number remained essentially constant. The mass transfer was believed to be limited by a slow, reversible, covalent binding step while the diffusional limitations were assumed to be negligible.

A temperature study on the phases led to Van 't Hoff plots that were strongly dependent on the mobile phase pH and also on the mobile phase composition. From linear portions of these plots values of ΔH and $\Delta S'$ (absolute for the D-enantiomer and apparent for the L-enantiomer) for the retention and $\Delta\Delta H_{app}$ and $\Delta\Delta S_{app}$ for the separation could be calculated. The exothermicity of both the retention and the separation decreases with decrease in pH and an endothermic process is observed when using an organic–acetic acid mobile phase. These effects were believed to be caused mainly by the desolvation required on interactions between

strongly solvated ammonium and carboxylate groups.

Acknowledgements

This work was supported by grants from the Swedish Natural Science Research Council and from the US National Science Foundation. Financial support from Lars Hiertas Minne is gratefully acknowledged.

References

[1] G.S. Weber and P.W. Carr, in P.R. Brown and R. Hartwick (Editors), *High Performance Liquid Chromatography*, Wiley-Interscience, New York, 1989, pp. 1–15.
[2] J.Å. Jönsson (Editor), *Chromatographic Theory and Basic Principles*, Marcel Dekker, New York, 1987.
[3] J.C. Giddings, *Anal. Chem.* 13 (1963) 1999.
[4] A.M. Katti and G.A. Guichon, *Adv. Chromatogr.*, 31 (1992) 1–119.
[5] W.R. Melander, B.-K. Chen and C. Horvath, *J. Chromatogr.*, 185 (1979) 99–109.
[6] W.R. Melander, J. Stoveken and C. Horvath, *J. Chromatogr.*, 185 (1979) 111–127.
[7] W.R. Melander, A. Nahum and C. Horvath, *J. Chromatogr.*, 185 (1979) 129–152.
[8] A. Nahum and C. Horvath, *J. Chromatogr.*, 203 (1981) 53–63.
[9] W.H. Pirkle, *J. Chromatogr.*, 558 (1991) 1–6.
[10] G. Wulff and W. Vesper, *J. Chromatogr.*, 167 (1978) 171.
[11] G. Wulff and M. Minárik, *J. High Resolut. Chromatogr. Chromatogr. Commun.*, 9 (1986) 607.
[12] For a review, see B. Sellergren, in G. Subramanian (Editor), *Chiral Separations by Liquid Chromatography*, VCH, Weinheim, 1994, pp. 69–93.
[13] B. Sellergren, B. Ekberg and K. Mosbach, *J. Chromatogr.*, 347 (1985) 1.
[14] B. Sellergren, M. Lepistö and K. Mosbach, *J. Am. Chem. Soc.*, 110 (1988) 5853.
[15] M. Lepistö and B. Sellergren, *J. Org. Chem.*, 54 (1989) 6010–6012.
[16] B. Sellergren and K.J. Shea, *J. Chromatogr.*, 635 (1993) 31–49.
[17] B. Sellergren and K.J. Shea, *J. Chromatogr.*, 654 (1993) 17–28.
[18] L.R. Snyder and J.J. Kirkland (Editors), *Introduction to Modern Liquid Chromatography*. Wiley, New York, 1979, pp. 234–237.
[19] J.H. Knox and G. Vasvari, *J. Chromatogr.*, 83 (1973) 181–194.
[20] J.H. Knox and H.M. Pyper, *J. Chromatogr.*, 363 (1986) 1.
[21] L.R. Snyder, G.B. Cox and P.E. Antle, *Chromatographia*, 24 (1987) 82–96.
[22] K.J. Shea, D.A. Spivak and B. Sellergren, *J. Am. Chem. Soc.*, 115 (1993) 3368–3369.
[23] S. Jacobson, S. Golshan-Shirazi and G. Guichon, *J. Am. Chem. Soc.*, 112 (1990) 6492.
[24] J.F.K. Huber, *Ber. Bunsenges. Phys. Chem.*, 77 (1973) 179.
[25] A. Jardy and R. Rosset, *J. Chromatogr.*, 83 (1973) 195–204.
[26] R. Eksteen, J.C. Kraak, P. Linssen, *J. Chromatogr.*, 148 (1978) 413–427.
[27] M. Meot-Ner, in J.F. Liebman and A. Greenberg (Editors), *Molecular Structure and Energetics*, Vol. 4, VCH, Weinheim, 1987, p. 71.
[28] R. Kuhn, F. Erni, T. Bereuter and J. Häusler, *Anal. Chem.*, 64 (1992) 2815–2820.

ELSEVIER

Journal of Chromatography A, 690 (1995) 41–54

JOURNAL OF CHROMATOGRAPHY A

Normal-phase high-performance liquid chromatography of volatile compounds
Selectivity and mobile phase effects on polar bonded silica

Markus Lübke[a,*], Jean-Luc le Quéré[a], Denis Barron[b,1]

[a]*INRA, Laboratoire de Recherche sur les Arômes, 17 rue Sully, 21034 Dijon Cédex, France*

[b]*Université Joseph Fourier, UFR de Pharmacie, Laboratoire de Pharmacognosie, 38706 La Tronche Cédex, France*

First received 28 July 1994; revised manuscript received 25 October 1994

Abstract

Liquid chromatographic retention data of various volatile alcohols, phenols, ethers, aldehydes, ketones, esters, nitriles, isothiocyanates, and heterocyclic compounds were measured on diol-, cyano- and amino-bonded silica columns. The mobile phase was pentane–diethyl ether in varying compositions. The Snyder theory was applied to retention of polycyclic aromatic hydrocarbons and to selected other compounds. The role of diethyl ether in the retention process was examined. Restricted-access delocalization was observed on all three bonded phases, and was pronounced on diol and amino silica. Secondary solvent effects were important for most compounds, indicating differences in specific solvent–solute interactions between adsorbed and non-adsorbed mobile phase. Principal component analysis was performed on a large set of retention data. Esters and ethers showed clear affinity for diol silica, while alcohols and phenols were preferentially retained on amino silica.

1. Introduction

Reversed-phase high-performance liquid chromatography (HPLC) on octadecyl bonded silica continues to be the most popular technique in liquid chromatography. Nevertheless, polar bonded phases have gained in interest, both in the reversed-phase and in the normal-phase mode. Only three binding types have found wide application, dihydroxypropyl propyl ether (diol), aminopropyl, and cyanopropyl silica. In the normal-phase mode, these phases exhibit properties similar to bare silica, but they offer some important advantages, among which (1) no irreversible adsorption of very polar solutes, (2) faster column equilibration, and (3) less importance of water content of the mobile phase.

The Snyder model of adsorption chromatography [1] was originally designed for silica and alumina as adsorbents. It starts from the assumption that retention of a solute is governed by competitional adsorption on some active site on the adsorbent rather than by partition between two immiscible liquid phases. Several studies showed that this general assumption also holds

* Corresponding author.

[1] Present address: Université Claude Bernard, Laboratoire de Biochimie Végétale, 43 boulevard du 11 novembre 1918, 69622 Villeurbanne Cédex, France

0021-9673/95/$09.50
SSDI 0021-9673(94)01048-X

true on diol- [2,3], cyano- [2,4–7] and amino- [5,6,8,9] bonded silica, while details of retention mechanisms are still controversial.

The present work was conducted in the context of a study of the possible advantages of normal-phase HPLC in prefractionation of aroma extracts of various origins. It aims to further elucidate retention characteristics and selectivity effects of these adsorbents for a wide range of volatile solutes, with consideration of the role of the mobile phase. Especially for diol bonded silica, there is still a deficiency of precise differentiation from the other two adsorbents. With respect to easy concentration of fractions in semi-preparative chromatography, only one mobile phase system, pentane–diethyl ether, was used in varying compositions throughout the study. Its volatility largely exceeds that of the solutes studied.

2. Experimental

2.1. Chemicals

Pentane and diethyl ether were of HPLC grade (Fisons, Loughborough, UK). Prior to use all solvents were filtered through a 0.45 μm membrane filter (Millipore, Bedford, MA, USA). The standards were from Sigma (St. Quentin Fallavier, France) or from our laboratory collection of volatile compounds.

2.2. Equipment

All experimental conditions were as previously published [10]. The columns, a LiChrospher 100 diol (5 μm), a Hypersil Cyanopropyl (5 μm), and a Hypersil Aminopropyl (5 μm), all 250 × 4.6 mm, were obtained from Shandon (Eragny, France). Dead time determination was performed using a Waters R 401 refractometer. The flow rate was set to 1.5 ml/min.

2.3. Procedures

Capacity factors were calculated from the mean of three injections. Correction for variations in the mobile phase composition via selectivity coefficients and for flow rate variations were performed as described previously [10].

3. Results and discussion

3.1. Dead time determination

Column dead time was measured by injection of 20 μl of a solution of 1% hexane in the mobile phase. It was found to depend on the mobile phase composition. Experimental data show a decrease in dead time, when varying the mobile phase composition from 100% pentane to 100% diethyl ether (Fig. 1). The maximum dead time shift is more pronounced on diol (9 s) than on amino (5 s) and cyano (2 s).

3.2. Solvent strength

The experimental data obtained in this study were interpreted using the Snyder displacement model [1]. For a non-localizing compound, retention is given by

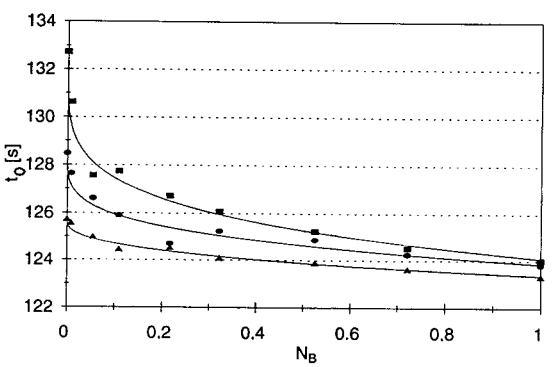

Fig. 1. Dead time on diol (□), cyano (▲) and amino (○) columns as a function of mobile phase diethyl ether content. Flow rate 1.5 ml/min. Dead time marker: hexane. Refractometric detection. Each point is a mean of 10 repetitions. Mean standard deviations are 0.15 for diol, 0.15 for cyano, and 0.20 for amino. Curves result from regression analysis with the model: $t_0 = a\,N_B^b + c$; N_B is molar fraction of diethyl ether.

$$\log (k'_{AB}/k'_A) = \alpha' A_S(\epsilon_A - \epsilon_{AB}) \quad (1)$$

where k'_A and k'_{AB} are the capacity factors for pure mobile phase A and for a mixture of A and B (A being a weaker eluent than B), α' is the adsorbent activity factor (arbitrarily defined as one for all adsorbents in this study), A_S is the molecular cross-sectional area of the solute, and ϵ_A and ϵ_{AB} are the solvent strength values of solvent A and the mixture of A and B, respectively. For pentane, ϵ_A is equal to zero.

The solvent strengths of pure solvent A and B are related to that of their mixture by

$$\epsilon_{AB} = \epsilon_A + \left[\log \left(N_B\, 10^{\alpha' n_B(\epsilon_B - \epsilon_A)} + 1 - N_B\right)\right] / \alpha' n_B \quad (2)$$

where N_B is the mole fraction of solvent B in the mixture, and n_B is the molecular cross-sectional area of solvent B (in multiples of 8.5 Å^2, equal to 4.5 for diethyl ether). When the capacity factor of a solute for pure mobile phase A and for a mixture of A and B is known along with its molecular cross-sectional area, substitution of ϵ_{AB} in Eq. 2 by Eq. 1 and subsequential solution for ϵ_B allows calculation of the solvent strength of pure solvent B in this mixture.

Retention of phenanthrene and triphenylene was measured on all three adsorbents with seven mobile phase compositions (ranging from 100% pentane to 50% diethyl ether). Capacity factors and calculated ϵ_B are given in Table 1. As can be seen, ϵ_B increases with decreasing molar fraction

Table 1
Retention of aromatic hydrocarbons and experimental mobile phase strengths

Modifier (%)	log k'		ϵ_{AB}	ϵ_B	θ_B	ϵ''	ϵ'	Determination coefficient[c]
	Phenanthrene[a]	Triphenylene[b]						
Diol						0.101	0.291	0.996
0	0.078	0.486						
0.8	−0.042	0.320	0.012 ± 0.001	0.265 ± 0.006	0.123			
5	−0.182	0.131	0.025 ± 0.001	0.180 ± 0.005	0.273			
10	−0.268	0.029	0.033 ± 0.001	0.150 ± 0.004	0.368			
20	−0.345	−0.080	0.041 ± 0.002	0.119 ± 0.004	0.487			
50	−0.639	−0.331	0.064 ± 0.002	0.099 ± 0.003	0.755			
Cyano						0.061	0.094	0.934
0	−0.386	−0.096						
0.8	−0.401	−0.112	0.0013 ± 0.0001	0.091 ± 0.003	0.022			
5	−0.485	−0.202	0.0086 ± 0.0005	0.095 ± 0.004	0.135			
10	−0.538	−0.252	0.0129 ± 0.0011	0.080 ± 0.005	0.221			
20	−0.608	−0.350	0.0198 ± 0.0007	0.069 ± 0.002	0.362			
50	−0.814	−0.587	0.0382 ± 0.0012	0.063 ± 0.002	0.681			
Amino						0.145	0.423	0.998
0	0.309	0.818						
0.8	−0.106	0.278	0.040 ± 0.001	0.392 ± 0.004	0.342			
5	−0.380	−0.053	0.065 ± 0.001	0.280 ± 0.002	0.516			
10	−0.456	−0.143	0.072 ± 0.001	0.232 ± 0.002	0.576			
20	−0.567	−0.276	0.082 ± 0.001	0.190 ± 0.001	0.664			
50	−0.770	−0.522	0.100 ± 0.001	0.145 ± 0.001	0.832			

[a] $A_S = 10.84$.
[b] $A_S = 13.26$.
[c] Non-linear regression model: $\%_{lc} = 1 - \int_0^x e^{-25(0.5-x^a)^2} dx / \int_0^1 e^{-25(0.5-x^a)^2} dx$.

of diethyl ether. The pure solvent strength of diethyl ether can furthermore be related to its fractional surface coverage on the adsorbent θ_B by

$$\theta_B = N_B 10^{\alpha' n_B(\epsilon_B - \epsilon_A)} / \left[1 - N_B + N_B 10^{\alpha' n_B(\epsilon_B - \epsilon_A)}\right] \quad (3)$$

The plot of ϵ_B against θ_B (Fig. 2) permits us to visualize the capability of solvent B to localize on the adsorbent surface. For solvent–adsorbate combinations where the solvent does not localize, a horizontal graph is obtained (ϵ_B is independent of concentration). If the solvent molecule is able to undergo strong interactions with active sites on the adsorbent, the graph will be non-linear. In order to quantitatively describe the relationship of ϵ_B and θ_B in these cases, Snyder [11,12] introduced a localization function $\%_{lc}$ as follows:

$$\epsilon_B = \epsilon'' + \%_{lc}(\epsilon' - \epsilon'') \quad (4)$$

At low solvent B concentration, ϵ_B will be independent of the surface coverage (plateau on the left side of the graphs, $\epsilon_B = \epsilon'$), but with increasing concentration the active sites will become saturated with solvent B and solvent strength decreases until a state where all active sites are occupied by solvent B molecules and solvent strength becomes again independent of surface coverage, now reflecting the solvent strength of delocalized B ($\epsilon_B = \epsilon''$). This effect is commonly referred to as restricted-access delocalization.

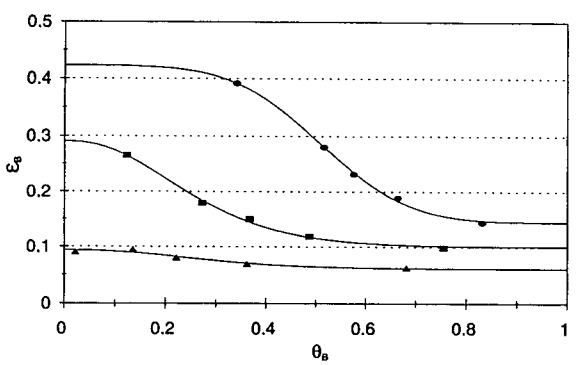

Fig. 2. Solvent strength of pure diethyl ether ϵ_{AB} as a function of its fractional surface coverage θ_B. Symbols of columns as in Fig. 1.

The empirical term of function $\%_{lc}$ proposed by Snyder for silica cannot be sufficiently adapted to the bonded phases of this study, because an additional minimum occurs on the right half of the graph when varying the parameters in this function so that it approaches the experimental points. Therefore, another function, the integral of a slightly modified Gaussian curve, was used for the regression analysis generating the curves in Fig. 2 (see legend of Table 1).

Snyder and Schunk [8] assumed that no restricted-access delocalization should occur on polar bonded phases, since the flexibility of the functional group, attached to the silica by a propyl chain, precludes formation of strong interactions. The authors found this theory confirmed by the experimental data they obtained on an amino column with hexane–tetrahydrofurane mixtures as a mobile phase. However, ϵ_B values calculated in the above described way (Eq. 2) from their experimental ϵ_{AB} data show significant decrease when increasing the mobile phase modifier content. In a subsequent publication [13], Snyder argued that this variation of ϵ_B does not signify the occurrence of restricted access delocalization. This hypothesis was based on the observation that the shapes of their graphs of ϵ_B against θ_B differ markedly from the equivalent graph on bare silica, and that ϵ_B varied even when non-localizing solvents like chlorinated hydrocarbons were used as modifiers.

Cooper and Smith [2,7] studied retention on diol, cyano and amino columns with hexane–methyl *tert.*-butyl ether as a mobile phase and found that ϵ_B varies with the ether content only in the case of the cyano column. They attributed this phenomenon to remaining accessible silanols rather than to interactions with the cyano group, although this column was the only endcapped column in their experiments. From retention data of an aromatic nitro compound with localization effects on all three columns, however, the authors concluded that restricted-access delocalization may also occur on diol and amino, but

that this phenomenon does not affect the retention of the large aromatic hydrocarbons that served for ϵ_B calculation, due to a lesser extent of accessibility of the silanols.

Our data show localization of diethyl ether on active sites of all three columns. While the cyano column exhibits only a slight non-linearity, this effect is pronounced on the diol and amino columns. The sigmoidal shapes of the graphs of ϵ_B against θ_B (Fig. 2) resemble the relationship observed on silica [12]. Total obstruction of the active sites for large molecules by the aliphatic groups bonded to the silica could not be observed. We believe furthermore that the functional groups on the organic moiety are involved in localization. Two observations support this hypothesis.

First, Fig. 2 reveals that the position of the point of inflection depends on the bounding type. It was found at $\theta_B = 0.25$ (diol), 0.27 (cyano) et 0.51 (amino). On bare silica, independently of the solvents used, this transition point is found at $\theta_B = 0.75$ [12]. This last value means that, at saturation of the active sites by the modifier, 75% of the adsorbent surface are occupied by localized modifier molecules. 25% of the surface remain unoccupied due to steric hindrance of the modifier molecules among each other. An analogous conclusion suggests that on diol and cyano, a quarter of the surface can be occupied by localized solvent molecules, whereas on amino, one half is accessible. It is not clear why, at comparable bonding densities (ca. 4 μmol/m^2) and thus comparable silanol density of all three adsorbents, silanol accessibility is double on amino compared to diol and cyano.

Second, we found that the value of the delocalization function $f(Q_k^\circ)$, defined by

$$f(Q_k^\circ) = 1 - \epsilon''/\epsilon' \quad (5)$$

also depends on the type of adsorbent. This function indicates to which amount the standard adsorption energy Q_k° of a group k (here–O–in diethyl ether) is lowered as a result of its delocalization. On diol, cyano and amino, this function takes the values 0.64, 0.35 and 0.66, respectively. When supposing only residual silanols as sites of localization, $f(Q_k^\circ)$ should be independent of the adsorbent type. For cyano, this is clearly not the case. Its $f(Q_k^\circ)$ value is similar to that of bare silica (0.45).

We conclude that localization of ether molecules on residual silanols occurs on all three stationary phases, and that, on diol and amino, it also takes place on the functional groups of the organic moieties. The cyano phase appears, in terms of the analysis of primary solvent effects, equivalent to partially deactivated silica.

In this context it is interesting to look at the observed dead time shifts when increasing the modifier concentration (Fig. 1). At a bonded phase load of 1.4 mmol/g on diol, and 0.8 mmol/g on cyano and amino, and at an apparent density of 0.6 g/cm^3 for these bonded silicas, solvation volumes are 16 μl/mmol on diol, 7.5 μl/mmol on cyano, and 15 μl/mmol on amino. This reflects quite well the order of importance of localization.

3.3. Solute retention

When the solute to be injected is at least moderately polar, it specifically interacts with the adsorbent, and competes with solvent molecules for active sites on the adsorbent. This effect, referred to as site-competition delocalization [14], leads to a weakening of the theoretical adsorption energy of the solute (i.e., the adsorption energy that would be observed without any interacting solvent molecule), and thus, because ϵ is by definition independent of solute nature, to an apparent increase in A_S values of Eq. 1. On the other hand, one condition of validity of Eq. 1 (interactions of solutes with solvent molecules in the mobile phase and in the stationary phase essentially cancel) may no longer be true. Deviations can be described quantitatively by the introduction of a secondary solvent term [1]. The variation of this secondary solvent term is responsible for changes in selectivity in adsorption chromatography. Eq. 1 becomes

$$\log (k'_{AB}/k'_A) = \alpha'(A_S + \Delta A_S)(\epsilon_A - \epsilon_{AB}) + (\Delta_{AB} - \Delta_A) \quad (6)$$

where Δ_A and Δ_{AB} are the secondary solvent terms for solvent A and the mixture of A and B, respectively. Since pentane can be considered not to induce such effects, Δ_A is assumed equal to zero. With $\alpha' = 1$ and $\epsilon_A = 0$ Eq. 6 can be simplified to

$$\log (k'_{AB}/k'_A) = -(A_S + \Delta A_S)\epsilon_{AB} + \Delta_{AB} \quad (7)$$

It can be seen from Eq. 7 that, if the secondary solvent term remains constant, a plot of $\log (k'_{AB}/k'_A)$ against ϵ_{AB} should be linear, with a slope of $-(A_S + \Delta A_S)$ and an intercept of Δ_{AB}.

Table 2 presents capacity factors of some moderately to highly polar solutes as a function of mobile phase composition (ϵ_{AB}). Figs. 3 to 6 show graphs of $\log k'$ versus mobile phase strength for the same solutes. Aldehydes and ketones were not injected on the amino column, since formation of Schiff's bases may occur. Obvious non-linearity can be observed in some cases, especially on the diol and cyano column. This effect is not correlated with solute polarity, since strongly retained 1-octene-3-ol (A16) and anisaldehyde (ALD6) show linear behaviour, and moderately retained esters do not. We believe Δ_{AB} to be responsible for the non-linearity of the graphs. For $\epsilon = 0$, $\Delta_{AB} = \Delta_A = 0$, and thus, for solutes with Δ_B different from zero, Δ_{AB} is dependent on diethyl ether concentration. This leads to non-linearity of the $\log k'$ versus mobile phase strength plot. However, since solute concentration is infinitely lower than diethyl ether concentration even at low modifier percentages, rapid stabilization of Δ_{AB} to a maximum value of Δ_B with increasing diethyl ether concentration should be expected.

We attribute this discrepancy with the experimental behaviour to the heterogeneity of the surface of polar bonded silicas. At low modifier concentrations, ether molecules occupy preferentially the residual silanols, due to the higher resulting adsorption energies compared to the functional groups of the organic moieties. At higher concentrations, the mobile phase will also progressively occupy the bonded moieties. The solvent–solute interactions in the adsorbed mobile phase depend on properties of solvent, solute and stationary phase. Since the nature of the latter varies with increasing modifier concentration, secondary solvent effects, which are the difference between solvent–solute interactions in the adsorbed and the non-adsorbed mobile phase, should vary as well.

We intended to model changes in secondary solvent effects throughout the entire concentration range from 0% to 50% diethyl ether. Therefore, all capacity factors measured, including those at 0% modifier, were considered in our mathematical treatment in Table 2. The regression analysis is based on the approximation that the ratio Δ_{AB}/Δ_B is constant at a given diethyl ether concentration, and independent of the stationary phase. The substitution of the empirical relationship

$$\Delta_{AB} = \Delta_B \log \left(1 + N_B^{0.25}\right) / \log 2 \quad (8)$$

for Δ_{AB} in Eq. 7 yields, via regression, $(A_S + \Delta A_S)$ and Δ_B. Theoretical A_S were calculated from van der Waals surfaces [15] of the parts of the molecules which are totally adsorbed, plus increments for the partially adsorbed alkyl chains [1]. Due to the experimental error inherent in small k', precision of the values seems rather low. Calculation of the ratio of experimental $(A_S + \Delta A_S)$ and theoretical A_S lets us estimate the extent of site-competition delocalization. As expected, this effect occurs for most of the solute–stationary phase combinations of Table 2. On diol, it seems in general to be less pronounced than on cyano and amino. The regression also makes Δ_B directly accessible, and the relative importance of solvent–solute interactions can be discussed. The observed secondary solvent terms significantly different from zero have all negative values, which means that diethyl ether further weakens retention by solute–solvent interaction.

The weakly polar isothiocyanates (butyl isothiocyanate, I1, and 2-phenylethyl isothiocyanate, I2) show Δ_B values near zero, as does the moderately polar aliphatic ketone (2-undecanone, K2). On diol and cyano, esters [ethyl acetate, ES4, and ethyl (E)-2-butenoate, ES13] exhibit high secondary solvent terms,

Table 2
Retention data of moderately to highly polar compounds

Modifier (%)	ϵ_{AB}	log k'									
		I1[a]	I2	ES4	ES13	K2	L2	A16	ALD6	HE8	P1
A_S[b]		[c]	[c]	4.6	6.8	6.0	8.1	7.3	8.6	7.4	6.8
Diol											
0	0	−0.27	0.21	0.34	0.35	0.37	–	–	–	–	–
0.8	0.0118	−0.37	0.07	−0.07	−0.02	0.03	0.99	1.02	0.69	–	–
5	0.0253	−0.55	−0.07	−0.30	−0.28	−0.27	0.63	0.66	0.42	0.90	0.98
20	0.0408	−0.70	−0.27	−0.60	−0.62	−0.64	0.25	0.18	0.13	0.40	0.39
50	0.0639	−0.82	−0.62	−0.82	−0.80	−0.85	−0.16	−0.28	−0.19	−0.05	−0.08
$A_S + \Delta A_S$		6.5	15.0	5.8	6.7	21.4	10.8	13.8	9.0		
$(A_S + \Delta A_S)/A_S$				1.3	1.0	3.6	1.3	1.9	1.1		
Δ_B		−0.17	0.16	−0.90	−0.84	0.00	−1.17	−1.20	−0.82		
Determination coefficient[d]		0.982	0.998	0.998	0.993	0.941	1.000	0.998	1.000		
Degrees of freedom		3	3	3	3	3	2	2	2		
Cyano											
0	0	−0.46	−0.16	−0.32	−0.30	−0.41	0.94	0.04	0.38	0.69	1.17
0.8	0.0013	−0.47	−0.18	−0.46	−0.43	−0.44	0.79	−0.04	0.26	0.60	0.83
5	0.0086	−0.55	−0.29	−0.66	−0.62	−0.62	0.53	−0.30	0.09	0.24	0.21
20	0.0198	−0.72	−0.43	−0.82	−0.82	−0.77	0.27	−0.68	−0.10	−0.17	−0.34
50	0.0382	−0.92	−0.74	−0.96	−0.85	−1.10	−0.09	−1.22	−0.39	−0.62	−0.80
$A_S + \Delta A_S$		12.2	14.9	6.6	14.6	18.3	17.6	29.8	13.5	27.4	25.6
$(A_S + \Delta A_S)/A_S$				1.4	2.1	2.1	2.2	4.1	1.6	3.7	3.8
Δ_B		0.00	0.00	−0.46	−0.32	0.00	−0.41	−0.15	−0.29	−0.34	−1.19
Determination coefficient[d]		0.996	0.997	0.987	0.998	0.991	0.997	0.999	1.000	0.990	0.984
Degrees of freedom		3	3	3	2	3	3	3	3	3	3
Amino											
0	0	−0.17	0.34	0.40	0.42		–	–		–	–
0.8	0.0395	−0.47	0.02	−0.12	−0.09		–	–		–	–
5	0.0646	−0.64	−0.16	−0.51	−0.51		1.17	0.64		1.04	–
20	0.0816	−0.85	−0.41	−0.82	−0.82		0.26	0.11		0.49	0.82
50	0.1003	−1.00	−0.90	−1.00	−1.00		−0.18	−0.37		0.00	0.33
$A_S + \Delta A_S$		7.6	10.3	13.2	14.4						
$(A_S + \Delta A_S)/A_S$				1.9	1.1						
Δ_B		−0.05	0.00	−0.11	0.00						
Determination coefficient[d]		0.991	0.902	0.995	0.994						
Degrees of freedom		3	3	3	2						

[a] Explanation of compound codes: see Table 3.
[b] From molecular dimensions.
[c] A_S for these compounds not available.
[d] Regression model: $\log k_{AB} = \log k_A - (A_S + \Delta A_S)\epsilon_{AB} + \Delta_B \log(1 + N_B^{0.25}) / \log 2$.

while on amino, although most strongly retained, they do not. The aliphatic alcohol (1-octen-3-ol, A16) shows a high Δ_B on diol, but not on cyano. On amino, although no regression could be performed, values suggest a secondary solvent term even higher than on diol.

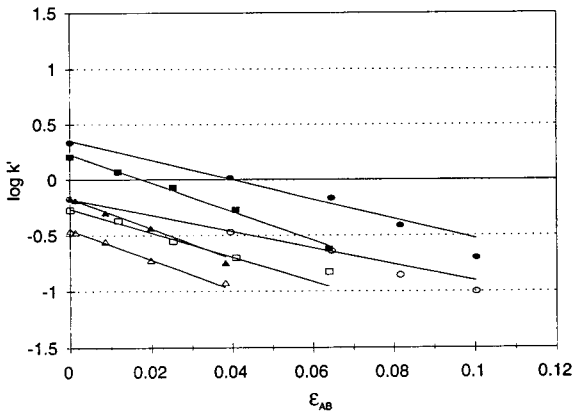

Fig. 3. Logarithm of capacity factors for butyl isothiocyanate (I1, open symbols) and 2-phenylethyl isothiocyanate (I2, black symbols) as a function of solvent strength ϵ_{AB}. Column symbols: rectangles are on diol, triangles on cyano, and circles on amino.

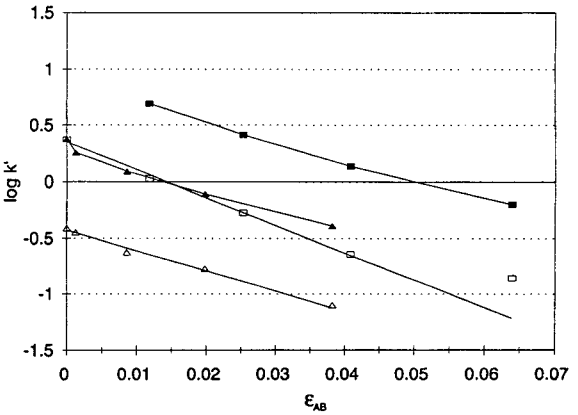

Fig. 5. Logarithm of capacity factors for 2-undecanone (K2, open symbols) and anisaldehyde (ALD6, black symbols) as a function of solvent strength ϵ_{AB}. Symbols of columns as in Fig. 3.

These few examples illustrate that (1) only solutes capable of forming hydrogen bonds exhibit significant secondary solvent terms; (2) the characteristics of the stationary phase are largely responsible for the importance of secondary solvent effects. In fact, while hydroxyl groups on diol can form hydrogen bonds with alcohols (acidic compounds) as well as with esters (basic compounds), no such interaction occurs between amino groups and esters. This means that, although interactions between diethyl ether and esters certainly exist in the non-adsorbed mobile phase regardless of adsorbent type, they are, due

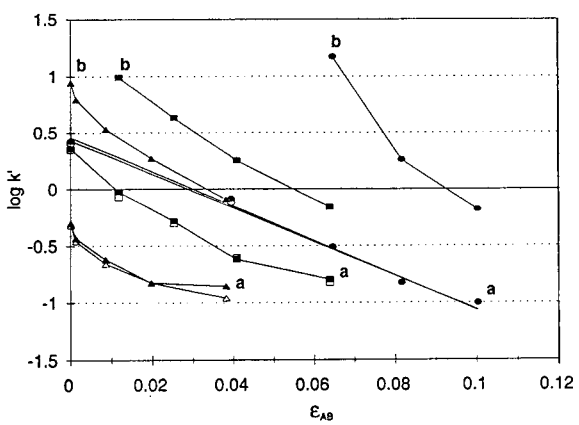

Fig. 4. Logarithm of capacity factors for ethyl acetate (ES1, open symbols), ethyl (E)-2-butenoate (ES2, a) and γ-decalactone (L2, b) as a function of solvent strength ϵ_{AB}. Symbols of columns as in Fig. 3.

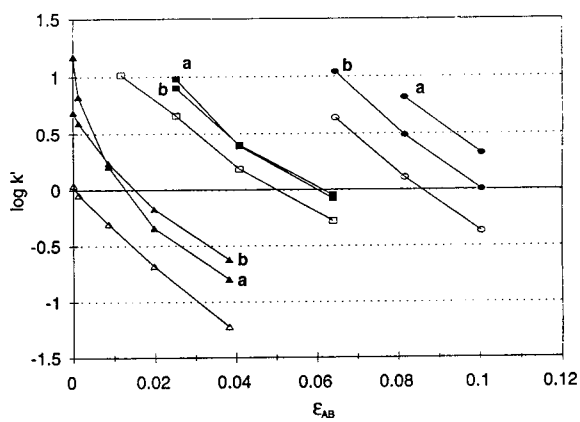

Fig. 6. Logarithm of capacity factors for 1-octene-3-ol (A16, open symbols), phenol (P1, a) and indole (HE8, b) as a function of solvent strength ϵ_{AB}. Symbols of columns as in Fig. 3.

to the low interaction of esters with amino groups on the silica, cancelled by equivalent interactions in the adsorbed mobile phase.

3.4. Column selectivity

About 100 volatile compounds of a wide variety of chemical classes were injected with pentane–diethyl ether mixtures on all three columns. The diol data were taken from a previous publication [10]. The mobile phase composition used for each compound was as previously defined for the diol column. Table 3 summarizes the capacity factors obtained.

The great number of values makes it difficult to interpret this table directly. We therefore believed it was useful to apply principal component analysis (PCA) to the data. This statistical tool allows to define an n-dimensional space (n being the variables, here the three adsorbent types) containing the total variation of the subjects (the solutes). Within this space, $n-1$ planes are defined so that the projection of the subjects and the vectors of the variables onto the first plane visualizes the maximum of variation, the projection onto the second plane the maximum of the remaining variation, and so on. Several types of information are now accessible:
- the greater the angles between the vectors of the variables, the greater their differences;
- the farther the subjects from the center of the plot, the farther their characteristics from the totality of the subjects;
- the nearer two subjects, the closer their relationship;
- the longer the orthogonal projection of a subject onto a vector, the stronger its correlation with the corresponding variable.

The two axes spanning the first plane represent the principal factors responsible for the variations. Its is however rarely possible to attribute to them a physical meaning. Thus, PCA cannot be used for prediction of solutes not included in the original data matrix. Some researchers have already applied this tool to the analysis of chromatographic data [16–19].

PCA was performed on the log (k'/mean k') values, mean k' referring to the mean capacity factor of one solute on all three columns. Fig. 7 shows the plot corresponding to the two principal axes, representing together 97.5% of the variation. All three columns are well distinguished from another and occupy different sectors of the plot. This illustrates important differences in the interaction of solutes with the diol, cyano and amino silica and hence differences in selectivity. Contrary to the discussion of secondary solvent effects in the preceding section, this analysis shows differences in absolute retention, and does not differentiate between the effects responsible for it (ΔA_S or Δ_B). As expected, essentially acidic compounds (alcohols, phenols) are, due to hydrogen bonding with the adsorbent, clearly correlated with the amino column. Predominantly dipolar compounds (nitriles, isothiocyanates), and, more surprisingly, also lactones, are correlated with the cyano column. Ethers and esters are, in their great majority, correlated with the diol column. This indicates a strong interaction of this phase with ether bridges (sp^3 hybridized oxygen). On the other hand, a negative correlation of these compounds with the cyano column can be observed. Ethyl lactate (ES23) behaves like an alcohol because it contains a hydroxyl group.

These results are in general agreement with those obtained in earlier studies on diol, cyano and amino columns. However, it must be pointed out that meaningful comparisons can only be made for specific column–mobile phase combinations, not for columns as a whole, since the same column can exhibit very different characteristics with two different mobile phases. Salotto et al. [3] used group retention values to characterize selectivity differences. They found, for dichloromethane as mobile phase modifier, no significant difference between the amino and the diol column, while the cyano column was described as retaining preferentially dipolar solutes. Smith and Cooper [2] used nitrobenzenes, phenol and aniline as test solutes. They presented their results as selectivity matrices, which describe column characteristics as a function of the selectivity of the mobile phase modifier. In

Table 3
Capacity factors on diol, cyano and amino columns

Code	Compound	Mobile phase[a]	Diol	Cyano	Amino
Saturated alcohols					
A1	Ethanol	4	3.40	0.39	
A2	1-pentanol	4	2.82	0.35	1.86
A3	1-Dodecanol	4	2.41	0.30	1.88
A4	2-Pentanol	4	2.39	0.28	1.81
A5	2-Methyl-1-butanol	4	2.20	0.29	1.84
A6	3-Methyl-1-butanol	4	2.75	0.34	1.87
A7	2-methyl-2-butanol	4	2.39	0.25	1.71
A8	3-Methyl-2-butanol	4	1.99	0.24	1.60
A9	Menthol	4	1.85	0.24	1.45
A10	Fenchyl alcohol	3	4.18	0.14	2.79
Unsaturated alcohols					
A11	2-Buten-1-ol	4	3.16	0.43	3.21
A12	(*E*)-2-Octen-1-ol	4	2.72	0.35	2.50
A13	(*Z*)-3-Octen-1-ol	4	2.68	0.34	2.38
A14	(*Z*)-6-Nonen-1-ol	4	3.22	0.37	2.60
A15	1-Penten-3-ol	3	7.19	0.57	4.86
A16	1-Octen-3-ol	2	9.53	0.91	
A17	α-Terpineol	4	2.38	0.28	1.70
A18	4-Terpineol	3	4.36	0.33	2.27
A19	Carveol	4	2.25	0.32	1.97
A20	α-Bisabolol	3	6.84	0.45	3.11
A21	Geraniol	4	3.70	0.45	3.11
A22	Nerol	4	3.17	0.40	2.60
Aromatic alcohols					
A23	Benzyl alcohol	4	3.88	0.59	4.75
A24	Cinnamyl alcohol	4	5.42	0.79	6.11
A25	Veratryl alcohol	5	5.31	0.68	6.65
A26	Furfuryl alcohol	4	4.15	0.70	5.69
Phenols					
P1	Phenol	4	2.01	0.50	6.59
P2	4-Vinylphenol	4	1.58	0.56	3.33
P3	2-Methoxyphenol	3	4.39	0.76	1.84
P4	2,6-Dimethoxyphenol	5	3.33	0.57	7.64
Ethers and epoxides					
ET1	Diethylether	1	1.09		0.60
ET2	Vitispirane	1	1.15	0.05	0.34
ET3	Methoxybenzene	1	0.74	0.15	0.26
ET4	1,4-Dimethoxybenzene	1	3.83	0.33	1.24
ET5	α-Caryophyllene oxide	2	3.54		1.31
Thiols and sulfides					
S1	Butanethiol	1		0.06	0.05
S2	Dimethyldisulfide	1		0.11	0.15
S3	Dimethyltrisulfide	1		0.11	0.15

Table 3 (*continued*)

Code	Compound	Mobile phase[a]	Diol	Cyano	Amino
Saturated aldehydes					
ALD1	Formaldehyde	4	1.59	0.37	
ALD2	Nonanal	1	1.65	0.24	
Unsaturated aldehydes					
ALD3	Geranial	2	5.49	1.04	
ALD4	Citronellal	1	2.61	0.38	
Aromatic aldehydes					
ALD5	4-Hydroxybenzaldehyde	4	9.33	1.78	
ALD6	Anisaldehyde	3	4.67	1.06	
ALD7	Vanillin	4	7.04	1.66	
ALD8	Coniferaldehyde	5	3.32	1.18	
ALD9	Sinapaldehyde	5	6.72	2.08	
Saturated ketones					
K1	Acetone	3	4.68	1.11	
K2	2-Undecanone	2	2.37	0.36	
K3	5-Undecanone	1	3.17	0.23	
K4	Camphor	2	3.43	0.52	
K5	Menthone	1	2.42	0.36	
Unsaturated ketones					
K6	Artemisia ketone	1	2.20	0.19	
K7	Carvone	2	4.43	0.61	
K8	Dihydrocarvone	2	2.61	0.50	
K9	Verbenone	3	6.76	1.16	
K10	Damascenone	2	2.99	0.47	
Aromatic ketones					
K11	Acetophenone	2	3.73	0.65	
K12	Indonone	3	5.16	0.97	
K13	Benzyl methyl ketone	2	6.32	0.94	
K14	Acetovanillone	4	7.74	1.54	
Miscellaneous ketones					
K15	Acetoine	4	5.00	0.75	
K16	Diacetyl	2	1.69	0.86	
K17	Sotolon	2	3.61	0.59	
Saturated esters					
ES1	Methyl acetate	1	5.40	0.32	1.72
ES2	Methyl tetradecanoate	1	2.31	0.15	0.85
ES3	Ethyl formiate	1	2.47	0.28	
ES4	Ethyl acetate	1	5.42	0.27	1.52
ES5	Pentyl pentanoate	1	1.98	0.15	0.77
ES6	Isopentyl pentanoate	1	1.89	0.16	0.80
ES7	Pentyl isopentanoate	1	1.86	0.15	0.80
ES8	Pentyl 2-methylbutyrate	1	1.75	0.14	0.76
ES9	Isopentyl 2-methylbutyrate	1	1.68	0.14	0.73
ES10	Isopentyl isopentanoate	1	1.72	0.14	0.77
ES11	Bornyl acetate	1	1.87	0.25	1.38
ES12	Fenchyl acetate	1	2.02	0.18	0.82

(Continued on p. 52)

Table 3 (*continued*)

Code	Compound	Mobile phase[a]	Diol	Cyano	Amino
Unsaturated esters					
ES13	Ethyl (*E*)-2-butenoate	1	4.71	0.28	1.60
ES14	Ethyl (*E*)-4-decenoate	1	2.71	0.18	1.03
ES15	Ethyl (*Z*)-4-decenoate	1	2.55	0.17	0.94
ES16	Geranyl acetate	1	5.07	0.27	1.64
ES17	Terpinyl acetate	1	3.49	0.21	1.16
Aromatic esters					
ES18	Benzyl acetate	1	6.90	0.48	2.36
ES19	2-Phenylethyl acetate	2	3.01	0.46	0.62
ES20	Methyl benzoate	1	3.22	0.34	1.24
ES21	Ethyl benzoate	1	2.96	0.32	1.28
ES22	Methyl cinnamate	2	3.39	0.56	1.51
Miscellaneous esters					
ES23	Ethyl lactate	4	2.74	0.34	3.87
ES24	Diethyl malonate	3	2.87	0.66	1.04
ES25	Tributyrine	3	5.10	0.94	1.23
ES26	Tristearine	3	9.09	0.40	0.43
Lactones					
L1	γ-Butyrolactone	2	6.47	1.28	3.20
L2	γ-Decalactone	2	6.43	1.29	3.19
L3	δ-Decalactone	2	6.39	1.27	3.14
Nitriles					
N1	Allyl cyanide	2	2.86	0.79	2.88
N2	Benzyl cyanide	3	3.56	1.52	2.20
Isothiocyanates					
I1	Butyl isothiocyanate	1	0.54	0.23	0.41
I2	2-Phenylethyl isothiocyanate	1	1.73	0.69	1.31
Heterocyclics					
HE1	Menthofuran	1	0.21	0.08	0.05
HE2	Thiophene	1	0.17	0.09	
HE3	Furfural	3	4.34	1.00	
HE4	5-Hydroxymethylfurfural	5	4.63	0.87	
HE5	Pyridine	5	3.50	2.50	0.84
HE6	2-Acetylpyridine	3	4.19	0.44	
HE7	Pyrrole	3	3.90	0.92	1.00
HE8	Indole	4	2.20	0.68	3.08
HE9	2-Acetylpyrrole	4	4.81	0.70	3.52
HE10	Pyrazine	5	2.28	0.34	0.56
HE11	Ethylpyrazine	4	2.48	0.22	0.60
HE12	2-Isobutyl-3-methoxypyrazine	3	1.78	0.07	0.35
HE13	Thiazole	4	2.38	0.48	0.83
HE14	4-Methyl-5-vinylthiazole	4	1.77	0.22	0.54
HE15	2-Acetylthiazole	3	3.11	0.46	1.07

[a] 1 = 100% pentane, 2 = 0.8%, 3 = 5%, 4 = 20%, 5 = 50% diethyl ether.

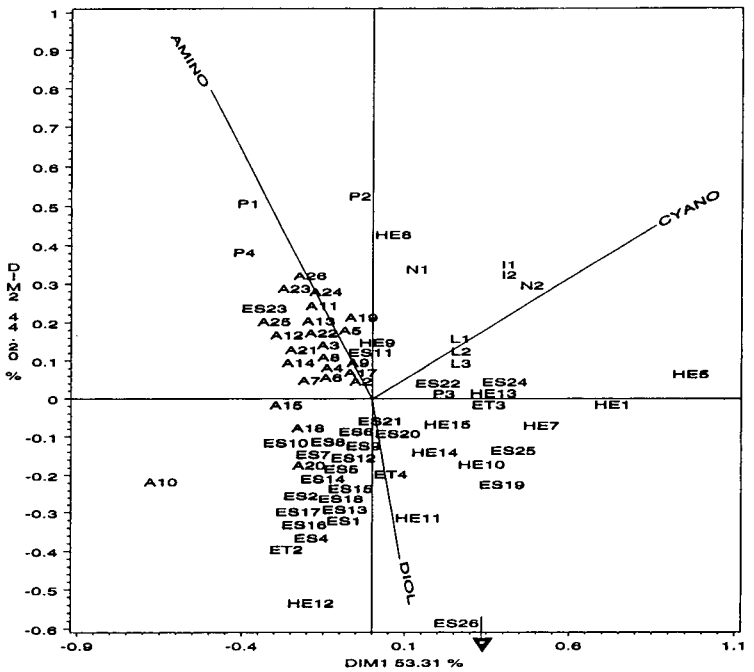

Fig. 7. Principal component analysis on log (k'/mean k') values of Table 3. Correlation coefficients (r): diol–cyano −0.18, diol–amino −0.80, cyano–amino −0.15. Explanation of compound codes: see Table 3. For better legibility of the plot, compound ES26 was shifted upwards. Its original coordinates are: 0.25, −1.02.

an other paper [20], these authors determined extended solubility parameters for the same three columns, and situated the stationary phases in a selectivity triangle. Again, cyano silica was found to be essentially dipolar, while amino and diol silica were basic and dipolar, with little difference.

4. Conclusions

The adsorption model has proven to successfully describe retention on polar bonded silicas, and allowed the quantification of the various phenomena intervening in the retention behaviour. Localization effects were observed on all three stationary phases, although they were less important on the cyano phase. From our results we conclude that restricted-access delocalization not only occurs on residual silanols, but also on the functional groups of the hydrocarbon chains attached to the silica. The order of solute retention corresponds approximately to that found for bare silica. Absolute average retention is weakest on cyano, and highest on diol. However, important differences exist in secondary solvent effects and localization strength, leading to differences in selectivity. The principal component analysis presented here confirms these selectivity effects. It shows particular affinity of diol silica for ethers and esters, while amino silica preferentially retains acidic compounds.

The diol bonded silica seems to be the most versatile phase, since low retention on cyano and the restriction of amino to non-carbonyl compounds may preclude some applications. Nevertheless, both amino and cyano phases can be attractive for on- or off-line multi-column prefractionation techniques, when advantage is

taken of selectivity effects for particular compounds.

Acknowledgements

We are grateful to Shandon France for the loan of two of the three columns used in this study.

References

[1] L.R. Snyder, *Principles of Adsorption Chromatography*, Marcel Dekker, New York, 1968.
[2] P.L. Smith and W.T. Cooper, *J. Chromatogr.*, 410 (1987) 249–265.
[3] A.W. Salotto, E.L. Weiser, K.P. Caffey, R.L. Carty, S.C. Racine and L.R. Snyder, *J. Chromatogr.*, 498 (1990) 55–65.
[4] E.L. Weiser, A.W. Salotto, S.M. Flach and L.R. Snyder, *J. Chromatogr.*, 303 (1984) 1–12.
[5] S. Hara and S. Ohnishi, *J. Liq. Chromatogr.*, 7 (1984) 59–68.
[6] S. Hara and S. Ohnishi, *J. Liq. Chromatogr.*, 7 (1984) 69–82.
[7] W.T. Cooper and P.L. Smith, *J. Chromatogr.*, 355 (1986) 57–74.
[8] L.R. Snyder and T.C. Schunk, *Anal. Chem.*, 54 (1982) 1764–1772.
[9] L.D. Olsen and R.J. Hurtubise, *J. Chromatogr.*, 479 (1989) 5–16.
[10] M. Lübke, J.L. Le Quéré and D. Barron, *J. Chromatogr.*, 646 (1993) 307–316.
[11] L.R. Snyder and J.L. Glajch, *J. Chromatogr.*, 214 (1981) 1–19.
[12] L.R. Snyder, *J. Chromatogr.*, 255 (1983) 3–26.
[13] L.R. Snyder, in Cs. Horváth (Editor), *Mobile-phase Effects in Liquid–Solid Chromatography*, Academic Press, New York, 1983, pp. 157-223.
[14] L.R. Snyder and J.L. Glajch, *J. Chromatogr.*, 248 (1982) 165-182.
[15] A. Bondi, *Physical Properties of Molecular Crystals and Liquids*, John Wiley and Sons, New York, 1968.
[16] M. Righezza and J.R. Chrétien, *J. Chromatogr.*, 556 (1991) 169-180.
[17] T. Cserháti and Z. Illés, *J. Pharm. Biomed. Anal.*, 9 (1991) 685-691.
[18] L. Morin-Allory and B. Herbreteau, *J. Chromatogr.*, 590 (1992) 203–213.
[19] M.C. Pietrogrande, M.I. Turnes Carou and F. Dondi, *Analusis*, 20 (1992) 111–116.
[20] P.L. Smith and W.T. Cooper, *Chromatographia*, 25 (1988) 55–60.

ELSEVIER

Journal of Chromatography A, 690 (1995) 55–63

JOURNAL OF CHROMATOGRAPHY A

Determination of α-dialkylamino acids and their enantiomers in geological samples by high-performance liquid chromatography after derivatization with a chiral adduct of *o*-phthaldialdehyde

Meixun Zhao[1], Jeffrey L. Bada

Scripps Institution of Oceanography, University of California at San Diego, La Jolla, CA 92093, USA

First received 13 June 1994; revised manuscript received 23 September 1994

Abstract

Derivatization with *o*-phthaldialdehyde (OPA) and the chiral thiol N-acetyl-L-cysteine (NAC) is a convenient and sensitive technique for the HPLC detection and resolution of protein amino acid enantiomers. The kinetics of the reaction of OPA-NAC with α-dialkylamino acids was investigated. The fluorescence yield of α-dialkylamino acids was only about 10% of that of protein amino acids when the derivatization was carried out at room temperature for 1–2 min, which is the procedure generally used for protein amino acid analyses. The fluorescence yield of α-dialkylamino acids can be enhanced by up to ten-fold when the derivatization reaction time is increased to 15 min at room temperature. The OPA–NAC technique was optimized for the detection and enantiomeric resolution of α-dialkylamino acids in geological samples which contain a large excess of protein amino acids. The estimated detection limit for α-dialkylamino acids is 1–2 pmol, comparable to that for protein amino acids.

1. Introduction

Developments in two areas of research have resulted in efforts to detect α-dialkylamino acids in nature. For example, α-dialkylamino acids have been identified in abiotic synthesis experiments simulating primitive Earth conditions [1], in carbonaceous condritic meteorites [2] and in sediments (the Cretaceous/Tertiary boundary) associated with the impact of a large asteroid or comet with the Earth [3]. In addition, α-dialkylamino acids have also been shown to be present in several polypepetidic antibiotics [4] and have been incorporated into enzymes without greatly affecting their activity [5]. The observation that these amino acids may serve as specific inhibitors of enzymes that use protein amino acids as substrates has raised interest in their potential as pharmacologically active agents [6].

Interest in the α-dialkylamino acids has led to the utilization of several chromatographic methods for their detection and optical isomer separation. The separation of isovaline enantiomers by gas chromatography (GC) after derivatization with N-trifluoroacetyl anhydride (TFA) and a

[1] Present address: Environmental Sciences Program, University of Massachusetts, Boston, MA 02125-3393, USA.

0021-9673/95/$09.50
SSDI 0021-9673(94)00927-9

chiral alcohol has been successfully achieved [7]. However, attempts to separate optical isomers of α-dialkylamino acids using commercial chiral GC columns has been largely unsuccessful: either poor isomer separation or on-column degradation was observed [8, 9]. Separations by high-performance liquid chromatography (HPLC) either utilizing a chiral mobile complex or employing pre- or postcolumn chiral derivatization have been more successful [10].

Almost all of the reports of the attempted resolution of the enantiomers of α-dialkylamino acids either used authentic compounds, or α-dialkylamino acids were the major components in the mixtures [11]. In efforts to detect α-dialkylamino acids in marine sediments and other geological samples where α-dialkylamino acids are minor components, we have found that most of these methods do not give satisfactory results. Interfering peaks often hindered the identification of the α-dialkylamino acids. In other instances higher sensitivity was required.

The purpose of this study was to develop a sensitive, reliable and routine HPLC method for the detection and simultaneous resolution of optical isomers of α-dialkylamino acids in geological samples in the presence of a large excess of the protein amino acids. A widely used HPLC method for the determination of amino acids is based on the reaction of amino acids with OPA and a thiol [12]. The derivatives formed can be separated on reversed-phase HPLC columns and detected using a fluorescence detector. If the thiol also has a chiral centre, diastereomers will be formed and they often can be separated by HPLC. Aswad [13] used NAC as the chiral thiol and successfully separated the enantiomers of aspartic acid. Nimura and Kinoshita [14] extended the OPA–NAC method to resolve most of the protein amino acids enantiomers. No attempt was made to separate α-dialkylamino acid enantiomers using OPA–NAC in these studies. We demonstrate here that the OPA–NAC method can be used for the detection and resolution of several α-dialkylamino acid enantiomers. Derivatization conditions for the OPA–NAC technique were optimized to enhance the detection of α-dialkylamino acids. The geochemical applications of this method are demonstrated by the identification of α-aminoisobutyric acid (AIB) and racemic isovaline in Cretaceous/Tertiary (K/T) boundary sediments.

2. Experimental

2.1. Reagents and standards

α-aminoisobutyric acid (AIB), α-methylaspartic acid (α-Me-Asp) and α-methylglutamic acid (α-Me-Glu) were obtained from Sigma. Isovaline (Isoval), α-methylvaline (α-Me-Val), α-methylnorvaline (α-Me-n-Val) and α-ethyl-α-aminobutyric acid (α-Et-ABA) were kindly synthesized by Professor Stanley Miller (Department of Chemistry, University of California, San Diego, CA, USA).

HPLC-grade methanol and sodium acetate were obtained from Fisher and OPA and NAC from Sigma. Doubly distilled water was prepared in the laboratory by two consecutive distillations of deionized water in all-glass stills.

NAC solution (1*M*) was prepared by dissolving NAC in doubly distilled water and adjusting the pH to 5–6 with 2 *M* sodium hydroxide. The 1 *M* NAC solution was stored frozen. OPA–NAC derivatization solution was prepared by (1) dissolving 4.00 mg of OPA in 300 μl of methanol, (2) adding 250 μl of 0.4 *M* sodium borate buffer (pH 9.4) to ensure that the solution would be basic, (3) adding 15 μl of 1 *M* NAC and (4) adding 435 μl of water to give a total volume of 1 ml. OPA–NAC solution was prepared fresh weekly and kept frozen in the dark.

2.2. HPLC analysis

Derivatization of amino acids with OPA–NAC was carried out by thoroughly mixing 20 μl of an amino acid solution (normally 1–100 pmol/μl) with 5 μl of OPA–NAC reagent in a poly-

ethylene "microfuge" tube. After 1–15 min, 475 μl of 50 m*M* sodium acetate buffer (pH 5.2) were added to stop the reaction. A 50-μl volume of this solution was injected into an Altex Model 332 HPLC system. The highly fluorogenic derivatives were separated on an Alltech Econosphere C_{18} column (250 × 4.6 mm I.D.). The mobile phases were (A) methanol and (B) 50 m*M* sodium acetate (pH 5.4)–methanol (92 : 8). The column was equilibrated with 100% B. Four minutes after injection, a gradient was started to change the mobile phase to 63% B in 10 min, then to 58% B in another 10 min and to 40% B in 5 min, and this concentration of B then maintained to the end of the analysis. Finally, the mobile phase was changed back to 100% B in 15 min and the system was ready for the next injection. The flow-rate was 1 ml/min. The column effluent was monitored with a Shimadzu RF-530 fluorescence HPLC monitor at an excitation wavelength of 340 nm and an emission wavelength of 450 nm. The results were recorded with a Hitachi D-2500 Chromato-Integrator. The amino acid concentrations in an actual sample were calculated from peak-area integration using the peak area determined from a known amount of authentic standard for comparison.

2.3. HCl cation-exchange chromatography

A preparative-scale acid cation-exchange chromatographic method was utilized to separate AIB and isovaline from interfering protein amino acids [15]. A column of cation-exchange resin (AG 50W-X8, 100–250 μm, hydrogen form) was equilibrated with 1.0 *M* HCl. A mixture of amino acids was placed on the top of the column. Increasing concentrations of HCl were used to elute the amino acids from the column; the eluate was collected with a Gilson fraction collector at a flow-rate of 0.2 ml/min. Each fraction consisted of 2–4ml of solution. Evaporation of the HCl fractions in a desiccator yielded the purified amino acids. The fractions were then dissolved in 1 ml of water and analyzed by the technique described above.

3. Results and discussion

3.1. Kinetics of the derivatization reaction

Under the derivatization conditions given by Aswad [13] and Nimura and Kinosita [14], protein amino acids react with OPA–NAC rapidly at room temperature. However, it has been noted that α-dialkylamino acids react much more slowly with OPA under similar conditions [16]. We therefore decided to carry out a systematic investigation of the reaction kinetics of α-dialkylamino acids with OPA–NAC to test whether this technique can be modified for their sensitive detection.

Initially the same reaction conditions as recommended by Aswad [13] were used, with OPA at 6 m*M* and NAC at 12 m*M* in the derivatization solution (OPA to NAC ratio = 0.5). The amino acid concentration is normally adjusted to about 10–100 μM. Alanine was chosen as an example to observe the reaction of OPA–NAC with protein amino acids. Under these conditions the reaction of alanine with OPA–NAC reaches its maximum yield in less than 2 min, as observed by Aswad [13]. In the next step, the concentrations of OPA and NAC were varied and the reaction kinetics monitored. The results indicated that as long as the concentration of NAC is within the range 1–20 m*M* and the concentration of OPA is more than 10–20 times that of alanine, the reaction is completed within 1–2 min. The rate of reaction and the fluorescence yield are not very sensitive to the ratio of OPA to NAC. If the concentration of OPA is comparable to that of alanine, the derivatization slows considerably. Svedas et al. [17] observed a similar behavior for the reaction of protein amino acids with OPA and mercaptoethanol. They concluded that the OPA concentration should be 2–3 times higher than that of the amino acid. Based on our study and earlier reports, it is recommended that the OPA concentration be at least ten times higher than that of the amino acid for protein amino acid analysis using OPA–NAC.

The same approach was utilized to investigate

the reaction of α-dialkylamino acids with OPA–NAC using AIB as an example. Under the same conditions as used by Aswad [13], this reaction proceeds much more slowly than that with alanine. A detailed study of the kinetics of the AIB reaction was carried out by using various combinations of OPA, NAC and AIB concentrations to determine the best reaction parameters (Fig. 1). These experiments demonstrated that as long as the OPA and NAC concentrations are roughly 10–20 times higher than that of AIB, both the rate of the derivatization reaction and the maximum fluorescence yield are a function of the ratio of OPA to NAC. Fig. 1 shows the fluorescence response of OPA–NAC with AIB as a function of derivatization time at room temperature using various OPA to NAC ratios from 0.25 to 4. It is clear that, at room temperature, this reaction needs at least 15 min to reach equilibrium. When the OPA to NAC ratio is low (e.g., 0.25 and 0.5), equilibrium is not reached even after 25 min. When the OPA to NAC ratio is increased to 1, the reaction is accelerated and equilibrium is achieved within 15 min. At an OPA to NAC ratio of 2, the rate of the reaction is the fastest and the maximum yield is the highest. When the OPA to NAC ratio is increased to 4, the reaction proceeds at roughly the same rate as with a ratio of 2, but the maximum fluorescence yield is about 15% lower. Fig. 1 clearly demonstrates that for the OPA–NAC reaction with AIB, an OPA to NAC ratio of 2 is the optimum to maximize both the reaction rate and the final fluorescence yield.

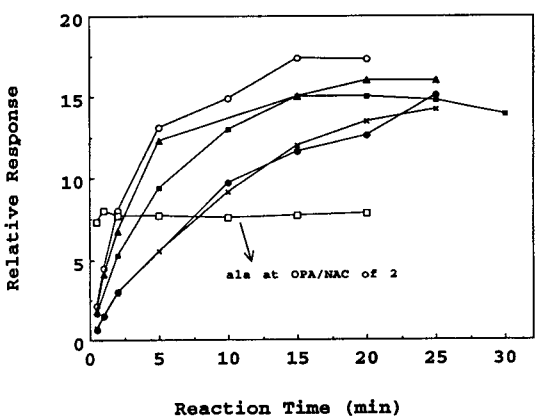

Fig. 1. Kinetics of the reaction of AIB with OPA–NAC with different ratios of OPA to NAC: ○ = 2; ▲ = 4; □ = 1; ● = 0.5; × = 0.25. □ = Alanine. Also shown are the reaction kinetics of alanine with OPA–NAC for OPA/NAC = 2. Concentrations in the derivatization reaction: OPA = 6 m*M*, AIB = 12 μ*M* and alanine = 6 μ*M*. The amount of AIB injected into the column was 30 pmol and that of alanine was 15 pmol.

Our results are in agreement with the report by Cronin et al. [16] that the fluorescent yield of the OPA–β-mercaptoethanol derivative of α-dialkyl-substituted amino acids is much less than that for amino acids with an α-hydrogen when derivatization is carried out for 1–2 min at room temperature. Cronin et al. [16] were able to increase the yield of α-dialkylamino acids by carrying out the reaction at 100°C. Based on our results and those of Cronin et al. [16], it seems that there are two approaches to improve the detection of α-dialkylamino acids: (1) carry out the derivatization at higher temperature (100°C) for 1–2 min, or (2) carry out the derivatization at room temperature for 15–20 min. With the OPA–NAC reaction, derivatization at 100°C increased the fluorescence yield of α-dialkylamino acids but the response of the α-hydrogen amino acids was also substantially affected (e.g., the yield for glycine was decreased by a factor of 10–15). Also, when amino acids extracted from sediments were derivatized at 100°C, several side-reactions occurred that gave rise to unknown peaks which interfered with the detection of several amino acids.

Our kinetic studies of the OPA–NAC reaction with AIB imply that the fluorescent yield for the α-dialkylamino acids can also be increased up to eight-fold if derivatization is carried out for 15 min compared with 1–2 min at room temperature while the yield for the α-hydrogen amino acids is more or less unaffected (see Table 1). This not only improves the detection for α-dialkylamino acids, but also provides another criterion for the identification of the α-dialkylamino acids. By carrying out the derivatization for both 1 and 15 min, we can easily recognize the α-dialkylamino acids by observing the dramatic increase of 5–10-fold in their fluorescent peak size when the chromatograms

Table 1
Retention time, Y15/Y1 ratio and relative molar fluorescence for protein and α-dialkylamino acids

Amino acid	Retention time (min)	Y15/Y1[a]	Molar fluorescence[b]
Asp	7.5–8.9	1	1.04
Glu	11.3	1	1.14
α-Me-Asp	12–12.5	4.6	0.40
α-Me-Glu	12.9–13.6	3.9	1.06
Gly	14.7	0.8	1
Ala	16.7–16.9	1	1.47
AIB	18	8	1.19
Isovaline	19.3–19.6	12	0.93
Val	20.4–21.7	6.1–12	0.43
α-Et-ABA	21.7	6.1–12	0.43
α-Me-Val	22.7–23.5	8–10	0.64
α-Me-Nva	22.5–22.9	3.7–6.8	0.40
Leu	26.8	1	0.73

The retention times would be expected to vary depending on the instrument, column and elution scheme used in the analyses. The values of Y15/Y1 and the molar fluorescence depend on the room temperature and the age of the OPA-NAC reagent. The values given here are those which were found to be representative of those routinely obtained with the present analytical set-up.
[a] Y15/Y1 is the relative fluorescence yield ratio for the 15- and 1-min derivatization times.
[b] Relative to the glycine = 1.0.

for the two reaction times are compared. It is therefore recommended that the OPA–NAC derivatization be carried out for both 1 and 15 min at room temperature for the identification of α-dialkylamino acids.

3.2. OPA–NAC reaction with several α-dialkylamino acids

Our study was extended to include several other α-dialkylamino acids to test whether this method could be generally applied for their identification. The derivatization conditions for all these amino acids were 6 m*M* OPA and 3 m*M* NAC (OPA to NAC ratio = 2) in the derivatization solution. Fig. 2 shows chromatograms for several α-dialkylamino acids. The results in Fig. 2 demonstrate that the same reaction condition as used for AIB analysis can also be applied for other α-dialkylamino acids. With all the α-dialkylamino acids that we have investigated, the yield for the 15-min derivatization (Y15) increased compared with those for 1-min derivatization (Y1). However, the yield enhancement was not the same for all α-dialkylamino acids. The Y15/Y1 ratio ranged from 4 to 12, with isovaline showing the largest increase and α-methylglutamic acid the smallest. Even with the same amino acid, the Y15/Y1 ratio can vary by up to a factor of 2 depending on the age of the OPA–NAC reagent and the room temperature when the analyses are carried out. However, the derivatization yield for all the α-dialkylamino acids is always significantly greater for the 15-min reaction time. The approximate HPLC elution times for several amino acids (both protein and α-dialkyl) are summarized in Table 1 along with the Y15/Y1 ratio.

With the 15-min derivatization, the molar fluorescence yields of α-dialkylamino acids are comparable to those of protein amino acids (see Table 1). In fact, the yields for AIB and isovaline are higher than those for some protein amino acids, such as valine and leucine. The estimated detection limit is 0.3–1 pmol for α-dialkylamino acids based on analyses of authentic compounds. The detection limit for geological samples would be expected to be higher owing to interference from other components present in these complex mixtures.

In studying the OPA–NAC reaction with α-substituted glutamic acid analogues, Maurs et al.

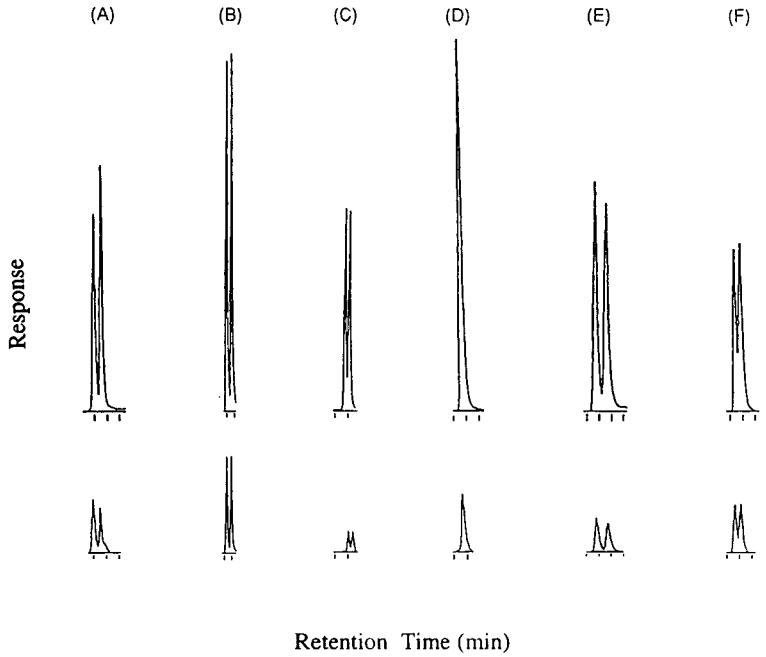

Fig. 2. HPLC of OPA–NAC derivatives of α-dialkylamino acids, obtained with derivatization for (bottom) 1 min and (top) 15 min. (A) D/L-α-Me-Asp; (B) D/L-α-Me-Glu; (C) D/L-Isoval; (D) α-Et-ABA; (E): D/L-α-Me-Val; (F) D/L-α-Me-n-Val. The approximate retention times for these various amino acids are given in Table 1.

[18] gave some conflicting results. They first stated that, despite the steric congestion around the amino group due to α-substitution, α-substituted analogues of glutamic acid react as rapidly as protein amino acids with the OPA–NAC reagent under alkaline conditions. However, they then noticed a significant decrease in the fluoresence response with all the α-substituted amino acids compared with protein amino acids (10–30%). Our results unambiguously demonstrate that α-dialkylamino acids react much more slowly with OPA–NAC at room temperature, but the fluorescence response can be increased with a longer reaction time.

3.3. Resolution of enantiomers

It is critical to evaluate the stereochemistry of α-dialkylamino acids in order to establish their possible biotic or abiotic origin [2]. Although the OPA–NAC technique was originally designed for the detection of protein amino acids and their enantiomers, the chromatograms shown in Fig. 2 illustrate that this technique can also be used to separate the enantiomers of α-dialkylamino acids. It should be pointed out that we do not know the elution order of the enantiomers for the α-dialkylamino acids as we do not have pure isomers. For protein amino acids, the D-enantiomers elute before the L-enantiomers with hydrophilic amino acids such as aspartic acid, whereas the L-enantiomers elute before the D-enantiomers with hydrophobic amino acids such as valine [11, 14]. We predict that the same elution order would also apply to α-dialkylamino acids.

3.4. Detection of AIB and isovaline in geological samples

To demonstrate the application of the OPA–NAC technique for the detection of α-dialkylamino acids in geological samples, we

selected sediments from the K/T boundary sequence at Stevns Klint, Denmark. The K/T boundary marks one of the largest mass extinction episodes in the Earth's history [19]. Convincing evidence has suggested that this mass extinction was caused by the collision of a large extraterrestrial object with the Earth [20–23]. The collision of an asteroid or comet with the Earth may have added extraterrestrial organic matter to the earth since certain meteorites and comets contain a variety of organic compounds [24]. We decided to investigate AIB and isovaline in K/T boundary sediments as these two amino acids have been found to be among the most abundant non-protein amino acids in the Murchison meteorite [2].

Fig. 3 shows the HPLC traces for the total amino acid extract from a Stevns Klint K/T boundary sediment sample. Regions where AIB and isovaline are expected to elute are indicated by arrows. Examination of the chromatograms for the 1- and 15-min derivatization times indicate that AIB and isovaline are probably present in this sample. However, it is obvious that their concentrations are minute compared with those of the protein amino acids. This complicates the detection and quantitation of the α-dialkylamino acids because many small unknown peaks in the chromatogram of the sediment extract may co-elute with AIB and isovaline. However, careful evaluation of the chromatograms still provides preliminary evidence that AIB and isovaline are present. Comparing the 1- and 15-min results, it is seen that, for the peak in the AIB retention time region, the fluorescence yield for the 15-min derivatization was double that for the 1-min derivatization. However, if we examine this peak carefully in the 15-min chromatogram, we notice that peak 9 appears to be a doublet. One explanation is that there are two peaks with a retention time roughly corresponding to AIB. For the 1-min analysis the AIB peak is much smaller than the unknown peak so AIB is totally hidden beneath this unknown peak. For the 15-min analysis, the AIB peak increases 5–8-fold whereas the unknown peak stays more or less the same. As a result, the AIB peak height is comparable to that of the unknown peak.

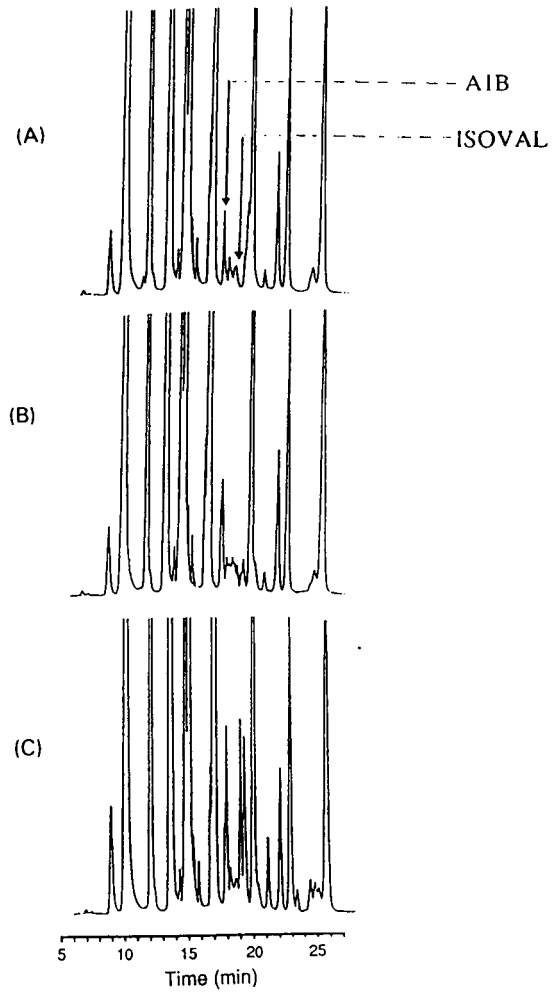

Fig. 3. HPLC of the total amino acid fraction from a sediment sample 0.5 m below the K/T boundary at Stevns Klint, Denmark. HPLC conditions are given in the text. (A) 1-min derivatization; (B) 15-min derivatization; (C) 15-min derivatization after spiking with authentic AIB and racemic isovaline.

Because their retention times are not exactly the same, AIB and the unknown peak appear to be partially separated. The 1-min analysis gives no indication of isovaline in the sample. However, when the sample is derivatized for 15-min the corresponding isovaline peaks apparently emerge. There seems to be two peaks, as would be expected if racemic isovaline was present.

The retention times of both AIB and racemic isovaline in this sample were confirmed by spiking the sediment extract with the authentic amino acids (Fig. 3C).

The analyses of bulk amino acids in K/T boundary sediment extracts gave an indication that K/T boundary sediments probably contain AIB and racemic isovaline, and demonstrated that the OPA–NAC technique could be applied for the detection of these unusual non-protein amino acids in geological samples. However, these analyses are by no means satisfactory. Because the concentrations of AIB and isovaline in K/T boundary sediments are very low compared with those of protein amino acids (the AIB concentration is about 5% of that of alanine in the sample shown), impurities that normally do not interfere with the detection of protein amino acids may interfere with the detection of AIB and isovaline.

To improve this situation, the total amino acid extracts were further separated into fractions using HCl cation-exchange chromatography (see Experimental). With this separation procedure, AIB and isovaline are partially resolved from protein amino acids. Their relative concentration compared with the background of protein amino acids is increased and co-eluting peaks are usually eliminated. The chromatograms of the AIB and isovaline fractions for the same sample shown in Fig. 3 are given in Fig. 4. Here the presence of AIB and racemic isovaline in this K/T boundary sample is clearly demonstrated. By analyzing known amounts of authentic AIB and racemic isovaline, and comparing the resulting peak areas with those in the K/T boundary sample, we were able to estimate [3] that this sediment contains 350 ng/g of AIB and 120 ng/g of racemic isovaline.

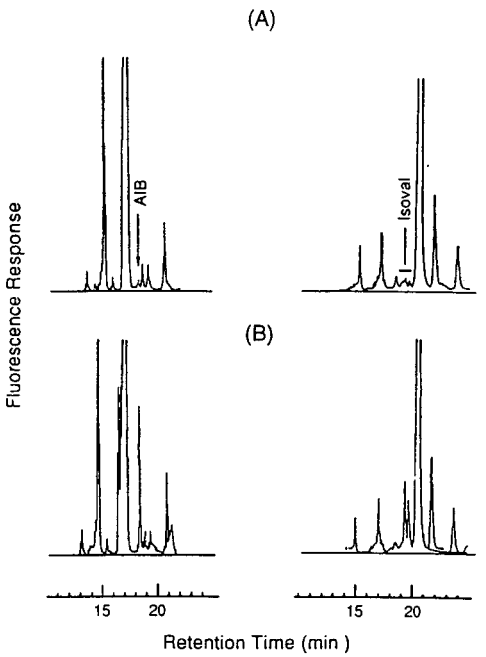

Fig. 4. HPLC of AIB and isovaline HCl cation-exchange chromatographic fractions from the same K/T boundary sample as shown in Fig. 3. HPLC conditions are given in the text. (A) 1-min derivatization; (B) 15-min derivatization.

4. Conclusions

Based on these investigations, we recommended the following procedure for the detection of α-dialkylamino acids in geological samples. The total amino acid extract obtained from a sample should be analyzed using the OPA–NAC technique with both 1- and 15-min derivatization times. If a peak, or peaks, corresponding to a specific α-dialkylamino acid increases several-fold, this provides the first indication that an α-dialkylamino acid is present. Further verification can be accomplished by first partly separating the amino acids using either HCl cation exchange chromatography or some other technique, and then repeating the OPA–NAC analyses. The method provides for the highly sensitive and selective detection of α-dialkylamino acids in natural samples which are dominated by the protein amino acids.

Acknowledgments

This research was supported by NSF grant EAR89-15829. We thank Professor Stanley Miller for synthesizing and providing several of the α-dialkylamino acids used in this study.

References

[1] S.L. Miller, *J. Am. Chem. Soc.*, 77 (1955) 2351.
[2] K.A. Kvenvolden, J.G. Lawless and C. Ponnamperuma, *Proc. Natl. Acad. Sci.* U.S.A., 68 (1971) 486.
[3] M. Zhao and J.L. Bada, *Nature*, 339 (1989) 463.
[4] M.K. Das, S. Raghothama and P. Balaram, *Biochemistry*, 25 (1986) 7110.
[5] J.A. Ellman, D. Mendel and P.G. Schultz, *Science*, 255 (1992) 197.
[6] R.C. Sheppard (Senior Reporter), *Amino Acids, Peptides, and Proteins* (Specialist Periodical Report, Vol. 10), Chemical Society, London, 1979, p. 11.
[7] G.E. Pollock, C.-N. Cheng, S.E. Cronin and K.A. Kvenvolden, *Geochim. Cosmochim. Acta*, 39 (1975) 1571.
[8] S.-C. Chang, R. Charles and E. Gil-Av, *J. Chromatogr.*, 238 (1982) 29.
[9] S. Weinstein, B. Feibush and E. Gil-Av, *J. Chromatogr.*, 126 (1976) 97.
[10] M.H. Engel and B. Nagy, *Nature*, 296 (1982) 837.
[11] H. Bruckner, I. Bosch, T. Graser and P. Furst, *J. Chromatogr.*, 395 (1987) 569.
[12] M. Roth, *Anal. Chem.*, 43 (1971) 880.
[13] D.W. Aswad, *Anal. Biochem.*, 137 (1984) 405.
[14] N. Nimura and T. Kinoshita, *J. Chromatogr.*, 352 (1986) 169.
[15] C.H.W. Hirs, S. Moore and W.H. Stein, *J. Am. Chem. Soc.*, 76 (1954) 6063.
[16] J.R. Cronin, S. Pizzarello and W.E. Gandy, *Anal. Biochem.*, 93 (1979) 174.
[17] V.J.K. Svedas, I.J. Galaev, I.L. Borisov and I.V. Berezin, *Anal. Biochem.*, 101 (1980) 188.
[18] M. Maurs, F. Trigalo and R. Azerad, *J. Chromatogr.*, 440 (1988) 209.
[19] D.M. Raup, *Science*, 231 (1986) 1528.
[20] L.W. Alvarez, F. Asaro and H.V. Michel, *Science*, 208 (1980) 1095.
[21] A. Montanari, R.L. Hay, W. Alvarez, F. Asaro, H.V. Michel, L.W. Alvarez and J. Smit, *Geology*, 11 (1983) 668.
[22] B.F. Bohor, P.J. Modreski and E.E. Foord, *Science*, 236 (1987) 705.
[23] J.F. McHone, R.A. Nieman, C.F. Lewis and A.M. Yates, *Science*, 243 (1989) 1182.
[24] F. Mullie and J. Reisse, *Top. Curr. Chem.*, 139 (1987) 83.

ELSEVIER

Journal of Chromatography A, 690 (1995) 65–70

JOURNAL OF CHROMATOGRAPHY A

Oligonucleotide model with non-identical complementary strands for chromatographic studies of structure-dependent photosusceptibility☆

Vladimir N. Potaman[a,b,*], Valery N. Soyfer[a]

[a]*Department of Biology, George Mason University, Fairfax, VA 22030, USA*
[b]*Institute of Molecular Genetics, Kurchatov Square, Moscow 123182, Russian Federation*

First received 16 August 1994; revised manuscript received 4 October 1994

Abstract

In a previous work, we used a quantitative chromatographic analysis of two self-complementary oligonucleotides to correlate the conformational differences between the oligonucleotide duplexes and photochemical susceptibilities of constituent oligomers. In this work we describe a new double-stranded oligonucleotide model with non-identical complementary strands. To separately analyze photoproducts in two strands, one of them is used in a partially protected form (the hydrophobic 5′-dimethoxytrityl group uncleaved). Using a reversed-phase column, the oligomers and products of their UV photomodification are separated into two groups of peaks. This facilitates the quantitation of photoproducts in each of the complementary strands. Three 15-mer oligonucleotides, 5′-TTTTTAT-TAAATATA-3′ (F5), 5′-AAAAATAATTTATAT-3′ (F6) and 5′-TATATTTAATAAAAA-3′ (F7) form the parallel-stranded (*ps*) F5 · F6 and the ordinary antiparallel-stranded (*aps*) F5 · F7 duplexes. For these particular sequences, the rate of cyclobutane thymine dimer formation in the *ps* DNA has been estimated as ca. 1.5–2 times that in the ordinary *aps* DNA.

1. Introduction

We are developing a chromatographic approach to conformational studies of nucleic acids [1,2]. The positions and/or mobilities of adjacent pyrimidines favorable for the photodimerization depend on the structural details and rigidity of nucleic acid conformations as shown for the double-stranded A, B, B′ forms and the triple-stranded helix [1–5]. Self-complementary decanucleotides were previously used for the reversed-phase chromatographic analysis of the B and B′ form double-stranded helices, and a decreased photoproduct yield in the structurally rigid B′ conformation was shown [1,2]. These decamers and the products of their modification were chromatographically resolved enough to provide their quantitative analysis. However, such self-complementary models are not always available. Another oligonucleotide model could consist of the complementary strands with different sequences. In this approach, it is desirable to separately analyze the photoproducts in both

* Corresponding author.

☆ Part IV in the series High-performance liquid chromatography of the photoproducts of nucleic acid components. For Part III, see Ref. [1].

0021-9673/95/$09.50
SSDI 0021-9673(94)00950-3

```
5'-DMTr-TTTTTATTAAATATA-3' (F5)  ps duplex
     5'-AAAAATAATTTATAT-3' (F6)

5'-DMTr-TTTTTATTAAATATA-3' (F5)  aps duplex
     3'-AAAAATAATTTATAT-5' (F7)
```

strands. In a reversed-phase chromatography this could be achieved by deliberately increasing the hydrophobicity of one strand.

As a new model we chose to study the three 15-mer oligonucleotides, 5′-TTTTTATTAAATATA-3′ (F5), 5′-AAAAATAATTTATAT-3′ (F6) and 5′-TATATTTAATAAAAA-3′ (F7) which form the ordinary antiparallel-stranded (*aps*) F5·F7 and parallel-stranded (*ps*) F5·F6 duplexes [6,7]. They were used to compare the photoproduct yields under UV irradiation. To separately analyze the photoproducts in both duplex strands, one of them was rendered hydrophobic by leaving the 5′-dimethoxytrityl protecting group uncleaved. UV irradiation of oligomers combined into either *aps* or *ps* duplexes resulted in the hydrophobicity changes which were low in comparison with the initial differences in hydrophobicity between complementary (protected and deprotected) oligomers. This allowed the elution of two strands and products of their photomodification out of the reversed-phase column as well separated groups of peaks. Quantitation of the modified oligomers with these specific sequences allowed estimation of the thymine dimerization in the *ps* DNA as ca. 1.5–2 times greater than that in the ordinary *aps* DNA.

2. Experimental

2.1. Materials

Oligonucleotides DMT-d(TTTTTATTAAATATA) (F5), d(AAAAATAATTTATAT) (F6), d(TATATTTAATAAAAA) (F7), d(CCTTTAAAGG) and d(GCGCGCACGTGGGCCCTTGCAGCGCTCTAGACC) were synthesized using standard phosphoramidite chemistry. They were purified by electrophoresis and RP-HPLC. Snake venom phoshodiesterase I (PDE I) was from Pharmacia (Piscataway, NJ, USA). All other chemicals of analytical-reagent grade were from various commercial sources.

2.2. UV Irradiation

Oligonucleotides and their double-stranded complexes were UV irradiated at 300 nm using a Model 1-1430 Foto/Phoresis UV transilluminator (Fotodyne, New Berlin, WI, USA) equipped with four 15 W lamps. The oligonucleotide mixtures of F5·F6 and F5·F7 (1:1 molar ratio chromatographically determined after an exhaustive PDE I digestion) were prepared in 20 m*M* sodium cacodylate, 0.5 *M* NaCl (pH 7.2). The duplexes were annealed from 90°C by a slow cooling (90 min) to −7.5°C. The 1 mm length quartz cells containing oligonucleotide solutions (10 μM strand concentration) were placed just underneath the surface of the partially melted ice prepared with 2.1 *M* NaCl solution (freezing point of −7.5°C [8]) and irradiated from a 1 cm distance for various periods of times.

2.3. Chromatographic conditions

Chromatography was accomplished using a Millipore–Waters system (Milford, MA, USA) consisting of a 600E solvent-delivery unit, a 717 autosampler, and a 996 photodiode array detector, operated under a control of a Millenium 2010 Chromatographic Manager. The products of oligonucleotide photomodification were separated on a NovaPak C_{18} (150 × 3.9 mm) reversed-phase column immersed in a Shel-Lab water bath (Sheldon, Cornelius, OR, USA) using a 0–10% B (10 min), 10–20% B (20 min), 20–50% B (30 min) gradient of 0.1 *M* ammonium acetate, pH 6.8 (eluent A), and acetonitrile–water (1:1, eluent B) at a flow-rate of 1.2 ml/min and 45°C. The chromatographic peak areas were calculated using detector traces at 260 nm, the wavelength for which the extinction coefficients of nucleic acid components are well known.

2.4. Characterization of photoproducts

To localize photoproducts in the oligonucleotide sequences, peaks were collected in Eppendorf tubes; volatile salt was evaporated in a Speed-Vac; the residue was redissolved in a buffer; and then the collected peaks of modified oligomers were subjected to digestion with PDE I which sequentially cleaves 5′-nucleoside monophosphates from the oligomer 3′-end and stops at the photoproduct position. Resulting monucleotides were chromatographically quantitated using a reversed-phase column. Peak areas and molar absorption coefficients were used to calculate the 5′-AMP/5′-TMP ratios that allowed determination of the number of residues between the photoproduct and the 3′-end, that is the sequence position of the photoproducts. Peaks containing cyclobutane thymine dimers were identified using oligonucleotide irradiation at 300 nm in the presence of 5% acetone which promotes the formation of cyclobutane pyrimidine dimers [9,10].

3. Results and discussion

In order to test a new model of nucleic acid structure with the different complementary strands appropriate for chromatographic studies, we chose the partially characterized oligonucleotide system [6,7]. The *ps* F5 · F6 and *aps* F5 · F7 duplexes at 2 m*M* strand concentrations melted at 8°C and 27°C in 10 m*M* cacodylate, 100 m*M* NaCl, pH 7.2 [6]. Under our experimental conditions, the melting temperatures are expected to be several degrees higher due to the increases in strand and salt concentrations [11]. However, to be sure that we irradiated the double-stranded complexes, we used the conditions well below the melting points for F5 · F6 and F5 · F7. The primary photoproducts of UV irradiation under conditions employed are expected to be thymine dimers [9]. To avoid artifacts during the analysis of irradiated samples due to possible on-column association of complementary strands, chromatography was accomplished at the temperature above the melting points for both *ps* and *aps* duplexes.

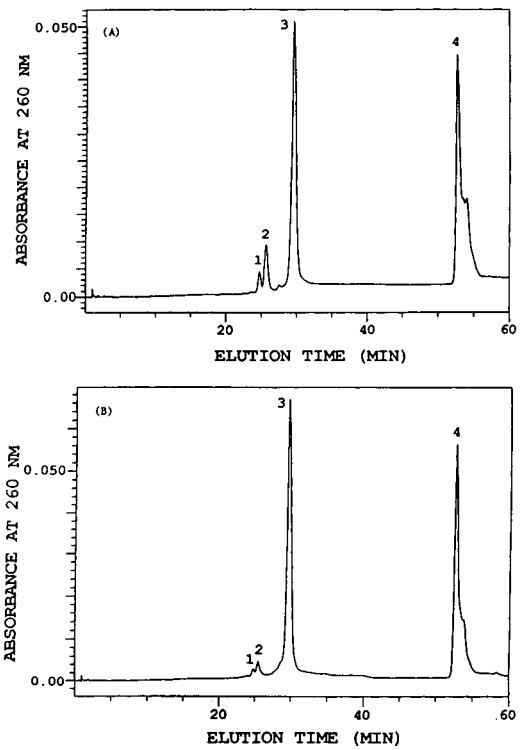

Fig. 1. Chromatograms of the oligonucleotide complexes UV irradiated for 5 min under the conditions in which the double-stranded structures exist (20 m*M* sodium cacodylate, 0.5 *M* NaCl, pH 7.2, −7°C). Column: NovaPak C_{18} (150 × 3.9 mm). Eluents: A, 0.1 *M* ammonium acetate (pH 6.8); B, 50% acetonitrile in water. Gradient: 0–10% B (10 min), 10–20% B (20 min), 20–50% B (30 min) at 45°C. Flow-rate, 1.2 ml/min. (A) *ps* duplex F5 · F6. Peaks: 1 = d(AAAAATAAT< >TTATAT); 2 = d(AAAAATAATT< >TATAT) and other photoproducts of F6; 3 = F6; 4 = DMT-F5 and its photoproducts. (B) *aps* duplex F5 · F7. Peaks: 1 = d(TATAT< >TTAATAAAAA); 2 = d(TATATT< > TAATAAAAA) and other photoproducts of F7; 3 = F7; 4 = DMT-F5 and its photoproducts.

Fig. 1A and B show the chromatograms of UV-irradiated oligonucleotide complexes F5 · F6 (*ps*) and F5 · F7 (*aps*), respectively. The group of peaks 1–3 in panel A corresponds to the oligomer F6 and its photomodification products which have lower retention times. Digestion of collected fractions with PDE I, which sequentially cleaves 5′-nucleoside monophosphates from the oligomer 3′-end and stops at the photoproduct

position, as well as the acetone-sensitized irradiation were used for peak identification. The acetone-sensitized irradiation producing mostly cyclobutane thymine dimers T< >T resulted in accumulation of modified oligomers in peaks 1 and 2. An HPLC quantitation of enzymatically cleaved mononucleotides for peak 1 (data not shown) gave the 5′-AMP/5′-TMP ratio which within a few percent experimental error was that expected for 5′-AAAAATAAT< >TTATAT-3′. Significantly higher peak 2 is a composite one. Its appearance under acetone-sensitized irradiation shows that it contains a modified oligomer 5′-AAAAATAATT< >TATAT-3′. Yet, the 5′-AMP/5′-TMP ratio derived from quantitation of the PDE I digestion products for peak 2 indicates the presence of other photoproducts. Presumably they result from an accumulation of non-cyclobutane photoproducts, the T[6-4]T photoadducts [9]. This suggestion is consistent with our earlier data according to which non-cyclobutane pyrimidine adducts are slightly more hydrophobic than cyclobutane dimers that results in later off-column elution of T[6-4]T-modified oligomers [1,2,12]. The magnitude of peak 2 is closer to that of peak 1 when a single-stranded oligomer is irradiated and these peaks are approximately equal under acetone-sensitized irradiation. The second important feature of this chromatogram is the poor-resolved group of peaks 4 corresponding to the protected oligomer DMT-F5 and the numerous products which result from its modification. In this case, the number of photoproducts is expected to be large since F5 contains several thymine dinucleotide units. Similarly, the panel B contains peaks 1 (5′-TATAT< >TTAATAAAAA-3′), 2 (5′-TATATT< >TAATAAAAA-3′ and some uncharacterized products), 3(F7) and 4 (F5 and its photoproducts). Note that in the case of DMT-F5, photomodified oligomers have longer retention times relative to the parent compound. The reason for this is not clear. However, it is not an artifact: the chromatogram of UV-irradiated partially deprotected F5 has two groups of photoproduct peaks, one in the front of deprotected oligomer and second at the tail of tritylated oligomer (Fig. 2).

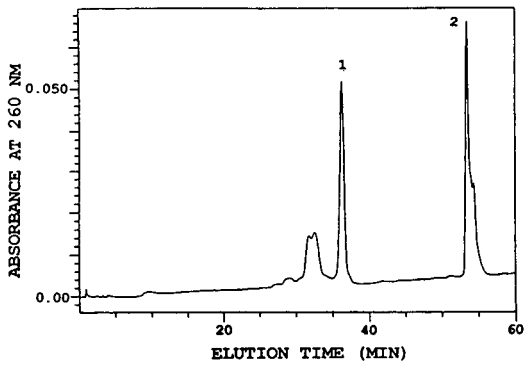

Fig. 2. Chromatogram of the partially protected oligonucleotide F5 UV irradiated for 5 min. Chromatographic conditions as in Fig. 1. Peaks: 1 = F5; 2 = DMT-F5 and its photoproducts.

Thus, it is clear that protected and deprotected oligomers and their photomodification products are eluted out of the reversed-phase column as the separate groups of peaks. This allows a separate analysis of photomodifications in each of the complementary strands. A purposeful optimization may result in the resolution of numerous peaks allowing their total quantitation. At this stage we limited ourselves to the quantitation of only early eluted photoproduct peaks. As mentioned above, these are the homogeneous peaks of primary modification products containing 5′-AAAAATAAT< > TTATAT-3′ and 5′-TATAT< >TTAATAAAAA-3′. A comparison of the rates of cyclobutane dimer formation revealed that they are approximately equal for the adjacent thymine dinucleotides of the same oligomer (data not shown). Therefore, the peaks 1 in these chromatograms can be used as quantitative markers for the primary photodamages in the *ps* and *aps* duplex DNA. Fig. 3 shows that at low extents of modification (several percent of oligomers contain damaged sites, i.e., oligomers contain single dimers), the photosusceptibility of the *ps* DNA is higher than that of the *aps* DNA. The initial accumulation rate for the cyclobutane thymine dimers in the *ps* duplex F5 · F6 is two times greater than that in the *aps* duplex F5 · F7 and 1.5 times greater than in the *aps* duplex form of self-complementary oligonucleotide d(CCTTTAAAGG) which was used as an additional double-

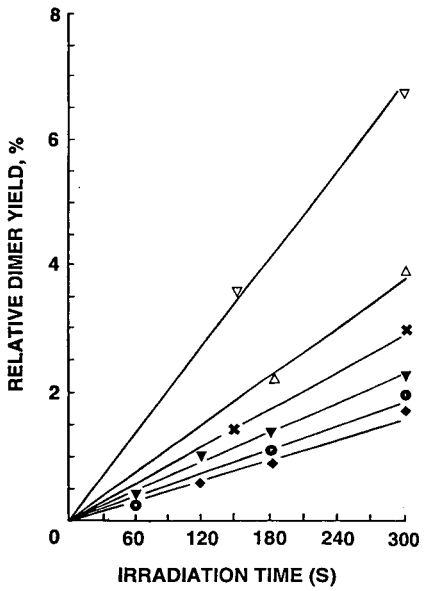

Fig. 3. Time courses of a single-position cyclobutane thymine dimer accumulation (calculated relative to the initial amounts of unmodified oligomers) in oligonucleotides in the different structural forms. Conditions: 20 m*M* sodium cacodylate, 0.5 *M* NaCl, pH 7.2, −7.5°C. ▽ = single-stranded d(GCGCGCACGTGGGCCCT< >TGCAGCGCTCTAGACC); △ = AAAAATAAT< >TTATAT in *ps* F5·F6 duplex; × = CCT< >TTAAAGG in *aps* duplex; ○ = TATATT< >TAATAAAAA in *aps* F5·F7 duplex; ▼ = AAAAATAAT< >TTATAT in F6 alone; ◆ = TATATT< >TAATAAAA in F7 alone.

stranded control. Under the same conditions the single strands F6 and F7, which we planned to use for the determination of the photosusceptibility of single-stranded nucleic acids, have lower degrees of modification than expected [9]. Examination of their sequences shows a possibility of their self-aggregation as they can form imperfect self duplexes with 10 base pairs (compare with 15 base pairs in perfect duplexes). The photomodification properties of these aggregated single strands were similar to those of the duplex conformations. In another single-stranded con trol, d(GCGCGCACGTGGGCCCTTGCAGCGCTCTAGACC), the cyclobutane thymine dimers formed faster than in both *ps* and *aps* duplexes.

According to the early studies, the photosusceptibility of single-stranded DNA is greater than that of its double-stranded form [9,13]. The rate of thymine dimer formation in the *ps* F5·F6 duplex is intermediate between those for single-stranded form and the ordinary *aps* F5·F7 duplex. This could be explained by the conformational differences between the *ps* and *aps* duplexes and/or increased structural mobility of bases in the *ps* duplex relative to the *aps* duplex. Compared to the B-DNA *aps* duplex, the *ps* duplex has a very different surface shape, and the two grooves are of approximately equal width [14]. There was no direct experimental measurement of the base mobilities in the *ps* nucleic acids. Molecular dynamics calculations show that in comparison with the *aps* DNA the *ps* DNA is more fluctuating structure [15]. This gives it some single-stranded character, which is confirmed by its increased susceptibility to the single-strand specific reagents (e.g., Os-pyridine, or potassium permanganate) [16]. However, the photosusceptibility of adjacent thymines in both single- and double-stranded nucleic acids may significantly depend on the nearest neighbors [13]. Clearly, more possible sequence variants should be tested to reach a general conclusion about the differences in photosusceptibilities of *ps* and *aps* nucleic acids. Yet, the present results allow us to conclude that unlike other non-B DNA forms (A, B′, triplex) where the formation of dipyrimidine photoproducts is significantly inhibited, the *ps* DNA has the photosusceptibility comparable to that of the usual *aps* B-DNA.

The oligonucleotide models are useful because (i) the short lengths and relative simplicities allow a quantitative analysis of various modifications in them by a chromatographic technique, and (ii) they approximate short DNA sequences (a few dozen nucleotides long) where unusual structures (B′, Z forms, cruciform, triplex, etc.) different from a regular B form DNA have been found [17–19]. The present results show the usefulness of a new oligonucleotide model of nucleic acid structure which can be analyzed by the HPLC technique. In order to separately quantify the photoproducts formed in different strands of the double-stranded DNA fragment, we artificially increased the hydrophobicity of one strand leaving it in a partially protected form. This allowed the products of

photomodification to be separately analyzed for each of the complementary strands. We used the simplest way to obtain the hydrophobically modified oligonucleotide. Yet, other hydrophobicity modifications (e.g., oligonucleotide conjugation with cholesterol [20]) can be used for a significant increase in the oligonucleotide retention time.

We described a new oligonucleotide model which is suitable for the structure-dependent UV modification. Many chemical compounds known to react with DNA are used as the structure-dependent probes or to produce some mutagenic lesions [21,22]. Their sequence specificity and the structures of adducts are often studied using the oligonucleotide models. The new oligonucleotide model is suitable also for such multiple-site reacting chemicals. In many cases the formation of chemical adducts results in an increase of the on-column oligomer retention, which is significantly lower than expected for the difference in retention between partially protected and completely deprotected unmodified strands [23–25]. Thus, our model seems to be applicable to the chromatographic analysis of both chemical and photochemical modifications of oligonucleotide duplexes.

Acknowledgements

We are grateful to Dr. Vikas Chandhoke, Director, and Mr. Michael Southall of the Shared Research Instrumentation Facilities at George Mason University for their help during chromatographic experiments. We are also indebted to Dr. Oleg Voloshin of the National Institutes of Health for supplying most of the oligonucleotides studied.

References

[1] V.N. Potaman, I.P. Chernov and V.V. Demidov, *J. Chromatogr.*, 648 (1993) 151–156.
[2] V.V. Demidov and V.N. Potaman, *Nucleic Acids Res.*, 21 (1993) 2691–2696.
[3] M.M. Becker and Z. Wang, *J. Biol. Chem.*, 264 (1989) 4163–4167.
[4] V.I. Lyamichev, M.D. Frank-Kamenetskii and V.N. Soyfer, *Nature*, 344 (1990) 568–570.
[5] V. Lyamichev, *Nucleic Acids Res.*, 19 (1991) 4491–4496.
[6] T.M. Jovin, K. Rippe, N.B. Ramsing, R. Klement, W. Elhorst and M. Vorlickova, in R.H. Sarma and M.H. Sarma (Editors), *Structure and Methods: Vol. 3: DNA and RNA*, Adenine Press, New York, 1990, pp. 155–174.
[7] K. Rippe and T.M. Jovin, *Methods Enzymol.*, 211 (1992) 199–220.
[8] V.I. Perelman (Editor) *The Concise Chemist Handbook*, Khimiya Press, Moscow, Leningrad, 1964, p. 394.
[9] N.K. Kochetkov and E.I. Budovskii (Editors), *Organic Chemistry of Nucleic Acids*, Part B, Plenum Press, London, New York, 1972, pp. 543–618.
[10] R. Rycyna, J.C. Wallace, M. Sharma and J.L. Alderfer, *Biochemistry*, 27 (1988) 3152–3163.
[11] D. Rentzeperis, K. Rippe, T.M. Jovin and L.A. Marky, *J. Am. Chem. Soc.*, 114 (1992) 5926–5928.
[12] V.V. Demidov and V.N. Potaman, *J. Chromatogr.*, 285 (1984) 135–142.
[13] J. Cadet and P. Vigny, in H. Morrison (Editor) *Bioorganic Photochemistry*, Vol. 1. Wiley, New York, 1990, pp. 1–272.
[14] N. Zhou, M.W. Germann, J.H. van de Sande, N. Pattabiraman and H.J. Vogel, *Biochemistry*, 32 (1993) 646–656.
[15] A.E. Garcia, D.M. Soumpasis and T.M. Jovin, *Biophys. J.*, 66 (1994) 1742–1755.
[16] J. Klysik, K. Rippe and T.M. Jovin, *Biochemistry*, 29 (1990) 9831–9839.
[17] R.D. Wells and S.C. Harvey (Editors), *Unusual DNA Structures*, Springer, New York, 1988.
[18] E. Palecek, *Crit. Rev. Biochem. Mol. Biol.*, 26 (1991) 151–226.
[19] G. Yagil, *Crit. Rev. Biochem. Mol. Biol.*, 26 (1991) 475–559.
[20] S.M. Gryaznov and D.H. Lloyd, *Nucleic Acids Res.*, (1993) 5909–5915.
[21] D.M.J. Lilley, *Methods Enzymol.*, 212 (1992) 133–139.
[22] B. Singer and D. Grunberger, *Molecular Biology of Mutagens and Carcinogens*, Plenum Press, New York, 1983.
[23] M.J. Pillaire, G. Villani, J.S. Hoffmann, A.M. Mazard and M. Defais, *Nucleic Acids Res.*, 20 (1992) 6473–6479.
[24] M. Cosman, V. Ibanez, N.E. Geacintov and R.G. Harvey, *Carcinogenesis*, 11 (1990) 1667–1672.
[25] T. Oida, W.G. Humphreys and F.P. Guengerich, *Biochemistry*, 30 (1991) 10 513–10 522.

ELSEVIER

Journal of Chromatography A, 690 (1995) 71–76

JOURNAL OF CHROMATOGRAPHY A

Stability study and content uniformity of prochlorperazine in pharmaceutical preparations by liquid chromatography

Adnan El-Yazigi[a,*], Fida Abdel Wahab[a], Barma Afrane[b]

[a]*Department of Biological and Medical Research, King Faisal Specialist Hospital and Research Centre, Riyadh 11211, Saudi Arabia*

[b]*Department of Pharmacy Services, King Faisal Specialist Hospital and Research Centre, Riyadh 11211, Saudi Arabia*

First received 22 March 1994; revised manuscript received 5 August 1994

Abstract

The stability of prochlorperazine (PCZ) in pharmaceutical admixtures and the content uniformity of its dosage forms were examined by liquid chromatography. The drug and internal standard (imipramine) were separated on a CN Radial-Pak cartridge using sodium acetate solution (0.018 *M*)–acetonitrile (5:95, v/v) as the mobile phase, and were detected in the eluate at 250 nm. The assay was highly linear ($r > 0.993$), and the relative standard deviations (R.S.D.s) at 5, 12.5 and 25 μg/ml were 7.8, 4.1, and 4.3%, respectively. The deviations from perfect accuracy at these concentrations were 6.4, 1.6, and 6.0%, respectively. The mean percentages (with R.S.D.s) of the labelled claim found in a commercially available injection, syrup, tablet and suppository were 103.9 (3.5%), 103.8 (3.6%), 100.5 (1.5%) and 101.1 (5.0%), respectively. Although the drug was stable in sterile dextrose solution (5%, w/v) at 4°C (refrigeration) with protection from light, it degraded rapidly in a bi-exponential fashion at 23°C (room temperature), particularly when unprotected from light. Poorer stability was observed under all conditions examined when PCZ was formulated in normal saline.

1. Introduction

Prochlorperazine, 2-chloro-10-[3-(1-methylpiperazinyl)propyl]phenothiazine (PCZ), is an antiemetic and antipsychotic agent widely used in the prevention and control of nausea and vomiting [1,2] associated with chemotherapy or radiation treatment of cancer. The drug is often dispensed by the hospital pharmacy to the patient's bedside in the form of an intravenous admixture; however, for clinical reasons or after death it may remain unused, requiring disposal. This may prove to be expensive and troublesome if it occurs frequently, particularly in major cancer centres. Unfortunately, no data are available on the stability of PCZ to evaluate the feasibility of preserving these preparations for use in different patients.

Although a few liquid chromatographic (LC) methods have been reported for the determination of PCZ [3–6], LC has not been used to examine the stability of the drug in pharmaceutical admixtures. Unlike in spectrophotometry, in LC the compounds are separated prior to determination.

This study was undertaken to examine the

* Corresponding author.

0021-9673/95/$09.50
SSDI 0021-9673(94)00897-3

stability of prochlorperazine in intravenous admixtures under different storage conditions and to investigate the content uniformity of its commercially available dosage forms by use of an LC method.

2. Experimental

2.1. Materials

Analytical samples of prochlorperazine edisylate and imipramine hydrochloride (internal standard) were supplied by Sigma (St. Louis, MO, USA). Acetonitrile, pentane, 2-propanol (all from Fisher, Fair Lawn, NJ, USA) and sodium acetate (Fluka, Buchs, Switzerland) were of HPLC grade. Water for HPLC was generated by passing "reverse osmosis" water through a 0.45-μm membrane filter (Millipore, Milford, MA, USA).

2.2. Pharmaceutical formulations

Four commercially available formulations of prochlorperazine, i.e., 10-mg tablets, 5-mg suppositories, 5 mg per 5 ml syrup (Compazine; Smith Kline and French, Philadelphia, PA, USA) and 5 mg/ml injections (Prochlorperazine Edisylate USP; Wyeth, Philadelphia, PA, USA), obtained from a local hospital pharmacy were analysed for their content uniformity of PCZ.

2.3. Instrument

The chromatograph (Waters, Milford, MA, USA) consisted of a system controller (Model 720), a solvent-delivery pump (Model 6000A), an autosampler (Model 710B WISP), a radial compression module (RCM 8×10) equipped with a μBondpack CN Radial-Pak cartridge and a Guard-Pak precolumn module with a CN insert, a variable-wavelength UV–visible detector (Lambda-Max Model 480) set at 250 nm and a data module (Model 730). The mobile phase was a mixture of sodium acetate solution (0.018 *M*) and acetonitrile (5:95, v/v), filtered and degassed before use. The flow-rate was 4 ml/min at a pressure of <1000 lb/in.^{2}.

2.4. Calibration

The concentration of PCZ in the test samples was calculated by use of calibration graphs (peak-height ratio versus concentration) in the range 5–25 μg/ml of PCZ on different days. The linearity of the assay was also established by constructing calibration graphs in the range 2–50 μg/ml. To 200-μl aliquots of a freshly prepared stock standard solution of the internal standard in water (100 μg/ml), different volumes of a freshly prepared stock standard solution of PCZ in water (1 mg/ml) were added and the final volume of each sample was brought to 2 ml with water to yield concentrations in the above range. The solutions were transferred to microvials and the autosampler was programmed to inject 200 μl of each solution.

2.5. Precision

The intra-run (within-day) precision was investigated by analysing replicate samples of PCZ in aqueous solutions at concentrations of 5, 12.5 and 25 μg/ml. The preparation of the samples and the analysis were performed as described above.

2.6. Stability study

The stability of PCZ in sterile normal saline (NS) and dextrose (5%, w/v) (DX) solutions was investigated under three different conditions: room temperature (i.e., 23°C) with protection from light (RT-LP), room temperature with no protection from light (RT-LUP) and at 4°C (refrigeration) with protection from light (RF-LP). On the day of the experiment, an appropriate volume of an injection of PCZ (5 mg/ml) was thoroughly mixed with sterile NS or DX solution to yield a concentration of PCZ equivalent to 20 mg/l. A 200-μl volume of this solution stored under RT-LP, RT-LUP or RF-LP conditions was diluted to 2 ml with water and placed in an autosampler vial, and the autosampler

(which was protected from light with aluminium foil for the LP experiment) was programmed to inject 200 μl every 15 min for 13 h. To maintain the RF-LP condition, a 200-μl autosampler microvial placed in an autosampler vial filled with ice was used, and the diluted solution, which was kept at 4°C, was replenished between injections. The concentration of PCZ was calculated using calibration graphs constructed daily from fresh stock standard solutions prepared immediately prior to each experiment.

2.7. Determination of prochlorperazine in dosage forms

Tablets

The tablet was pulverized into a fine powder and carefully placed in a 1-l volumetric flask. After dilution to volume with water, the liquid was thoroughly mixed and stirred for 2 h using a magnetic stirrer and filtered. Triplicate samples (9 ml each) of the filtrate were taken quickly and analysed as described above after the addition of the internal standard (1 ml of 100 μl/ml solution). The concentration of PCZ was calculated using a calibration graph prepared under similar conditions. Ten different tablets were analysed.

Injections

A 2-ml aliquot of the injection solution (5 mg/ml) was carefully placed in a 1-l volumetric flask and diluted to volume with water. After the liquid has been thoroughly mixed, triplicate samples (9 ml each) of the solution were taken and analysed as described above after the addition of internal standard (1 ml of 100 μg/ml solution). Ten different injection units were analysed.

Syrup

A 1-ml volume of syrup (5 mg per 5 ml) was placed in a 100-ml volumetric flask and diluted to volume with water. After the liquid had been thoroughly mixed, triplicate samples (9 ml each) of the solution were taken and analysed as described above after the addition of internal standard (1 ml of 100 μg/ml solution). Five different batches of syrup were analysed.

Suppositories

A suppository was carefully unwrapped and weighed, and one fifth of the total mass (equivalent to 1 mg of PCZ) was cut out and placed in a 100-ml volumetric flask containing 80 ml of 2-propanol–pentane (3:97, v/v). After the flask had been tightly sealed, the liquid was thoroughly shaken then stirred for 15 min. After dilution to volume with the above organic solvent mixture and thorough mixing, the extract was filtered. Duplicate samples of the filtrate were dried under a stream of nitrogen after addition of the internal standard, and the residue was reconstituted with 200 μl of the mobile phase and analysed as described above. Complete recovery (>97%) was obtained with this extraction procedure. Ten different suppositories were analysed.

3. Results and discussion

Fig. 1 shows a typical chromatogram for PCZ in a diluted tablet extract sample supplemented with an appropriate amount of the internal standard (I.S.). Under the described conditions the compounds were fully resolved and yielded sharp and symmetrical peaks with a total chromatographic time of less than 7.5 min.

The concentration of PCZ in the pharmaceutical preparations examined was calculated by use of peak-height ratio (PCZ/I.S.) (PHR) versus concentration (C) calibration graphs constructed immediately prior to analysis under similar conditions. The assay was highly linear ($PHR = 0.0068 \pm 0.00066 + 0.1147 \pm 0.0072C$) with correlation coefficients (r) ranging between 0.993 and 0.999. The intercept and slope of this equation represent the mean ± S.D. of ten determinations. The intra-run precision was equally good with relative standard deviations (R.S.D.s) at 5, 12.5 and 25 μg/ml of 7.8, 4.1 and 4.3% (Table 1); the deviations from perfect accuracy at these concentrations were 6.4, 1.6, and 6.0%, respectively (Table 1).

The content uniformity of four different commercially available dosage forms of PCZ were examined according to the described procedure,

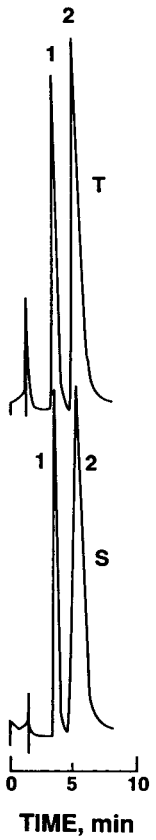

Fig. 1. Representative chromatograms of a tablet extract (T) and a standard sample (S) of PCZ (peak 2). Each of these samples contained 10 μg/ml of the internal standard (peak 1), and the concentrations of PCZ were 13.6 μg/ml (measured) and 12.5 μg/ml, respectively.

and the results obtained are presented in Table 2. The mean percentages (with R.S.D.s) of the labelled claim found in ten injections, five syrups, ten tablets and ten suppositories were 103.9 (3.5%), 103.8 (3.6%), 100.5 (1.5%) and 101.1 (5.0%), respectively, which fall within the content uniformity limits specified by the USP (Table 2).

Table 2
Content uniformity of commercial prochlorperazine formulations

Unit no.	Percentage of labelled claim			
	Tablet	Suppository	Injection	Syrup
1	99.3	106.5	102.2	105.3
2	99.5	96.6	106.8	104.1
3	100.1	93.4	108.7	97.6
4	99.0	105.6	103.8	104.3
5	100.0	99.5	101.0	107.6
6	98.6	102.4	105.8	
7	102.3	102.0	101.2	
8	102.5	98.0	96.9	
9	102.5	97.7	104.6	
10	101.3	109.5	107.7	
Mean	100.5	101.1	103.9	103.8
R.S.D. (%)	1.5	5.0	3.5	3.6

The stability of PCZ in sterile normal saline (NS) and dextrose (5%, w/v) (DX) solutions at a concentration equivalent to 20 mg/l was examined under RM-LP, RM-LUP and RF-LP conditions as described above. Although the drug was stable in DX solution when kept in a refrigerator (RF-LP), it degraded rapidly at room temperature in a bi-exponential fashion (Fig. 2):

$$C = Q\,e^{-\sigma t} + R\,e^{-\delta t} \quad (1)$$

where C is the concentration of the drug remain-

Table 1
Accuracy and precision of the method

Concentration prepared (μg/ml)	Concentration found[a] (μg/ml)	R.S.D. of concentration[a] (%)	Deviation from perfect accuracy[b] (%)
5.0	4.68	7.8	6.4
12.5	12.70	4.3	1.6
25.0	26.50	4.1	6.0

[a] $n = 10$.
[b] Estimated as 100(concentration prepared − concentration found)/concentration prepared.

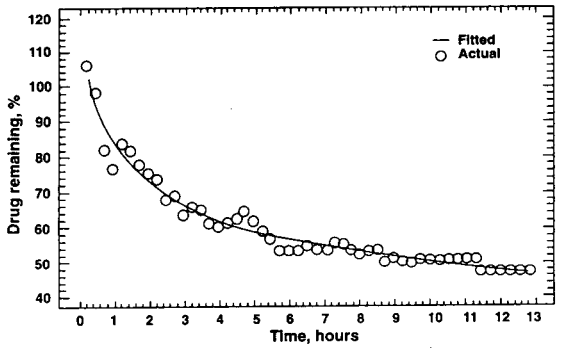

Fig. 2. Stability profile of PCZ (20 mg/l) in sterile dextrose solution (5%, w/v) stored at room temperature (23°C) unprotected from light (DX, RT-LUP). The data were fitted to a bi-exponential equation and the solid line represents the best fit.

ing, σ and Q are the apparent first-order rate constant and pre-exponential coefficient for the rapid phase of degradation (or disappearance) of the drug, respectively, and δ and R are the apparent first-order rate constant and pre-exponential coefficient for the slow phase of degradation, respectively. Hence it appears that the drug undergoes a reversible reaction ($A \rightleftharpoons B$), and its chemical decomposition occurs irreversibly (to an unspecified specie) only when it is in the original form (A), or

$$\begin{array}{c} A \rightleftharpoons B \\ \downarrow \end{array}$$

The percentage of the drug remaining was fitted non-linearly to Eq. 1 using the STATGRAPHICS Statistical Graphic System package (Statistical Graphics, Rockville, MD, USA), and the rapid (σ) and slow (δ) rate constants of degradation of PCZ in solution were generated (Table 3). The corresponding half-lives ($t_{1/2\sigma}$ and $t_{1/2\delta}$, respectively) ranged between 0.082 h (NS, RT-LUP) and 1.31 h (DX, RT-LP) for the rapid phase of degradation and between 24.6 h (DX, RT-LUP) and 71.7 h (NS, RT-LP) for the slow phase of degradation. These half-lives were readily calculated from the relationship $t_{1/2\sigma} = 0.693/\sigma$ or $t_{1/2\delta} = 0.693/\delta$. As shown in Table 3, the drug in both DX and NS solutions was as expected more stable under LP than under LUP conditions. It is noteworthy that whereas the drug was stable in DX solution under refrigeration, it lost about 21% of its original amount in NS within 1.75 h, after which it remained constant for the duration of the experiment. It appears that the drug under the same temperature or light-protection conditions was more stable in the dextrose solution than in normal saline, possibly owing to the primary and secondary salt effect of sodium chloride on the velocity of the degradative reaction. Hence it may be recommended that the intravenous admixture of PCZ should be used immediately after preparation, and if there is any delay in administration, it may be utilized in patients only if formulated in dextrose solution and stored in a refrigerator away from light.

Table 3
Apparent rate constants for degradation of prochlorperazine

Storage conditions	Degradation rate constant (h^{-1})		r^2
	σ	δ	
DX, RT-LUP	0.709	0.0282	0.963
DX, RT-LP	0.527	0.0190	0.948
NS, RT-LUP	8.503	0.0265	0.940
NS, RT-LP	0.574	0.00967	0.933

NS = Normal saline; DX = dextrose (5%, w/v) sterile solutions; LP = protection from light; LUP = no protection from light; RT = room temperature (23°C); σ and δ = apparent first-order rate constants for rapid and slow phases of degradation of PCZ, respectively; r = correlation coefficient.

Acknowledgement

The authors thank the Administration of the King Faisal Specialist Hospital and Research Centre for its support of the drug analysis research programme in this institution.

References

[1] J. Lapiere, M. Amin and S. Hattargadi, *Can. Psychiatr. Assoc. J.*, 14 (1969) 267.
[2] M.C. Nahata, C. Ford and F.B. Ruymann, *J. Clin. Pharmacol. Ther.*, 17 (1992) 121.

[3] A. Fowler, W. Taylor and D.N. Bateman, *J. Chromatogr.*, 380 (1986) 202.
[4] M.G. Sankey, J.E. Holt and C.M. Kaye, *Br. J. Clin. Pharmacol.*, 13 (1982) 578.
[5] J.K. Cooper, G. McKay and K.K. Midha, *J. Pharm. Sci.*, 72 (1983) 1259.
[6] J.E. Kountourellis and C.K. Markopoulou, *J. Liq. Chromatogr.*, 14 (1991) 2969.

ELSEVIER

Journal of Chromatography A, 690 (1995) 77–82

JOURNAL OF CHROMATOGRAPHY A

Determination of cyanide by high-performance liquid chromatography using postcolumn derivatization with *o*-phthalaldehyde

Koichi Sumiyoshi[a,*], Takao Yagi[a], Hiroshi Nakamura[b]

[a]*Tokyo Customer Support Centre, Shimadzu Corporation, 380-1 Horiyamashita Hadano-city, Kanagawa 259-13, Japan*
[b]*Department of Analytical Chemistry, Faculty of Pharmaceutical Sciences, University of Tokyo, 7-3-1 Hongo, Bunkyo-ku, Tokyo 113, Japan*

First received 31 January 1994; revised manuscript received 11 October 1994; accepted 11 October 1994

Abstract

A simple, highly sensitive and selective method for the determination of cyanide ion by high-performance liquid chromatography (HPLC) with postcolumn fluorescence derivatization is described. Cyanide ion was separated on an ion-exclusion chromatographic column and derivatized with two reagents, ammonium ion in the mobile phase and *o*-phthalaldehyde in the postcolumn reagent solution at pH 9.5. Sulfite ion, 2-mercaptoethanol and 3-mercaptopropionic acid did not interfere with the analysis. The average recovery of cyanide from spiked environmental water samples (river water) was 99.0% ($n = 6$). The relative standard deviation was 2.5% (based on peak area) for cyanide standard solutions (0.1 μg/ml, $n = 10$). The linear determination range was from 2.5 ng/ml to 1 μg/ml. The detection limit was 0.1 ng/ml (signal-to-noise ratio = 3, injection volume 200 μl).

1. Introduction

Cyanide ion is found in industrial wastewater and river water. Because of its extreme toxicity, the development of a sensitive and selective analytical method is highly desirable. HPLC and ion chromatography (IC) using various detection methods have been reported for this purpose. The electrochemical method, which has been considered the most sensitive, has interference problems [1]. The conductivity method [2], based on the formation of cyanate ion, and the spectrophotometric method [3], based on the König reaction, are often limited by low sensitivity. The precolumn fluorescence derivatization method, based on the reaction of cyanide with 1,4-benzoquinone, which has high selectivity, has the problem that the calibration graph is non-linear below 1 μg/ml for a potassium cyanide solution [4]. It is known that *o*-phthalaldehyde (OPA) reacts with cyanide ion and primary amines or primary amino acids to afford highly fluorescent isoindole derivatives [5,6]. These methods can be utilized in precolumn or postcolumn derivatization modes, but for the former a complicated procedure is necessary to

* Corresponding author.

0021-9673/95/$09.50
SSDI 0021-9673(94)00976-7

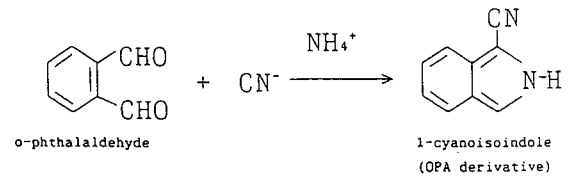

Fig. 1. Fluorogenic reaction of cyanide ion with OPA and ammonium ion.

remove contaminants and block thiols, sulfite and sulfide ion prior to derivatization, whereas for the latter it is necessary to use two pumps for the derivatizing reagents, i.e., OPA and primary amines or primary amino acids [5,6].

Cyanide ion can be derivatized to a fluorescent substance by reaction with ammonium ion and OPA according to the scheme in Fig. 1 [5]. This work was aimed at establishing a simple and sensitive fluorimetric method for determining cyanide ion by utilizing this reaction. Specifically, cyanide ion was separated from related compounds on an ion-exclusion chromatographic column and was then derivatized with two reagents, ammonium ion in the mobile phase and OPA in the postcolumn reagent solution, requiring only two pumps. The method described is simple and highly effective in decreasing the noise level cause by pumping the two postcolumn reagent solutions in addition to the pumping of the mobile phase.

Additionally, we describe its application to the determination of cyanide ion in river water and industrial wastepaper, demonstrating the utility of the proposed method.

2. Experimental

2.1. Reagents

OPA, potassium cyanide, boric acid, diammonium hydrogencitrate, perchloric acid, sodium hydroxide, 2-mercaptoethanol, 3-mercaptopropionic acid, sodium sulfite and methanol were obtained from Wako (Osaka, Japan).

A standard solution of cyanide (0.10 μg/ml) was prepared by dissolving potassium cyanide in 0.1 *M* sodium hydroxide solution. The concentration of cyanide was calibrated by titration with silver nitrate according to the Japanese Industrial Standard (JIS) method [7].

2.2. HPLC apparatus and analytical conditions

Fig. 2 shown a flow diagram of the HPLC postcolumn derivatization system, which consists of two microvolume double-plunger pumps (LC-10AD) for the eluent and the postcolumn derivatization reagent, a variable-wavelength fluorimetric detector (RF-10A) equipped with a xenon lamp and a 12-μL flow cell, a sample autoinjector (SIL-10A), a column oven (CTO-10A) and PTFE tubing (5–30 m × 0.5 mm I.D.) for the mixing coil (all from Shimadzu, Kyoto, Japan).

The HPLC conditions were as follows: column, Shim-pack SCR-102H polystyrene matrix strong cation exchanger (d_p = 7 μm, 300 mm × 8.0 mm I.D.) (Shimadzu); eluent, 10 m*M* ammonium citrate buffer (pH 3.3) at a flow-rate of 0.8 ml/min; postcolumn derivatization reagent,

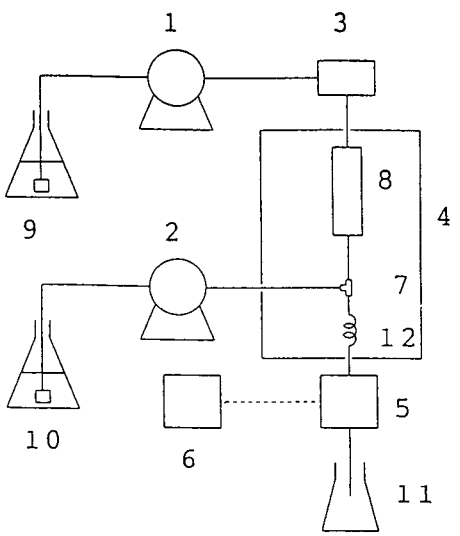

Fig. 2. Flow diagram for the HPLC postcolumn derivatization of cyanide ion. 1, 2 = Pumps; 3 = sample injector; 4 = column oven; 5 = fluorescence detector; 6 = data processor; 7 = mixing joint; 8 = analytical column; 9 = mobile phase; 10 = OPA reagent; 11 = waste; 12 = mixing coil (15 m × 0.5 mm i.d.).

0.5 *M* sodium borate buffer (pH 7–13) containing 54 m*M* OPA methanolic solution (flow-rate 0.15 ml/min); excitation and emission wavelengths of the spectrofluorimeter set at 328 and 370 nm, respectively; column and mixing coil maintained at 30–50°C in the column oven. Chromatograms were recorded with a Shimadzu Model C-R7A recording integrator.

3. Results and discussion

Diammonium hydrogencitrate was selected as the source of ammonium ions because it contained essentially no contaminants such as sulfide or sulfite, which gave interfering fluorescence on reaction with OPA in the presence of ammonium ion and thus caused interference.

In the following investigation, the reaction coil length, the pH of the OPA buffer, the reaction temperature and the excitation and emission wavelengths were optimized. Sano et al. [5] reported the optimum pH for the reaction of cyanide with OPA and taurine to be 9.0. Using flow-injection fluorimetry, with ammonium in place of taurine, the effect of the pH of the borate solution on the fluorescence intensity of the derivatized cyanide ion was investigated. The reaction conditions were as follows: reaction time, 15 min at room temperature; 1.0 mg/ml cyanide standard solution 50 μL; 0.5 *M* sodium borate buffer (pH 7–13, adjusted with concentrated sodium hydroxide) containing 54 mmol/l OPA methanolic solution, 750 μl; 10 m*M* diammonium hydrogencitrate (pH 3.3), 4 ml; wavelengths, $\lambda_{ex} = 328$ nm, $\lambda_{em} = 370$ nm. In the pH region above 9, the fluorescence intensity increased, as was reported using taurine [5], and the maximum intensity was achieved at pH 9.5.

The effect of the reaction coil length on the peak height and the peak area was examined. As shown in Fig. 3, the peak height and peak area increased with increasing reaction coil length up to 15 m. On the other hand, when a coil length of 15 m or more was used, the peak height decreased significantly for the diffusion, but the peak area remained stable and high. Consequently, a reaction coil length of 15 m was suitable in this method. When using a coil length of 15 m at a total flow-rate of 0.95 ml/min, it took 3.1 min (186 s) for the eluate to reach the detector after exiting the column.

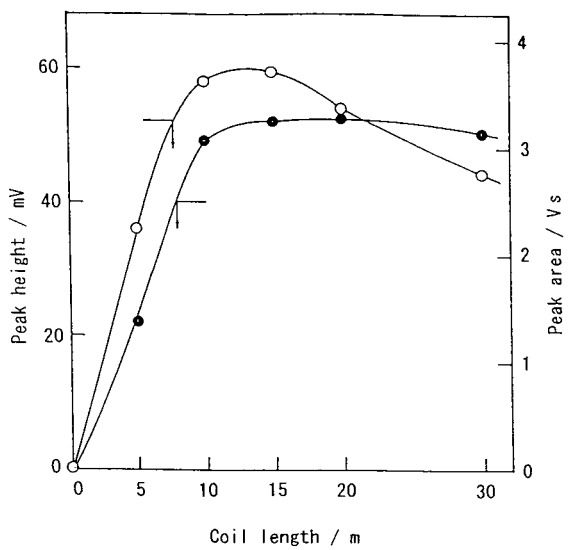

Fig. 3. Effects of reaction coil length on (○) peak height and (●) peak area. pH of OPA reagent, 9.5; 0.1 μg/ml cyanide standard solution, 10 μl; other conditions as in Section 2.2.

The effect of the reaction temperature on the fluorescence peak area was investigated. The reaction conditions were as follows: reaction time, 3.1 min; pH of OPA reagent, 9.5; 1.0 μg/ml cyanide standard solution, 10 μl; other conditions as those given in Section 2.2. The fluorescence peak area for the cyanide derivative increased with increasing temperature from 30 to 50°C. However, when the reaction temperature was 45°C or above, the background noise level of the eluent itself was relatively high. In consideration of the sensitivity, the optimum reaction temperature was determined to be 40°C.

Following the fluorescence scanning technique using the stopped-flow method, the excitation and emission spectra of OPA-derivatized cyanide were investigated under the above-selected conditions. The maximum excitation and omission wavelengths obtained were at 328 and 370 nm, respectively, which are close to the reported maximum excitation (330 nm) and emission

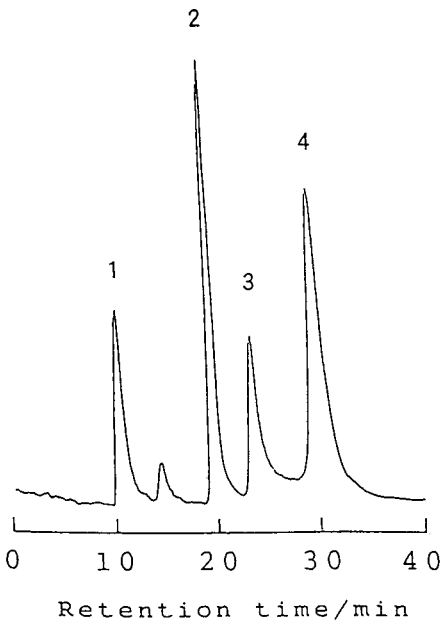

Fig. 4. Chromatogram of sulfite ion, cyanide ion, 2-mercaptoethanol and 3-mercaptopropionic acid, derivatized with OPA and ammonium ion. Peaks: 1 = sulfite ion (1 ng); 2 = cyanide ion (1 ng); 3 = 2-mercaptoethanol (100 ng); 4 = 3-mercaptopropionic acid (100 ng). Chromatographic conditions as in Section 2.2.

wavelengths (371 nm) of OPA-derivatized cyanide using taurine [5].

The proposed method should show no interference from the presence of primary amines or primary amino acids in the samples, because of the difference in excitation and emission wavelengths normally used in the determination of these substances with OPA derivatization (λ_{ex} = 360 nm and λ_{em} = 450 nm, respectively) [8]. It is well known that OPA also reacts with organic thiols such as 2-mercaptoethanol and 3-mercaptopropionic acid and with sulfite ion in the presence of primary amines or primary amino acids to afford the fluorescent isoindole derivatives [9,10]. Therefore, the separation of those compounds and cyanide ion was investigated. A typical chromatogram of the above compounds and cyanide ion in standard solution is depicted in Fig. 4. It was found that the determination of cyanide ion was not interfered with by the sulfur compounds because they were completely separated in the ion-exclusion mode. This also suggests that it is possible to determine these compounds and cyanide ion simultaneously.

3.1. Calibration graph and accuracy

The reliability of the proposed method was tested by the following experiments. A linear calibration graph was obtained over the concentration range 2.5–1000 ng/ml cyanide ion per 20 μl of sample. Linear regression analysis resulted in the following equation: $y = -1.06 + 3.821x$, where y = peak area (mVs) and x = concentration (ng/ml). The regression coefficient was 0.9999. The relative standard deviation was 2.5% for 0.1 ng/ml cyanide standard solution (n = 10) (Table 1).

A series of recovery tests were performed by adding one volume of cyanide standard (1 μg/ml) to nine volumes of the river water and comparing the results with those for an equivalent cyanide standard solution (0.1 μg/ml). The mean recovery of cyanide ion was 99% with a relative standard deviation of 2.2% (n = 6) (Table 1). Before the recovery tests, metal ions in the river water were determined by cation-exchange chromatography. As the concentration of Fe(III) from the river water was below about 10 ng/ml and other metal-related complex

Table 1
Accuracy and precision of the postcolumn derivatization system

Sample	n	Peak area (Vs) (mean ± S.D.)	R.S.D. (%)	Recovery (%)
Standard	10	2.37 ± 0.06	2.5	
Spiked river water	6	1.11 ± 0.02	2.2	99.0

cyanides were not detected, spiked cyanide (100 ng/ml) was completely recovered from the river water.

One of the standard methods for determining of cyanide is molecular absorptiometric analysis (pyridine–pyrazolone spectrophotometric method), which is the recommended JIS method [7]. The cyanide in water is classified into free cyanide (HCN, CN^-) and complex cyanide [$Fe(CN)_6^{4-}$, $Fe(CN)_6^{3-}$, $Cu(CN)_4^{3-}$, etc.]. The cyanide in an environmental sample is determined after converting cyanide ion by pretreatment distillation in acidic solution in accordance with the JIS method.

The analytical data for the proposed method were in fair agreement with those for the JIS method in the range above 0.1 ppm. Consequently, using the proposed method without the distillation pretreatment, the analytical data for an environmental sample indicated the concentration of free cyanide. As the detection limit of the JIS method is 0.1 ppm, the proposed method could not be compared with it in the range below 0.1 ppm.

It was found that the resolving power of the analytical column and the stability of the pumping pressure were unchanged over the ca. 1000 samples used during the investigation.

The detection limit for cyanide ion in standard solution obtained by the present method is about 0.1 ng/ml for 200 μl of sample with a signal-to-noise ratio of 3. The sensitivity reported here is approximately two orders of magnitude higher than that reported for the taurine and OPA system [5].

3.2. Application

One of the major advantages of the present method is its extremely high sensitivity and selectivity compared with other HPLC and IC techniques for cyanide ion. The method is particularly well suited for the determination of cyanide ion in environmental waters such as industrial wastewater and river water. In order to test the utility of the proposed method, such samples were analysed and typical chromatograms are shown in Fig. 5. By use of ion-exclusion chromatography as described above, a sample could be injected without clean-up steps. Cyanide ion was not detected in the river water. In contrast, cyanide ion was detected in industrial wastewater from a plating bath prior to treatment with wastewater treatment equipment. The proposed method showed no interference from complex cyanides, because the latter in environmental water eluted at the retention volume of the exclusion limit and separated completely with free cyanide in the ion-exclusion mode.

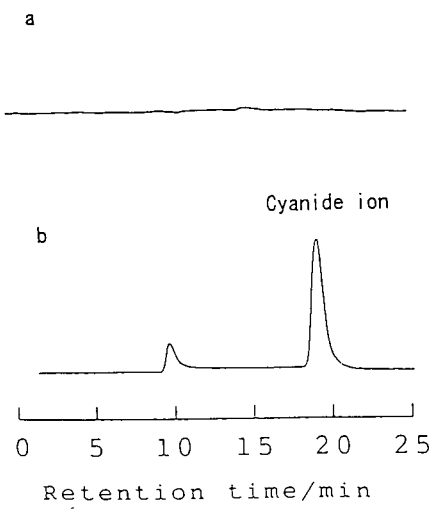

Fig. 5. Chromatograms of (a) river water and (b) industrial wastewater from a plating bath. (a) Sampling from the River Nogawa, Japan; (b) sampling prior to treatment with wastewater treatment equipment. Chromatographic conditions as in Section 2.2.

4. Conclusions

In conclusion, a highly sensitive, reproducible and selective determination of cyanide was performed using ion-exclusion chromatography employing a simplified postcolumn derivatization with OPA and ammonium ion. This method allows cyanide ion to be detected at the level of 0.1 ppb in environmental waters.

References

[1] R.D. Rocklin and E.L. Johnson, *Anal. Chem.*, 55 (1983) 4.
[2] M. Nonomura, *Anal. Chem.*, 59 (1987) 2073.
[3] T. Imanari, S. Tanabe and T. Toida, *Chem. Pharm. Bull.*, 30 (1982) 3800.
[4] Y. Suzuki and T. Inoue, *Bunseki Kagaku*, 33 (1984) 425.
[5] A. Sano, S. Takitani and M. Takezawa, *Anal. Sci.*, 2 (1986) 491.
[6] K. Gamoh and H. Sawamoto, *Anal. Sci.*, 4 (1988) 665.
[7] Japanese Industrial Standards Committee (Editor), *Testing Method for Industrial Wastewater (JIS K 0102)*, Japanese Standards Association, Tokyo, 1986.
[8] M. Roth, *Anal. Chem.*, 43 (1971) 880.
[9] H. Nakamura and Z. Tamura, *Anal. Chem.*, 53 (1981) 2190.
[10] K. Mopper and D. Delmas, *Anal. Chem.*, 56 (1984) 2557.

ELSEVIER

Journal of Chromatography A, 690 (1995) 83–91

JOURNAL OF CHROMATOGRAPHY A

Physico-chemical characterization of chemically bonded stationary phases including metal complexes by inverse gas chromatography

W. Wasiak[a,*], A. Voelkel[b], I. Rykowska[a]

[a]*Faculty of Chemistry, Adam Mickiewicz University, ul. Grunwaldzka 6, 60-780 Poznań, Poland*

[b]*Institute of Chemical Technology and Engineering, Poznań University of Technology, Pl.M. Skłodowskiej-Curie 2, 60-965 Poznań, Poland*

First received 8 June 1994; revised manuscript received 22 September 1994

Abstract

The solubility parameter δ_2 and dispersive force parameters were estimated for a group of chemically bonded stationary phases. Selected physico-chemical parameters were determined by means of inverse gas chromatography. The influence of the structure of the liquid phases examined on their properties was evaluated and discussed.

1. Introduction

The retention mechanism of components of mixtures to be separated by complexation gas chromatography is based on at least two systems. In one case, they are organic complexes formed by analyte molecules and stationary phases with electron-donor or electron-acceptor properties. Aromatic or unsaturated compounds with several electron-withdrawing substituents, such as NO_2, Cl or CN, are efficient electron acceptors. Tetracyanoethylene or 1,3,5-trinitrobenzene may serve as examples. Such compounds when supported on a support, dissolved in an inert stationary phase or chemically bound to a silica surface are employed in GC, TLC and HPLC [1].

The other group consists of packings where metal cations are the main factor responsible for the chromatographic separation. Electron-deficient species, such as many metal cations, have at least one empty valence orbital available for extra coordination. As a result, they are capable of complexing appropriate electron-donating species. A typical example is Ag^+, cation which has been widely used since 1962 for the separation of unsaturated compounds. Most frequently it is employed in the form of $AgNO_3$ dissolved in glycol or squalane [2]. The stabilities of complexes formed by alkenes and silver depend on the anion of the silver salt ($BF_4^- > ClO_4 \gg NO_3^-$). Other factors influencing the stability of a complex of a metal cation and solute molecules are valency, electronic structure and radius of the central metal ion. A significant role is also played by steric effects and the basicity of molecules to be separated on a column. In addition to unsaturated hydrocar-

* Corresponding author.

0021-9673/95/$09.50
SSDI 0021-9673(94)00921-X

bons, other soft bases containing N, O or S heteroatoms (n-donors) have been separated on complexing stationary phases in GC [3–5]. In addition to silver, various complexing metal ion compounds containing, e.g., Hg^{2+}, Cu^{2+}, Pd^{2+}, Ni^{2+} and Co^{2+} have also been investigated.

In order to eliminate the effect of the liquid stationary phase (which acts as a solvent for a metal salt) and to increase the packing stability, metal cations are bound to a silica surface with the help of suitable silanes having their hydrocarbon chain terminated with an appropriate functional group, e.g., diphenylphosphine, thiol, cyano, amino [6–8]. One such group is β-diketone, the complex-forming properties of which were used in this study in order to bind Cu(II), Ni(II) and Pd(II) cations to a SiO_2 surface.

These compounds have not so far been characterized with respect to physico-chemical parameters often used in the description of the properties of commercial stationary phases, surfactants and extractants [9–14]. One of the most interesting parameters used in characterization of polymers [14–17], commercial stationary phases [18–20] and surfactants [21–24] is the solubility parameter δ_2, defined by Hildebrand and Scott [25] and introduced into inverse gas chromatographic experiments by DiPaola-Baranyi and Guillet [15,26].

In an inverse gas chromatographic (IGC) process, a volatile diluent injected on to the column has a tendency to be absorbed by the liquid phase, i.e. the examined compound (product). This tendency is a function of the solute–solvent interaction parameter κ and is measured in terms of retention, e.g., specific retention volume V_g. The interaction parameter was usually obtained at the limit of zero concentration of the solute and was calculated as follows:

$$\kappa_{12}^{\infty} = \ln\left(\frac{273.15R}{P_1^0 V_g M_1}\right) - \frac{P_1^0}{RT}(B_{11} - V_1^0) + \ln\left(\frac{\rho_1}{\rho_2}\right) - \left(1 - \frac{V_1^0}{V_2^0}\right) \quad (1)$$

where M_1, P_1^0, B_{11}, V_1^0, ρ_1 and V_g^0 are the molecular mass, saturated vapour pressure, second virial coefficient, molar volume and specific retention volume of the solute, respectively, ρ_2 and V_2^0 are the density and molar volume of the stationary phase, respectively, T is the column temperature and R is the gas constant.

The solubility parameter δ_2 of the liquid phase was calculated from the following equation:

$$\frac{\delta_1^2}{RT} - \frac{\kappa_{12}^{\infty}}{V_1^0} = \frac{2\delta_2}{RT} \cdot \delta_1 - \left(\frac{\delta_2^2}{RT} + \frac{\kappa_S^{\infty}}{V_1^0}\right) \quad (2)$$

where δ_1 is solute solubility parameter and κ_S^{∞} is entropic term of the interaction parameter. On plotting the left-hand side of Eq. 2 versus δ_1 one obtains a straight line with slope proportional to δ_2 of the polymer. Most often excellent linearity of Eq. 2 was found [14]. However, in some instances deviations from a straight line were reported [21–24,27].

The procedure proposed by Voelkel and coworkers [21–24] allowed the calculation of the increments of the solubility parameter corresponding to dispersive (δ_d), polar non-hydrogen bonding (δ_p) and hydrogen bonding (δ_h) interactions. There have been numerous reports of the examination of the properties of surfactants and extractants by IGC [11,14,21–24,28–36]. The parameters used therein may be divided into two groups: (i) empirical parameters (e.g., polarity index) and (ii) parameters having a strong physical meaning (e.g., thermodynamic functions of solution, Gibbs excess function of solution, criterion A). The advantages and restrictions in using these parameters have been discussed [11]. A number of empirical relationships were evaluated between the surfactant properties and their polarity parameters [14].

The importance of the dispersive forces in solute–solvent intermolecular interactions in GC experiments has been reported [13,37–42]. The proposed dispersive force parameters have been used for the characterization of the properties of commercial stationary phases and surface-active species [13,32,37–42].

The criterion A was proposed by Sevcik and Lowentap [39] and defined as

$$A = \frac{t'_{Rn+1} t'_{Rn}}{t'_{Rn} - t'_{Rn-1}} \quad (3)$$

where t'_{Rn+1}, t'_{Rn} and t'_{Rn-1} are the adjusted retention times of n-alkanes having $n+1$, n and $n-1$ carbon atoms, respectively, used as test solutes. It was proposed to describe the dispersive properties of stationary phases. An increasing value of A corresponds to decreasing polarity of the liquid phase.

The partial excess Gibbs function of solution per methylene group, $\Delta G^E(CH_2)$, represents the ability of the stationary phase to interact with solutes by means of intermolecular interactions other than dispersive interactions.

Roth and Novak [41] proposed to calculate $\Delta G^E(CH_2)$ from the retention data for two consecutive members of homologous series:

$$\Delta G^E(CH_2) = RT \ln[(V^0_{gn} P^0_n)/(V^0_{gn+1} P^0_{gn+1})] \quad (4)$$

where V_g is the specific retention volume, P^0 is the saturated vapour pressure and the subscripts n and $n+1$ refer to the two consecutive homologues.

Commercial stationary phases are usually characterized by McReynolds' constants [43] calculated in the standard way using the retention indices of benzene, 2-butanol, 2-pentanone, pyridine and 1-nitropropane. The sum of the values for these test solutes is represented by $\Sigma_{i=1}^{5} \Delta I_i$.

The aims of this investigation were (i) to characterize the examined stationary phases by the solubility parameter, dispersive force parameters and thermodynamic parameters of solution and (ii) to determine the influence of the molecular structure of the compounds on the parameters considered.

2. Experimental

2.1. Preparation of packings

Preparation of packing with bonded trichlorooctylsilane

Dry silica was immersed in a solution consisting of 3 ml of trichlorooctylsilane and 80 ml of water-free xylene. The mixture was heated at boiling point and stirred in an evaporator for 12 h. The packing was then washed with xylene and transferred into a Soxhlet apparatus, where it was subjected to extraction with the same solvent. The next stage was an end-capping reaction using hexamethyldisilazane (HMDS). The reaction proceeded in xylene. After the above stage, the packing was extracted and dried.

Preparation of packing with bonded 3-(3-trimethoxysilylpropyl)pentane-2,4-dione (TMSPP)

Silica was dried under vacuum at 180°C for 12 h, then a solution of silane (10 ml) in water-free xylene (250 ml) was added and the mixture obtained was boiled under reflux for 15 h. The system was protected from moisture. Unreacted silane was extracted with xylene and then with hexane in a Soxhlet extractor. Finally the packing was dried.

Preparation of packings with TMSPP-bonded $CuCl_2$, $PdCl_2$, $Cu(acac)_2$, $Ni(acac)_2$ and $Ni(hfac)_2$

A packing with bonded silane (TMSPP) was covered with a saturated, water-free solution of the appropriate salt in tetrahydrofuran (THF). The reagent system was allowed to stand for 7 days at room temperature, being protected from any access of moisture during that period. The excess of salt was then removed by extraction with THF in a Soxhlet extractor. After the extraction, packings were dried *in vacuo*.

2.2. Apparatus

All chromatographic measurements were carried out on a GCHF 18.3 gas chromatographic manufactured by Chromatron (Berlin, Germany), equipped with a flame ionization detector and a digital thermometer (Slandi, Warsaw, Poland) for measuring the column temperature. Argon was used as the carrier gas. The packings were placed in stainless-steel columns (1 m × 0.3 cm I.D.) and conditioned at 150°C for 12 h. Sample volumes were 0.01 μl of solute vapour.

Injection was repeated at least three times. The peaks were sharp and symmetrical.

Elemental compositions (C, N, H) of the investigated packings were determined on a Perkin-Elmer (Norwalk, CT, USA) Model 240 elemental analyser. Surface-area measurements were performed on a Grawimat Sorptometer (Sartorius, Gottingen, Germany). Results of the physico-chemical measurements are given in Table 1.

2.3. Calculations

The solubility parameter was calculated according to the procedure of DiPaola-Baranyi and Guillet [15], i.e. from Eq. 2. Criterion A and $\Delta G^{E}(CH_2)$ were calculated from Eqs. 3 and 4, respectively. In the calculation of $\Delta G^{E}(CH_2)$, C_5–C_{10} n-alkanes were used as test solutes. $\Delta G_s^m(CH_2)$ was calculated according to the procedure of Risby and co-workers [42–45], also with the use of n-alkanes as test solutes.

The examined compounds were not characterized by McReynolds' $\Sigma_{i=1}^{5} \Delta I_i$ values. However, Kováts retention indices for several test solutes were calculated and are discussed in the following section.

3. Results and discussion

Values of all parameters obtained for the examined stationary phases are summarized in Table 2. The solubility parameters δ_2 are in the range $(10.2–15.8)\cdot 10^3$ $(J/mol)^{1/2}$ at the lowest temperature, i.e., they are similar to those reported earlier for silicone stationary phases (ca. 13.2 units for OV-101) [19], but lower than those of broad and narrow distributed oligooxyethylene derivatives of cetyl alcohol (15.0–17.8 units) [21] or oligooxyethylates containing highly fluorinated hydrophobes (18.2–19.4 units [22]. However, the solubility parameter generally decreases with increasing temperature of the experiment and the comparison of results obtained at different temperatures may be dubious. Even in our case the temperatures of the experiments varied slightly. As no linear relationship was found between the solubility parameter and the temperature of the experiment, we cannot

Table 1
Physico-chemical characteristics of the investigated packings

Packing	Elemental analysis (%)				Surface area (m^2/g)	Surface concentration of silane ($\mu mol/m^2$)
	C	H	Cl	M (metal)		
I[a]	2.41	0.43	–	–	65	4.87
II[b]	2.54	0.61	–	–	75	3.33
III[c]	2.84	0.78	0.27	0.49	82	3.33
IV[d]	2.94	0.75	0.25	0.75	81	3.33
V[e]	2.08	0.44	–	0.1	71	2.41
VI[f]	2.46	0.74	–	0.11	74	2.88
VII[g]	1.84	0.33	–	1.73	71	2.04

[a] $(CH_2)_7CH_3$.
[b] $(CH_2)_3CH(COCH_3)_2$.
[c] $(CH_2)_3CH(COCH_3)_2 \cdot CuCl$.
[d] $(CH_2)_3CH(COCH_3)_2 \cdot PdCl$.
[e] $(CH_2)_3CH(COCH_3)_2 \cdot Cu(acac)$ (acac = acetylacetonate).
[f] $(CH_2)_3CH(COCH_3)_2 \cdot Ni(acac)$.
[g] $(CH_2)_3CH(COCH_3)_2 \cdot Ni(hfac)$ (hfac = hexafluoroacetylacetonate).

Table 2
Solubility parameter δ_2, dispersive force parameters and retention indices for the investigated packings

Liquid phase[a]	Temperature (°C)	δ_2 [10^3 (J/m^3)$^{1/2}$]	Criterion A	$\Delta G_S(CH_2)$ (J/mol)	$\Delta G^E(CH_2)$ (J/mol)	Retention index		
						Benzene	Thiophene	Furan
I	120.8	13.920	1.634	−1245.0	1422.4	612.5	605.3	457.8
	130.8	13.791	1.563	−1114.1	1576.9	592.4	609.9	459.4
	140.8	13.675	1.528	−983.1	1634.0	603.4	613.1	458.4
II	120.4	14.615	1.717	−1473.1	1199.3	682.1	683.9	524.0
	130.6	14.288	1.681	−1337.7	1265.2	681.6	695.1	544.5
	140.1	14.793	1.616	−1227.9	1396.4	674.1	691.3	529.9
III	124.7	15.789	1.690	−1390.6	1205.0	737.8	724.9	556.0
	137.3	15.489	1.656	−1521.1	1296.6	716.1	714.1	537.1
	146.2	16.359	1.656	−1620.8	770.8	760.6	761.9	665.4
IV	126.4	15.396	1.709	−1380.4	1202.7	678.3	690.8	528.9
	136.1	15.254	1.629	−1348.7	1324.7	676.2	695.8	544.2
	145.5	15.653	1.590	−1220.0	1421.5	676.2	690.1	539.9
V	120.6	13.631	1.826	−1734.3	894.4	671.8	676.9	521.4
	130.3	13.531	1.736	−1589.3	1052.5	689.1	689.2	524.8
	140.3	13.934	1.669	−1439.8	1177.8	687.2	692.5	549.1
VI	120.6	10.187	1.816	−1628.4	968.2	703.1	710.6	571.8
	130.4	10.002	1.703	−1490.7	1147.5	698.2	684.7	519.4
	140.4	10.537	1.658	−1350.3	1240.9	710.6	714.5	564.6
VII	120.7	10.470	1.816	−1628.2	968.5	703.7	710.6	571.8
	130.4	10.269	1.703	−1491.9	1147.5	698.2	684.7	519.4
	140.5	10.802	1.658	−1350.0	1241.2	710.6	714.5	564.6

[a] Numbers as in Table 1.

extrapolate our results to a temperature of 90°C and compare the δ_2 values for compounds examined in this work with those reported earlier for other liquid phases. We may only qualitatively judge that δ_2 values for chemically bonded phases at lower temperatures, e.g., at room temperature, would be slightly higher than those for other classes of compounds.

Eq. 2 is linear and the correlation coefficient in all instances was above 0.97. This means that despite the relatively low molecular mass of the liquid phases no significant deviations from linearity of the basic relationship was observed. Therefore, estimation of increments of the solubility parameter was impossible. However, such deviations may appear if one extends the list of test solutes, i.e., by using typical polar test solutes such as alcohols, ketones, pyridine or nitropropane.

For the stationary phases examined the lowest (δ_2) values were obtained for two Ni-containing materials, i.e., $Ni(hfac)_2$ and $Ni(acac)_2$, and the highest values were found for these phases modified by $PdCl_2$ and $CuCl_2$. This means that the lowest polarity (as measured by δ_2) is exhibited by chemically bonded phases in which metal ion is screened by the relatively large organic part of the molecule. Higher values were found for acetylacetonate derivatives having a copper atom as the complexing centre (Fig. 1).

The criterion A for non-polar stationary phases is high, i.e., usually slightly above 2 units [32, 41]. An increase in the polarity of the liquid phase causes a decrease in this parameter. The highest values of criterion A were found for phases modified by $Cu(acac)_2$, $Ni(acac)_2$ and $Ni(hfac)_2$ and the lowest one for a C_8 liquid phase.

The partial molar excess Gibbs free energy of solution per methylene group, $\Delta G^E(CH_2)$, re-

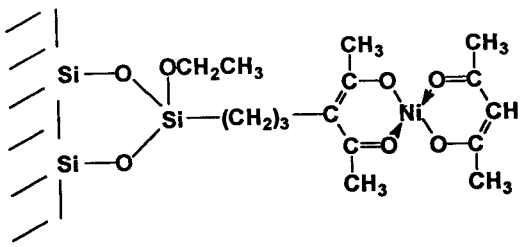

Fig. 1. Schematic diagram of packing.

flects the resistence of the liquid phase to dissolve the non-polar methylene fragment. The values of this parameter increases with increase in the polarity of the liquid phase. A stationary phase modified by $Cu(acac)_2$ seems to be the least polar and C_8 the most polar phase.

The partial molar Gibbs free energy of solution per methylene group increases with increase in the polarity of the stationary phase. The lowest value -1.628 kJ/mol was found for phases having $Ni(hfac)_2$ and $Ni(acac)_2$ and these two stationary phases should be indicated as the least polar [according to $\Delta G_s^m(CH_2)$].

Generally, in all instances, despite the parameters considered, investigated phases containing large organic molecules were selected as those exhibiting the lowest polarity. A C_8 chemically bonded phase was ordered by δ_2 (Table 3) as slightly more polar than those modified by $Cu(acac)_2$. However, C_8 is the most polar when judged on all the dispersive force parameters. If this difference is not taken into account, the arrangement of the examined stationary phases is similar with the use of all the parameters considered: $Ni(hfac)_2 \approx Ni(acac)_2 \approx Cu(acac)_2 < TMSPP \approx C_8 < CuCl_2 \approx PdCl_2$.

n-Alkanes used as test solutes interact with the stationary phase only by dispersive interaction. In such a case the strongest relationships are observed for a C_8 chemically bonded phase. Here the dispersive interactions are predominant as no steric effects characteristic of complexes and free β-diketonate groups are observed. The solubility parameter δ_2 was calculated with the use of retention data for *n*-alkanes, aromatics and polar solutes, and strong specific interactions were taken into account. Therefore, the ordering based on δ_2 differs from the others where dispersive force parameters were considered.

Straight-line relationships (Figs. 2 and 3a) were found between dispersive force parameters and the surface concentration of silane (SC):

$$\Delta G^E(CH_2) = 2.192 - 3.988 \times 10^{-4} SC$$
$$R = 0.987$$
$$\Delta G_s^m(CH_2) = 1.104 - 4.237 \times 10^{-4} SC$$
$$R = 9.979$$
$$\text{Criterion } A = 1.1983 - 0.075SC$$
$$R = 0.905$$

The relationship between δ_2 and surface concentration is characterized by a low value of the correlation coefficient, $R = 0.7$ (Fig. 3b).

The application of ligands containing a β-diketonate group allowed a comparison of their specific interaction ability with typical electron donors. In fluorinated acetylacetonates, substitution of the hydrogen atom in the methyl group causes a decrease in the σ-donor and π-donor abilities of ligands. The small differences between stationary phases with $Ni(hfac)_2$ and

Table 3
Influence of modifying agent on investigated parameters

Parameter	Order
Criterion *A*	$Cu(acac)_2 < Ni(acac)_2 = Ni(hfac)_2 < TMSPP < PdCl_2 < CuCl_2 < C_8$
$\Delta G^E(CH_2)$	$Cu(acac)_2 < Ni(acac)_2 = Ni(hfac)_2 < TMSPP < CuCl_2 < PdCl_2 < C_8$
$\Delta G_s^m(CH_2)$	$Cu(acac)_2 < Ni(acac)_2 = Ni(hfac)_2 < TMSPP < PdCl_2 < CuCl_2 < C_8$
δ_2	$Ni(acac)_2 < Ni(hfac)_2 < Cu(acac)_2 < C_8 < TMSPP < PdCl_2 < CuCl_2$

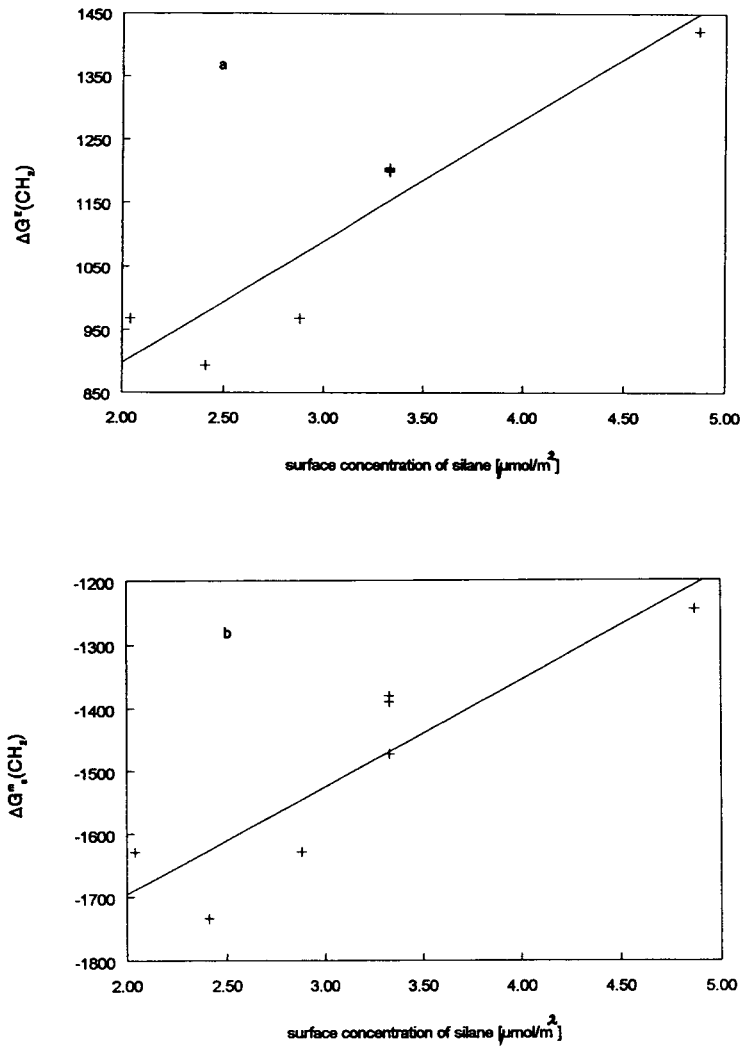

Fig. 2. Relationships between Gibbs functions of solution and surface concentration of silane (*SC*): (a) $\Delta G^{E}(CH_2)$ vs. *SC*; (b) $\Delta G_s^{m}(CH_2)$ vs. *SC*.

$Ni(acac)_2$ as judged by dispersive force parameters are probably caused by transformations occurring during the reaction of nickel salts with the TMSPP surface. One of hexafluoroacetylacetonate groups in $Ni(hfac)_2$ is replaced by an acetylacetonate group bonded to the silica surface. Therefore, only six instead of twelve fluorine atoms are present in the final complex. This causes lower than expected differences in the physico-chemical properties of both types of chemically bonded stationary phases.

Acknowledgements

This work was partly supported by Poznań University of Technology grant and KBN grant

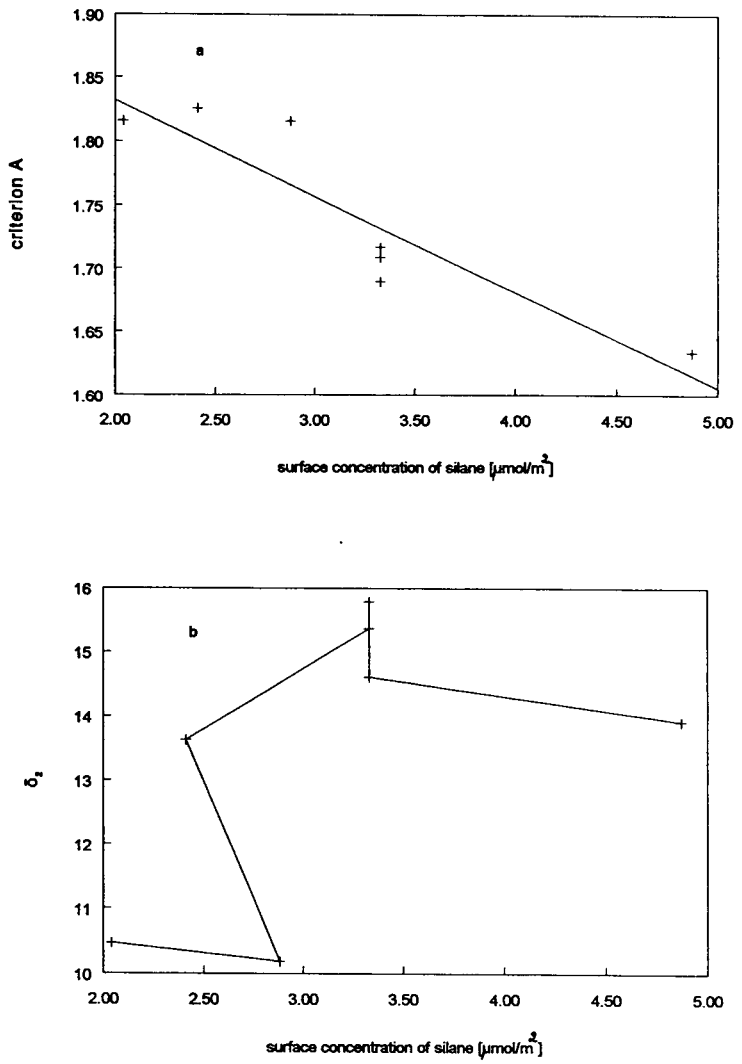

Fig. 3. Relationships between physico-chemical parameters and surface concentration of silane (*SC*): (a) criterion *A* vs. *SC*; (b) δ_2 vs. *SC*.

BW 32/237/94 and KBN grant 207499101, which are gratefully acknowledged.

References

[1] D. Cagniant (Editor), *Complexation Chromatography*, Marcel Dekker, New York, 1992.
[2] W. Szczepaniak, J. Nawrocki and W. Wasiak, *Chromatographia*, 12 (1977) 484 and 559.
[3] W. Wasiak, *J. Chromatogr. A*, 653 (1993) 63.
[4] I. Rykowska, R. Wawrzyniak and W. Wasiak, *Chem. Anal. (Warsaw)*, 39 (1994) 335.
[5] W. Wasiak, *Chromatographia*, 22 (1986) 147.
[6] W. Wasiak, *Chromatographia*, 23 (1987) 423.
[7] W. Wasiak, *Chromatographia*, 23 (1987) 427.
[8] W. Wasiak, *J. Chromatogr.*, 547 (1991) 259.
[9] A. Voelkel, *Wiad. Chem.*, 41 (1987) 77.
[10] A. Voelkel, *Wiad. Chem.*, 41 (1987) 671.
[11] J. Szymanowski, *CRC Crit. Rev. Anal. Chem.*, 21 (1990) 407.
[12] C.F. Poole and S.K. Poole, *Chem. Rev.*, 89 (1989) 377.
[13] S.K. Poole and C.F. Poole, *J. Chromatogr.*, 500 (1990) 329.

[14] A. Voelkel, *CRC Crit. Rev. Analyt. Chem.*, 22 (1991) 411.
[15] G. DiPaola-Baranyi and J.E. Guillet, *Macromolecules*, 11 (1978) 228.
[16] Y. Ren and P. Zhu, *J. Chromatogr.*, 457 (1988) 354.
[17] P.J. Hoftyzer and D.W. Van Krevelen, in *Properties of Polymers*, Elsevier, Amsterdam, 2nd ed., 1976, Ch. 7, pp. 152–155.
[18] E. Fernandez-Sanchez, A. Fernandez-Torrez, J.A. Garcia-Dominguez and J.M. Santiuste, *J. Chromatogr.*, 457 (1988) 55.
[19] M.R. Becerra, E. Fernandez-Sanchez, A. Fernandez-Torrez, J.A. Garcia-Dominguez and J.M. Santiuste, *J. Chromatogr.*, 547 (1991) 269.
[20] E. Fernandez-Sanchez, A. Fernandez-Torrez, J.A. Garcia-Dominguez and M.D. Salvador Moya, *J. Chromatogr.*, 556 (1991) 485.
[21] A. Voelkel and J. Janas, *J. Chromatogr.*, 645 (1993) 141.
[22] A. Voelkel and J. Janas, *J. Fluorine Chem.*, 67 (1994) 75.
[23] A. Voelkel, J. Janas and J.A. Garcia-Dominguez, *J. Chromatogr. A*, 654 (1993) 135.
[24] A. Voelkel and J. Janas, *J. Chromatogr. A*, 669 (1994) 89.
[25] J.H. Hildebrand and R.L. Scott, *The Solubility of Nonelectrolytes*, Van Nostrand, Princeton, NJ, 1950.
[26] J.E. Guillet, *J. Macromol. Sci. Chem.*, 4 (1970) 1669.
[27] G.J. Price, in D.R. Lloyd, T.C. Ward and H.P. Schreiber (Editors), *Inverse Gas Chromatography. Characterization of Polymers and Other Materials* (*ACS Symposium Series*, No. 391), American Chemical Society, Washington, DC, 1989, Ch. 5, pp. 48–58.
[28] J. Szymanowski, A. Voelkel, J. Beger and H.-J. Binte, *J. Chromatogr.*, 327 (1985) 353.
[29] J. Szymanowski, A. Voelkel, J. Beger and H. Merkwitz, *J. Chromatogr.*, 330 (1985) 61.
[30] A. Voelkel, J. Szymanowski, J. Beger and K. Ebert, *J. Chromatogr.*, 398 (1987) 31.
[31] A. Voelkel, *Chromatographia*, 23 (1987) 195.
[32] A. Voelkel, *J. Chromatogr.*, 435 (1988) 29.
[33] J. Szymanowski, A. Sobczyńska and A. Voelkel, *J. Pharm. Sci.*, 77 (1988) 893.
[34] A. Voelkel, *Chromatographia*, 25 (1988) 95.
[35] A. Voelkel, J. Szymanowski, J. Beger and H. Rustig, *J. Chromatogr.*, 448 (1988) 219.
[36] A. Voelkel, *J. Chromatogr.*, 450 (1988) 291.
[37] I. Brown, *J. Chromatogr.*, 10 (1963) 284.
[38] L. Rohrschneider, *J. Chromatogr.*, 17 (1965) 1.
[39] J. Sevcik and M.S.H. Lowentrap, *J. Chromatogr.*, 217 (1981) 139.
[40] J. Novak, *J. Chromatogr.*, 78 (1973) 269.
[41] M. Roth and J. Novak, *J. Chromatogr.*, 234 (1982) 337.
[42] C.E. Figgins, B.L. Reinbold and T.H. Risby, *J. Chromatogr. Sci.*, 15 (1977) 208.
[43] T.H. Risby, P.C. Jurs and B.L. Reinbold, *J. Chromatogr.*, 99 (1974) 173.
[44] B.L. Reinbold and T.H. Risby, *J. Chromatogr. Sci.*, 13 (1975) 372.
[45] C.E. Figgins, T.H. Risby and P.C. Jurs, *J. Chromatogr. Sci.*, 14 (1976) 453.

ELSEVIER

Journal of Chromatography A, 690 (1995) 93–102

JOURNAL OF CHROMATOGRAPHY A

Chemically bonded chelates as selective complexing sorbents for gas chromatography
III. Silica chemically modified by N-benzoylthiourea groups

W. Wasiak

Faculty of Chemistry, A. Mickiewicz University, Grunwaldzka 6, 60-780 Poznań, Poland

First received 22 March 1994; revised manuscript received 30 June 1994

Abstract

High stability and simple synthesis from inexpensive starting materials make it possible to use the N-benzoylthiourea groups as modifiers of silica for complexation gas chromatography. Taking advantage of the chelating properties of N-benzoylthiourea, copper(II) ions were bonded with SiO_2 to give a packing capable of entering into π-type interactions with adsorbates with electron-donor properties such as linear and branched alkenes and aromatic and cyclic hydrocarbons. The high selectivity of the packing obtained permitted the separation of complex mixtures (including isomers) of different classes of organic compounds.

1. Introduction

In general, complexation gas chromatography uses two types of packings. One employs phases bonded to the surface of the support, which include electron-donor or electron-acceptor groups capable of forming organic electron-donor–acceptor complexes with molecules of mixtures to be separated. The first attempt at using the formation of organic complexes in chromatography was made by Godlewicz [1]. He used silica gel impregnated with trinitrobenzene to separate the organic fraction of lubricating oils. In many instances the same molecule can act as an electron donor or acceptor, depending on the circumstances. It is only essential to ensure that the rate of formation of surface complexes and their dissociation are high. Phases of this type are discussed in detail in Refs. [2–4].

The other type of packing employs electron-deficient species, such as many metal cations, which have at least an empty valence orbital available for extra coordination. These species are capable of complexing with electron-donating groups. Examples of packings of this type are those with transition metal complexes formed with such groups as diphenylphosphine, thiol, cyano, β-diketonate and iminoamine [5–10], bonded to the silica surface by a hydrocarbon chain.

The stability of the complexes which are formed by molecules of analyte compounds with a packing depends on at least six factors [2]: (1) valence, electronic structure and radius of the central metal ion; (2) spatial arrangement of

0021-9673/95/$09.50
SSDI 0021-9673(94)00903-1

overlapping orbitals of central ion and ligands; (3) basicity of ligands; (4) "internal" electric effects of ligands transmitted through the central ion; (5) steric effects due to direct contact between the atoms of different ligands; and (6) "external" effects due to changes in the outer coordination sphere (e.g., solvent effect).

From the point of view of the complexation mechanism and stoichiometry, the following two cases can be distinguished: change in the number of ligands coordinated in the inner coordination sphere and displacement of a ligand coordinated in the inner coordination sphere. The fact that so many factors affect the process of complexation ensures a high sensitivity of complexation gas chromatography and permits its control. As the role of the ligand binding the metal ion with the support surface is of key importance, attempts are still made to determine the effects of using different groups as ligands.

This paper reports results obtained with the N-benzoylthiourea group applied as a binding ligand. A high affinity of this group to metals has been described by Koenig and co-workers [11–13] and others [14].

A sorption–spectrophotometric method was developed for determining silver using dithizone and silica chemically modified with N-propyl-N′-benzoylthiourea groups. The sensitivity and selectivity of the above method are better than those for the known methods based on organic reagents [15].

Complex formation between the N-benzoylthiourea group and metal ions on the surface of modified silica can be depicted as shown below; where $n = 1$, 2 or 3. A metal ion bonded in such a way is capable of entering into coordinative interactions with electron-donor molecules, so it can be used for modification of silica for the purposes of complexation gas chromatography.

2. Experimental

2.1. Materials

In order to prepare the packings we used Porasil C, obtained from Waters (Milford, MA, USA), as a support. Its specific surface area was 89 m^2/g and the particle size was 177–149 μm (80–100 mesh). Hexamethyldisilazane and γ-aminopropyltriethoxysilane were purchased from Fluka (Buchs, Switzerland) and potassium thiocyanate, benzoyl chloride, toluene and acetone from POCh (Gliwice, Poland). The compounds used as sorbates were produced by different manufacturers and were either pure or of analytical-reagent grade.

2.2. Preparation of packings with N-benzoylthiourea groups

Synthesis of a packing was carried out in two stages. In the first stage, γ-aminopropyltriethoxysilane was bonded to the surface of silica dried at 180°C under reduced pressure. The reaction proceeded in anhydrous toluene under reflux. After washing and drying, an end-capping reaction was performed using hexamethyldisilazane. In the second stage, the reaction of the aminated silica with benzoyl isothiocyanate was carried out. The dry aminated silica was covered with a solution of benzoyl isothiocyanate in acetone. After 24 h, the packing was washed with dry acetone and then extracted with acetone in a Soxhlet extractor. Elemental analysis of the obtained dried packing gave N 1.16, C 5.43, H

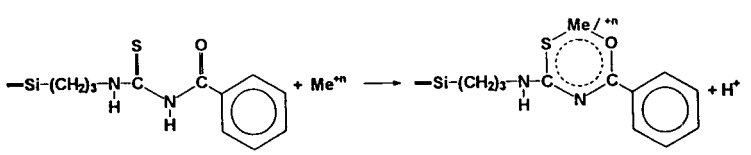

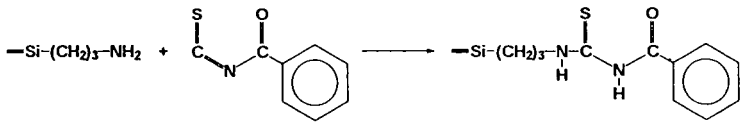

1.01, S 0.93%. This reaction can be represented schematically as shown above.

Part of the packing thus obtained was placed in a chromatographic column which was used as a reference for the packing subjected to reaction with copper(II) chloride. The reaction of isothiocyanate groups with copper(II) chloride was performed as follows: 9 g of the modified silica was covered with 50 ml of a saturated solution of $CuCl_2$ in acetone. The solution was light ochre in colour. At the moment of the contact with copper solution, the silica changed colour from light yellow to violet-ochre. After 12 h the packing was extracted with acetone in a Soxhlet extractor, dried and placed in a chromatographic column. The amount of bonded copper was 1.78% for the packing with a specific surface area of 81 m^2/g.

2.3. Apparatus

Chromatographic measurements were carried out on a GCHF 18.3 chromatograph (Chromatron, Berlin, Germany), equipped with a mercury manometer, digital thermometer and flame ionization detector with argon as the carrier gas. Stainless-steel columns of 1 m × 0.4 cm I.D. were used. The adsorbates were saturated and unsaturated linear and branched aliphatic hydrocarbons and cyclic and aromatic hydrocarbons. They were introduced by a Hamilton type syringe in doses of 0.01 μl or less.

3. Results and discussion

The measurements of retention time and calculations of retention parameters such as capacity factor (k'), retention index (I), molecular retention index (ΔM_e) and specific retention volume (V_g) were performed for both packings studied, i.e., that with Cu bonded via N-benzoylthiourea groups and that with free (without metal) N-benzoylthiourea groups, used as a reference. ΔM_e values can be calculated from $\Delta M_e = M_e - M$, where M = real molecular mass, $M_e = 0.14027I + 2.016$ and I = Kováts retention index. The results obtained for particular groups of adsorbates are given in Tables 1–4. The chromatographic measurements were carried out at three temperatures, 125, 135 and 145°C.

3.1. Aliphatic hydrocarbons

The presence of a metal capable of entering into coordinative interactions with additional ligands such as unsaturated hydrocarbons was responsible for the fact that the retention parameters determined under the same conditions were higher for the metal-containing packing. An increase in the strength of π-type specific interactions was accompanied by an increase in selectivity. A comparison of the differences in the capacity factors for alkene–alkane pairs obtained for the two packings (Table 2) provides clear evidence for the effect of a transition metal presence on specific interactions. Similar conclusions can be drawn from the retention indices (Table 1).

With the metal-containing packing, the difference (ΔI) between the extreme values of the retention indices for linear C_5 hydrocarbons ($\Delta I = I_{1\text{-pentyne}} - I_{\text{pentane}}$) was 110 u (u = unit of retention index), whereas with the packing free of metal, ΔI for the same compounds was only 39 u. This disproportion was much greater for subsequent hydrocarbons, C_6 and C_7. For C_6 hydrocarbons ΔI between an alkyne and alkane ($\Delta I = I_{1\text{-hexyne}} - I_{\text{hexane}}$) was 211 u with the metal-

Table 1
Values of capacity factors, retention indices, molecular retention indices and specific retention volumes for aliphatic hydrocarbons at 125°C

Solute	Packing with $-CuCl_2$				Packing without metal				B.p. (°C)
	k'	I	ΔM_e	V_g	k'	I	ΔM_e	V_g	
Pentane	1.73	500	0	1.27	1.74	500	0	2.14	36.07
1-Pentene	1.88	511	3.54	1.38	1.78	503	2.42	2.18	36.94
cis-2-Pentene	2.07	525	5.51	1.52	1.89	514	3.96	2.33	36.94
trans-2-Pentene	1.91	514	3.96	1.4	1.85	509	3.26	2.27	36.35
1-Pentyne	3.64	610	19.45	2.68	2.22	539	9.49	2.72	40.18
2-Methyl-1,3-butadiene	2.16	532	8.51	1.69	1.94	517	6.41	2.37	34.06
Hexane	3.41	600	0	2.5	3.22	600	0	3.95	68.74
1-Hexene	3.86	619	4.67	2.84	3.24	601	2.15	3.97	63.48
cis-2-Hexene	3.89	621	4.81	2.86	3.37	607	2.99	4.13	68.84
trans-2-Hexene	3.69	612	3.69	2.71	3.29	603	2.43	4.04	67.87
1,3-Hexadiene	5.14	662	12.71	3.78	3.96	613	5.85	4.85	73
1,4-Hexadiene	4.14	629	8.08	3.04	3.33	605	4.72	4.08	65
2,3-Hexadiene	4.68	647	10.61	3.44	3.78	626	7.66	4.63	68
2,4-Hexadiene	5.88	682	15.52	4.33	4.51	636	9.07	5.53	80
1-Hexyne	13.68	811	33.47	10.07	4.11	641	9.77	5.03	71.35
Heptane	6.61	700	0	4.86	5.85	700	0	7.17	98.42
1-Heptene	7.52	719	4.67	5.53	5.87	701	2.14	7.19	93.64
cis-2-Heptene	7.65	722	5.09	5.62	6.15	708	3.13	7.54	98.51
trans-2-Heptene	7.23	713	3.83	5.32	6.03	705	2.69	7.39	98.95
cis-3-Heptene	7.31	715	4.11	5.38	5.94	702	2.28	7.28	95.75
trans-3-Heptene	6.92	707	2.98	5.09	5.82	699	1.86	7.13	95.67
1-Heptyne	26.98	913	33.89	19.86	7.61	743	10.05	9.32	99.78
2-Methylpentane	2.97	581	−2.81	2.18	2.89	582	−2.53	3.54	60.27
3-Methylpentane	3.12	587	−1.83	2.29	3.04	594	−0.84	3.72	63.28
2-Methyl-1-pentene	3.53	605	2.71	2.6	2.94	586	0.05	3.85	60.7
4-Methyl-1-pentene	3.31	595	1.31	2.43	2.92	584	−0.23	3.58	53.88
2-Methyl-2-pentene	3.57	607	2.99	2.63	3.25	601	2.15	3.98	67.29
cis-3-Methyl-2-pentene	3.61	609	3.27	2.66	3.27	602	2.29	4.01	70.45
trans-3-Methyl-2-pentene	3.68	612	3.69	2.71	3.34	606	2.85	4.1	67.63
cis-4-Methyl-2-pentene	3.11	586	0.04	2.29	2.83	579	−0.93	3.47	56.3
trans-4-Methyl-2-pentene	3.12	587	0.18	2.3	2.88	582	−0.51	3.53	58.55
2,2-Dimethylbutane	2.59	559	−5.57	1.9	2.63	567	−4.63	3.22	49.7
2,3-Dimethylbutane	2.91	576	−3.33	2.14	2.86	580	−2.81	3.51	57.98
2,3-Mimethyl-1-butene	3.19	591	0.61	2.35	2.85	580	−2.79	3.41	55.67
2,3-Dimethyl-2-butene	6.15	615	4.11	2.78	3.42	611	3.41	4.19	73.21
3,3-Dimethyl-1-butene	2.29	559	−0.73	1.9	2.41	568	−4.72	2.95	41.24

containing packing and 41 u with the metal-free packing. For C_7 hydrocarbons these differences were 213 and 44 u for the packings with and without metal, respectively.

As far as the branched hydrocarbons are concerned, for which the steric effect must be taken into account, the effect of metal bonded on the packing surface on retention of the studied sorbates was much weaker. The difference in retention indices (ΔI) in the group of monosubstituted C_6 hydrocarbons calculated for 2-methylpentane and *trans*-3-methyl-2-pentene was 31 and 24 u for the packing with and without metal, respectively. For disubstituted derivatives of butene and butane, $\Delta I = I_{2,3\text{-dimethyl-2-butene}} - I_{2,3\text{-dimethylbutane}}$ was 39 and 31 u for the packing with and without metal, respectively. This indicates that the steric effect weakens the specific

Table 2
Values of $\Delta k' = k'_{alkene} - k'_{alkane}$ for the two packings investigated

Alkene–Alkane	125°C		136°C		145°C	
	Metal-containing packing	Metal-free packing	Metal-containing packing	Metal-free packing	Metal-containing packing	Metal-free packing
1-Pentene–pentane	0.18	0.04	0.13	0.01	0.09	−0.06
1-Hexene–hexane	0.45	0.02	0.29	0.03	0.24	0
1-Heptene–heptane	0.91	0.02	0.57	0.03	0.44	0.02
2-Methyl-1-pentene–2-methylpentane	0.56	0.05	0.29	0.14	0.27	0.11
2,3-Dimethyl-1-butene–2,3-dimethylbutane	0.28	−0.01	0.12	0.90	0.11	0

interactions between the bonded metal complex and the adsorbate, which, consequently, brings closer the selectivities of both kinds of packings towards the branched hydrocarbons. This conclusion is supported by the values of the molecular retention indices, which in a few cases are negative. According to the definition of this parameter, a negative value is evidence for repulsion between the electron-acceptor centre on the packing surface and the studied sorbate. The differences between the retention indices ($\Delta I = I_{cis\text{-isomer}} - I_{trans\text{-isomer}}$) obtained for the four pairs of geometric isomers of *n*-alkanes studied was within 9 u for the metal-containing packing, whereas for the metal-free packing the differences in the retention indices between these same pair of isomers were 3–5 u. The elution sequence of particular sorbates against their boiling temperatures also indicates the effect of π-type interactions on their retention parameters. Alkanes with higher boiling points were eluted first, before alkenes with lower boiling points (Table 1), e.g. pentane (b.p. = 36.07°C) was eluted before 2-methyl-1,3-butadiene (b.p. = 34.06°C), hexane before 1-hexene, *trans*-2-hexene and 1,4-hexadiene, etc.

3.2. Cyclic hydrocarbons

Similarly as for linear hydrocarbons, specific interactions were stronger in the case of the metal-containing packing (Table 3). The strength of the interactions increased with increase in the number of unsaturated bonds in a molecule. This can be illustrated by the results for unsaturated cyclooctane derivatives. Lower values of the retention parameters of cyclooctatetraene than those of 1,5-cyclooctadiene, despite a larger number of unsaturated bonds in the former, are a consequence of its specific (tube-like) structure [16,17]:

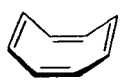

Because of its unique structure, cyclooctatetraene is capable of interacting with metals only through two unsaturated bonds. It should also be noted that the interactions were stronger for dienes with isolated bonds than for dienes with conjugated bonds (1,4-cyclohexadiene and 1,3-cyclohexadiene or 1,5-cyclooctadiene and 1,3-cyclooctadiene). This is contrary to the situation observed for linear dienes (e.g., 1,3- and 1,4-hexadiene), for which the lowest values of k', I and ΔM_e were noted for the isomer with isolated unsaturated bonds (1,4-hexadiene). The presence of methyl or ethyl substituents resulted in a significant decrease in the molecular retention index (ΔM_e), even to negative values (with saturated cyclic hydrocarbons).

The strength of specific interactions can be judged from the values of the retention parameters obtained for four pairs of cycloalkanes–cycloalkenes using the metal-containing packing. Cyclopentene (b.p. 44.24°C) is eluted after

Table 3
Values of capacity factors, retention indices, molecular retention indices and specific retention volumes for cyclic hydrocarbons at 137°C

Solute	Metal-containing packing				Metal-free packing				B.p. (°C)
	k'	I	ΔM_e	V_g	k'	I	ΔM_e	V_g	
Cyclopentane	1.42	506	2.84	1.54	0.99	502	2.28	1.11	49.26
Cyclopentene	1.63	528	7.95	1.52	0.98	518	6.55	1.27	44.24
Methylcyclopentane	2.38	588	0.32	2.58	1.67	601	3.54	1.86	71.81
1-Methyl-1-cyclopentene	2.73	610	5.42	2.76	1.78	608	3.13	2.13	75.8
Cyclohexane	2.57	601	2.15	2.87	1.86	617	4.39	2.01	80.73
Cyclohexene	3.15	632	8.51	3.11	2.01	620	6.82	2.46	82.97
1,3-Cyclohexadiene	3.91	667	15.43	3.25	2.1	637	11.23	3.05	81.5
1,4-Cyclohexadiene	4.16	677	16.84	3.57	2.21	642	11.93	3.25	88.5
Benzene	4.02	671	11.97	3.5	2.16	640	13.67	3.14	80.1
Methylcyclohexane	4.41	687	0.18	4.7	3.04	697	1.58	3.46	100.93
Ethylcyclohexane	5.46	748	−3.26	8.67	5.61	802	2.28	6.61	131.78
Cycloheptane	5.48	720	4.81	5.9	3.82	736	7.05	4.28	118.79
Cycloheptene	7.06	760	12.44	5.96	3.86	738	9.35	5.51	115
1,3,5-Cycloheptatriene	7.96	779	19.13	6.68	4.33	757	16.05	6.21	116
Cyclooctane	10.94	829	6.07	11.31	7.33	848	8.73	8.55	151.14
Cyclooctene	12.66	852	11.31	10.92	7.08	842	9.91	9.89	138
1,3-Cyclooctadiene	12.17	846	12.49	10.94	7.09	842	11.93	9.51	141
1,5-Cyclooctadiene	26.26	962	29.61	12.93	8.38	871	16.01	20.51	148.4
Cyclooctatetraene	16.58	895	23.39	11.16	7.23	846	16.52	12.95	143

cyclopentane (b.p. 49.26°C). The situation is similar for cycloheptane and cycloheptene and for cyclooctane and cyclooctene. Only for C_6 cyclic hydrocarbons (cyclohexane and cyclohexene) is the sequence of elution according to increasing boiling point, because the boiling point of cyclohexane is lower than that of cyclohexene. For the packing free of metal the sequence of elution is according to increasing boiling points. However, the values of molecular retention indices, which are higher for cycloalkenes in the four pairs considered, are indicative of the fact that also in this case retention is affected by specific interactions.

3.3. Aromatic hydrocarbons

Interactions of aromatic hydrocarbons with the studied packings are strongly dependent on the size and structure of the adsorbate molecule. This is particularly well evidence when comparing molecular retention indices obtained for different adsorbates (Table 4).

Values of this parameter, reflecting the strength of specific interactions between the metal and π-electrons, increased from benzene to C_9H_{12}, and for the isomers of the studied group the highest values were obtained for trimethylbenzenes. The more branched were the substituents on the benzene ring, the weaker was the specific π-type interaction owing to growing steric hindrance. The ΔM_e values for 4-isopropyltoluene, which are 0.61 and −2.60 (the only negative ΔM_e among the adsorbates in this group) for the packings with and without metal, respectively, provide a good example that confirms this observation. Low ΔM_e values were also obtained for *sec.*- and *tert.*-pentylbenzenes and for a pair of C_9H_{12} isomers, propylbenzene and cumene. A strong influence of π-electrons of the aromatic ring on specific interactions in the studied packing–sorbate systems is indicated by the values of the k'/k' ratio for pairs consisting of a halogenated benzene (chlorobenzene or bromobenzene) and an alkylbenzene (ethylbenzene or cumene) (Table 5).

Table 4
Values of capacity factors, retention indices, molecular retention indices and specific retention volumes for aromatic hydrocarbons at 145°C

Solute	Formula	B.p. (°C)	Metal-containing packing				Metal-free packing			
			V_g	k'	I	ΔM_e	V_g	k'	I	ΔM_e
Benzene	C_6H_6	80.1	2.49	3.24	672	18.16	2.7	1.82	643	14.09
Toluene	C_7H_8	110.62	4.9	6.38	786	20.1	4.93	3.32	753	15.49
Styrene	C_8H_8	145.2	12.13	15.79	939	29.57	9.97	6.72	882	21.57
Ethylbenzene	C_8H_{10}	136.18	8.49	11.05	879	19.13	8.28	5.38	848	14.78
p-Xylene	C_8H_{10}	138.35	9.41	12.25	896	21.51	8.73	5.88	857	16.04
o-Xylene	C_8H_{10}	144.41	10.38	13.51	913	23.9	9.69	6.53	877	18.85
m-Xylene	C_8H_{10}	139.1	9.33	12.15	895	21.37	8.79	5.92	859	16.32
α-Methylstyrene	C_9H_{10}	171.51	18.11	23.58	1006	33.55	15.28	10.3	962	18.76
Allylbenzene	C_9H_{10}	156.47	16.1	20.96	986	22.13	13.86	9.34	944	16.24
Propylbenzene	C_9H_{12}	159.21	14.86	19.35	973	18.28	14.03	9.46	946	14.5
Cumene	C_9H_{12}	152.39	12.56	16.35	944	14.22	12.44	8.38	923	11.27
1,2,3-Trimethylbenzene	C_9H_{12}	176.08	22.24	28.95	1038	27.4	18.53	12.48	999	21.93
1,2,4-Trimethylbenzene	C_9H_{12}	168.35	20.15	26.23	1023	25.3	16.53	11.13	977	18.8
1,3,5-Trimethylbenzene	C_9H_{12}	164.35	17.56	22.86	1001	22.21	14.92	10.05	958	16.18
2-Ethyltoluene	C_9H_{12}	165.15	16.91	22.02	994	21.23	15.4	10.38	964	17.02
3-Ethyltoluene	C_9H_{12}	161.3	14.77	19.22	972	18.14	14.3	9.63	950	15.06
n-Butylbenzene	$C_{10}H_{14}$	183.27	27.32	35.56	1071	18.01	25.9	16.45	1051	15.2
Isobutylbenzene	$C_{10}H_{14}$	172.75	23.2	30.2	1045	14.36	20.62	12.89	1019	10.8
tert.-Butylbenzene	$C_{10}H_{14}$	169.11	19.73	25.69	1019	10.72	18.54	12.49	999	7.81
sec.-Butylbenzene	$C_{10}H_{14}$	173.3	20.66	26.9	1027	11.84	19.52	13.15	1008	9.17
p-Diethylbenzene	$C_{10}H_{14}$	183.75	28.45	37.03	1078	18.99	24	16.17	1048	14.78
o-Diethylbenzene	$C_{10}H_{14}$	183.42	28.02	36.47	1075	18.57	23.87	16.09	1047	14.64
m-Diethylbenzene	$C_{10}H_{14}$	181.1	27.02	35.18	1069	17.73	23.1	15.56	1040	13.66
4-Isopropyltoluene	$C_{10}H_{14}$	177.1	23.47	30.54	1047	0.61	23.63	14.25	1024	−2.6
sec.-Pentylbenzene	$C_{11}H_{16}$	198.9	36.09	46.98	1116	10.29	31.91	21.5	1101	8.19
tert.-Pentylbenzene	$C_{11}H_{16}$	186	33.26	43.3	1102	8.33	30.04	20.24	1090	6.61
1,3,5-Triethylbenzene	$C_{12}H_{18}$	216.2	71.47	93.03	1224	11.41	55.53	37.42	1208	9.17
Fluorobenzene	C_6H_5F	85.1	3.01	3.92	704	4.65	3.17	2.13	672	0.17
Chlorobenzene	C_6H_5Cl	132.22	6.93	9.64	856	9.51	7.34	4.94	825	5.17
Bromobenzene	C_6H_5Br	156.43	9.73	15.27	933	−24.13	11.2	7.55	903	−25.62

The appropriate pairs of compounds (the first two) are characterized by similar boiling points (Table 5). In the case of alkylbenzenes, the electron density in the aromatic ring is increased as a result of the electron-donor character of the substituent. On the other hand, halogen sub-

Table 5
Values of k'/k' for selected pairs of adsorbates for the two packings investigated

Pairs of solutes	Metal-containing packing	Metal-free packing
Fluorobenzene–toluene	0.47	0.64
Chlorobenzene–ethylbenzene	0.62	0.91
Bromobenzene–cumene	0.59	0.9
Ethylbenzene–styrene	0.69	0.8
Propylbenzene–allylbenzene	0.95	1.01

stituents with electron-acceptor properties have a decreased electron density in the aromatic ring and thus reduce the ability of the ring to interact with metals. The presence of an unsaturated substituent increases the retention parameters, which is indicative of an increased strength of specific interactions. For example, for the pairs ethylbenzene–styrene or propylbenzene–allylbenzene, stronger interactions were observed for styrene and allylbenzene. This is a consequence of the fact that for, e.g., styrene the double bond of the vinyl group conjugated with the benzene ring exhibits an electron-releasing tendency [18].

3.4. Separation properties of the studied packings

As the data presented in the form of tables do not give a clear illustration of the analytical usefulness of the packings, we performed a number of analyses of mixtures of standard hydrocarbons belonging to the studied groups. As follows from the chromatograms presented, the analysis can be performed in a short time and a complete separation of the analysed mixtures can be achieved. As the column used was only 1 m long, we can expect a further improvement of the separating abilities of the packings when the optimum conditions are found. Moreover, it should be emphasized that the peaks obtained were highly symmetrical and showed no tails. Fig. 1 illustrates a separation of four alkane–alkene pairs (from C_6 to C_9). Fig. 2 presents the result of the separation of a mixture of branched hydrocarbons including two alkane–alkene pairs. Because of the π-type interactions, the alkene is always eluted after the corresponding alkane, e.g., 2,3-dimethyl-2-butene is eluted after 2,2-dimethylbutane and 2,2,4-trimethyl-1-pentene after 2,2,4-trimethylpentane. Fig. 3 presents a chromatogram of a mixture of cycloalkanes and cycloalkenes. Also in this instance a cycloalkene is eluted after the corresponding cycloalkane. The chromatograms in Figs. 4 and 5 illustrate the separating power of the packing modified by $CuCl_2$ towards aromatic hydrocarbons. Both mixtures analysed included isomers. Fig. 4 shows the separation of three C_9H_{12} isomers (cumene,

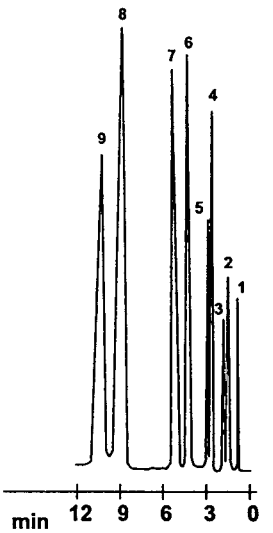

Fig. 1. Separation of a mixture of alkanes and alkenes on a Cu(II) complex-containing packing. Column temperature, 121°C; carrier gas flow-rate, 14 ml/min. Peaks: 1 = 1-pentene; 2 = hexane; 3 = 1-hexene; 4 = heptane; 5 = 1-heptene; 6 = octane; 7 = 1-octene; 8 = nonane; 9 = 1-nonene.

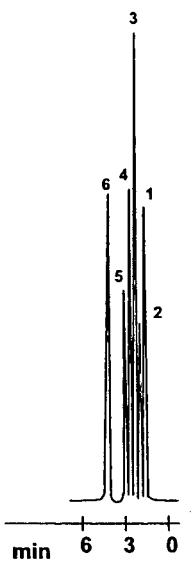

Fig. 2. Analysis of a mixture of branched hydrocarbons. Packing as in Fig. 1. Column temperature, 125°C; carrier gas flow-rate, 25.4 ml/min. Peaks: 1 = 2,2-dimethylbutane; 2 = 2,3-dimethyl-2-butene; 3 = 2,3-dimethylpentane; 4 = 2,2,4-trimethylpentane; 5 = 2,2,4-trimethyl-1-pentene; 6 = 2,2,5-trimethylhexane.

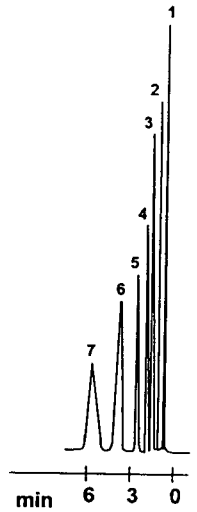

Fig. 3. Chromatogram of a mixture of cyclic hydrocarbons. Packing, column temperature and carrier gas flow-rate as in Fig. 2. Peaks: 1 = cyclopentane; 2 = cyclohexane; 3 = cyclohexene; 4 = cycloheptane; 5 = cycloheptene; 6 = cyclooctane; 7 = cyclooctene.

propylbenzene and *o*-ethyltoluene) and two $C_{10}H_{14}$ isomers (isobutylbenzene and *n*-butylbenzene), and Fig. 5 shows the separation

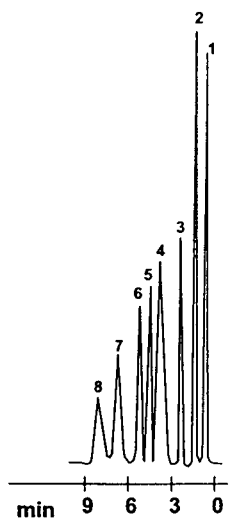

Fig. 4. Separation of a mixture of aromatic hydrocarbons. Packing as in Fig. 1. Column temperature, 147.5°C; carrier gas flow-rate, 18.8 ml/min. Peaks: 1 = benzene; 2 = toluene; 3 = ethylbenzene; 4 = cumene; 5 = propylbenzene; 6 = *o*-ethyltoluene; 7 = isobutylbenzene, 8 = *n*-butylbenzene.

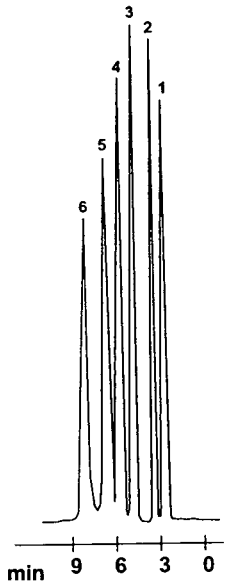

Fig. 5. Separation of a mixture of aromatic hydrocarbons. Packing, column temperature and carrier gas flow-rate as in Fig. 4. Peaks: 1 = *m*-xylene; 2 = styrene; 3 = allylbenzene; 4 = *tert.*-butylbenzene; 5 = isobutylbenzene; 6 = *n*-butylbenzene.

of three $C_{10}H_{14}$ isomers. Fig. 6 illustrates the separation of a mixture of three halogen derivatives of benzene and *p*-chlorotoluene. Also in this case the peaks are symmetrical.

4. Conclusions

Our earlier studies concerned packings capable of electron-donor–acceptor interactions obtained by modifying the silica support with chemically bonded simple functional groups such as cyano, thiol or diphenylphosphine [5–10]. The use of the N-benzoylthiourea group with chelating properties as a modifier has demonstrated that even spatially developed groups meet the requirements of complexation gas chromatography, in spite of the fact that their spatial structure may disturb the contact between the metal and electron donor. The packing modified with copper(II) chloride allowed the investigation of specific π-type interactions with unsaturated hydrocarbons. This packing can also be

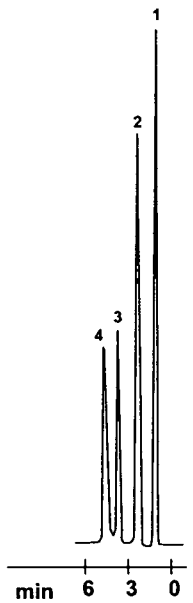

Fig. 6. Chromatogram of a mixture of halogen derivatives of benzene and toluene. Packing as in Fig. 1. Column temperature, 145°C; carrier gas flow-rate, 24 ml/min. Peaks: 1 = fluorobenzene; 2 = chlorobenzene; 3 = bromobenzene; 4 = *p*-chlorotoluene.

used in the chromatographic analysis of complex mixtures of hydrocarbons, including isomers. Its successful application to the separation of isomers confirms its high selectivity.

References

[1] M. Godlewicz, *Nature*, 164 (1949) 1132.
[2] D. Cagniant (Editor), *Complexation Chromatography*, Marcel Dekker, New York, 1992.
[3] W. Holstein and H. Hemetsberger, *Chromatographia*, 15 (1982) 186.
[4] W. Holstein and H. Hemetsberger, *Chromatographia*, 15 (1982) 251.
[5] W. Wasiak and W. Szczepaniak, *J. Chromatogr.*, 364 (1986) 257.
[6] W. Wasiak, *Chromatographia*, 23 (1987) 423.
[7] W. Wasiak, *Chromatographia*, 23 (1987) 427.
[8] W. Wasiak, *J. Chromatogr.*, 547 (1991) 259.
[9] W. Wasiak, W. Urbaniak, I. Obst and R. Wawrzyniak, *Acta Chromatogr. (Poland)*, 1 (1992) 56.
[10] W. Wasiak, *J. Chromatogr. A*, 653 (1993) 63.
[11] K.H. Koenig, M. Schuster, G. Schneeweis and B. Steinbrech, *Fresenius' Z. Anal. Chem.*, 319 (1984) 66.
[12] K.H. Koenig, M. Schuster, B. Steinbach, G. Schneeweis and R. Schlodder, *Fresenius' Z. Anal. Chem.*, 321 (1985) 457.
[13] P. Vest, M. Schuster and K.H. Koenig, *Fresenius' Z. Anal. Chem.*, 335 (1989) 759.
[14] L. Beyer, E. Hoyer, J. Liebscher and H. Hartmann, *Z. Chem.*, 21 (1981) 81.
[15] I.P. Alimarin, L.N. Zhukova, V.K. Runov, E.E. Simov, I.E. Talut and A.K. Trofimchuk, *Zh. Anal. Khim.*, 46 (1991) 695.
[16] O. Bastiansen, L. Hedberg and K. Hedberg, *J. Chem. Phys.*, 27 (1957) 1311.
[17] B. Dickens and W.N. Lipscomb, *J. Chem. Phys.*, 37 (1962) 2084.
[18] A.N. Nesmeyanov and N.A. Nesmeyanov, *Fundamentals of Organic Chemistry*, Mir, Moscow, 1977.

ELSEVIER

Journal of Chromatography A, 690 (1995) 103–108

JOURNAL OF CHROMATOGRAPHY A

Constant-current a.c. electron-capture detector☆

Hameraj Singh, Brian Millier, Walter A. Aue*

Department of Chemistry, Dalhousie University, Halifax, Nova Scotia B3H 4J3, Canada

Received 19 August 1994

Abstract

The constant-current drive is the most popular mode of polarization for the conventional (unipolar) electron-capture detector: in this mode, an increase in analyte produces an *increase* in frequency. In contrast, when the electron-capture detector is operated under a constant-current constraint in the bipolar a.c. mode, an increase in analyte produces a *decrease* in frequency in the, roughly, 10^4 to 10^5 Hz region (as well as an increase in frequency in the, roughly, 10^2 to 10^3 Hz region). Both constant-current mechanisms —similar to the mechanism of the conventional unipolar detector— rely on the increasing withdrawal of electrons from their reactions with increasing concentrations of analyte molecules and carrier cations.

1. Introduction

Often it is more rewarding —and far more interesting— to ask what a detector can*not* do than what it can do. Detectors are presumed to work under particular circumstances or follow particular mechanisms. But can they also work under circumstances opposite to those prescribed; can they also follow mechanisms opposite to those presumed?

We have used this stimulus of instrumental or perceptional inversion on several occasions. And every time we did [1–5], the detector could indeed be persuaded to act contrary to its conventional role. Two of these cases involved the subject of the present note, the electron-capture detector (ECD) (e.g. [6–18]). They will therefore be mentioned here, mainly for the opportunity to set the stage and cite the literature.

In the first case [3], the stimulus of inversion was applied to the undisputed fact that electron-capture peaks are negative, i.e. that they represent *decreases* in current. Could the ECD also produce positive peaks (*increases* in current)? The answer is yes —and that, inter alia, confirms the presence of negative space charges in the detector.

In the second case [4,5], the stimulus of inversion was applied to the well-established singular perception that the ECD, true to its name, monitors electrons —and nothing but. Naturally, then, drive regimes are designed to function in unipolar modes (note that the earliest ECD was d.c.-driven). Could they also function in bipolar modes (e.g., could the ECD be a.c.-driven)? The answer is again yes —in fact, even household current will say so [4]— and that leads, inter alia, to the "a.c. ECD" [5] prototype and to some interesting kinetic conclusions [19,20].

(Note that the common words "d.c." and

☆ Part of doctoral thesis of H.S.

* Corresponding author.

0021-9673/95/$09.50
SSDI 0021-9673(94)00912-0

"a.c." —which historically stand for "direct current" and "alternating current"— refer here to the *imposed polarization* regime: "d.c." implies a set unipolar potential; "a.c." implies an amplitudinally fixed, alternatingly bipolar square-wave potential free of pulse-free intervals.)

This study similarly pursues (and inverts) a common perception. In modern instruments, the most popular ECD drive uses a constant-current constraint. Its major experimental advantage —vis-a-vis the constant-frequency modes— is its much longer linear range [6,21–23]. (Note, however, that this linear-range advantage, particularly from the theoretician's view of strong capturers, remains controversial (cf. [10]).

In the popular constant-current mode, then, the current is maintained at a set level by a variable-frequency pulse generator operating as part of a feedback circuit [21]. As the analyte concentration increases, so does the pulse frequency. (The increased pulse frequency withdraws electrons that would otherwise be captured by analyte molecules or recombine with carrier gas cations.)

So how could this process be inverted? Inversion would mean that the passage of analyte, instead of being signalled by an increase, would have to be signalled by a *decrease* in frequency! Yet just such a frequency inversion was predicted on electronic grounds: at the end of our detailed description of the a.c. ECD, we remarked that the system could conceivably be made to "respond to analyte by a *decrease* in frequency", but cautioned at the same time that "the very idea of a.c.c. (alternating constant current) remains pure speculation" [5].

As a follow-up to that earlier prediction, then, we shall describe here a physical arrangement that inverts the frequency dependence of analyte response and thus reduces prediction to practice.

2. Experimental

This study employs a reliable and only slightly worn gas chromatograph (i.e., one safely beyond its teens): a Tracor Model 550 carrying a ^{63}Ni ECD. Its column is a 100 × 0.2 cm I.D. borosilicate tube, filled with 5% OV-101 on Chromosorb W AW, 100–120 mesh, and operated at 150°C by a nitrogen flow of 35 ml/min. The standard test analyte is α-1,2,3,4,5,6-hexachlorocyclohexane (α-HCCH), as obtained from ICN Labs. (Irvine, CA, USA), and used without further purification. Other GC conditions are similarly conventional (and their choice, we presume, similarly inconsequential to the outcome of this study).

The a.c. ECD is held at a constant current level by the feedback circuit shown schematically in Fig. 1. The circuit is designed to follow classical lines, operate in the simplest fashion possible, and make good use of already existing components. (Our prime objective in choosing the detector and in designing the drive is to answer a mechanistic question rather than to outperform existing instrumentation.)

In this context, the available Tracor electrometer is made to serve as the current-to-voltage converter. The voltage is further amplified, tenfold, by an inverting (or, by operator's choice, non-inverting) operational amplifier. It is then combined with the voltage from the reference potentiometer by a summing operational amplifier with a gain of 200.

The polarity of the reference potentiometer is opposite to that of the voltage resulting from the

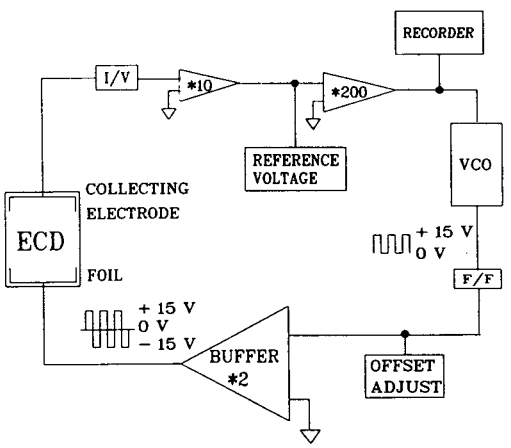

Fig. 1. Block diagram of a.c. constant-current drive. I/V = Current-to-voltage converter (Tracor electrometer); VCO = voltage-controlled oscillator, F/F = flip flop.

detector current (after the first operational amplifier). Setting the reference potentiometer thus sets the baseline current of the detector: it establishes, via the summing amplifier, the base frequency of the voltage-controlled oscillator (VCO).

The VCO converts voltage to frequency in a highly linear manner; its voltage input can hence be used to produce the chromatogram (a plot of frequency vs. time) on a stripchart recorder. At the VCO's extreme upper range, its square-wave output does not precisely conform to a 50% duty cycle. A simple flip-flop (F/F) therefore follows the VCO to yield a "perfect" waveform. (The flip-flop triggers on the *rising* potential only; it therefore reduces the frequency to one half of its original value). A potentiometer then introduces a d.c. offset voltage, chosen (for pure a.c.) such that the + 15 V unipolar pulses appear as + / − 7.5 V alternating pulses against ground. A buffer, which amplifies the a.c. square wave by 2 (to + / − 15 V) completes the circuit by polarizing the foil of the ECD.

The first operational amplifier can be set in either an inverting or a non-inverting configuration. This allows the feedback circuit to respond to chromatographic peaks, i.e. to higher cell impedances, by either a decrease or an increase in the frequency of the + / − 15 V pulses.

3. Results and discussion

To put the following results into context, and to facilitate their discussion by a visual aid, Fig. 2 displays a sample set of response and current profiles from the perceptionally more accessible and diagnostically more informative constant-*frequency* mode. (While this sample hails from the very detector of this study and covers all of its interesting a.c. frequency range, it must be realized that it represents only one possible set out of many: extent and location of the typical features of response and current profiles are highly dependent on the voltage chosen to measure them.)

Similar profiles have been measured [5,19] and/or simulated [3,19,24,25] in earlier work

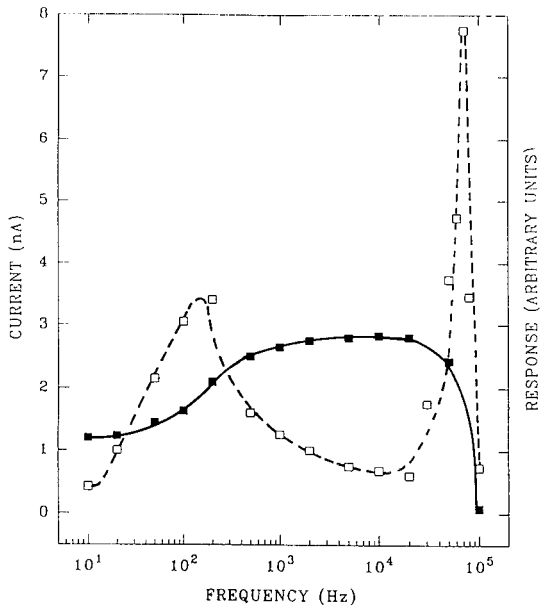

Fig. 2. Response profile of 10 pg α-HCCH (dashed line) superimposed on the current profile (solid line). Drive: + / − 20 V a.c. (square wave) in fixed-frequency mode.

—and descriptions have been given there of their various regions such as the two response maxima that by their nature coincide with the current's ascent to, and descent from, the "plateau". Ascent and descent occur in what we shall term here the "low-frequency" and "high-frequency" regions, respectively.

Fig. 2 suggests that it is these two frequency regions that offer the best chance of success for developing a constant-current a.c. mode. Of these, the low-frequency region (about 10^2 to 10^3 Hz at this voltage) should be closer in behavior to that of the conventional, unipolar constant-current mode. It should react with an *increase* in frequency to an increase in analyte.

On the other hand, the high-frequency region (about 10^5 to 10^4 Hz here) should react with a *decrease* in frequency to an increase in analyte. Since the high-frequency region has at its disposal about double the current the low-frequency region has, it should be capable of a better performance and a wider linear range.

Fig. 3 presents the calibration curve for the *low*-frequency region. As expected, the fre-

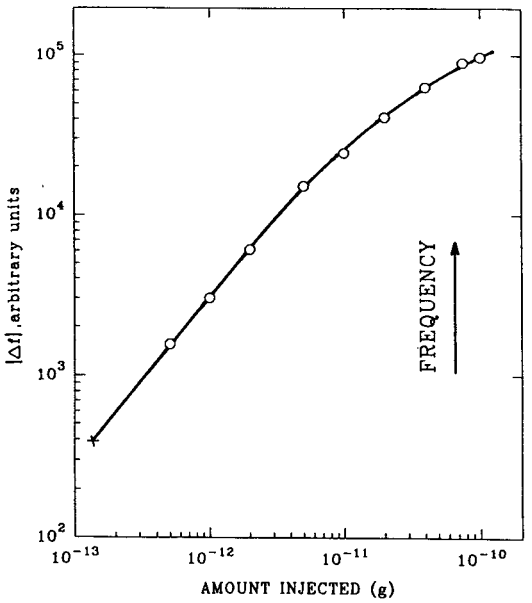

Fig. 3. Calibration curve of α-HCCH from the *low*-frequency region. Constant-current a.c. operation at 1.8 nA; base frequency 270 Hz. The frequency *increases* with increasing amounts of analyte. The lowest point on the calibration curve was not measured but represents extrapolation to the $S/N_{p\text{-}p} = 2$ detection limit, at a resistor–capacitor (RC) filter constant of 1 s and with drift and spikes excluded in measuring the peak-to-peak noise $N_{p\text{-}p}$. Δf = Difference in frequency (between baseline and peak apex).

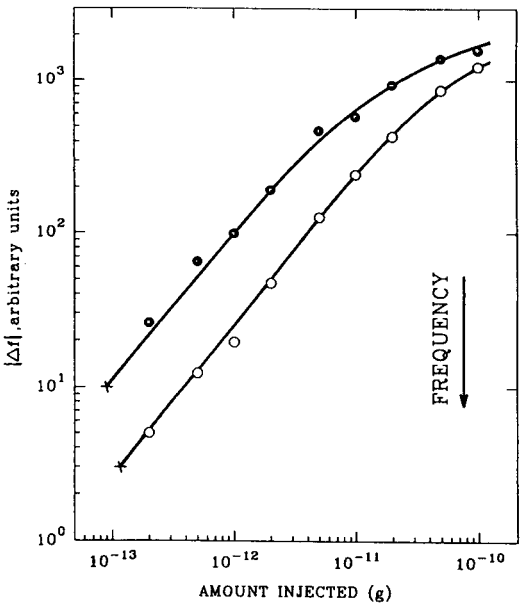

Fig. 4. Calibration curves of α-HCCH from the *high*-frequency region. Constant-current a.c. operation at 1.2 nA (●) and 0.5 nA (○); base frequencies 37.3 and 42.9 kHz, respectively. The frequency *decreases* with increasing amounts of analyte. The lowest points on the calibration curves are the $S/N_{p\text{-}p} = 2$ detection limits (defined as for Fig. 3).

quency *increases* with the analyte concentration (and the difference in frequency is proportional to the difference in analyte concentration). This behavior is similar to that of a typical unipolar constant-current pulse regime operating on the Tracor ECD, although the linear range of the latter is somewhat longer than that of the low-frequency a.c. mode. In light of the earlier discussion, this is neither overly surprising nor overly important.

What is important, however, is the clear experimental demonstration that a constant-current constraint can indeed be imposed on an *a.c.*-driven ECD. This makes it that much more interesting to check the *high*-frequency region —which is unique to a.c. operation— for compliance with the constant-current constraint and, more importantly, with the predicted [5] inversion of the frequency/concentration relationship.

Fig. 4 presents two calibration curves from the *high*-frequency a.c. regime, under constant-current constraints of 1.2 and 0.5 nA. The system does accept the constraints, and its frequency now *decreases* as the analyte concentration increases. In other words, the predicted inversion has been successfully realized.

Frequency inversion can, of course, occur only under a.c., i.e. under *bi*polar conditions. But *given* a bipolar regime, the *inverted*-frequency mode is, in fact, the one that offers the greater flexibility and the better performance.

That the lower of the two currents shown in Fig. 4 should yield the longer linear range comes as no surprise either. "Response" is the difference between baseline and peak, i.e. between analyte-free and analyte-carrying gas streams. The ECD reacts to analyte in the gas stream with a *reduction* of current (which the unipolar constant-current system counters with an increase in frequency [21] or voltage [23]). In (the constant-*frequency* system of) Fig. 2, the current profiles

for analyte-carrying gas streams would stack up below the profile shown for the analyte-free stream, with otherwise similar (i.e. vertically attenuated) shapes and plateaus.

The *constant*-current response to increasing concentration of analyte could thus be represented in Fig. 2 by two horizontal arrows that would start from the (baseline) current profile and point toward a central region under the plateau. Obviously, then, such an arrow would intersect more current profiles —i.e. such a system would be able to respond linearly to larger amounts of analyte— if it operated at a *lower* current level.

With linear response thus achieved, it may be interesting to discuss the similarities and dissimilarities between the low- and high-frequency regions of a.c. constant-current operation in *process*-minded terms. How does the system actually keep the current constant?

The *low*-frequency region exists because the drive —whether of the unipolar or bipolar, d.c. or a.c. variety— works there against the rate of recombination (of cations and electrons). The *high*-frequency region exists because the drive —now of the a.c. or bipolar pulsed variety only— can cycle so fast as to become (almost) ineffective: electrons are no longer driven all the way to the anode, but are pulled back in midflight by the reversing potential. In other words, they oscillate.

(Note: "oscillation" —applied here to the swaying of electrons as induced by the drive's external potential and as modified by the space charges' internal field— appears to be the appropriate term for very fast a.c. regimes. For bipolar regimes that contain pulse-*free* intervals, however, bidirectional *relaxation* kinetics [26] should be included in this so far mostly figurative characterization.)

In the constant-frequency system of Fig. 2, the current's plateau region is characterized by a small rate of recombination and a small concentration of electrons. In the current's valley regions at both sides of the plateau (and particularly so on the high-frequency side), the recombination rate is large and so is the concentration of electrons [5,19].

The electron-capture reaction is first order in electrons. Furthermore, electrons that are captured by analyte molecules and form heavy anions cause the cell impedance and the cation concentration to rise —which, in turn, increases the recombination rate of electrons that escape capture. A drive system set on keeping the current constant will thus have to pull electrons away from both the electron-capture and the recombination reaction, by collecting them with greater efficiency, i.e., by moving in frequency toward the plateau region of the (analyte-doped) current profile.

This means for the low-frequency regime an increase, for the high-frequency regime a decrease in frequency. (The former tries to tug more often; the latter tries to tug longer.)

The final effect is, however, always the same: when peaks arrive, the constant-current drive responds by working harder to herd its electrons to the safety of the anode —away from the greater chance of being captured by analyte molecules, away from the increased possibility of recombining with carrier gas cations.

Acknowledgements

This research was supported by NSERC operating grant A-9604. It followed a preliminary stab at the problem by M.P. Merrin in 1987.

References

[1] Y.-Z. Tang and W.A. Aue, *Mikrochim. Acta*, II (1987) 21.
[2] Y.-Z. Tang and W.A. Aue, *Mikrochim. Acta*, II (1987) 29.
[3] A. McMahon and W.A. Aue, *J. Chromatogr.*, 393 (1987) 221.
[4] K.W.M. Siu and W.A. Aue, *J. Chromatogr.*, 268 (1983) 273.
[5] W.A. Aue, K.W.M. Siu and S.S. Berman, *J. Chromatogr.*, 395 (1987) 335.
[6] A. Zlatkis and C.F. Poole (Editors), *Electron Capture* (*Journal of Chromatography Library*, Vol. 20), Elsevier, Amsterdam, 1981.

[7] M. Dressler, *Selective Gas Chromatographic Detectors (Journal of Chromatography Library*, Vol. 36), Elsevier, Amsterdam, 1986.
[8] E.D. Pellizzari, *J. Chromatogr.*, 98 (1974) 323.
[9] W.A. Aue and S. Kapila, *J. Chromatogr. Sci.*, 11 (1973) 255.
[10] E.P. Grimsrud, in H.H. Hill and D.G. McMinn (Editors), *Detectors for Capillary Chromatography*, Wiley, New York, 1992, Ch. 5.
[11] J. Connor, *J. Chromatogr.*, 200 (1980) 15.
[12] E.P. Grimsrud, *Mass Spectrom. Rev.*, 10 (1992) 457.
[13] S.O. Farwell, D.R. Gage and R.A. Kagel, *J. Chromatogr. Sci.*, 19 (1981) 358.
[14] W.E. Wentworth, E. Chen and J.E. Lovelock, *J. Phys. Chem.*, 70 (1966) 445.
[15] M.W. Siegel and M.C. McKeown, *J. Chromatogr.*, 122 (1976) 397.
[16] A. Neukermans, W. Kruger and D. McManigill, *J. Chromatogr.*, 235 (1982) 1.
[17] W.A. Aue and S. Kapila, *J. Chromatogr.*, 188 (1980) 1.
[18] W.A. Aue, K.W.M. Siu, D. Beauchemin and S.S. Berman, *J. Chromatogr.*, 500 (1990) 95.
[19] K.W.M. Siu, S.S. Berman and W.A. Aue, *J. Chromatogr.*, 408 (1987) 53.
[20] K.W.M. Siu, S.S. Berman and W.A. Aue, *J. Chromatogr.*, 391 (1987) 433.
[21] R.J. Maggs, P.L. Joynes, A.J. Davies and J.E. Lovelock, *Anal. Chem.*, 43 (1971) 1966.
[22] J.J. Baum and C. Josias, presented at the *27th Pittsburgh Conference, Cleveland, OH, March 1976*, abstract 437.
[23] W.A. Aue and K.W.M. Siu, *Anal. Chem.*, 52 (1980) 1544.
[24] A.W. McMahon and W.A. Aue, *Mikrochim. Acta*, III (1988) 11.
[25] A.W. McMahon, *Ph.D. Thesis*, Dalhousie University, Halifax, 1987.
[26] H. Singh, B. Millier and W.A. Aue, *J. Chromatogr. A*, 689 (1995) 45.

ELSEVIER

Journal of Chromatography A, 690 (1995) 109–118

JOURNAL OF CHROMATOGRAPHY A

Determination of nitrilotriacetic acid and ethylenediaminetetraacetic acid in environmental samples as their methyl ester derivatives by gas chromatography–mass spectrometry

Yoshinori Nishikawa*, Tameo Okumura

Environmental Pollution Control Centre, 62-3, 1 Chome, Nakamichi, Higashinari-ku, Osaka City 537, Japan

First received 6 July 1994; revised manuscript received 16 September 1994

Abstract

A method for the determination of nitrilotriacetic acid (NTA) and ethylenediaminetetraacetic acid (EDTA) in environmental samples such as river water and sediment is reported. An aqueous sample, after evaporation to dryness, was treated with a boron trifluoride–methanol mixture. The resulting methyl ester derivatives were determined by capillary GC–MS with selected-ion monitoring. NTA and EDTA could be determined in the ranges 4.1–12.2 and 3.9–11.8 ng/ml in water with relative standard deviations (R.S.D.s) of 3.1–7.8% and 11.0–19.7%, respectively. Their recoveries from river water and sediment were 74–92% with R.S.D. 1.5–6.8% and 51–60% with R.S.D. 14–16%, respectively.

1. Introduction

Nitrilotriacetic acid (NTA) and ethylenediaminetetraacetic acid (EDTA) have received much attention as chelating agents in analytical chemistry. As they form water-soluble and stable chelates with many metals, NTA and EDTA have been used as detergents and in a variety of other products, and their use results in their ultimate release to the environment. These chelating agents may affect the distribution of metals within aquatic ecosystems.

Early analytical procedures for NTA and EDTA [1] involved mainly three techniques, GC, polarography and spectrophotometry. GC methods mostly involve converting the analyte into a methyl or other volatile ester and determining the ester using a flame ionization [2–5] or a nitrogen-specific detector [6–8]. Polarographic and spectrophotometric techniques are critical with respect to selectivity. To increase the selectivity, ion-pair liquid chromatographic (LC) combined with electrochemical [9–10] or UV–Vis [11–13] detection has been used. Although the application of ion-pair LC to environmental samples has been investigated, considerable difficulties are encountered owing to the sample matrix effects.

The more recent GC–MS technique with selected-ion monitoring (SIM) provides excellent

* Corresponding author.

0021-9673/95/$09.50
SSDI 0021-9673(94)00919-8

sensitivity and selectivity. In this paper, a convenient method is presented for determining NTA and EDTA in environmental sample at ng/ml levels by capillary GC–MS-SIM via methylation with BF_3–CH_3OH.

2. Experimental

2.1. Reagents and apparatus

NTA disodium salt and EDTA disodium salt dihydrate, used as standards because their free acids are slightly soluble in water, *trans*-1,2-cyclohexanediamine-N,N,N′,N′-tetraacetic acid (CDTA) monohydrate, which was dissolved in 1 *M* NaOH and used as surrogate standard, and Fe(III)–EDTA were of special grade from Aldrich (Milwaukee, WI, USA) and Dotite (Kumamoto, Japan). $[^2H_{10}]$Acenaphthene (acenaphthene-d_{10}), $[^2H_{10}]$phenanthrene (phenanthrene-d_{10}) and $[^2H_{10}]$fluoranthene (fluoranthene-d_{10}), used as internal standards, were obtained from MSD Isotopes (Montreal, Canada). Boron trifluoride–methanol complex (BF_3–CH_3OH), containing ca. 14% BF_3 in gas chromatographic grade methanol, and other reagents of special grade were purchased from Wako (Osaka, Japan) and Tokyo Kasei (Tokyo, Japan).

A Yamato (Tokyo, Japan) RE-46 rotary evaporator was used for concentration of sample solutions. A Branson (Shelton, CT, USA) B-220 ultrasonic extractor and a Poly Toron PT10-30 homogenizer were used for extraction from sediment and fish samples, respectively. A Tomy Seiko (Tokyo, Japan) LC06-SP centrifuge was employed for phase separation of sediment or fish samples.

2.2. Gas chromatography–mass spectrometry

A Hewlett-Packard (Avondale, PA, USA) HP 5790 gas chromatograph and a Nihondenshi (Tokyo, Japan) JEOL-DX303 mass spectrometer with a DA-5000 data processing system were employed. The analytical column used was Ultra-2 cross-linked with 5% phenylmethylsilicone (25 m × 0.32 mm I.D., 0.52 μm film thickness). The GC temperature programme was as follows: initial temperature, 70°C held for 4 min, then increased at 15°C/min to 300°C and held there for 10 min. The temperatures of the injector, transfer line and ion source were 250°C. The carrier gas was helium at 7.5 psi (61 cm/s). Samples were injected in the splitless mode with a 2-min purge off. The mass spectrometer was

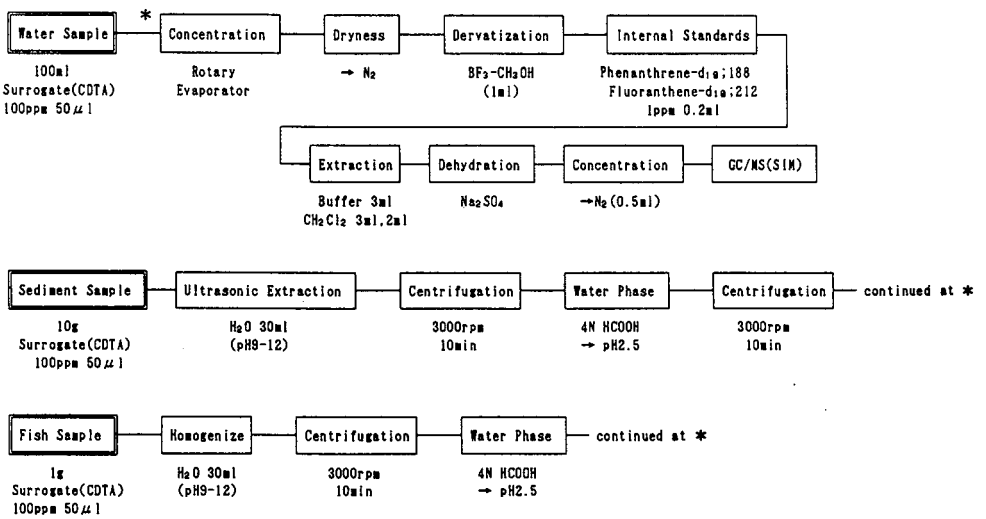

Fig. 1. Flow scheme for the determination of NTA and EDTA in environmental samples.

operated at 70 eV and 300 μA with electron impact ionization using the scan or SIM mode. Between retention times of 8 and 20 min, ions at *m/z* 174 (NTA and EDTA), 188 (phenanthrene-d_{10}), 212 (fluoranthene-d_{10}), 233 (NTA), 289 (EDTA), 348 (EDTA) and 402 (CDTA) were monitored.

2.3. Analytical procedure

The procedure for the determination of NTA and EDTA in environmental samples is outlined in Fig. 1. A 100-ml volume of the water sample was spiked with the surrogate standard and adjusted to pH 2.5 with 4 *M* formic acid. The sample was reduced to about 2–3 ml in a rotary evaporator, transferred into a 10-ml test-tube and evaporated completely to dryness under nitrogen. A 1-ml volume of BF_3–CH_3OH solution was added to the dry sample and the tube was stoppered tightly with a clamp and allowed to stand for 1 h at 60°C or 30 min at 80°C. To this reactant, 0.2 ml of the internal standard solution, 3 ml of buffer solution (1 *M* KH_2PO_4 adjusted to pH 7 with 10 *M* NaOH) and 3 ml of methylene chloride were added, followed by shaking in a separating funnel. The extracted organic phase was dehydrated by passing it through anhydrous Na_2SO_4. The aqueous phase was re-extracted with 2 ml of methylene chloride in the same way. The organic phase was combined with the first extract in a 10-ml test-tube. The organic phase was evaporated to 0.5 ml under a stream of nitrogen, then a 1-μl aliquot was analysed by GC–MS-SIM.

For sediment, 10 g of sample spiked with the surrogate were added to 30 ml of pure water with stirring and the pH was adjusted to 9–12. The muddy sample was extracted in an ultrasonic extractor for 10 min and then centrifuged at 3000 rpm (1600 *g*) for 10 min. The aqueous phase was adjusted to pH 2.5 with 4 *M* formic acid. As a small amount of precipitate was occasionally observed at this stage, the turbid solution was re-centrifuged and then the supernatant solution was subjected to the same procedure as for water samples.

For fish, 1 g of sample was homogenized and centrifuged in a similar way.

3. Results and discussion

3.1. Derivatization reaction

As aminopolycarboxylic acids such as NTA and EDTA are non-volatile, it is preferable that their carboxyl groups are derivatized to volatile ester groups. First, dimethylformamide dimethylacetal was used as a methylation reagent, but some difficulties were encountered, i.e., masking reagents and thorough prewashing of glassware with acid were required, and the

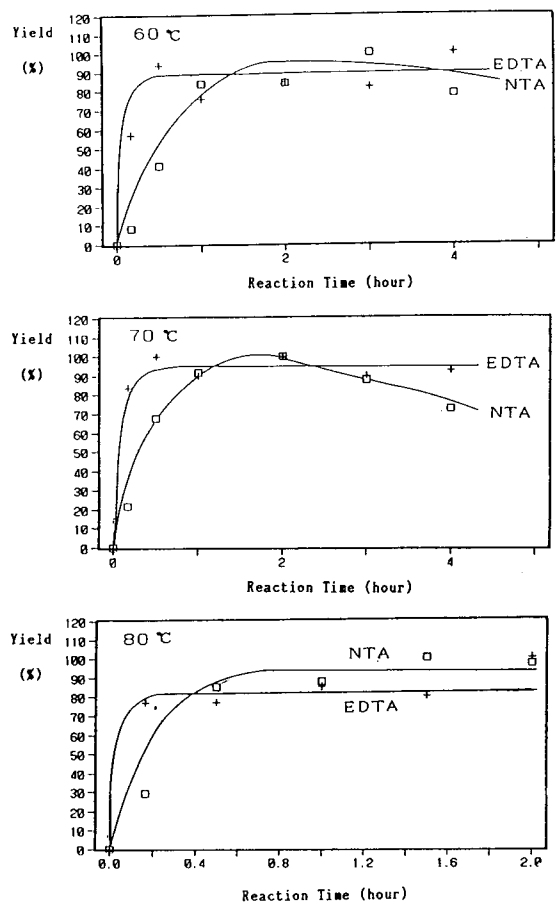

Fig. 2. Effects of reaction temperature and time on NTA and EDTA methyl esterfication yields.

results obtained varied widely, particularly at low μg/ml levels in the esterification reaction. The difficulties were overcome by using BF_3–CH_3OH instead of dimethylformamide dimethylacetal.

The reaction temperature and time were investigated using BF_3–CH_3OH. Fig. 2 shows the yields for NTA and EDTA at different temperatures and times. The optimum reaction conditions were 30 min at 80°C or 60 min at 60°C.

3.2. Internal standard and surrogate standard

It is preferable that deuterium-substituted substances with retention times near to those of the analytes are used as internal standards. The retention time of acenaphthene-d_{10} was near to that of NTA, but interference on the chromatogram was observed with real samples. The internal standards selected were phenanthrene-d_{10} for NTA and fluoranthene-d_{10} for EDTA. CDTA, which is a similar aminopolycarboxylic acid that is not present in the environmental samples, was used as a surrogate standard. When CDTA was added to an environmental sample just before processing, the reaction yield and losses due to manipulation compensated each other. The recovery of EDTA improved, but the precision was bad owing to the large retention time gap for NTA.

3.3. Mass spectra and GC–MS-SIM traces of standards

Fig. 3 shows the mass spectra of methyl esters of NTA, EDTA and CDTA. The base peak ions were at m/z 174, 174 and 168 and the molecular peak ions at 233, 348 and 402, respectively. The base peak ions of NTA and EDTA at m/z 174 are assumed to be ions of $[CH_2N(CH_2COOCH_3)_2]^+$. The base peaks showed lower selectivity than the molecular ions, so the latter ions were used for the determination. Fig. 4 shows typical GC–MS-SIM traces

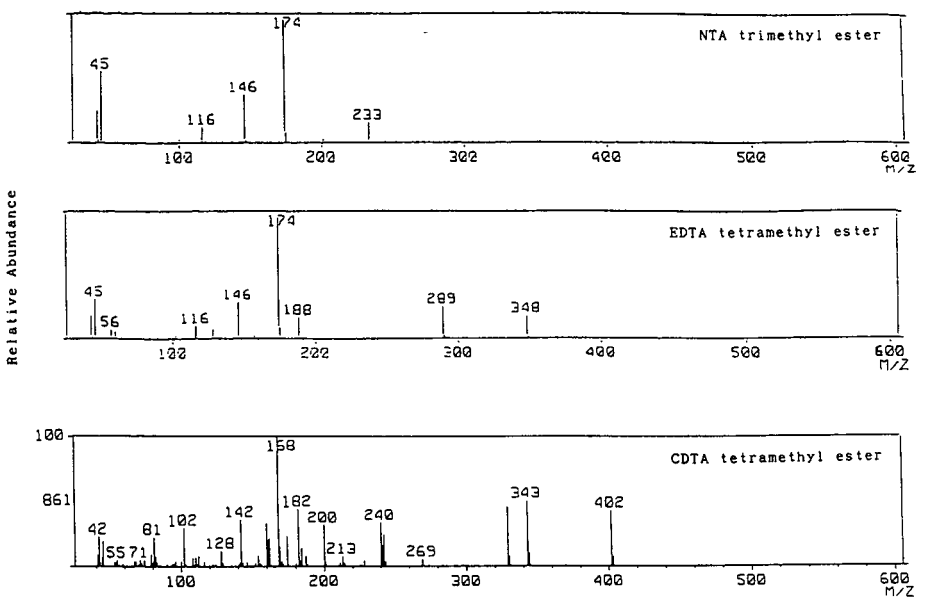

Fig. 3. GC–MS of methyl ester derivatives of NTA, EDTA and CDTA.

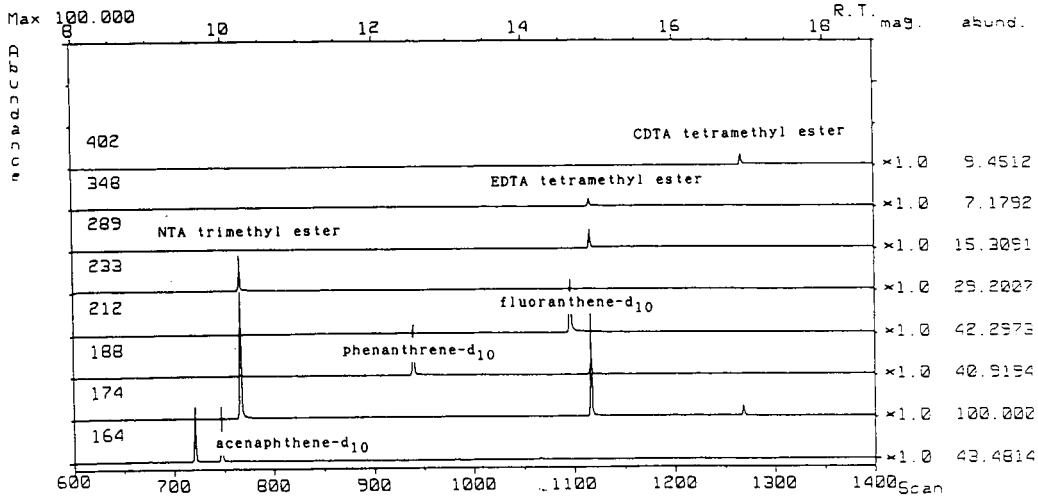

Fig. 4. Typical GC–MS-SIM traces of methyl ester derivatives of NTA, EDTA, CDTA and internal standards. R.T. = Retention time in min; mag. = magnitude; abund. = abundance.

for the standards. The retention times of the methyl esters of NTA, EDTA and CDTA were 10.2, 14.8 and 16.9 min, respectively.

3.4. Calibration

Calibration graphs for NTA and EDTA were obtained by plotting the amount injected against the peak-area ratio of the analyte to the internal or surrogate standard. Examples of calibration graphs are shown in Fig. 5. The concentration of NTA or EDTA in environmental sample was calculated as follows:

$$\text{Concentration(ng/ml or ng/g)} = F\ \text{(ng)} \cdot \text{FSV (ml)}/I\ \text{(ml)} \cdot \text{SV (ml or g)} \times \gamma$$

$$\gamma\ \text{(NTA)} = \text{NTA/NTA disodium} = 0.79$$

$$\gamma\ \text{(EDTA)} = \text{EDTA/EDTA disodium dihydrate} = 0.81$$

where F is the amount found by using the calibration graph, FSV the final sample volume, SV the sample volume, I the amount injected and γ the conversion coefficient to each free acid.

3.5. Esterfication reaction of Fe(III)–EDTA

NTA and EDTA form stable chelates with various metals. Fe(III)–EDTA is one of the

Table 1
Detection limits and precision for NTA and EDTA

Compound	DL (ng/ml)	Precision		
		Concentration (ng/ml)	Found[a] (ng/ml)	R.S.D. (%)
NTA	2.1	4.1	4.3	7.8
		8.1	7.7	5.6
		12.2	11.3	3.1
EDTA	6.2	3.9	3.5	11.0
		7.9	7.5	19.7
		11.8	9.7	11.8

Detection limits (DL) were calculated from the sensitivity of response estimating standard deviation as follows:

$$D = t(n-1, 0.05)\sigma/\sqrt{n}(\mathrm{d}C/\mathrm{d}R); \quad \mathrm{DL} = 3\bar{D},$$

where D is the detection power, $\bar{D}$ is the average value of D calculated from different concentrations (detection limits are defined as three times the detection power), $t(n-1, 0.05)$ is the t-distribution at 95% reliability, σ is the standard deviation of the response, n is the number of replicates, c is the concentration of NTA or EDTA and R is the peak-area ratio of analyte to internal standard.

[a] Average of four experiments.

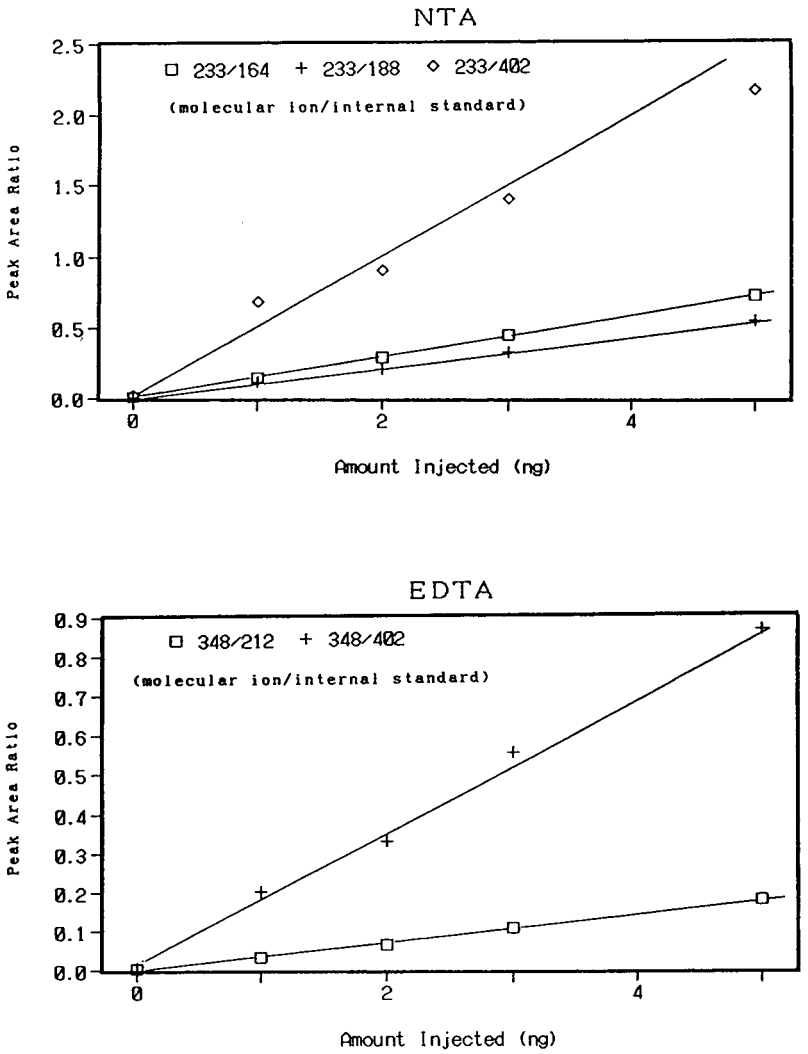

Fig. 5. Typical calibration graphs for NTA and EDTA with different internal and surrogate standards.

most stable chelate compounds and one of probable forms that exist in the environment. Its esterification yield with the proposed method was therefore investigated. The results show that for 23.7 nmol of Fe(III)–EDTA the amount determined was at 18.3 nmol (yield 77%) and 23.3 nmol (yield 98%) as EDTA when calibrating with fluoranthene-d_{10} internal standard and CDTA surrogate standard, respectively. This result indicates that a quantitative reaction proceed even in the metal chelate form.

3.6. Preservation in river water

Two sets of 100-ml river water samples spiked with 4.1 μg of NTA and 3.9 μg of EDTA were stored in a refrigerator for 7 days, then analyzed. The amounts determined were 3.5, 4.1 (5.7, 6.1) μg of NTA and 3.7, 3.5 (5.4, 5.7) μg of EDTA, and those for the non-spiked samples were 0.23 (0.06) μg of NTA and 1.6 (1.8) μg of EDTA, where the determined values calibrated with the CDTA surrogate standard are given in parenthe-

Table 2
Recovery of the methyl ester of NTA from environmental samples

Sample	Sample amount	Added (μg)	Found[a] (μg)	Recovery[a] (%)	No. of samples (n)	R.S.D. (%)
Pure water	100 ml	1.22	1.13 (1.90)	92 (156)	4	3.1 (17.2)
River water	100 ml	4.05	3.71 (6.26)	92 (155)	2	1.5 (6.5)
Sea water	10 ml	0.41	0.29 (0.99)	70 (241)	2	11.2 (20.1)
Sediment	10 g	4.05	2.05 (3.60)	51 (89)	7	16.4 (11.2)
Fish	1 g	0.81	0.97 (1.24)	120 (153)	7	24.9 (27.4)

The values in parentheses indicate the determined values calibrated with the CDTA surrogate standard.
[a] The amount found is the difference between the amount detected in spiked sample (S) and that in the non-spiked sample (N); recovery (%) = $[(S - N)/A] \cdot 100$, where A is the amount added.

ses. Based on the recovery, it appears that NTA and EDTA in river water do not decompose when stored in a cool location for up to 7 days.

3.7. Quantitative response

Table 1 reports the detection limits and precision for NTA and EDTA using the proposed procedure. A blank test was performed using a 100 ml of distilled water and with other chemicals used in analysis. No blank peaks corresponding to NTA and EDTA were observed in the chromatogram. NTA and EDTA were determined in the ranges 4.1–12.3 and 3.9–11.8 ng/ml in water samples with relative standard deviations (R.S.D.s) of 3.1–7.8% and 11.0–19.7%, respectively. The estimated detection limits of NTA and EDTA in water were 2.1 and 6.2 ng/ml, respectively, for a 100-ml water sample.

3.8. Determination in real samples

Analyte recovery was investigated by using 100 ml of pure and river water, 10 ml of sea water, 10 g of sediment and 1 g of fish sample spiked with 0.41–4.05 and 0.39–3.93 μg of NTA and EDTA, respectively. Tables 2 and 3 show that 92% and 74% of NTA and EDTA were recovered from the river water with R.S.D.s of 1.5% and 6.8%, respectively. For sea water, the recovery was lower, especially for EDTA. The low recovery could be due to matrix effects in sea water; in fact, a white, powdery salt was deposited during the analytical procedure. For sediment and fish samples, the recoveries were

Table 3
Recovery of the methyl ester of EDTA from environmental samples

Sample	Sample amount	Added (μg)	Found[a] (μg)	Recovery[a] (%)	No. of samples (n)	R.S.D. (%)
Pure water	100 ml	0.39	0.35 (0.48)	89 (124)	4	11.0 (12.4)
River water	100 ml	3.69	2.72 (4.54)	74 (123)	2	6.8 (3.6)
Sea water	10 ml	0.39	0.07 (0.54)	19 (139)	2	25.8 (34.0)
Sediment	10 g	3.93	2.36 (4.34)	60 (110)	7	14.1 (4.0)
Fish	1 g	0.79	0.50[b] (0.83)	63[b] (105)	7	12.3[b] (8.3)

The data in parentheses indicate the determined values calibrated with the CDTA surrogate standard.
[a] See Table 2 for definition of recovery.
[b] For fish samples, [$^2H_{10}$] = phenanthrene was used as the internal standard instead of [$^2H_{10}$]fluoranthene owing to interference on the chromatogram.

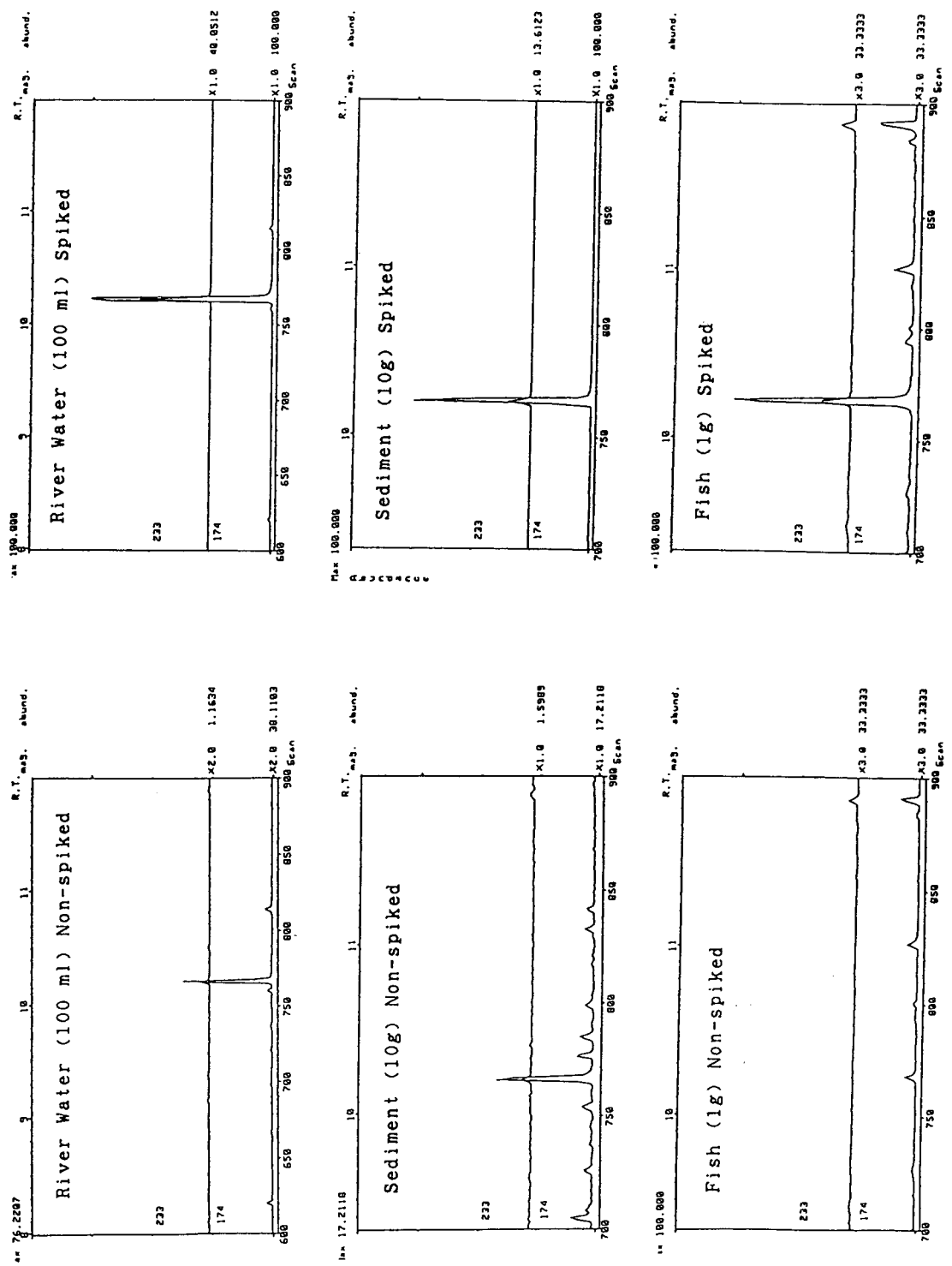

Fig. 6. Determination of NTA in normal and spiked river water, sediment and fish samples.

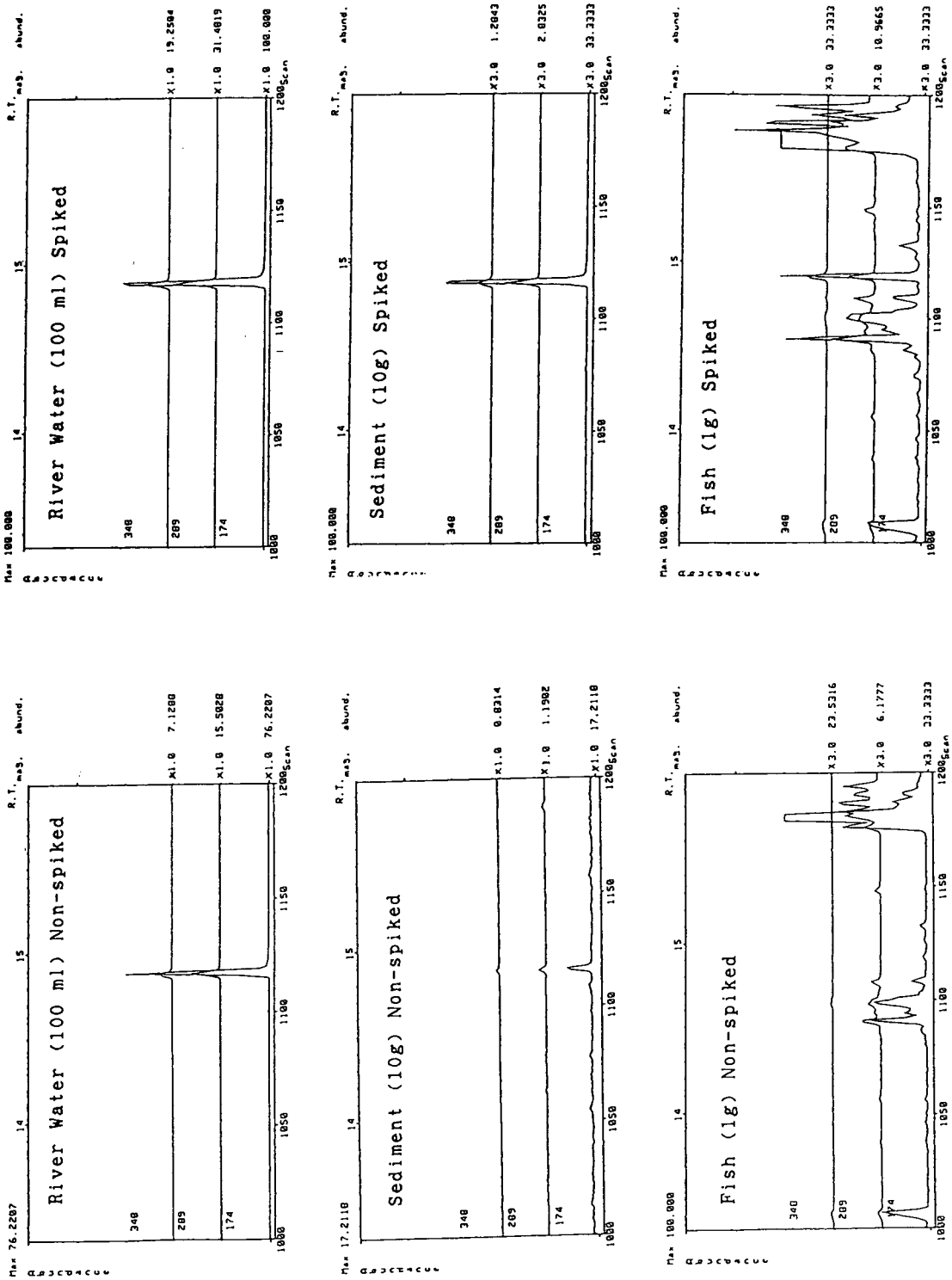

Fig. 7. Determination of EDTA in normal and spiked river water, sediment and fish samples.

51–60% and 63–120% with R.S.D.s of 14–18% and 12–25%, respectively. Whenever the recovery was calculated with the use of the CDTA surrogate standard, it became higher and was more than 100% in many instances. Figs. 6 and 7 show typical chromatograms for non-spiked and spiked samples of river water, sediment and fish. Both NTA (Fig. 6) and EDTA (Fig. 7) were detected in river water and sediment at low ng/ml and ng/g levels, respectively.

4. Conclusions

The proposed GC–MS-SIM method may be useful for the routine analysis of environmental samples at low ng/ml levels. However, it is difficult to analyse sea-water samples owing to the high concentration of salt. Determination of NTA and EDTA by this method could probably be applicable to their chelate forms in environmental samples.

Acknowledgement

This work was supported by the Office of Health Studies, Environmental Health Department, Japan Environmental Agency (Project for Development of Analytical Methods).

References

[1] K.L.E. Kaiser, *Water Res.* 7 (1973) 1465.
[2] M. Mihara, R. Amano, T. Kondo and H. Tanabe, *Shokuhin Eiseigaku Zasshi*, 11 (1970) 88.
[3] Y.K. Chau and M.E. Fox, *J. Chromatogr. Sci.*, 9 (1971) 271.
[4] L. Rudling, *Water Res.*, 6 (1972) 871.
[5] R.J. Stolzberg and D.N. Hume, *Anal. Chem.*, 49 (1977) 374.
[6] M. Malaiyandi, D.T. Williams and R. O'Grady, *Environ. Sci. Technol.*, 13 (1979) 59.
[7] D.T. Williams, F. Benoit, K. Muzika and R. O'Grady, *J. Chromatogr.*, 136 (1977) 423.
[8] C. Schaffner and W. Giger, *J. Chromatogr.*, 312 (1984) 413.
[9] J. Dai and G.R. Helz, *Anal. Chem.*, 60 (1988) 301.
[10] W. Buchberger, P.R. Haddad and P.W. Alexander, *J. Chromatogr.*, 546 (1991) 311.
[11] D.G. Parkes, M.G. Caruso and J.E. Spradling, III, *Anal. Chem.*, 53 (1981) 2154.
[12] C.C.T. Chinnick, *Analyst*, 106 (1981) 1203.
[13] W. Huber, *Acta Hydrochim. Hydrobiol.*, 20 (1992) 6.

ELSEVIER

Journal of Chromatography A, 690 (1995) 119–129

JOURNAL OF CHROMATOGRAPHY A

Gas chromatographic determination of triclopyr in fruits and vegetables

Keh-Chuh Ting*, Chang-Sook Lee

State of California, Department of Food and Agriculture, Pesticide Residue Laboratory, 169 East Liberty Avenue, Anaheim, CA 92801, USA

First received 1 July 1994; revised manuscript received 18 October 1994

Abstract

This research was comprised of two parts: quantitative analyses, and confirmatory test. In the quantitative analyses, five classes of fruits and vegetables comprising 10 individual commodities were fortified with triclopyr herbicide at 0.4 and 0.8 ppm level. Triclopyr was extracted from the matrices and derivatized separately to 2-chloroethylene ester with 2-chloroethanol–BCl_3 and methyl ester with diazomethane. The esters were then quantitated by GC–ECD and GC–NPD. The GC–ECD recoveries for 2-chloroethylene ester were 100.0% and 100.7% at 0.4 ppm and 0.8 ppm fortification levels, respectively, whereas methyl ester recovery was 103.9% at 0.4 ppm fortification level. Similarly, the GC–NPD recoveries for 2-chloroethylene ester were 99.0% and 97.9% at 0.4 ppm and 0.8 ppm fortification levels respectively, whereas methyl ester recovery was 102.0% at 0.4 ppm fortification level.

In the confirmatory test, the 2-chloroethylene ester was introduced into a GC–ion trap. The EI mass spectrum was then interpreted based on the criteria of molecular ion, isotopes, base ion, characteristic ions and the nitrogen rule. Compared to existing methods, this method has reduced partition solvents to nearly one-tenth. In addition, this method proved to be simple, fast, safe and accurate.

1. Introduction

Triclopyr is a systemic herbicide manufactured by DowElanco, its chemical name is 3,5,6-trichloro-2-pyridyloxyacetic acid by IUPAC [1]. It is often used in mixed formulation with other phenoxyalkanoic acids (e.g. 2,4-D, dicamba, mecoprop, etc.) for control of woody plants and many broad leaved weeds in grasslands, uncultivated lands, and rice fields [1,2]. As the rice market becomes more liberal in Japan and other Asian countries, California rice could become an important export in the near future. Consequently, rice production related chemicals, such as triclopyr, may be used more frequently than in the past. As a result, the occurrence of illegal applications and/or other crop violations due to drift from adjacent rice fields would rise. Therefore, the development of an effective and accurate analysis method is crucial for a regulatory agency like ours.

Conventionally, triclopyr is analyzed like phenoxyalkanoic herbicides [3–5]. This method requires a large amount of solvents for partition clean-up in sample extraction. Additionally, diazomethane, which is both explosive and exceed-

* Corresponding author.

0021-9673/95/$09.50
SSDI 0021-9673(94)01010-2

ingly toxic [6], must be generated on site in the existing method for the methyl ester derivatization reaction. Methyl ester is an early eluting compound which is vulnerable to certain commodity (e.g. citrus, onion and cabbage) matrix interferences. Chromatographically, early eluting matrix interferences from fruits and vegetables create difficulty in identification and quantitation.

Therefore, the first objective in method development was to reduce the volume of solvents in the sample preparation procedures. The second objective was to replace diazomethane with a derivatizing reagent that was (1) comparatively non-explosive, (2) low in toxicity, (3) an enhancement for detector response, (4) an improvement for separation and/or resolution (longer retention time or late peak) and (5) equivalently or better interpreted by an advanced instrument such as a mass spectrometer. The third objective was to establish an accurate method which was confirmed by applying multiple instrumentation strategy. In the method, we use GC–ECD and GC–NPD for quantitation and GC–ion trap for confirmation. The multiple instrumentation approach would seem to be redundant; however, in case of enforcement action or litigation by a governmental agency such as ours, decisive scientific evidence beyond a shadow of doubt is necessary.

2. Experimental

2.1. Chemicals

The solvents used in the experiment were analysis-grade reagents from J.T. Baker. The sodium sulfate (Na_2SO_4) anhydrous granular was purchased from EM Science. The derivatization reagent, 2-chloroethanol–boron trichloride (10%), was purchased from Applied Science Laboratories. The triclopyr standard (100%) was supplied and purity certified by the California Department of Food and Agriculture (CDFA), standards repository.

2.2. Instrumentation

Three instruments were used in this study.

(a) A Varian 3300 GC system was equipped with a Ni63 electron capture detector (ECD). The temperature program was: initial temperature 150°C held for 2 min, ramp rate 10°C/min, 1st final temperature 180°C held for 7 min, ramp rate 20°C/min, 2nd final temperature 250°C held for 2 min. The injection mode was splitless, held for 0.75 min and the injection volume was 1 μl. A J&W Scientific DB-210 column (50% trifluoropropyl methyl poly siloxane) was installed for the study. The column size was 15 m × 0.32 mm I.D. and coated film thickness was 1.0 μm.

(b) A Perkin-Elmer Sigma 2 GC system was equipped with a thermionic nitrogen–phosphorus detector (NPD). The temperature program was: initial temperature 150°C held for 2 min, ramp rate 10°C/min, final temperature 225°C held for 2 min. The injection volume was 2 μl. A Hewlett Packard HP-1 column (methyl silicone gum) was installed. The column size was 10 m × 0.53 mm I.D. and coated film thickness was 2.65 μm.

(c) A Varian 3400 GC system was equipped with a Finnigan MAT ITS-40 mass spectrometry detector. The temperature program was: initial temperature 150°C held for 1 min, ramp rate 10°C/min, final temperature 280°C held for 6 min. The injection mode was splitless, held for 0.75 min and the injection volume was 2 μl. For the ion trap ITS-40 system, the parameters were: mass range 50 to 400 amu, 1 second/scan, acquire time 20 min, fil/mul delay 240 s, peak threshold 50 counts, mass defect 50 mmu/100 amu, background mass 49 amu, ionize mode EI, and auto ion control on. A J&W Scientific DB-5 column (5% phenyl methyl poly siloxane) was used. The column size was 30 m × 0.25 mm I.D. and coated film thickness was 0.25 μm.

2.3. Preparation of spiked produce samples

Produce was grouped into 5 classes consisting of leafy vegetables, roots, fruits, citrus and spices. Each group contained 2 commodities in

the experiment. A unit of 3 Mason jars with 50 g per jar of chopped commodity was prepared for fortification. The first jar was fortified with 20 μg triclopyr (0.4 ppm level) for diazomethane derivatization as the control. The second and third jars were spiked with 20 μg and 40 μg triclopyr, respectively, to form 0.4 ppm and 0.8 ppm level for 2-chloroethanol–BCl_3 ethylation studies.

2.4. Sample extraction, derivatization and micro partition clean-up procedure

Vegetable or fruit was chopped and mixed in a food chopper. Only 50 g of the well chopped sample was placed in a 1-pt (470-ml) Mason jar. Then, 10 ml H_2SO_4 (1:1 in H_2O), 50 ml ethyl ether–hexane (1:1) and 25 g Na_2SO_4 were added into the jar. The contents of the jar were then blended by an Omni-Mixer for 2 min. The entire mixture was transferred into a 200-ml wide-mouth centrifuge bottle and the bottle was centrifuged for 2 min at 201 *g* (1500 rpm). The top 5 ml ethyl ether–hexane layer was pipetted into a 15-ml conical tube and evaporated to ca 0.5 ml with gentle air concentrator (N- EVAP) at ambient temperature.

Methylation

Approximately 0.25 ml or 10 drops of diazomethane was added into the conical tube. The tube was capped, and the contents were mixed and allowed to react for 30 min.

Ethylation

Approximately 0.2 ml or 7 drops of 2-chloroethanol–BCl_3 was added into the conical tube. The tube was capped, and then the cap was wrapped with a piece of parafilm so that it was sealed. The contents were mixed and allowed to react in a water bath at 70°C for 30 min. A volume of 5 ml of hexane was transferred into the conical tube and thoroughly mixed to dissolve methyl or ethylene ester.

Micro partition clean-up procedure

Approximately 5 ml of distilled water was added into the conical tube, mixed and allowed to settle for a couple of minutes. The bottom aqueous layer was discarded using a disposable pipette. This partition clean-up step was repeated two more times. Approximately 1.5 g of Na_2SO_4 was added into the tube to prepare it for GC injection. For GC–ion trap analysis, 3 ml of the solute was concentrated to 0.3 ml before injection.

3. Results

3.1. The quantitative analyses by GC–ECD and GC–NPD

The herbicide residues 0.4 ppm and 0.8 ppm were fortified into five classes of fruits and vegetables based on experimental design by Ting and Kho [7]. The 2-chloroethylene esters were then tested by GC–ECD and GC–NPD methods and the recovery data were compared with diazomethane derivatized methyl ester results in Tables 1 and 2.

In Table 1, the recovery means were 100.0% (0.4 ppm) and 100.7% (0.8 ppm) for 2-chloroethylene esters and 103.9% (0.4 ppm) for methyl esters. All of the results were excellent; however, in the comparison of R.S.D.s (13.5% and 3.5% for 2-chloroethylene esters versus 17.3% for methyl esters) there was a slight advantage when using 2-chloroethylene esters. This was because 2-chloroethylene esters had later eluting peaks; there was longer retention time, better separation, better resolution and less interference from matrices. This is illustrated by the orange samples in Figs. 1 and 2. The methyl ester had a retention time of 3.65 min which almost overlapped the co-eluting interference peak at 3.84 min in Fig. 1. Conversely, in Fig. 2, the 2-chloroethylene ester had a longer retention time, $t_R = 7.35$ min, and was totally separated from early eluting matrix interferences.

Triclopyr is a herbicide containing a pyridine ring; in addition to GC–ECD, GC–NPD is also a logical tool to be investigated. The recovery data are presented in Table 2. Again, the advantage of using 2-chloroethylene ester is demon-

Table 1
Recovery data (%) by GC–ECD analyses

Vegetables and fruits		2-Chloroethylene ester		Methyl ester
		0.4 ppm	0.8 ppm	0.4 ppm
Leafy vegetables	Lettuce	90.2	99.5	101.1
	Cabbage	97.2	103.6	96.4
Roots	Carrot	101.3	94.5	95.4
	Potato	105.9	99.8	98.7
Fruits	Apple	81.6	102.5	89.9
	Cantaloupe	102.8	105.6	99.1
Citrus	Orange	97.1	104.3	98.6
	Lemon	96.6	100.6	99.9
Spices	Green Onion	133.1	100.6	153.6[a]
	Pepper	94.5	96.2	105.9
Statistics	Mean	100.0	100.7	103.9
	S.D. ($n = 10$)	13.5	3.5	17.9
	R.S.D.	13.5	3.5	17.3

[a] Elevated result due to coeluting interferences from matrix.

Table 2
Recovery data (%) by GC–NPD analyses

Vegetables and fruits		2-Chloroethylene ester		Methyl ester
		0.4 ppm	0.8 ppm	0.4 ppm
Leafy vegetables	Lettuce	100.1	95.9	105.9
	Cabbage	96.7	88.9	123.2[a]
Roots	Carrot	101.4	99.5	97.7
	Potato	90.3	107.9	101.6
Fruits	Apple	101.6	95.2	99.7
	Cantaloupe	104.0	88.2	104.1
Citrus	Orange	91.0	106.5	95.7
	Lemon	94.1	92.0	104.9
Spices	Green Onion	102.0	102.0	97.9
	Pepper	108.6	102.9	89.3
Statistics	Mean	99.0	97.9	102.0
	S.D. ($n = 10$)	5.9	7.0	8.9
	R.S.D.	5.9	7.1	8.8

[a] Elevated result due to coeluting interference from matrix.

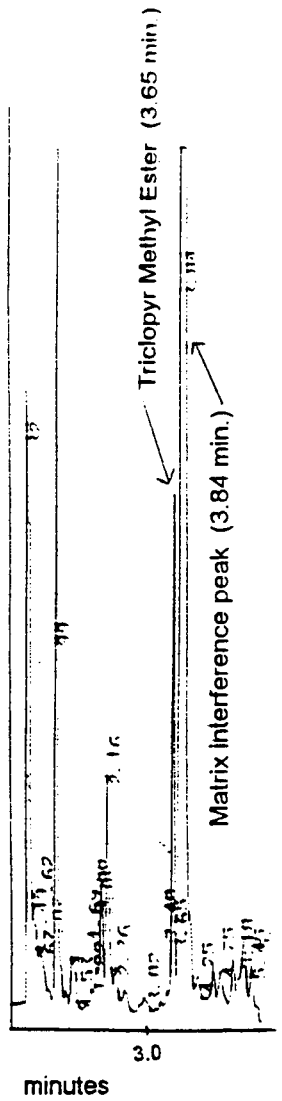

Fig. 1. Chromatogram of triclopyr methyl ester in orange by GC–ECD.

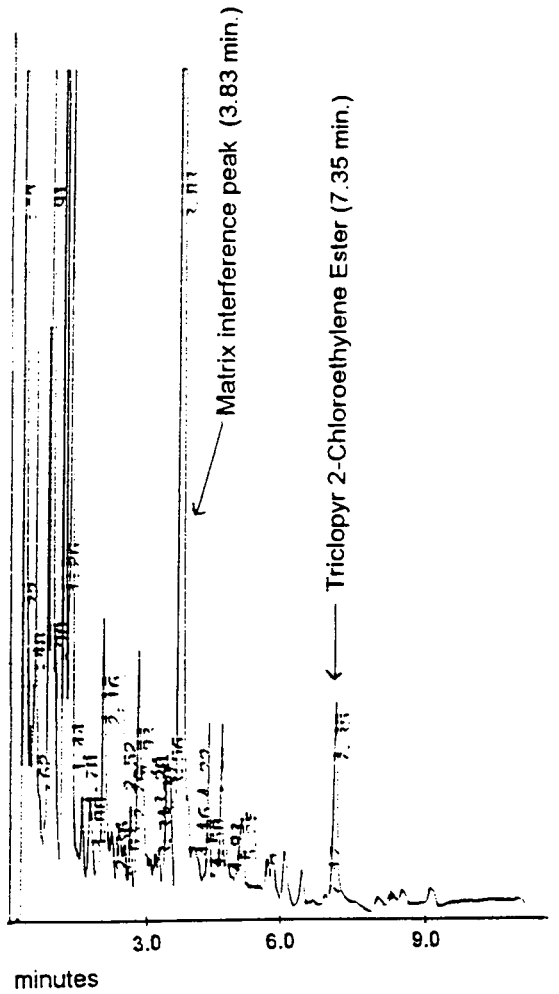

Fig. 2. Chromatogram of triclopyr 2-chloroethylene ester in orange by GC–ECD.

strated in the nitrogen rich commodity cabbages. The recovery for 2-chloroethylene ester in cabbage was 96.7%, which was better than the 123.2% for methyl ester at the same fortification level, 0.4 ppm. The elevated recovery result occurred as the methyl ester peak at 3.556 min had a shorter retention time (Fig. 3); it was thus susceptible to co-eluting interferences in the matrix. Meanwhile, the 2-chloroethylene ester peak at 6.729 min in Fig. 4 was completely separated and had better resolution because of the longer retention time. Therefore, the recovery of 2-chloroethylene ester was much more reasonable. Overall, the GC–NPD data (99.0% and 97.9% for 2-chloroethylene esters versus 102.0% for methyl ester) were as good as the GC–ECD as regards the recovery mean percentages. Keep in mind that the GC–NPD was not affected by chloride interferences from derivatizing reagents and consequently, the background noise was far less for the GC–NPD in comparison to the GC–ECD. Therefore, at the

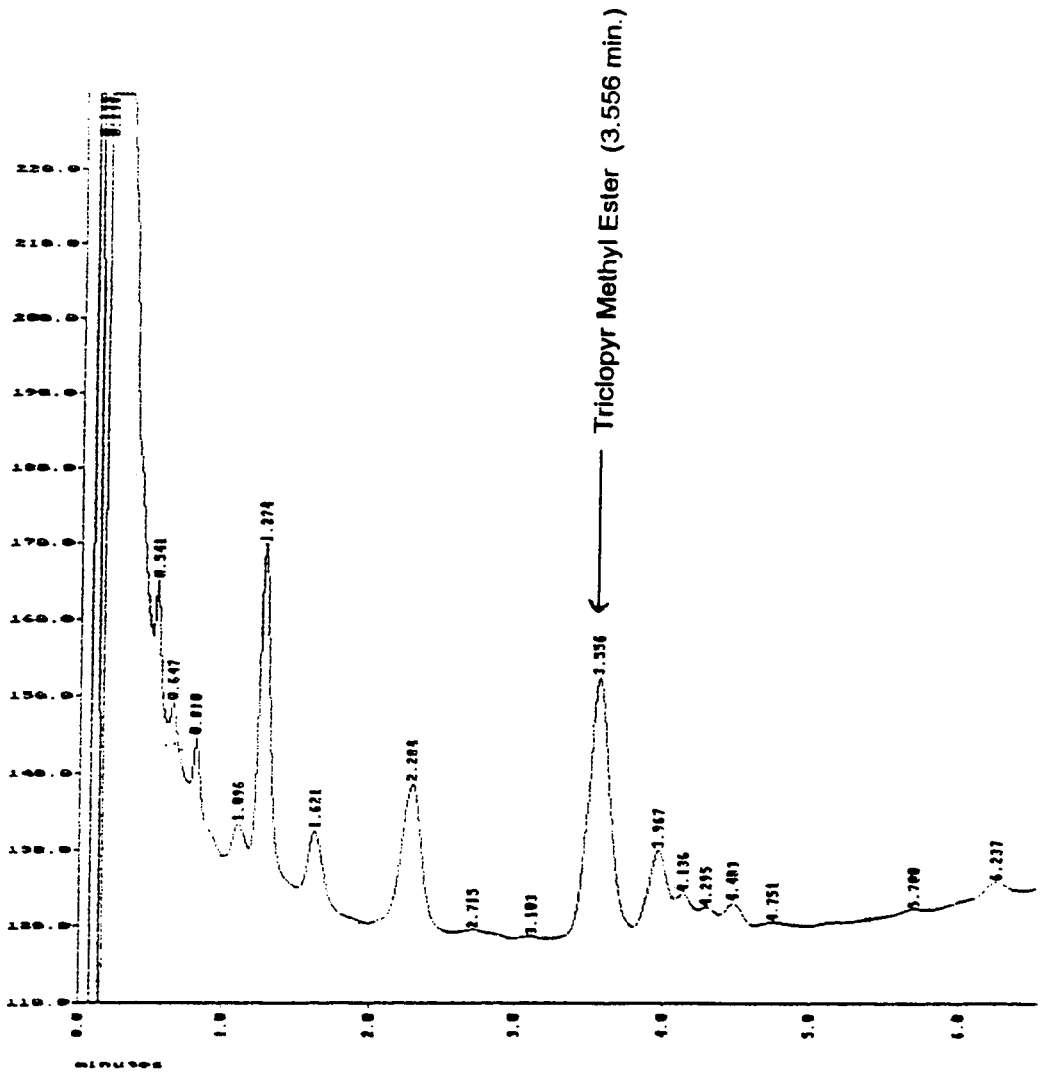

Fig. 3. Chromatogram of triclopyr methyl ester in cabbage by GC–NPD.

lower fortification level (0.4 ppm), the R.S.D. data for GC–NPD appeared less variable, e.g. $8.8 < 17.3$ and $5.9 < 13.5$.

One point worth mentioning is that the signal-to-noise ratio in the chromatograms was generally lower for GC–NPD than in GC–ECD analyses. This observation was to be expected since there is only one nitrogen atom on the pyridine ring in comparison to three or four chloride atoms, on methyl or ethylene esters, respectively. Therefore, the detection responses were restricted. If the fortified level had to be lower than 0.4 ppm, the GC–NPD method would consequently be more difficult to use.

Throughout the quantitative study, data were gathered from peak height rather then peak area. At low level residue analyses, the peaks were small, unsymmetrical and often distorted by background noise and/or matrix interferences. The impact was disastrous when peak

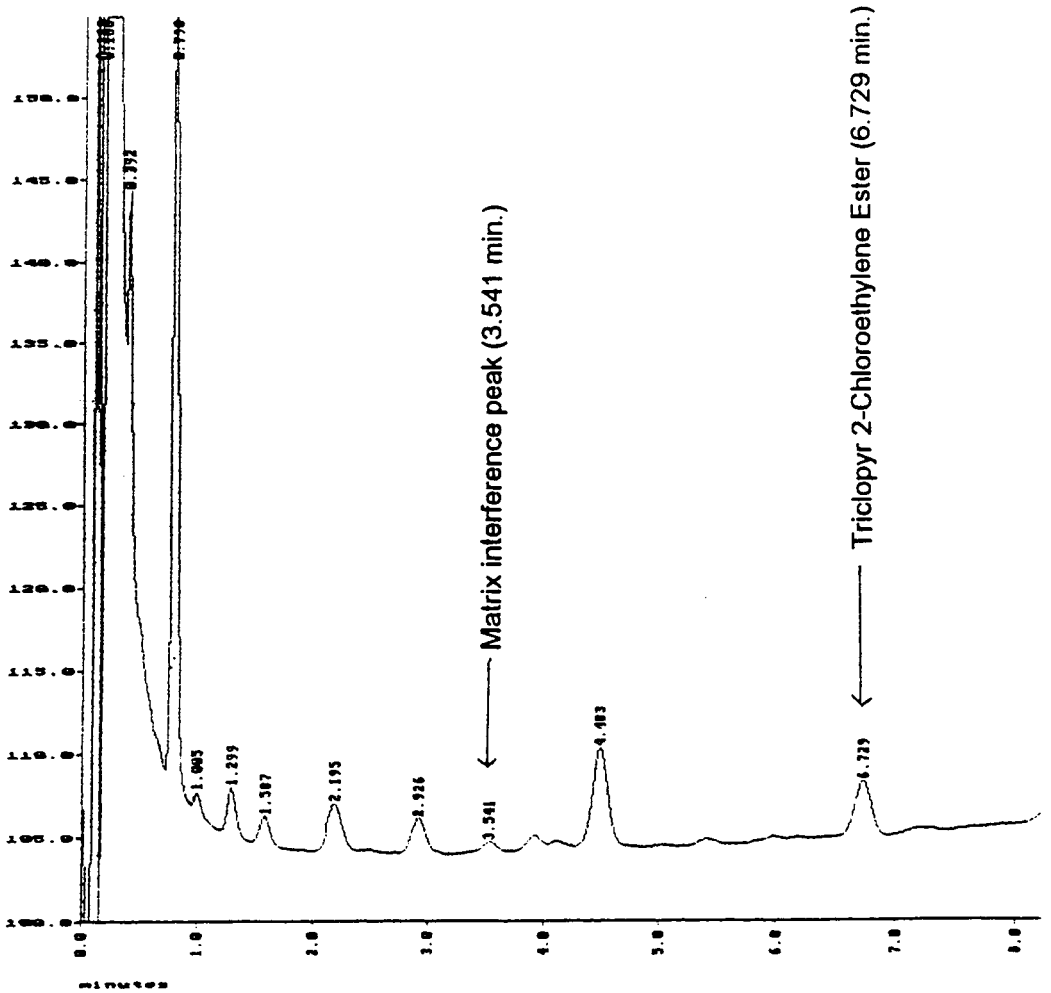

Fig. 4. Chromatogram of triclopyr 2-chloroethylene ester in cabbage by GC–NPD.

area was tried in the preliminary trials. Peak height was definitely the better data to take into account.

3.2. The qualitative or confirmation study by GC–ion trap

Triclopyr was first derivatized by 2-chloroethanol–BCl_3 and the ethylene ester synthesis was based on the acid chloride conversion and alcoholysis [8]. The reactions are presented in Fig. 5.

The 2-chloroethylene ester was then introduced into a GC–ion trap [9]. The GC–ion trap was first tuned to meet DFTPP (decafluorotriphenylphosphine) criteria based on the US EPA requirement for pesticide analyses [10]. An injection of 8 ng of ethylene ester was found to be the adequate concentration in order to obtain the full spectrum of the molecular ion and its fragment ions. However, a double concentration in citrus was needed because of the complexity of matrix interferences in the citrus peels. An injection concentration of 1 to 2 ng was also

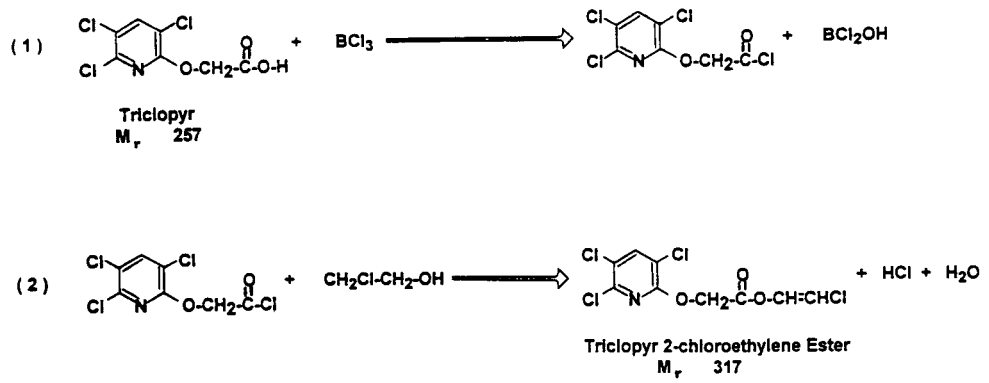

Fig. 5. (1) Acid chloride conversion, and (2) esterification through alcoholysis.

tested, the end result was that the isotopes' information around the major ions became unavailable.

The essence of MS in EI mode was shown in the spectra profile which provided significant information in terms of molecular structure [11]. The result was indisputable when the identification data were complemented with the injunction of elemental instrument analyses, such as the GC–ECD and the GC–NPD. Therefore, in order to distinguish this method, spectrum interpretation was the focal point of the study (Table 3). As mentioned before, 2-chloroethylene ester was a relatively stable compound in which the molecular ion ($m/z = 317$) could be found in the spectrum at the concentration level of 8 ng in

Table 3
MS interpretation of triclopyr 2-chloroethylene ester

Molecular ion	$m/z = 317$, $C_9H_5O_3NCl_4$				
Base ion	$m/z = 210$, $C_6H_2NOCl_3$				
Isotopes	Relative abundance				
	X	$X+2$	$X+4$	$X+6$	$X+8$
$m/z = 317$, Cl = 4	76.9	100	48.7	10.5	0.9
$m/z = 210$, Cl = 3	100	97.5	31.7	3.4	–
$m/z = 146$, Cl = 2	100	65.0	10.6	–	–
Appearance of characteristic ions	$m/z = 238$, $C_7H_2NO_2Cl_3$ $m/z = 210$, $C_6H_2NOCl_3$ $m/z = 182$, C_5HNCl_3 $m/z = 146$, C_5HNCl_2				
Nitrogen rule	Molecular weight = odd $m/z = 317$ Fragment ions = even mass $m/z = 238, 210, 182, 146$				

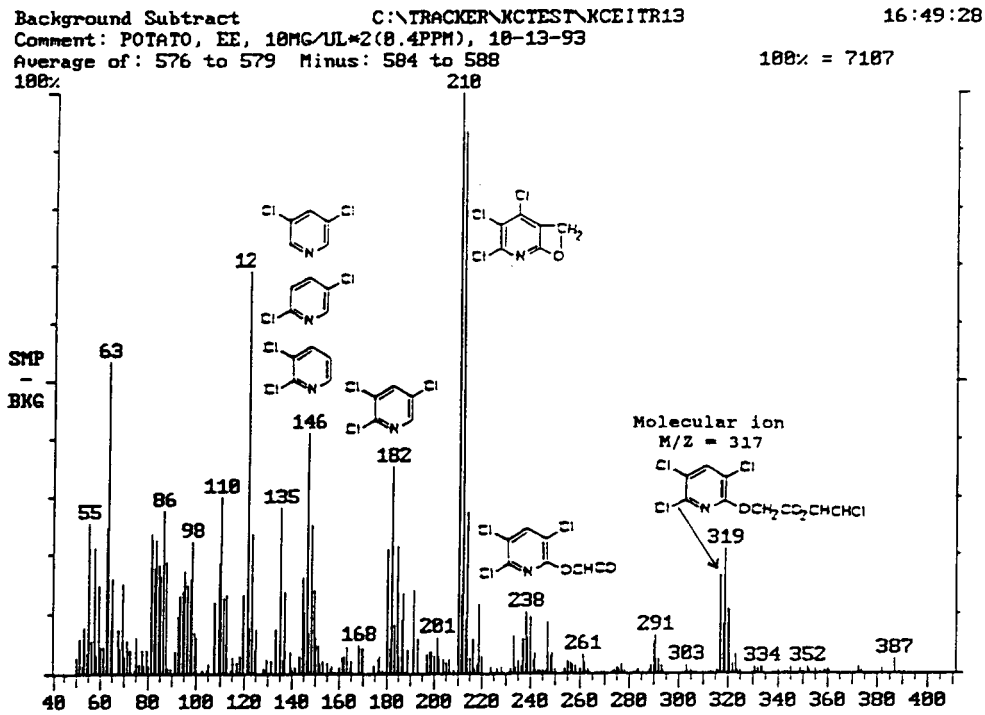

Fig. 6. Mass spectrum of triclopyr 2-chloroethylene ester in potato (0.4 ppm fortification).

Fig. 6. In the case of a synthesized compound like triclopyr 2-chloroethylene ester, the molecular ion information was very important as one can never be certain about the derivative process without this vital information. The base ion ($m/z = 210$) was the most abundant or frequently occurring ion in the profile because of the sigma-bond dissociation mechanism at a weakly bonded link between carbon and carboxyl, RC–COR', which, consequently, induced the McLafferty hydrogen atom rearrangement. Structurally, the base ion ($m/z = 210$) was $C_6H_2NOCl_3$ which was also the major ion used for methyl ester identification since the molecular ion was sometimes absent in the spectrum at the 8 ng concentration level. With a chlorinated compound, one of the unique displacements was the distribution of a isotope abundance ratio in the spectrum. For example, in Table 3, the molecular ion ($m/z = 317$) contained 4 chloride atoms, the isotope abundance ratios being $X = 76.9$, $X + 2 = 100$, $X + 4 = 48.7$, $X + 6 = 10.5$ and $X + 8 = 0.9$. In other examples, the base ion ($m/z = 210$) contained 3 chloride atoms, the isotope abundance ratios being $X = 100$, $X + 2 = 97.5$, $X + 4 = 31.7$ and $X + 6 = 3.4$ in Fig. 7, and the fragment ion ($m/z = 146$) had 2 chloride atoms, its isotope abundance ratios being $X = 100$, $X + 2 = 65.0$, and $X + 4 = 10.6$. These were excellent clues for a fingerprint match. In the fragmentation profile, there were character ions, such as $m/z = 238$, $C_7H_2NO_2Cl_3$; $m/z = 182$, C_5HNCl_3; and $m/z = 146$, C_5HNCl_2 and these were used as a means of identification in case of cleavage patterns. As mentioned before, the pyridine structure was a nitrogen containing compound; therefore, the nitrogen rule could be applied for more thorough identification. In this case, for example, the molecular weight should be odd and matched $m = 317$ (odd). Also, the fragment ions should have even mass, while the nitrogen containing fragment ions were $m/z = 238$, 182 and 146 (even). Again, these were great identifiers for the newly derivatized compound.

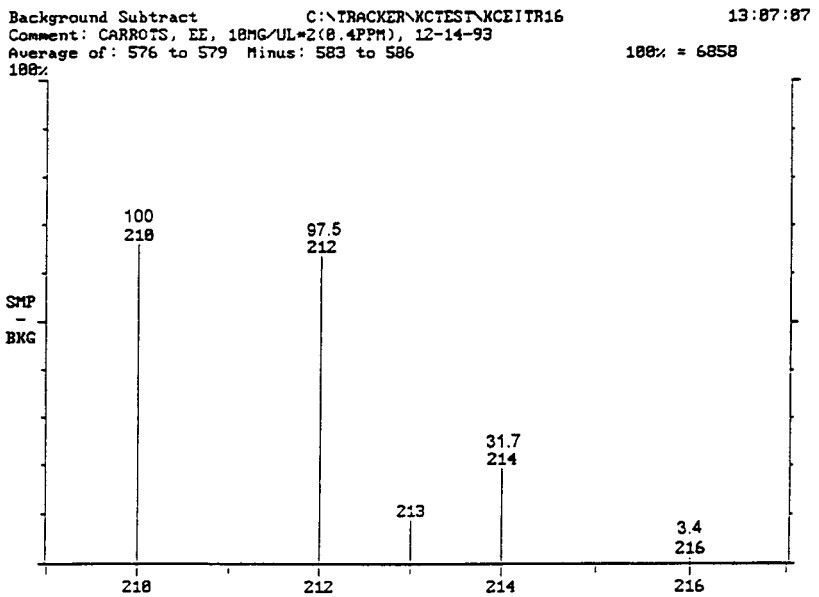

Fig. 7. Chlorine isotope peaks of $m/z = 210$ in the spectrum of carrots (0.4 ppm fortification).

4. Discussion

Structurally, triclopyr has many similarities to 2,4-D, 2,4,5-T and other phenoxyalkanoic acids. They are made up of aromatic rings (pyridine verses phenol) and carboxylic acid; and because of this, triclopyr had been analyzed like phenoxyacetic acids very successfully. However, sample preparation of the phenoxyacetic acid method is time consuming as it requires at least 6 hours processing time for a set of 2 to 3 samples per analyst without taking the GC analysis time into account. Furthermore, the method uses a large volume of solvents in the partition clean-up procedure and consequently, the disposal of liquid waste becomes an expensive process. In our method, we eliminated the partition steps prior to esterification and later used a micro-scale clean-up procedure that only required 5 ml water partition with hexane by repeating the step 3 times. This modification has reduced solvent waste almost to one-tenth and is a significant improvement in terms of decreasing waste and thus helps to protect the environment. In addition, one analyst could easily complete a set of 6 samples in 4 hours using our fast and simple sample preparation procedure.

Traditionally, diazomethane has been the single most popular derivatizing reagent for phenoxyacetic acid analyses [6]. However, because of its highly unstable and volatile nature, fresh diazomethane must be prepared for each batch of sample analyses. Long term storage is not recommended due to the problem of degradation. In addition, because diazomethane is both explosive and exceedingly toxic, it causes much fear and anxiety among analysts during its usage in laboratories. Analytically, diazomethane reacts with carboxylic acid to form methyl ester which has a short retention time under usual GC conditions. This is an unfortunate situation as interferences from sample co-extractives generally appear in the early region of the chromatogram.

Keeping all the diazomethane associated deficiencies in mind, 2-chloroethanol–BCl_3 is an obvious replacement in this line of research [12]. 2-Chloroethanol–BCl_3 is a non-explosive, and less toxic chemical than diazomethane. The reagent is capable of enhancing the halogen

detector response due to an extra chloride atom added to the original compound. Furthermore, the added chloride moiety increases the derivative compound's polarity or electronegativity which in turn prolongs retention time in the GC column and leads to better separation and resolution. In addition, 2-chloroethanol derivative is a better compound for GC–MS analysis as it is more stable than methyl ester at the ion source. In other words, some molecular ions could survive the ion beam bombardment without undergoing fragmentation and ultimately reach the detector intact. Because the mass ion could then be found in the spectrum, identification is simpler and faster.

Although 2-chloroethanol–BCl_3 has many advantages, one should also be aware of its weaknesses. In comparison to diazomethane, 2-chloroethanol–BCl_3 contributes more background noise in the halogen detector. During the preliminary trial, the reagent was first washed with hexane before use and then incorporated with 5 ml of NaOH (5 *M*) after esterification in the partition clean-up step so as to neutralize excessive chlorides [12]. These treatments proved to be insignificant as there was no noticeable improvement. For this reason, combined GC–MS identification and GC quantitation is a crucial step in obtaining quality data.

5. Conclusion

Triclopyr residue in fruits and vegetables is analyzed like other phenoxyalkanoic acids; the current method is time consuming, needs a large amount of solvents, and involves a dangerous chemical, diazomethane, as a derivatizing reagent.

In this research, the entire solvent volume used for analysis was reduced to one-tenth of that used in the existing method. Diazomethane was replace by 2-chloroethanol–BCl_3, a stable and safe reagent. In order to overcome the identification or qualitative difficulty which was caused by 2-chloroethanol–BCl_3 background noise, the multiple instrumentation approach was taken to assure a high standard of quantitative and qualitative data. The results generated by these experiments demonstrate that this method is simple, fast, safe and reliable.

Acknowledgments

The author wishes to thank Bill Cusick (Chief of Chemistry, CDFA) and Ton Joe (Program Supervisor of Chemistry, CDFA) for their support of this research work. The author would also like to acknowledge Angie C. Ting for her efforts in the editing of this work.

References

[1] *The Agrochemicals Handbook*, Royal Society of Chemistry, Cambridge, 1989, A530/Aug87.
[2] *Farm Chemical Handbook*, Meister Publishing Co., Willoughby, OH, 1993.
[3] G. Yip, *J. Assoc. Off. Anal. Chem.*, 45 (1962) 367.
[4] G. Yip, *J. Assoc. Off. Anal. Chem.*, 47 (1964) 1116.
[5] G. Yip, *J. Assoc. Off. Anal. Chem.*, 54 (1971) 970.
[6] *Aldrichimica Acta*, 17 (1984) 1.
[7] K.C. Ting and P. Kho, *J. Assoc. Off. Anal. Chem.*, 74 (1991) 991.
[8] R.T. Morrison and R.W. Boyd, *Organic Chemistry*, Allyn and Bacon, Boston, MA, 3rd ed.
[9] Finnigan Corporation, *Ion Trap System Operators' Manual*, San Jose, CA, 1990.
[10] J.R. Donnelly, G.W. Sovocool and R.K. Mitchum, *J. Assoc. Off. Anal. Chem.*, 71 (1988) 434.
[11] F.W. McLafferty, *Interpretation of Mass Spectra*, University Science Books, Mill Valley, CA, 3rd ed.
[12] A.S.Y. Chau and K. Terry, *J. Assoc. Off. Anal. Chem.*, 58 (1975) 1294.

ELSEVIER

Journal of Chromatography A, 690 (1995) 131–139

JOURNAL OF CHROMATOGRAPHY A

Estimating flow-rates for sub- and supercritical fluid extractions with linear restrictors

Yu Yang, Steven B. Hawthorne*, David J. Miller

Energy and Environmental Research Center, University of North Dakota, Grand Forks, ND 58202-9018, USA

First received 24 June 1994; revised manuscript received 7 September 1994

Abstract

The fluid flow-rate through a linear capillary restrictor depends on the type, pressure and temperature of the fluid as well as the length and internal diameter of the restrictor. A simple mathematical correlation was established for calculating the flow-rate of CO_2 and water through a capillary restrictor during dynamic flowing sub- and supercritical fluid extractions. Calculated flow-rate values compared favorably with the experimentally determined values for three cases: supercritical CO_2 extraction with the entire restrictor out of the supercritical fluid extraction oven, supercritical CO_2 extraction with restrictor inlet inside the supercritical fluid extraction oven, and sub- and supercritical water extraction.

1. Introduction

Since supercritical fluid extraction (SFE) is mostly performed under dynamic flowing extraction conditions [1], flow-rate is one of the important parameters which can influence extraction efficiencies for both supercritical CO_2 [2,3] and subcritical water extraction [4,5]. Because of their low cost, linear restrictors made from fused-silica tubing are often used for flow control in SFE. While there are several reports on estimating fluid flow-rate in supercritical fluid chromatography (SFC) [6–8], the calculations are frequently complex and fail to predict flow-rates for SFE. For example, differences between calculated and measured SFE flow-rates using the methods in Refs. [6–8] were typically up to ± 100%, possibly because in SFC, the restrictor is inside the SFC oven or heated detector (therefore, restrictor temperature ≥ SFC oven temperature); while for SFE, the entire restrictor (or at least the outlet of the restrictor) is outside the SFE oven during the extraction (restrictor temperature ≤ SFE oven temperature). Another reason might be that SFE flow-rates (ml/min) are normally much higher than SFC flow-rates (μl/min). In the present study, a simple mathematical correlation was developed for calculating fluid flow-rates through linear restrictors during sub- and supercritical fluid extractions with CO_2 and water.

2. Experimental

2.1. CO_2 extractions

CO_2 was pressurized by an ISCO (Lincoln,

* Corresponding author.

0021-9673/95/$09.50
SSDI 0021-9673(94)00884-1

NE, USA) Model 260D syringe pump into a 0.8-ml cell (50 mm × 4.6 mm I.D., Keystone Scientific, Bellefonte, PA, USA). The extraction temperature was controlled by placing both the extraction cell and a 1-m-long preheating coil made from 1/16 in. O.D. × 0.020 in. I.D. (1 in. = 2.54 cm) stainless-steel tubing inside a Hewlett-Packard 5890 Series II gas chromatograph. Fused-silica tubing with 9 to 50 μm I.D. (Polymicro Technologies, Phoenix, AZ, USA) was used for outlet restrictors to obtain flow-rates of ca. 0.005 to 5 ml/min (measured as liquid CO_2 at the pump). Exact internal diameters of the restrictors were measured and specified by the manufacturer. Since it takes ca. 10 min to get flow-rate equilibrium after refilling the pump or filling the extraction cells, an accurate CO_2 flow-rate can only be read after this equilibrium time. CO_2 flow-rates were determined for two different arrangements for the restrictor. The first approach had the entire restrictor outside the SFE oven (there is a shut-off valve between extraction cell and restrictor). In the second approach, the restrictor was directly connected to the extraction cell, which means that the restrictor inlet was inside the SFE oven, and the restrictor outlet was outside the SFE oven.

2.2. Water extractions

The setup for water extractions was similar to CO_2 extractions with the entire restrictor outside the SFE oven except that an ISCO Model μLC-500 pump was used instead of an ISCO Model 260D pump. Because the polyimide seals used in the SFE cells failed at high temperatures, empty HPLC columns (30 mm × 4.6 mm I.D., 0.48 ml; Keystone Scientific) were used as extraction cells for the higher extraction temperatures (250–400°C). Water flow-rate was measured as liquid water at the pump.

3. Results and discussion

3.1. Flow-rate dependence on pressure

Fig. 1 shows that flow-rates obtained experimentally are directly proportional to pressure; therefore, an equation expressing flow-rate in terms of pressure can be delivered as follows:

$$F = \chi_p P \quad (1)$$

where F is flow-rate in ml/min (liquid CO_2 or liquid water); P is pressure in atm (1 atm = 101 325 Pa); χ_p is a constant which is dependent on the type and temperature of the fluids, and the length and internal diameter of the restrictor. χ_p can be experimentally determined. Please note that χ_p is different if one of the parameters (the type and temperature of the fluids; the length and internal diameter of the restrictor) is changed [e.g.: the χ_p values in Fig. 1 (bottom) are $3 \cdot 10^{-3}$, $1.8 \cdot 10^{-3}$ and $4.8 \cdot 10^{-4}$ for restrictor lengths 10, 20 and 50 cm, respectively]. Flow-rate can be estimated by Eq. 1 with the help of experimentally determined χ_p. The calculated flow-rates using Eq. 1 are also shown in Fig. 1 (solid lines) which indicates a good agreement with experimental values. Once χ_p is known, Eq. 1 is applicable for all three extraction cases: CO_2 extraction with the entire restrictor outside the SFE oven, CO_2 extraction with the inlet of the restrictor inside the SFE oven, and water extraction.

3.2. Flow-rate dependence on internal radius of the restrictor

Restrictor internal radius (I.D./2) has a very strong influence on flow-rate for both CO_2 and water. Based on the experimental values as shown in Fig. 2, functions between flow-rate and restrictor internal radius can be established as below

$$F = \chi_r R^3 \quad (2)$$

for CO_2 and

$$F = \chi_r R^5 \quad (3)$$

for water, respectively;

where R is the internal radius of the restrictor in μm; χ_r is a constant dependent on the type, pressure and temperature of the fluids, and restrictor length. Using experimentally determined χ_r, Eqs. 2 and 3 give very close values

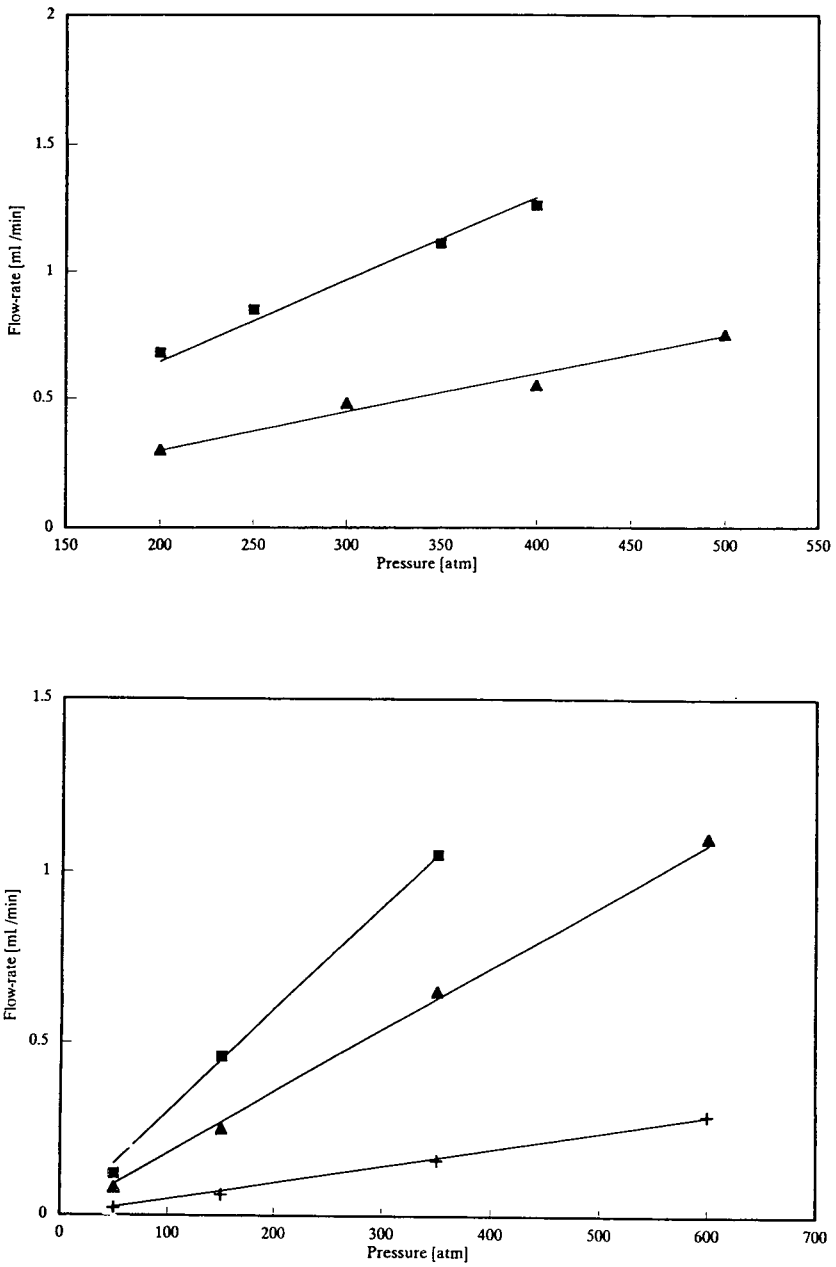

Fig. 1. Influence of pressure on flow-rate of CO_2 (top) and water (250°C, bottom). Experimental and calculated flow-rates are shown in symbols and lines, respectively. Top: ■ = 10 cm × 30 μm I.D. restrictor, outside the oven, 200°C; ▲ = 10 cm × 25 μm I.D. restrictor, inlet inside the oven, 80°C. Bottom: ■ = 10 cm × 30 μm I.D. restrictor; ▲ = 20 cm × 30 μm I.D. restrictor; + = 50 cm × 30 μm I.D. restrictor.

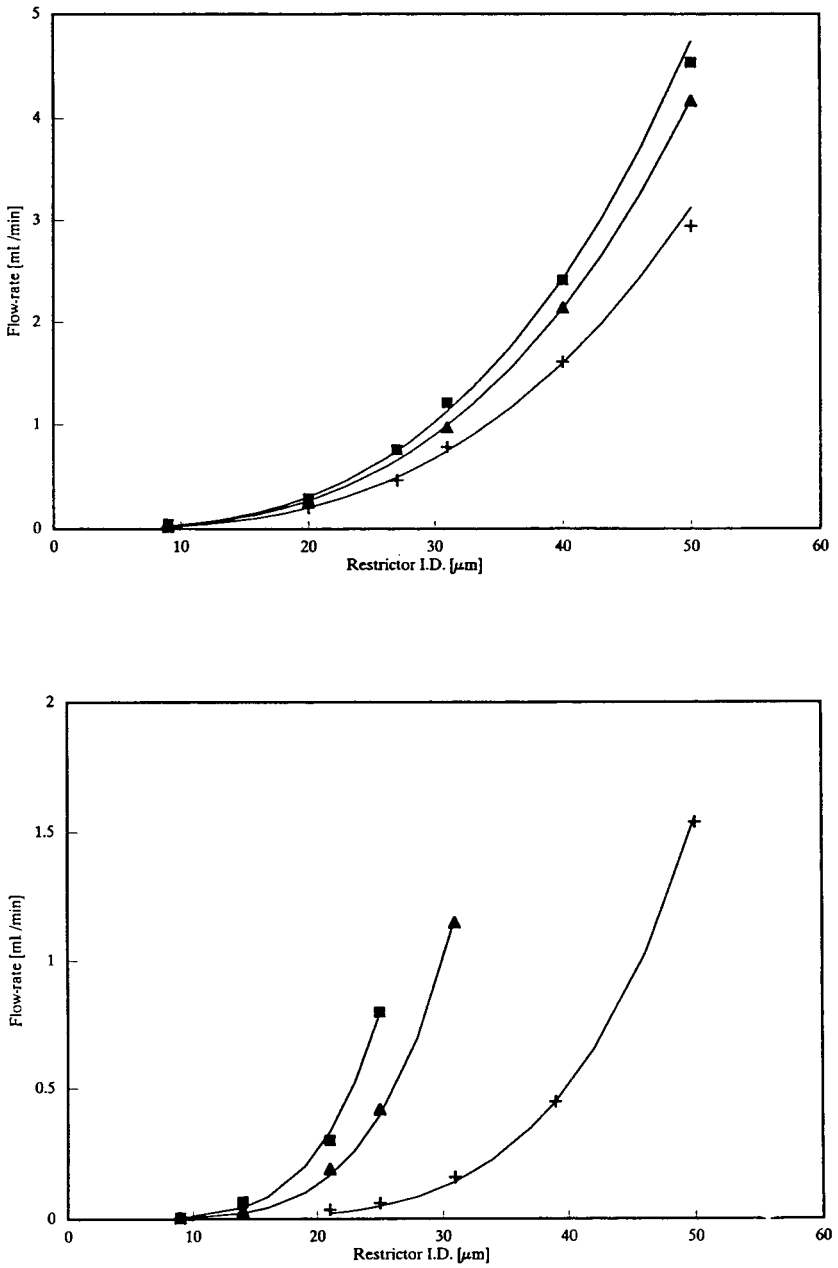

Fig. 2. Influence of internal diameter of restrictor on flow-rate of CO_2 (80°C, top) and water (250°C, bottom). Experimental and calculated flow-rates are shown in symbols and lines, respectively. Top: ■ = 10 cm restrictor (outside the oven), 400 atm; ▲ = 10 cm restrictor (inlet inside the oven), 400 atm; + = 10 cm restrictor (inlet inside the oven), 200 atm. Bottom: ■ = 10 cm restrictor, 600 atm; ▲ = 10 cm restrictor, 350 atm; + = 10 cm restrictor, 50 atm.

(solid lines) compared to experimental flow-rates (Fig. 2).

3.3. Flow-rate dependence on the length of the restrictor

Inverse proportional relationships between flow-rate and restrictor length were found and expressed by following equations

$$F = \chi_1 / L^{0.5} \quad (4)$$

for CO_2 and

$$F = \chi_1 / L \quad (5)$$

for water, respectively;

where L is restrictor length in cm; χ_1 is a constant dependent on the type, pressure and temperature of the fluids, and the internal radius of the restrictor. χ_1 can be determined by experimental flow-rates. Fig. 3 shows both experimental and calculated flow-rates using restrictors having different lengths.

3.4. Flow-rate dependence on temperature

The flow-rate of CO_2 extractions with the entire restrictor outside the SFE oven remained unchanged at extraction temperatures from 50 to 250°C (Fig. 4, top). The reason might be that the entire restrictor is out of the SFE oven (the temperature being much lower than that inside the oven), so that the flow-rate is much less influenced by extraction temperature. Once the restrictor inlet is directly connected to the extraction cell (the inlet of the restrictor is inside the SFE oven and the outlet of the restrictor is outside the oven), the extraction temperature does influence the CO_2 flow-rate (Fig. 4, top). In this case, the influence of temperature on CO_2 flow-rate can be expressed as

$$F = \chi_t / T \quad (6)$$

where T is extraction temperature in K; χ_t is a constant dependent on the pressure CO_2, and the length and internal radius of the restrictor and can be experimentally determined.

Like the flow-rate of CO_2 with the entire restrictor outside the SFE oven, water flow-rate is almost constant for high-temperature (200–450°C) extractions. However, at temperatures lower than 200°C, water flow-rate was decreased by lowering extraction temperatures (Fig. 4, bottom). Since a temperature around or higher than 250°C is required to extract non-polar organics using water [4,5], the mathematical correlation given below is established for a temperature range of 200–450°C. However, it should be easy to correct water flow-rates at temperatures lower than 200°C based on the relationship between water flow-rate and temperature (50–200°C) shown in Fig. 4, bottom (as discussed below).

3.5. Mathematical correlation of flow-rate

CO_2 flow-rates with the entire restrictor out of the SFE oven

Since the flow-rate of CO_2 is constant at a temperature range of 50–250°C, only Eqs. 1, 2 and 4 need to be considered. Thus, the expression of CO_2 flow-rate can be given by

$$F = 2.8 \cdot 10^{-6} P R^3 / L^{0.5} \quad (7)$$

where the constant $2.8 \cdot 10^{-6}$ was determined by experimental flow-rates, F is the flow-rate in ml/min, P is pressure in atm, R is the internal radius of the restrictor in μm and L is the restrictor length in cm. Table 1 gives some calculated flow-rates using Eq. 7 in comparing with experimental values, and good agreement was obtained.

CO_2 flow-rates with the restrictor inlet inside the SFE oven

In this case, we have to consider the influence of temperature on CO_2 flow-rate. To do this, we need to combine Eqs. 6 and 7, and obtain CO_2 flow-rate by

$$F = 7.6 \cdot 10^{-4} P R^3 / (T L^{0.5}) \quad (8)$$

where the constant $7.6 \cdot 10^{-4}$ was experimentally

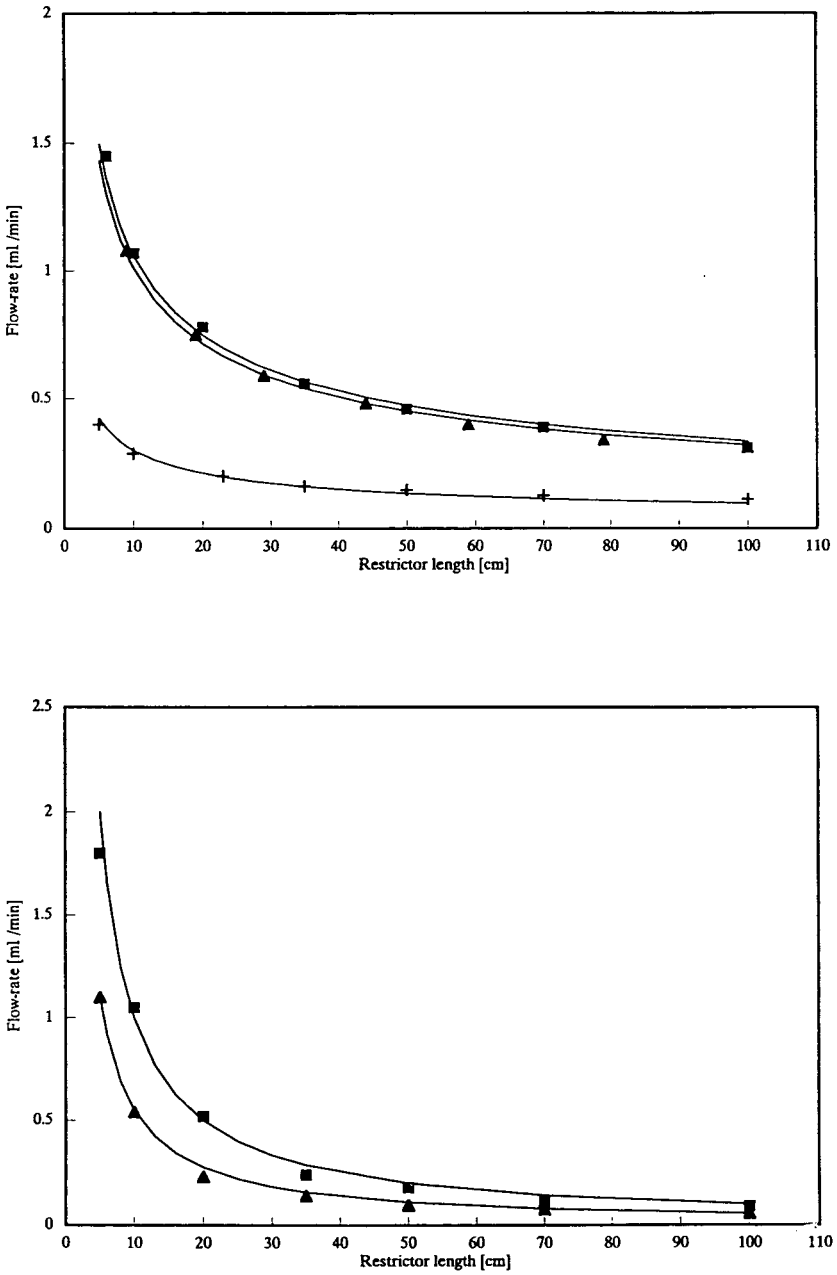

Fig. 3. Influence of restrictor length on flow-rate of CO_2 (top) and water (250°C, 350 atm; bottom). Experimental and calculated flow-rates are shown in symbols and lines, respectively. Top: ■ = 30 μm I.D. restrictor (outside the oven), 250°C, 350 atm; ▲ = 30 μm I.D. restrictor (inlet inside the oven), 80°C, 400 atm; + = 20 μm I.D. restrictor (outside the oven), 80°C, 400 atm. Bottom: ■ = 31 μm I.D. restrictor; ▲ = 26 μm I.D. restrictor.

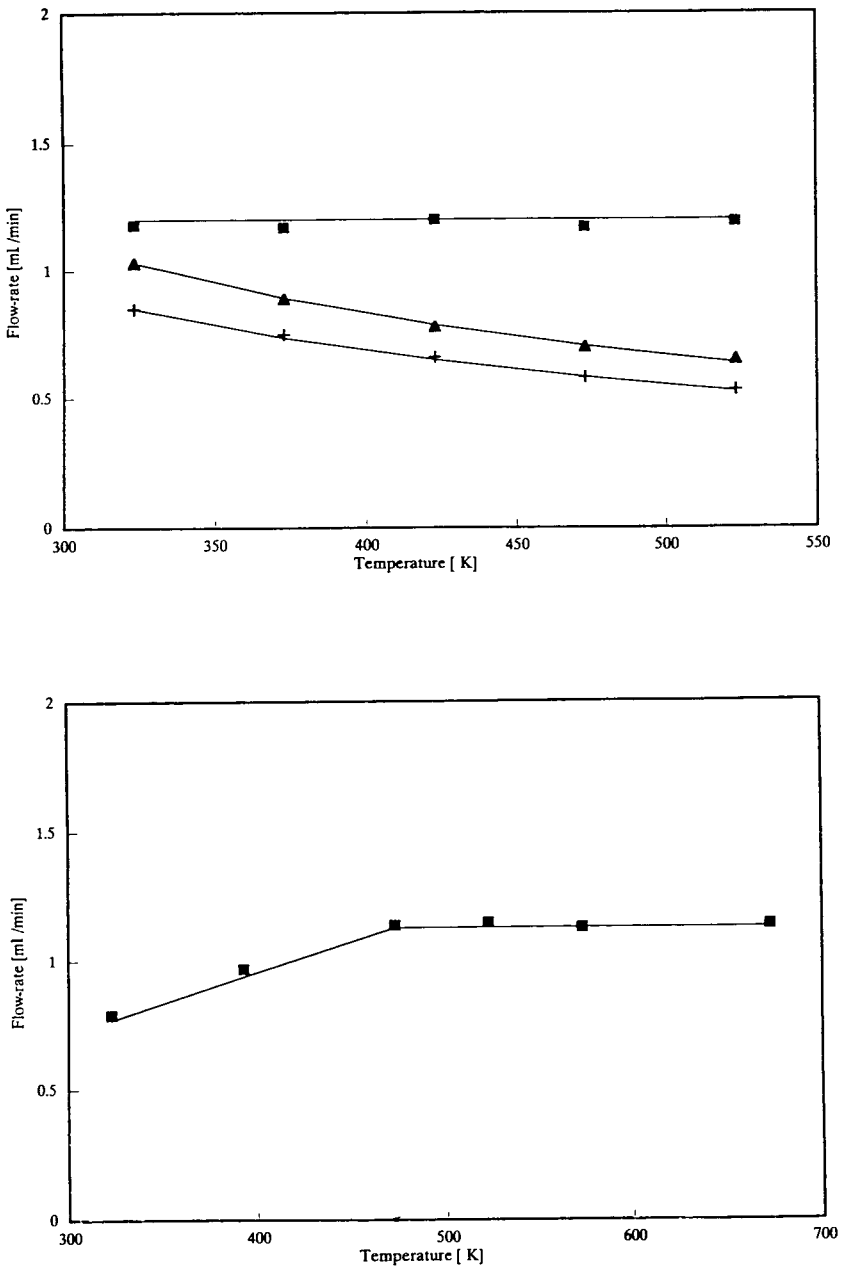

Fig. 4. Influence of temperature on flow-rate of CO_2 (400 atm, top) and water (350 atm, 10 cm × 31 μm I.D. restrictor; bottom). Experimental and calculated flow-rates are shown in symbols and lines, respectively. Top: ■ = 10 cm × 30 μm restrictor (outside the oven); ▲ = 10 cm × 30 μm I.D. restrictor (inlet inside the oven); + = 15 cm × 30 μm I.D. restrictor (inlet inside the oven).

Table 1
Comparison of calculated and experimental flow-rates for supercritical CO_2 extractions

Entire restrictor outside the SFE oven													
Pressure (atm)	200	200	200	200	350	350	350	350	400	400	400	450	600
Temperature (°C)	80	80	80	80	200	200	200	250	50	150	250	200	80
Restrictor length (cm)	10	10	10	10	20	50	100	10	10	10	10	10	10
Restrictor I.D. (μm)[a]	9	20	40	50	30	30	30	14	30	30	30	30	30
Calculated flow-rate (ml/min)	0.016	0.18	1.42	2.77	0.74	0.47	0.33	0.11	1.20	1.20	1.20	1.34	1.79
Experimental flow-rate (ml/min)[b]	0.022	0.20	1.61	2.92	0.76	0.46	0.33	0.16	1.18	1.20	1.19	1.23	1.45
Restrictor inlet inside the SFE oven													
Pressure (atm)	200	400	400	400	400	400	400	400	400	400	400	400	500
Temperature (°C)[c]	80	50	80	80	80	80	80	80	150	200	250	300	80
Restrictor length (cm)	10	10	10	10	10	10	50	100	10	10	10	10	10
Restrictor I.D. (μm)[a]	26	30	9	20	40	50	30	30	30	30	30	30	30
Calculated flow-rate (ml/min)	0.30	1.00	0.025	0.27	2.18	4.26	0.41	0.29	0.77	0.69	0.62	0.57	1.15
Experimental flow-rate (ml/min)[b]	0.31	1.03	0.023	0.27	2.15	4.19	0.40	0.29	0.77	0.69	0.65	0.60	1.08

[a] Values used in the correlation are internal radii (I.D./2).
[b] Experimental flow-rates were obtained by triplicate measurements, and the R.S.D. was less than 10%.
[c] Values used in the correlation are in K.

determined. As shown in Table 1, calculated flow-rates using Eq. 8 compared favorably with the experimentally determined values.

Water flow-rates

Based on Eqs. 1, 3 and 5, a mathematical correlation for water flow-rate can be expressed as

$$F = \chi PR^5/L \quad (9)$$

where χ is a temperature-dependent constant. For temperatures at or higher than 200°C, χ equals $3.6 \cdot 10^{-8}$ (determined by experimental flow-rates) if F is in ml/min, P is in atm, R is in μm and L is in cm. Thus, Eq. 9 can be changed into

$$F = 3.6 \cdot 10^{-8} PR^5/L \quad (10)$$

for $T \geq 200$°C (473 K)

For water extractions at temperatures lower than 200°C, the calculated flow-rate in Eq. 10 need to be corrected by a factor of $T/473$, where T is the extraction temperature in K. As shown in Table 2, the correlation for water flow-rates gives very close values compared with experimental flow-rates.

Table 2
Comparison of calculated and experimental flow-rates for sub- and supercritical water extractions

Pressure (atm)	50	50	350	350	350	350	350	350	350	350	600	600	600
Temperature (°C)[a]	250	250	50	120	200	250	400	250	250	250	250	250	250
Restrictor length (cm)	10	10	10	10	10	10	10	20	50	100	10	10	10
Restrictor I.D. (μm)[b]	39	50	31	31	31	31	31	31	31	31	9	21	31
Calculated flow-rate (ml/min)	0.51	1.76	0.77	0.94	1.13	1.13	1.13	0.56	0.23	0.11	0.004	0.28	0.97
Experimental flow-rate (ml/min)[c]	0.45	1.54	0.79	0.97	1.14	1.15	1.14	0.52	0.18	0.09	0.006	0.30	1.05

[a] Values used in the correlation are in K.
[b] Values used in the correlation are internal radii (I.D./2).
[c] Experimental flow-rates were obtained by triplicate measurements, and the R.S.D. was less than 10%.

3.6. General expression for predicting flow-rates

Eqs. 7, 8 and 10 are the practical calculating equations for flow-rates in the three cases discussed above. We can still combine Eqs. 7, 8 and 10; and the flow-rate for all three cases can be expressed by one general form

$$F = \chi_a P R^b / (T^c L^d) \quad (11)$$

For CO_2 with entire restrictor outside the oven, CO_2 with restrictor inlet inside the oven, and water, χ_a is $2.8 \cdot 10^{-6}$, $7.6 \cdot 10^{-4}$ and $3.6 \cdot 10^{-8}$; b is 3, 3 and 5; c is 0, 1 and 0; d is 0.5, 0.5 and 1, respectively. Eq. 11 is valid for: pressure from 150 to 500 atm (CO_2), and from 50 to 600 atm (water); restrictor internal diameter from 9 to 50 μm; restrictor length from 5 to 100 cm; temperature from 50 to 250°C (CO_2), and 200 to 450°C (water). For water flow-rates at temperatures lower than 200°C, the calculated flow using Eq. 11 need to be multiplied by $T/473$. As shown in Tables 1 and 2, this expression can be used to calculate flow-rates of CO_2 and water to ± 10% in most cases.

Acknowledgements

The financial support of the US Environmental Protection Agency (EMSL, Las Vegas) and instrument loans from ISCO are gratefully acknowledged.

References

[1] S.B. Hawthorne, *Anal. Chem.*, 62 (1990) 633A.
[2] S.B. Hawthorne, D.J. Miller, M.D. Burford, J.J. Langenfeld, S. Eckert-Tilotta and P.K. Louie, *J. Chromatogr.*, 642 (1993) 301.
[3] K.G. Furton and Q. Lin, *J. Chromatogr. Sci.*, 31 (1993) 201.
[4] Y. Yang, S.B. Hawthorne and D.J. Miller, presented at the *5th International Symposium on Supercritical Fluid Chromatography and Extraction, Baltimore, MD, January 1994*, poster D9.
[5] S.B. Hawthorne, Y. Yang and D.J. Miller, *Anal. Chem.*, 66 (1994) 2912.
[6] Y. Hirata and F. Nakata, *Chromatographia*, 21 (1986) 627.
[7] R.D. Smith, J.L. Fulton, R.C. Petersen, A.J. Kopriva and B.W. Wright, *Anal. Chem.*, 58 (1986) 2057.
[8] R.D. Smith and H.R. Udseth, *Anal. Chem.*, 59 (1987) 13.

ELSEVIER

Journal of Chromatography A, 690 (1995) 141–148

JOURNAL OF CHROMATOGRAPHY A

Theoretical estimation of capillary zone electrophoresis behaviour of metal complexes using multivariate regression analysis

A.R. Timerbaev*, O.P. Semenova

Department of Analytical Chemistry, Johannes Kepler University, A-4040 Linz, Austria

First received 22 July 1994; revised manuscript received 7 October 1994; accepted 7 October 1994

Abstract

The migration of lanthanide metal ions complexed with aminopolycarboxylic reagents (ethylenediaminetetraacetic acid and chemically similar analogues containing varying degrees of basicity and size) in capillary zone electrophoresis was investigated. Electrophoretic mobilities were measured for a series of complexes in borate buffer electrolytes of variable pH and buffer concentration (62 different compositions). A migration model was developed to relate the electrophoretic mobility with charge density parameters of a metal complex (the net charge, the stability constant and ligand structural increments) and electrophoretic system variables such as the electrolyte pH. The predictive ability of the derived regression equation was evaluated in terms of its statistical significance. The good agreement observed between the calculated electrophoretic mobilities and experimental values demonstrates the applicability of the multivariate regression approach to the prediction of migration behaviour in capillary electrophoresis on the basis of small-number measurements. The results confirm also that the separation mechanism for metal complexes is based on the differential electrophoretic migration governed by differences in charge-to-size parameters.

1. Introduction

High-performance capillary electrophoresis (CE) is receiving considerable attention as a highly efficient tool for separating and detecting metal ions. Significant advances have been made by a number of workers, as summarized in recent books [1–3] and reviews [4,5]. In CE it is now common to use the complexing agent added to the capillary electrolyte or to the sample, to complex metal ions, partially or completely, and thereby to facilitate the resolution. This CE methodology holds even greater promise than ion chromatography regarding the achievement of multi-element separations. Nevertheless, as metal ion analysis is a relatively new area of CE application, specific advances are still needed to develop the method as an alternative separation technique.

In this respect, a better understanding of the migration mechanism and the ionic or molecular properties that control the separation of metal

* Corresponding author. On leave from Mendeleev Russian University of Chemical Technology, Moscow, Russian Federation.

0021-9673/95/$09.50
SSDI 0021-9673(94)00968-6

species during CE would be of great value. Further, optimization of the electrophoretic behaviour requires the use of the quantitative relationships between migration parameters and different charge-to-size characteristics of the analytes. To the best of our knowledge, there has been only one published report, by Shi and Fritz [6], where a correlation was established between the migration times of lanthanide cations in the presence of a weak complexing agent, 2-hydroxyisobutyric acid (HIBA), and a charge-related parameter such as the average number of ligands associated with a metal atom. No-one seems to have addressed the issue of how the separand parameters affect the electrophoretic behaviour of precapillary-formed metal complexes, which are generally distinguished by a more complicated migration mechanism than partially complexed metal ions. This feature is related to a diversity of interactions between the complexes and electrolyte components such as those involved in acid–base equilibria, ion pairing, mixed-ligand complex or adduct formation, dissociation, micellization, etc.

In addition, method development in metal ion CE needs a systematic investigation of the effects of operating variables on the migration behaviour. Few studies have been published which deal with this subject. Jimidar et al. [7] showed that the separation of rare earth metal ions is mainly influenced by the pH and the concentration of HIBA and selected optimized conditions by using computer-assisted modelling. More recently, a mathematical model relating the electrophoretic mobility of a metal cation with the same two experimental factors was reported by Quang and Khaledi [8].

We have previously demonstrated that the iterative regression strategy can be successfully applied to the theoretical estimation of the retention of metal complexes in HPLC, when using well known molecular properties (e.g., the stability constants or the orbital electronegativity of the metal atom) and physico-chemical characteristics of the mobile phase as predictors [9]. Here we describe the extension of this approach to the interpretation of migration properties in CE for a range of metal complexes with the aim of developing a simple linear model of electrophoretic behaviour. The migration mechanism for lanthanide metal complexes of aminopolycarboxylic acids used as test solutes and the capability of derived multiparametric regression equations to predict migration parameters are discussed.

2. Experimental

2.1. Chemicals

Lanthanide metal ion solutions were prepared by dilution of 1000 μg/ml AAS standard concentrates (Aldrich, Milwaukee, WI, USA), except for lanthanum, thulium and lutetium, which were prepared from the nitrates dissolved in 0.01 *M* HNO_3. The aminopolycarboxylic acids used were purchased from Aldrich (Steinheim, Germany), Sigma (St. Louis, MO, USA) or Merck (Darmstadt, Germany). They included ethylenediaminetetraacetic, *trans*-1,2-cyclohexanediaminetetraacetic, diethylenetriaminepentaacetic and triethylenetetraaminehexaacetic acid and were used as 0.005 or 0.01 *M* solutions in 0.01 *M* sodium tetraborate. Metal complexes were prepared as described elsewhere [10]. All chemicals were of analytical-reagent grade and doubly distilled water was used for all solutions.

Sodium tetraborate was used for the preparation of electrolyte buffers. The pH of the electrolytes, varied as specified below, was adjusted by adding sodium hydroxide solution or hydrochloric acid to the sodium borate solutions. The borate concentration was varied as described under Results and discussion. The carrier electrolytes also contained an appropriate amount of a chelating reagent (usually $1 \cdot 10^{-3}$ *M*).

2.2. Instrumentation

Capillary electrophoresis was performed by using a Waters (Milford, MA, USA) Quanta 4000 capillary electrophoresis system and fused-silica capillaries of 50 cm total length × 75 μm I.D. (Polymicro Technologies, Phoenix, AZ, USA). A positive power supply of 15 kV was

used for electrophoresis. On-column direct detection was performed at 214 nm. The injection time was 10 s with hydrostatic injections from a height of 10 cm. Electropherograms were recorded and processed with a Hewlett-Packard Model 3359 data acquisition system. To ensure run-to-run reproducibility of migration times, 2-min purges of the capillary with running electrolyte were programmed. The electroosmotic flow velocity was determined from the migration time of acetophenone added to a sample. The electrophoretic mobility, μ_{ep}, was calculated as the difference between the observed mobility and electroosmotic mobility and expressed as negative values because it is opposed to the latter.

2.3. Calculations

Migration values (logarithms of electrophoretic mobilities) were related to analyte and electrolyte parameters by means of multiparametric regression analysis processed with the program SigmaPlot (Jandel Scientific, Corte Madera, CA, USA) on a personal computer. The equations derived were tested according to the requirements of a meaningful correlation analysis, taking into account the correlation coefficient, standard deviation, significance level of the whole equation and number of data points used to derive the equation. Calculated dependences of the electrophoretic mobility on the pH of the electrolyte were obtained by iteration based on a least-squares fit using a standard statistical package.

3. Results and discussion

In free-solution CE with simple electrolytes such as sodium borate buffers, the electrophoretic mobility of ionic species is commonly dependent on the charge and size of the solutes. For the metal complexes under investigation, as for negatively charged species, it can be assumed that adsorption interactions with the capillary wall are negligible. Neither could ion-pairing interactions substantially influence the migration behaviour. Differences in the mobility of the complexes can thus be ascribed to differential charge densities. Lanthanide metal ions have an equal formal charge (3+) and differ only slightly in the ionic radius. Hence as a central metal atom of the chelate complex, they contribute to the net charge and molecular size to a much lesser extent than an aminopolycarboxylic ligand. Therefore, we shall first discuss the effect of differences in charge-to-size ratio arising from differences in the structure of the organic part of the metal complex.

3.1. Correlations using ligand structural descriptors

As pointed out under Experimental, the four sets of lanthanide metal complexes with different aminopolycarboxylic ligands listed in Table 1 were subjected to CE experiments. Variations in the number of carboxylic groups impart different charges to the lanthanide complex, which should affect the migration behaviour. Indeed, superficial examination of the raw data showed that the migration times of the complexes of any given metal increased in the order CDTA < EDTA < DTPA < TTHA. This order followed the expected trend, i.e., the more charged solutes, having higher electrophoretic mobilities in the direction opposite to the electroosmotic flow,

Table 1
Characteristics of the complexing reagents used

Reagent	Charge of lanthanide complex	Ligand structural descriptors			
		$n_{COOH} - 3$	n_{COOH}	n_{CH_2}	n_N
Ethylenediaminetetraacetic acid (EDTA)	−1	1	4	6	2
Cyclohexanediaminetetraacetic acid (CDTA)	−1	1	4	10	2
Diethylenetriaminepentaacetic acid (DTPA)	−2	2	5	9	3
Triethylenetetraaminehexaacetic acid (TTHA)	−3	3	6	12	4

migrated longer than less charged species. DTPA and especially TTHA complexes as the compounds carrying charges of 2− and 3−, respectively, are strongly attracted to the anode (injection end of the capillary), resulting in a decreased apparent velocity compared with that of monocharged EDTA and CDTA complexes. For the latter, equally charged, complexes, the difference in size must have been substantial. As a result, CDTA complexes, being larger and thus possessing a smaller charge density, always migrated faster than EDTA complexes.

On the basis of the above observation, the net charge of the complex (Z) as the main parameter, determining the electrophoretic mobility of a solute, was taken for the initial analysis of the data. Evidently, the Z value strictly depends on the number of carboxylic groups, n_{COOH}, and can be expressed, in absolute units, as $n_{COOH} - 3$. While the charge is a very simple function of the ligand structural fragment, the size of the ligand, having an additive character, can be only presented as a sum of contributions (increments) of the various functional groups. In our case these are carboxylic and methylene groups as well as tertiary nitrogen atoms quantified by n_{COOH}, n_{CH_2} and n_N, respectively. Combination of all four variables was used for analysing the migration data using stepwise multiple regression. The best regression equation describing log μ_{ep} in the CE system based on a 10 mM borate buffer at pH 9.5 was

$$\log \mu_{ep} = -2.673 + 0.522(\pm 0.181)(n_{COOH} - 3) - 0.262(\pm 0.109)n_{COOH} - 0.031(\pm 0.002)n_{CH_2} - 0.091(\pm 0.182)n_N \quad (1)$$

$R = 0.9851$; S.D. $= 0.019$; $p \leq 9.44 \cdot 10^{-31}$; $n = 40$

In this and subsequent equations the values in parentheses are standard deviations of regression coefficients, R is the correlation coefficient, S.D. and p are standard deviation and significance level of the whole equation, respectively, and n is the number of data points used to derive the regression.

Eq. 1 is highly significant statistically, as expressed by the correlation coefficient, and consistent with the qualitative consideration of migration behaviour given above. This equation shows that a charge-related structural descriptor, $n_{COOH} - 3$, as expected, provides a positive input to electrophoretic mobility (positive sign of the corresponding coefficient), whereas the size-related parameters, n_{COOH}, n_{CH_2} and n_N, account for mobility-decreasing effects in CE. At the same time it suggests that the apparent size of the molecule, as estimated from the number of elementary fragments, is less marked as a factor controlling the migration ability relative to the charge. Although all functional groups are shown to contribute negatively to the mobility, the regression coefficients for the corresponding variables differ significantly. This can be rationalized as the input of $-CH_2-$ and =N– fragments appears to be of lesser importance than that of COOH groups. This observation fits well with the relative sizes of different molecular increments. Also, the comparison of the absolute values of the coefficients for $n_{COOH} - 3$ and n_{COOH} variables would assume that the free carboxylic group reflects the changes in the charge rather than in solute's size.

3.2. Correlations with the stability constant

Regardless of the nature of the ligand, the migration order of lanthanide complexes remained constant with a regular increase in migration times with increasing atomic number across the lanthanide series (Fig. 1). In a recent paper [10], we interpreted such a migration behaviour in terms of the effective charge of the metal ion. Evidently, the lower the electron-acceptor ability of the lanthanide ion, the larger is the negative charge of the complex and therefore the faster will be its electrophoretic mobility. Consequently, the complexes of lanthanide ions with higher atomic number migrate more slowly towards the cathode. However, to the best of our knowledge, no published data on effective charge calculations for the complexes under consideration are available. On the other hand, there are abundant reports on the overall stability constants, β_n (e.g., see Ref. [11] or more recent editions of

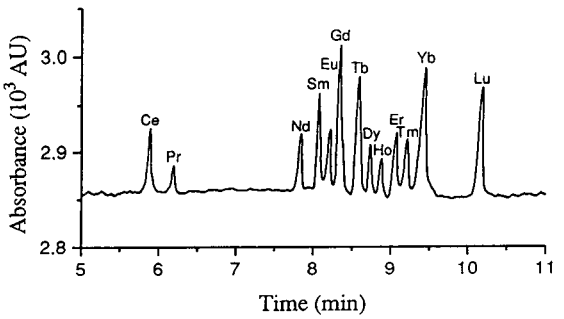

Fig. 1. CE separation of lanthanide metal–CDTA complexes. Capillary, 42/50 cm × 75 μm I.D.; electrolyte, 20 m*M* borate buffer containing $1 \cdot 10^{-3}$ *M* CDTA (pH 11.1); applied voltage, +15 kV; direct UV detection at 214 nm.

that publication) as a parameter closely connected with the electron-acceptor strength of metal ions. This universal structure-dependent characteristic of metal complexes is commonly accepted as a variable for quantitative structure–chromatographic retention relationships [12,13]. Further, in earlier work [14], the log β_n values were applied successfully in the regression equation describing the observed mobility of transition metal complexes with 8-hydroxyquinoline-5-sulphonic acid in CE.

With that in mind, we subjected the experimental migration data for lanthanide–aminopolycarboxylic acid complexes to linear regression analysis. A simple correlation of log β_n against log μ_{ep} values gave the following equation (in this example, for CDTA complexes).

$$\log \mu_{ep} = -2.840 - 0.038(\pm 0.005) \log \beta_n \qquad (2)$$

$$R = 0.9308;\ \text{S.D.} = 0.024;\ p \leq 3.901 \cdot 10^{-6};\ n = 13$$

Eq. 2 is of rather good statistical quality that proves the ability of log β_n to approximate mobility differences. It should be also stressed that the coefficient relating log μ_{ep} and log β_n is negative. This indicates that more stable complexes with the electron charge density shifted stronger to the central atom are less mobile than less stable complexes and additionally confirms the usefulness of β_n as a reliable measure for the effective charge estimations.

3.3. Dependences of electrophoretic mobility on electrolyte composition

Until now, migration data were analysed separately for each electrophoretic buffer system. For an approximation of the whole data set, knowledge of the electrolyte variables influencing the migration behaviour and selection of the most important ones are required. Included in a single equation with solute descriptors, as carried out below, they can provide a sufficiently complete answer. As borate buffer electrolytes were indicated to be the optimum electrolyte system for metal–aminopolycarboxylic acid complexes [10,15], the parameters considered were the pH and borate concentration.

pH

The electrophoretic mobility can reflect the changes in the electrolyte pH provided that the analytes undergo certain charge density alterations. For negatively charged metal complexes, this may concern the influence of pH on acid–base or complexation equilibria. The effect of pH variation was examined experimentally in the range 8.5–11.0 using 10 m*M* borate buffer. At less basic pH, the mobilities of the complexes were very close or even identical, as for separands with very similar pK_a (or effective charge) values. However, above pH 9.5, a significant increase in μ_{ep} as a function of pH was observed. This increase is thought to be related to the formation of hydroxo forms of the lanthanide complexes, presumably $M(OH)Y^{(n+1)-}$ (M and Y represent a lanthanide ion and the fully deprotonated form of a reagent, respectively). Evidently, an increased negative charge of lanthanide species, following a shift in the equilibrium

$$MY^{n-} + OH^- \rightleftharpoons M(OH)Y^{(n+1)-}$$

in favour of the mixed-ligand form, leads to correspondingly higher mobilities. The observed pH dependence is contrary to the results reported by Motomizu et al. [16], who found that the electrophoretic mobilities of alkaline earth metal–EDTA complexes were identical over the

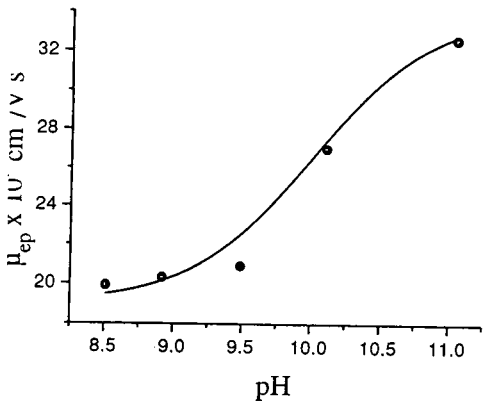

Fig. 2. Electrophoretic mobility of erbium–CDTA complex as a function of pH. O = experimentally determined values; solid line = theoretical curve calculated according to Eq. 3.

pH range 8–10.5. This contradiction can be explained by a stronger tendency of lanthanide(III) ions to hydrolyse and, consequently, to form hydroxymetal species. Note that the same workers suggested the formation of a mixed-ligand chelate, $Fe(OH)Y^{2-}$, for iron(III) with a high tendency for hydrolysis.

To find the relationship between the observed electrophoretic mobility of the complexes and pH of the electrolyte, the above equilibrium was treated in a similar way to an acid–base equilibrium (e.g., Ref. [17]). The resulting theoretical relationship between μ_{ep} and pH is

$$\mu_{ep} = \frac{\mu_{ep}^{M(OH)Y} - \mu_{ep}^{M(OH)}}{1 + 10^{pK-pH}} \quad (3)$$

where μ_{ep}^{MY} and $\mu_{ep}^{M(OH)Y}$ are the mobilities of individual complexed forms (the charges are omitted) and K is the formation constant of a mixed-ligand complex. Curves for μ_{ep} vs. pH dependences were approximated by an iteration procedure using Eq. 3. A typical example of the least-squares fit of the experimental data to the function as given in Eq. 3 is shown in Fig. 2 for the erbium–CDTA complex. The pK values resulting from this approximation were used for further evaluation of the electrolyte pH effect within a multivariative migration model.

Borate buffer concentration

Different borate concentrations of the electrolyte were then investigated. In these experiments, the electrolyte pH was kept constant at 9.5. The results are presented in Table 2. As can be seen, the mobility of all the complexes first decreases (up to ca. 10–15 mM) and then increases when the buffer concentration is further increased. This behaviour is probably due to the competing effects of changes in the ionic strength of the electrophoretic medium. At relatively low electrolyte concentrations, the mobilities become lower following a decreased ζ potential, as follows from the double-layer theory. In contrast, when high-ionic-strength buffer solutions are used, an excessive Joule heating, which is likely to occur, leads to an increase in mobilities owing to an influence of temperature on the electrolyte viscosity.

Nevertheless, these results indicate that the buffer concentration alters the electrophoretic mobility of lanthanide complexes only moderately and thus is a less important controllable factor than the pH; it is therefore not considered further. Hence pH was chosen as a variable that has the greatest impact on migration parameters

Table 2
Effect of borate buffer concentration on the electrophoretic mobilities of lanthanide complexes (pH 9.5)

Sodium tetraborate (mM)	$-\mu_{ep} \times 10^5$ (cm^2 V^{-1} s^{-1})			
	Ce–EDTA	Eu–EDTA	Dy–CDTA	Gd–CDTA
5	26.8	26.6	23.1	23.2
10	25.4	25.3	19.5	19.4
15	22.8	21.8	20.6	20.0
20	23.2	24.0	22.1	21.7

which can be described by a non-empirical function.

3.4. Multiparametric migration model for lanthanide complexes

Obviously, we approached the situation when a migration model relating log μ_{ep} values to solute and electrolyte parameters taken simultaneously into consideration as predictors can be derived to evaluate the migration behaviour of lanthanide complexes in different buffer systems. Therefore, an attempt was made to incorporate all of the above variables in one regression equation to be utilized for analysing all of the data combined into one set. The resulting migration model is expressed by the following six-term equation:

$$\log \mu_{ep} = -2.575 + 0.510(\pm 0.169)Z + 0.0041(\pm 0.0022) \log \beta_n - 0.285(\pm 0.099)n_{COOH} - 0.016(\pm 0.002)n_{CH_2} - 0.141(\pm 0.171)n_N - 0.077(\pm 0.006) \times \log(1 + 10^{pK-pH}) \quad (4)$$

$R = 0.9643$; S.D. $= 0.025$; $p \leq 3.17 \cdot 10^{-50}$; $n = 86$

This equation describes the linear change in log μ_{ep} as a function of charge and structure characteristics for any pH of borate buffer electrolyte. The last term was included after taking the common logarithm of both sides of Eq. 3 and operated with pK values determined by electrophoretic measurements. As the magnitude of the regression coefficient reflects both the contribution and the individual scale of each parameter, it is not easy to interpret their relevance. Nonetheless, as might be expected, the largest parameter is the net charge of the metal complex. Also, the coefficients for this parameter and ligand structural variables (terms 3–5) are in accord with those for similar terms of Eq. 1.

The statistical goodness of Eq. 4 is high enough to predict the mobility of a metal complex. In order to illustrate this value of the proposed model, the calculated logarithms of electrophoretic mobility were plotted against the observed values. Fig. 3 shows the result of applying Eq. 4 to the experimental data set for 43 complexes under 14 different electrolyte conditions (80 data points). A linear relationship with zero intercept and unit slope was obtained. The predictive quality expressed as the percentage deviation of the calculated and observed log μ_{ep} values is generally less than 1%.

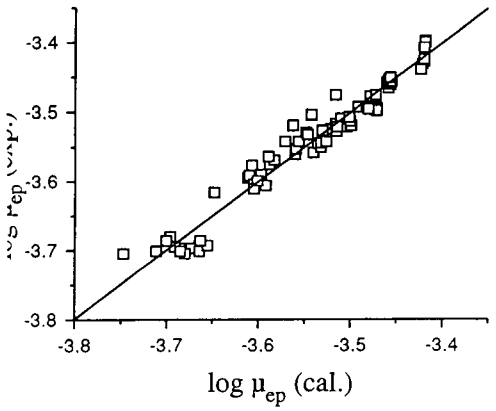

Fig. 3. Relationship between the migration parameters of lanthanide complexes determined experimentally and calculated using Eq. 4 ($\mu_{ep} \times 10^5$ cm^2 V^{-1} s^{-1}). The correlation coefficient (R) is 0.9791. The average deviation of the calculated and observed log μ_{ep} values is 0.40%.

4. Conclusions

The results of this study demonstrate that the multivariate regression strategy for analysing mobility dependences provides an adequate description and rational interpretation of CE data. The statistically significant relationships derived here can be widely employed to approximate differences in the migration properties of metal ion complexes arising from differences in structure and compositional electrolyte changes. At the same time, they support the validity of the generally observed mechanism of free-solution CE in the case of precapillary-formed metal complexes. The migration behaviour has been revealed to be a pure electrophoretic effect affected solely by charge density parameters of solute molecules without any observable influ-

ence of auxiliary solute–electrolyte or solute–capillary wall interactions. The fact that it is possible to correlate the mobility data directly with simple, readily determinable parameters, possessing a definite physical meaning, confirms also a straightforward theoretical foundation of CE.

As demonstrated above, accurate predictions of migration can be achieved from multiple linear regression when operating meaningful migration models consisting of certain sets of structural and electrolyte variables. It is worth noting that owing to its simplicity, the multivariate statistical approach can be easily adapted to other kinds of metal complexes and further developed to be applicable to partially complexed metal ions. Likely advances with this approach may also concern the migration behaviour of metal complexes in more sophisticated CE modes (e.g., micellar-mediated [18] or ion-association [19] CE), taking into account the inputs to mobility due to the corresponding solute and electrolyte parameters.

Acknowledgement

The authors are grateful to Professor Oleg M. Petrukhin for stimulating discussions.

References

[1] P. Jandik and G. Bonn, *Capillary Electrophoresis of Small Molecules and Ions*, VCH, New York, 1993.
[2] R. Kuhn and S. Hoffstetter-Kuhn, *Capillary Electrophoresis: Principles and Practice*, Springer, Berlin, 1993.
[3] F. Foret, L. Krivankova and P. Bocek, *Capillary Zone Electrophoresis*, VCH, Weinheim, 1993.
[4] P.E. Jackson and P.R. Haddad, *Trends Anal. Chem.*, 12 (1993) 231.
[5] A.R. Timerbaev, *J. Capillary Electrophoresis*, in press.
[6] Y. Shi and J.S. Fritz, *J. Chromatogr.*, 640 (1993) 473.
[7] M. Jimidar, T. Hamoir, W. Degezelle, D.L. Massart, S. Soykenç and P. Van de Winkel, *Anal. Chim. Acta*, 284 (1993) 217.
[8] C. Quang and M.G. Khaledi, *J. Chromatogr. A*, 659 (1994) 459.
[9] A.R. Timerbaev, O.P. Semenova, I.G. Tsoi and O.M. Petrukhin, *J. Chromatogr.*, 648 (1993) 307.
[10] A.R. Timerbaev, O.P. Semenova and G.K. Bonn, *Analyst*, in press.
[11] A.E. Martell and R.M. Smith, *Critical Stability Constants*, Plenum Press, New York, 1974.
[12] A.R. Timerbaev, I.G. Tsoi and O.M. Petrukhin, *J. Chromatogr.*, 498 (1990) 337.
[13] A.R. Timerbaev and G.K. Bonn, *J. Chromatogr.*, 640 (1993) 195.
[14] A.R. Timerbaev, W. Buchberger, O.P. Semenova and G.K. Bonn, *J. Chromatogr.*, 630 (1993) 379.
[15] S. Motomizu, S. Nishimura, Y. Obata and H. Tanaka, *Anal. Sci.*, 7 (1991) 253.
[16] S. Motomizu, M. Oshima, S. Matsuda, Y. Obata and H. Tanaka, *Anal. Sci.*, 8 (1992) 619.
[17] J. Vindevogel and P. Sandra, *Introduction to Micellar Electrokinetic Chromatography*, Hüthig, Heidelberg, 1992.
[18] A.R. Timerbaev, O.P. Semenova, P. Jandik and G.K. Bonn, *J. Chromatogr. A*, 671 (1994) 419.
[19] N. Iki, H. Hoshino and T. Yotsuyanagi, *J. Chromatogr. A*, 652 (1993) 539.

ELSEVIER

Journal of Chromatography A, 690 (1995) 149–154

JOURNAL OF CHROMATOGRAPHY A

Short communication

Separation of estrogens by micellar electrokinetic chromatography

King C. Chan[a], Gary M. Muschik[a], Haleem J. Issaq[a,*], Pentti K. Siiteri[b]

[a]*Program Resources, Inc./DynCorp, National Cancer Institute, Frederick Cancer and Research Development Center, Frederick, MD 21702, USA*

[b]*DCE, National Cancer Institute, Bethesda, MD, USA*

Received 6 September 1994; accepted 17 October 1994

Abstract

Capillary electrophoresis of the sex hormone estrogens using different buffer components was investigated. Free zone electrophoresis with 10 m*M* phosphate buffer (pH 11.5) or 10 m*M* phosphate buffer with 10–20% methanol was not effective in separating the ten estrogens used in this study. However, nine estrogens were resolved by micellar electrokinetic chromatography using a 10 m*M* borate buffer (pH 9.2) containing 100 m*M* sodium cholate. In addition, some estrogens were partially separated using sodium dodecyl sulfate (SDS) micellar buffers; however, the addition of modifiers such as organic solvents or cyclodextrins improved resolutions significantly. Using a 10 m*M* phosphate buffer (pH 7.0) containing 50 m*M* SDS and 20% methanol, or a 10 m*M* borate buffer (pH 9.2) containing 50 m*M* SDS and 20 m*M* γ-cyclodextrin, all ten of the tested estrogens were separated. However, the cyclodextrin-modified buffer allowed faster separation.

1. Introduction

Estrogens are steroidal sex hormones formed from the precursors androstenedione and testosterone [1]. The most potent naturally occurring estrogen is 17β-estradiol, which is interconvertable to the less potent compound, estrone. Both of these estrogens can also be metabolized to estriol, which also has limited estrogenic activity. All of these transformations take place mainly in the liver. Estrogen determinations are widely used to monitor pregnancy [2], osteoporosis [3], breast cancer [4] and uterine corpus cancer [5]. Radioimmunoassay [6] or enzyme immunoassay [7] have been used for the sensitive detection of estrogens. Also, chromatographic methods allow simultaneous determinations of various estrogens. High-performance liquid chromatography (HPLC) with UV absorption [8–11], fluorescence [12] or electrochemical detection [13,14], gas chromatography or gas chromatography–mass spectrometry [15–17] and supercritical fluid chromatography have been used for the analyses of estrogens [18]. Estrogens prelabeled with a 2-(4-carboxyphenyl)-5,6-dimethylbenzimidazole have also been separated by HPLC followed by fluorescence detection [19]. In addition, post-column chemiluminescence detection of estrogen derivatized with dansyl chloride was also demonstrated [20].

* Corresponding author.

0021-9673/95/$09.50
SSDI 0021-9673(94)00990-2

Due to its high resolution, rapid separation, low mass detectability, and easy operation, capillary electrophoresis (CE) has recently emerged as a very attractive separation tool complementary to HPLC [21]. Capillary zone electrophoresis (CZE) has been used exclusively for the separations of charged compounds. Another mode of CE, micellar electrokinetic chromatography (MEKC), is widely used for the separation of non-polar molecules [22]. This technique uses buffers containing organic micelles to separate analytes based on their differential partitions between the aqueous and the micellar phases.

Separations of steroidal compounds using MEKC have been demonstrated. For example, MEKC using sodium dodecyl sulfate (SDS) micelles was applied to the separation of the insect and plant hormones, ecdysteroids [23]. In addition, MEKC or MEKC modified with urea or cyclodextrins (CDs) were applied to the separations of corticosteroids [24–27]. MEKC of corticosteroids using mixed micelles was also shown [28]. Recently, separation of three estrogens by CZE using aqueous or aqueous–methanolic buffers was reported [29]. In this study, separations of estrogens under different MEKC conditions were investigated.

2. Experimental

2.1. Chemicals

Estrogen standards were obtained from Steraloids (Wilton, NH, USA). Stock estrogen solutions were prepared in methanol and stored at −20°C when not in use. CDs were obtained from Advanced Separation Technologies (Whippany, NJ, USA). SDS, sodium cholate, sodium deoxycholate and other reagent-grade chemicals were obtained from Sigma (St. Louis, MO, USA) or Fisher (Fairlawn, NJ, USA). All buffers were filtered with a 0.2-μm membrane filter before use.

2.2. Apparatus

A Beckman P/ACE 2050 CE system was used. Separations were performed at 20°C and +17 kV with 47 cm × 50 μm fused-silica capillaries (Polymicro Technologies, Phoenix, AZ, USA). Injection samples were prepared by diluting the estrogen stock solutions in either 50 m*M* of SDS, sodium cholate or sodium deoxycholate. Samples were introduced into a capillary by applying pressure (0.5 p.s.i.; 1 p.s.i. = 6894.76 Pa) for 2 s. The capillaries were flushed with the electrophoretic buffers for 2 min between runs. Peaks were detected by UV absorption at 200 nm.

3. Results and discussion

The most potent estrogen in humans is 17β-estradiol, followed by estrone and estriol. Each of these molecules contain a 17-carbon nucleus (steroid) with a methyl group at C-13, and an aromatic ring with a hydroxyl group at C-3 (Fig. 1). The derivatives are designated by the presence of a ketone (estrone) or hydroxyl (estradiol) group at C-17 and frequently at C-16 (16-keto-17β-estradiol, estriol). Estrogens are negatively charged at alkaline solution due to the ionization of the phenolic hydroxyl group. CZE has been used to separate 17β-estradiol, estrone and estriol [29]; but it was not adequate in resolving the ten estrogens used in our study (Fig. 2a) because these estrogens have similar electrophoretic mobilities. Although the addition of organic solvents to running buffers is a common method for enhancing separations by lowering electroosmotic flow and increasing solvation of solutes [28–30], separation of most estrogens was still unsuccessful using buffers containing 10–20% methanol (Fig. 2b and c).

MEKC of estrogens using bile salts as micelles was investigated. Using a 10 m*M* borate buffer (pH 9.2) containing 100 m*M* deoxycholate, partial separation of the estrogens was possible (Fig. 3a), while nine estrogens were separated using 100 m*M* sodium cholate (Fig. 3b). 4-Hydroxyestrone and 2-hydroxyestradiol were not resolved using the indicated running conditions. MEKC of estrogens using SDS micelles was also investigated. In contrast to the bile salts, SDS micelles strongly retain the estrogens, resulting in poor separation (Fig. 4a). Organic modifiers are often used in MEKC to decrease the af-

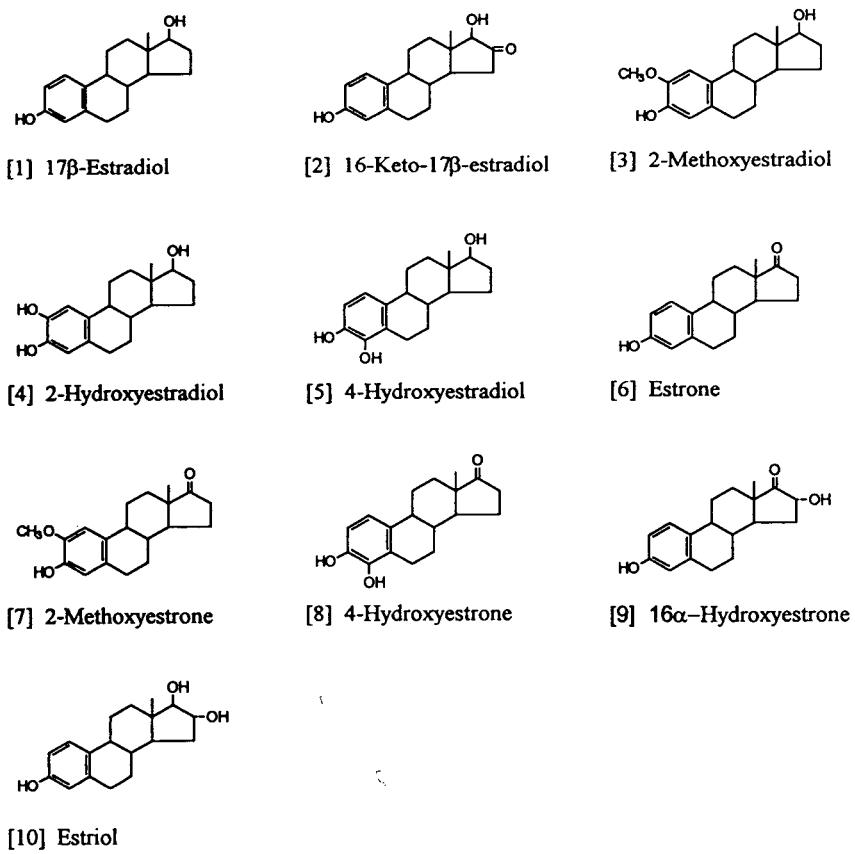

Fig. 1. Chemical structures of ten estrogens.

finities of hydrophobic solutes for the micellar phase. In addition, organic solvents reduce electroosmotic flow and subsequently expand the migration window [31–34]. As a result, resolution of highly hydrophobic compounds in MEKC is enhanced. Addition of 15% acetonitrile to the SDS buffer allows for the separations of all estrogens, except 4-hydroxyestrone and 4-hydroxyestradiol (Fig. 4b), while all ten estrogens were separated with 20% methanol (Fig. 4c).

SDS micellar buffers modified with CDs have been used to separate the highly hydrophobic compounds, corticosteroids [25–27], which share the steroidal nucleus of estrogens. CD reduces the capacity factors for the micellar phase by forming inclusion complexes with corticosteroids. The separations are based on the differential partitions of the solutes among the aqueous phase, CD, and SDS micelles. Compared to corticosteroids, estrogens are more hydrophilic because of the presence of phenolic hydroxyl groups. Nevertheless, CD also plays an important role in the MEKC of estrogens, as shown in Fig. 5a–c. Most of the ten estrogens were baseline separated with a 10 m*M* borate buffer (pH 9.2) containing 50 m*M* SDS and 20 m*M* β-CD, while the addition of 20 m*M* γ-CD in the SDS buffer allowed for the complete separation of the ten estrogens. The pair consisting of 2-methoxyestradiol and 2-methoxyestrone, which were partially resolved with the β-CD, were baseline separated with the γ-CD-modified buffer. This is because the larger size of the methoxy derivatives require a CD with a larger cavity (i.e., γ-CD) for more effective interaction. The migration orders of most estrogens were similar in either CD-modified buffers, except that the peaks of 16α-hydroxyestrone and 16-keto-17β-estradiol were reversed. MEKC modified with α-CD was also attempted, but

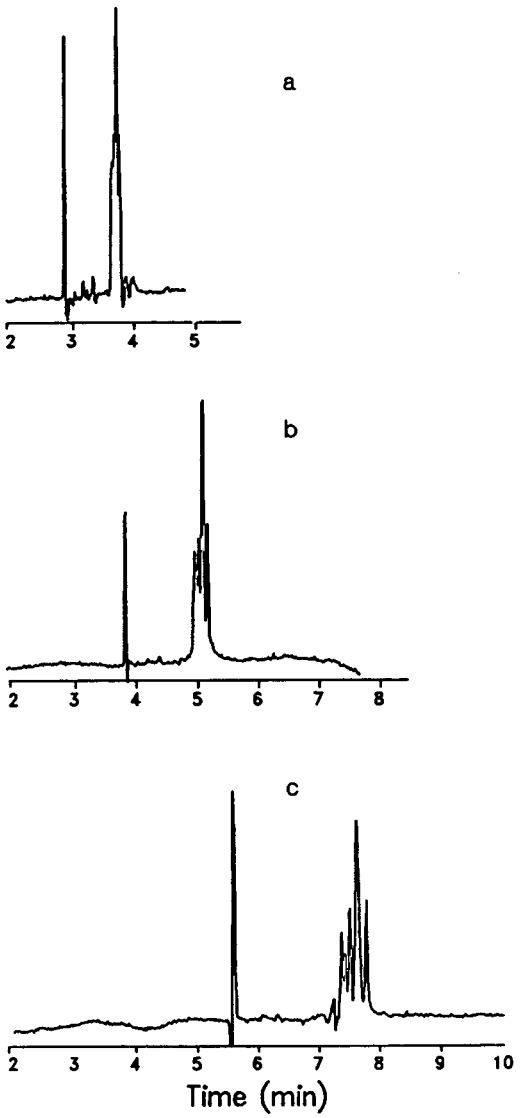

Fig. 2. CZE of ten estrogens. Buffers: 10 m*M* sodium phosphate (pH 11.5) containing (a) 0%, (b) 10% and (c) 20% of methanol; capillary: 47 cm × 50 μm; voltage: 17 kV; pressure injection: 2s; detection: absorption at 200 nm. Peak numbers correspond to Fig. 1.

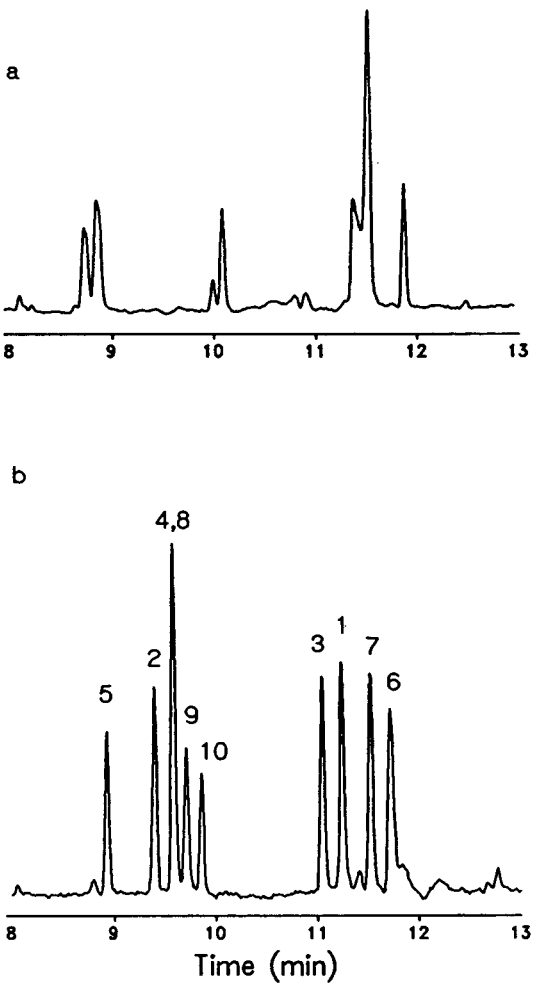

Fig. 3. MEKC of ten estrogens using bile salts. Buffers: 10 m*M* sodium borate (pH 9.2) containing (a) 100 m*M* sodium deoxycholate, and (b) 100 m*M* sodium cholate; capillary: 47 cm × 50 μm; voltage: 17 kV; pressure injection: 2 s; detection: absorption at 200 nm. Peak numbers correspond to Fig. 1.

separation of the estrogens was not successful (data not shown). This is because the estrogens did not form inclusion complexes with α-CD because its cavity is small compared to those of the β- and γ-CDs.

4. Conclusions

MEKC is a useful method for separating estrogens. With a 10 m*M* borate buffer (pH 9.2) containing 100 m*M* sodium cholate, nine of the ten tested estrogens were resolved. Buffers containing only SDS micelles allowed for partial separation of the estrogens. However, the addi-

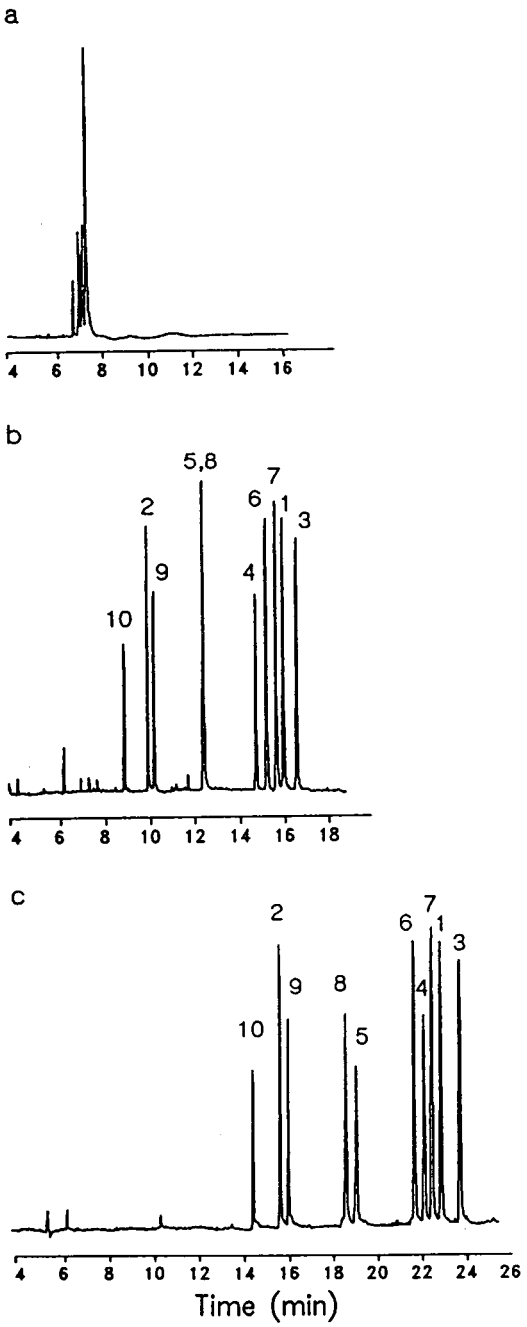

Fig. 4. Effects of organic solvents on MEKC of ten estrogens. Buffers: 10 m*M* sodium phosphate (pH 7.0) containing 50 m*M* SDS and (a) no organic solvent, (b) 15% acetonitrile and (c) 20% methanol; capillary: 47 cm × 50 μm; voltage: 20 kV; pressure injection: 2 s; detection: absorption at 200 nm. Peak numbers correspond to Fig. 1.

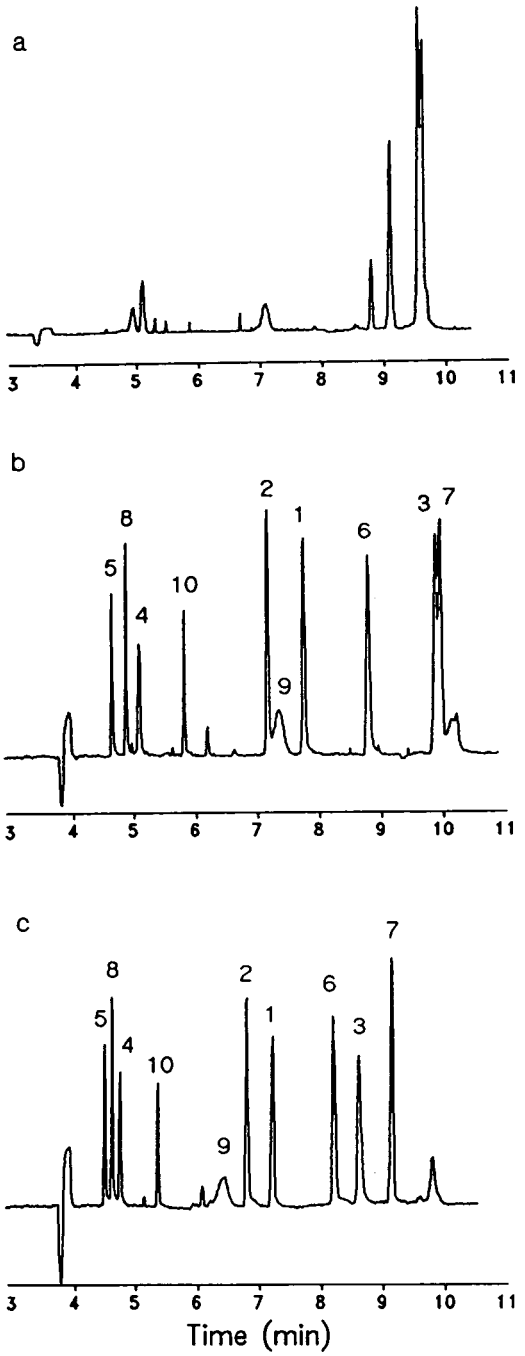

Fig. 5. Effects of cyclodextrins on MEKC of ten estrogens. Buffers: 10 m*M* sodium borate (pH 9.2) containing 50 m*M* SDS and (a) no CD, (b) 20 m*M* β-CD and (c) 20 m*M* γ-C; capillary: 47 cm × 50 μm; voltage: 17 kV; pressure injection: 2 s; detection: absorption at 200 nm. Peak numbers correspond to Fig. 1.

tion of modifiers to the SDS buffers, such as organic solvents or CDs, greatly improved the separations. Using either a 10 m*M* phosphate buffer (pH 7.0) containing 50 m*M* SDS and 20% methanol, or a 10 m*M* borate buffer (pH 9.2) containing 50 m*M* SDS and 20 m*M* γ-CD, all ten of the tested estrogens were separated. However, the CD-modified buffer is more desirable because it allows for a faster analysis time (ca. 10 min vs. 25 min). With UV absorption, the detection limits for the tested estrogens were ca. 2 μg/ml. An application of the described MEKC methods is the determination of estrogens in pharmaceutical dosage forms. For the determination of estrogens in biological samples, an extraction/concentration step or a more sensitive detection technique than absorption is needed and these are currently studied in our laboratory.

Acknowledgements

The content of this publication does not necessarily reflect the views or policies of the Department of Health and Human Services, nor does mention of trade names, commercial products, or organization imply endorsement by the US Government.

References

[1] C.A. Burtis and E.R. Ashwood (Editors), *Tietz Textbook of Clinical Chemistry*, W.B. Saunders, Philadelphia, PA, 2nd ed., 1994, p. 1857.
[2] J. Ishida, M. Kai and Y. Ohkura, *J. Chromatogr.*, 431 (1988) 249.
[3] T. Cundy, M. Evans, H. Roberts, D. Wattie, R. Ames and I.R. Reid, *Br. Med. J.*, 303 (1991) 13.
[4] J.L. Kelsey and M.D. Gammon, *Epidemiol. Rev.*, 12 (1990) 228.
[5] K. Iida, A. Imai and T. Tamaya, *Gen. Pharmacol.*, 22 (1991) 491.
[6] N. DeChene, B. McNamara and S. Breglio, *Clin. Chem.*, 38 (1992) 951.
[7] J.F.R. Robertson, D. Pearson, M.R. Price, C. Selby, R.W. Blamey and A. Howell, *Br. J. Cancer*, 64 (1991) 757.
[8] K. Shimada, H. Kaji and K. Kuwabara, *J. Chromatogr. Sci.*, 31 (1993) 363.
[9] L.A. Castagnetta, O.M. Granata, M.L. Casto, M. Calabro, F. Arcuri and G. Carruba, *J. Chromatogr.*, 572 (1991) 25.
[10] R.W. Townsend, V. Keuth, K. Embil, G. Mullersman, J.H. Perrin and H. Derendorf, *J. Chromatogr.*, 450 (1988) 414.
[11] P.E. Lonning, P. Skulstad, A. Sunde and T. Thorsen, *J. Steroid Biochem.*, 32 (1989) 91.
[12] H. Lamparczyk, P.K. Zarzycki, J. Nowakowska and R.J. Ochocka, *Chromatographia*, 38 (1994) 168.
[13] J. Noma, N. Hayashi and K. Sekiba, *J. Chromatogr.*, 568 (1991) 35.
[14] L. Castagnetta, O.M. Granata, G. Brignone, L. Blasi, F. Arcuri, M. Mesiti, A. D'Aquino and W. Preitano, *Ann. N.Y. Acad. Sci.*, 586 (1990) 121.
[15] E. Vanluchene, D. Vandekerckhove, J. Jonckheere and A. De Leenheer, *J. Chromatogr.*, 279 (1983) 573.
[16] D.C. Spink, D.W. Lincoln II, H.W. Dickerman and J.F. Gierthy, *Proc. Natl. Acad. Sci. U.S.A.*, 87 (1990) 6917.
[17] V. Vermoesen, J. Vercammen, C. Sanders, D. Courtheyn and H.F. De Brabander, *J. Chromatogr.*, 564 (1991) 385.
[18] N.K. Jagota and J.T. Stewart, *J. Pharm. Biomed. Anal.*, 10 (1992) 667.
[19] M. Katayama and H. Taniguchi, *J. Chromatogr.*, 616 (1993) 317.
[20] O. Nozaki, Y. Ohba and K. Imai, *Anal. Chim. Acta*, 205 (1988) 255.
[21] C.A. Monnig and R.T. Kennedy, *Anal. Chem.*, 66 (1994) 280R.
[22] S. Terabe, K. Otsuka, K. Ichikawa, A. Tsuchiya and T. Ando, *Anal. Chem.*, 56 (1984) 111.
[23] P. Davis, R. Lafon, T. Large, E.D. Morgan and I.D. Wilson, *Chromatographia*, 37 (1993) 37.
[24] H. Nishi, T. Fukuyama, M. Matsuo and S. Terabe, *J. Chromatogr.*, 513 (1990) 279.
[25] H. Nishi and M. Matsuo, *J. Liq. Chromatogr.*, 14 (1991) 973.
[26] S. Terabe, Y. Miyashita, Y. Ishihama and O. Shibata, *J. Chromatogr.*, 636 (1993) 47.
[27] J. Bumgarner and M. Khaledi, presented at the *6th International Symposium on High Performance Capillary Electrophoresis, San Diego, CA, 31 January–3 February 1994*, poster 615.
[28] K. Potter, R.J.B. Allington and J. Algaier, *J. Chromatogr. A*, 652 (1993) 427.
[29] C. Schwer and E. Kenndler, *Anal. Chem.*, 63 (1991) 1801.
[30] Y. Walbroehl and J.W. Jorgenson, *Anal. Chem.*, 58 (1986) 479.
[31] A.T. Balechunas and M.J. Sepaniak, *Anal. Chem.*, 59 (1987)1466.
[32] R.D. Holland and M.J. Sepaniak, *Anal. Chem.*, 65 (1993) 1140.
[33] T. Yashima, A. Tsuchiya, O. Morita and S. Terabe, *Anal. Chem.*, 64 (1992) 2981.
[34] R.O. Cole and M.J. Sepaniak, *LC·GC*, 10 (1992) 380.

PUBLICATION SCHEDULE FOR THE 1995 SUBSCRIPTION

Journal of Chromatography A and *Journal of Chromatography B: Biomedical Applications*

MONTH	O 1994	N 1994	D 1994	J 1995	
Journal of Chromatography A	683/1 683/2 684/1	684/2 685/1 685/2 686/1	686/2 687/1 687/2 688/1 + 2	689/1 689/2 690/1 690/2	The publication schedule for further issues will be published later.
Bibliography Section					
Journal of Chromatography B: Biomedical Applications				663/1 663/2	

INFORMATION FOR AUTHORS

(Detailed *Instructions to Authors* were published in *J. Chromatogr. A*, Vol. 657, pp. 463–469. A free reprint can be obtained by application to the publisher, Elsevier Science B.V., P.O. Box 330, 1000 AH Amsterdam, Netherlands.)

Types of Contributions. The following types of papers are published: Regular research papers (full-length papers), Review articles, Short Communications and Discussions. Short Communications are usually descriptions of short investigations, or they can report minor technical improvements of previously published procedures; they reflect the same quality of research as full-length papers, but should preferably not exceed five printed pages. Discussions (one or two pages) should explain, amplify, correct or otherwise comment substantively upon an article recently published in the journal. For Review articles, see inside front cover under Submission of Papers.

Submission. Every paper must be accompanied by a letter from the senior author, stating that he/she is submitting the paper for publication in the *Journal of Chromatography A* or *B*.

Manuscripts. Manuscripts should be typed in **double spacing** on consecutively numbered pages of uniform size. The manuscript should be preceded by a sheet of manuscript paper carrying the title of the paper and the name and full postal address of the person to whom the proofs are to be sent. As a rule, papers should be divided into sections, headed by a caption (*e.g.*, Abstract, Introduction, Experimental, Results, Discussion, etc.). All illustrations, photographs, tables, etc., should be on separate sheets.

Abstract. All articles should have an abstract of 50–100 words which clearly and briefly indicates what is new, different and significant. No references should be given.

Introduction. Every paper must have a concise introduction mentioning what has been done before on the topic described, and stating clearly what is new in the paper now submitted.

Experimental conditions should preferably be given on a *separate* sheet, headed "Conditions". These conditions will, if appropriate, be printed in a block, directly following the heading "Experimental".

Illustrations. The figures should be submitted in a form suitable for reproduction, drawn in Indian ink on drawing or tracing paper. Each illustration should have a caption, all the *captions* being typed (with double spacing) together on a *separate sheet*. If structures are given in the text, the original drawings should be provided. Coloured illustrations are reproduced at the author's expense, the cost being determined by the number of pages and by the number of colours needed. The written permission of the author and publisher must be obtained for the use of any figure already published. Its source must be indicated in the legend.

References. References should be numbered in the order in which they are cited in the text, and listed in numerical sequence on a separate sheet at the end of the article. Please check a recent issue for the layout of the reference list. Abbreviations for the titles of journals should follow the system used by *Chemical Abstracts*. Articles not yet published should be given as "in press" (journal should be specified), "submitted for publication" (journal should be specified), "in preparation" or "personal communication".

Vols. 1–651 of the *Journal of Chromatography*; *Journal of Chromatography, Biomedical Applications* and *Journal of Chromatography, Symposium Volumes* should be cited as *J. Chromatogr.* From Vol. 652 on, *Journal of Chromatography A* (incl. Symposium Volumes) should be cited as *J. Chromatogr. A* and *Journal of Chromatography B: Biomedical Applications* as *J. Chromatogr. B.*

Dispatch. Before sending the manuscript to the Editor please check that the envelope contains four copies of the paper complete with references, captions and figures. One of the sets of figures must be the originals suitable for direct reproduction. Please also ensure that permission to publish has been obtained from your institute.

Proofs. One set of proofs will be sent to the author to be carefully checked for printer's errors. Corrections must be restricted to instances in which the proof is at variance with the manuscript.

Reprints. Fifty reprints will be supplied free of charge. Additional reprints can be ordered by the authors. An order form containing price quotations will be sent to the authors together with the proofs of their article.

Environmental Analysis

Techniques, Applications and Quality Assurance

Edited by **D. Barceló**

Techniques and Instrumentation in Analytical Chemistry Volume 13

Three aspects of environmental analysis are treated in this book:

- the use of various analytical techniques
- their applications to trace analysis of pollutants, mainly organic compounds
- quality assurance aspects, including the use of certified reference materials for quality control of the whole analytical process.

The book will serve as a general reference for post-graduate students as well as a practical reference for environmental chemists who need to use the analytical techniques for environmental studies. Analytical chemists needing information on the complexity of environmental sample matrices and interferences will also find this an invaluable reference.

Contents: Part 1. Field Sampling Techniques and Sample Preparation.
1. Sampling techniques for air pollutants (R. Niessner).
2. Sample handling strategies for the analysis of organic contaminants from environmental samples (M.-C. Hennion, P. Scribe).
3. Extraction, clean-up and recoveries of persistent trace organic contaminants from sediment and biota samples (D.E. Wells).
Part 2. Application Areas.
4. Current developments in the analysis of polychlorinated biphenyls (PCBs) including planar and other toxic metabolites in environmental matrices (D.E. Wells).
5. Official methods of analysis of priority pesticides in water using gas chromatographic techniques (D. Barceló).
6. Coupled-column reversed phase liquid chromatography as a versatile technique for the determination of polar pesticides (E.A. Hogendoorn, P. van Zoonen). 7. Liquid chromatographic determination of phenols and substituted derivatives in water samples (G. Marko-Varga). 8. HPLC methods for the determination of mycotoxins and phycotoxins (J.F. Lawrence, P.M. Scott).
9. Determination of radionuclides in environmental samples (V. Valkovic).
Part 3. Quality Assurance and Reference Materials.
10. Quality assurance in environmental analysis (W.P. Cofino). 11. Certified reference materials for the quality control of measurements in environmental monitoring (E.A. Maier). 12. Standard reference materials for the determination of trace organic constituents in environmental samples (S.A. Wise).
Part 4. Emerging Techniques.
13. Application of fluorescence spectroscopic techniques in the determination of PAHs and PAH metabolites (F. Ariese, C. Gooijer, N.H. Velthorst).
14. Characterization of surfactants in water by desorption ionization methods (F. Ventura). 15. Utilization of various LC-MS interfacing systems in environmental analysis; application to polar pesticides (M.H. Lamoree, R.T. Ghijsen, U.A.Th. Brinkman).
16. Hyphenated techniques applied to the speciation of organometallic compounds in the environment (O.F.X. Donard, R. Ritsema). 17. The potential of capillary electrophoresis in environmental analysis (M.W.F. Nielen). Subject index.

©1993 658 pages Hardbound
Price: Dfl. 465.00 (US$ 273.50)
ISBN 0-444-89648-1

ELSEVIER
An imprint of Elsevier Science

ORDER INFORMATION

ELSEVIER SCIENCE B.V.
P.O. Box 330
1000 AH Amsterdam
The Netherlands
Fax: +31 (20) 485 2845

For USA and Canada:
P.O. Box 945
New York, NY 10159-0945
Fax: +1 (212) 633 3680

US$ prices are valid only for the USA & Canada and are subject to exchange rate fluctuations; in all other countries the Dutch guilder price (Dfl.) is definitive. Customers in the European Union should add the appropriate VAT rate applicable in their country to the price(s). Books are sent postfree if prepaid.

0021-9673(19950120)690:1;1-S